# ELECTRICAL CHARACTERIZATION AND APPLICATIONS OF CONDUCTIVE INFRASTRUCTURE MATERIALS

A Dissertation

by

YOUNHO REW

Submitted to the Office of Graduate and Professional Studies of
Texas A&M University
in partial fulfillment of the requirements for the degree of

DOCTOR OF PHILOSOPHY

| | |
|---|---|
| Chair of Committee, | Philip Park |
| Committee Members, | Dallas Little |
| | Marcelo Sanchez |
| | Gwan S. Choi |
| Head of Department, | Robin Autenrieth |

December 2017

Major Subject: Civil Engineering

## ABSTRACT

The feasibility of multifunctional applications of electrically conductive asphalt concrete is investigated. The conductive asphalt concrete has a huge potential for various multifunctional applications such as self-healing, self-sensing, and deicing. This study examines the method of controlling conductivity of asphalt composites, electrical characterization of the composites with alternating current impedance spectroscopy (ACIS), application for damage self-sensing, and application for removing snow and ice on pavements.

Aiming to control the electrical conductivity of asphalt concrete with a smooth transition from insulated to conductive phase, nine types of graphite having different particle shape, size, and origin were mixed with asphalt binders, and their effects on imparting conductivity were investigated. The natural flake graphite is effective to mitigate the percolation threshold, and a sufficiently high conductivity (up to $10^{-2}$ $\Omega \cdot cm$) can be achieved by replacing a part of fillers only with the graphite.

For the electrical characterization of the conductive asphalt composites, ACIS is employed. Through this technique, the equivalent electrical circuits in various levels of conductivity is constructed for the first time. The results show that a specific conductivity range containing 20-25% flake graphite by weight of the asphalt mastic is suitable for sensing applications.

Self-sensing of damage is one of probable multifunctional applications of the conductive asphalt concrete, and its feasibility is investigated using ACIS. The

experiments with dry and wet conditions show that the real and imaginary impedance increase with the increase of the damage, while the capacitance value does not show a clear relationship with the damage evolution. The results also show that the distance between electrodes is important for measuring damage with ACIS.

The feasibility of the heated pavement using the conductive asphalt as a cost-effective and pollution-free solution was investigated. Bench scale slab heating test, non-steady state heat transfer analysis, and life-cycle assessment (LCA) were conducted. The results of these methodologies reveal that the heating capacity of the conductive asphalt is sufficient for deicing on pavement surfaces.

The electrical and mechanical data obtained from this study provide essential information on multifunctional applications of conductive asphalt concrete, which will lead to technical innovations for more sustainable pavement systems.

## DEDICATION

To my beloved wife, Yunmi, my father, my mother

## ACKNOWLEDGEMENTS

First of all, I would like to thank my committee chair, Dr. Park, and my committee members, Dr. Little , Dr. Sanchez, and Dr. G. Choi, for their guidance and support throughout the course of this research.

Thanks also go to my friends and colleagues and the department faculty and staff for making my time at Texas A&M University a great experience. I also want to extend my gratitude to Korea Institute of Civil Engineering and Building Technology (KICT) and Southwest Region University Transportation Center (SWUTC), which provided the economic support of my degree.

Finally, thanks to my parents and parents-in-law for their encouragement, my brother and brother-in-law for continuous concern, and to my wife for her patience and love.

## CONTRIBUTORS AND FUNDING SOURCES

### Contributors

This work was supervised by a dissertation committee consisting of Professor Philip Park (committee chair), Dallas Little, and Marcelo Sanchez of the Zachry Department of Civil Engineering and Professor Gwan S. Choi of the Department of Electrical and Computer Engineering.

All work for the dissertation was completed independently by the student.

### Funding Sources

Graduate study was supported by a fellowship from Texas A&M University, by the Southwest Region University Transportation Center (SWUTC) under Grant Number DTRT12-G-UTC06, and by Korea Institute of Civil Engineering and Building Technology (KICT) by part.

## NOMENCLATURE

| | |
|---|---|
| ACIS | Alternating current impedance spectroscopy |
| AC | Alternating current |
| DC | Direct current |
| $I(t)$ | Sinusoidal excitation of input current |
| $V(t)$ | Sinusoidal excitation of output voltage |
| $\Delta V$ | Texas Department of Transportation |
| $\omega$ | Angular frequency ( $= 2\pi/t$ ) |
| $t$ | Time |
| $\theta$ | The phase angle (difference) between the voltage and the current |
| $R$ | Resistor |
| $C$ | Capacitor |
| CPE | Constant phase element |
| $L$ | Inductor |
| $\bar{F}(s)$ | Laplace transformation of a function $F(t)$ |
| $s$ | Complex number ( $s = \sigma + j\omega$ ) |
| $j$ | $\sqrt{-1}$ |
| $Y(\omega)$ | Admittance |
| $Z(\omega)$ | Impedance ($= 1/Y(\omega)$) |
| $\lvert Y(\omega)\rvert$ | The modulus of admittance |
| $\lvert Z(\omega)\rvert$ | The modulus of impedance |
| $Re\ Z(\omega)$ | Real part of $Z(\omega)$ |

| | |
|---|---|
| $Im\, Z(\omega)$ | Imaginary part of $Z(\omega)$ |
| $\Delta V(t)$ | A voltage in time domain |
| $\Delta I(t)$ | A current in time domain |
| $\Delta \bar{I}(\omega)$ | A Laplace transformation of $\Delta I(t)$ |
| $\Delta \bar{V}(\omega)$ | A Laplace transformation of $\Delta V(t)$ |
| $S(t)$ | $\frac{di}{dt}$ (time derivation of current I) |
| $V_{GM}$ | Graphite volume percentage by asphalt mastic volume |
| $V_{GC}$ | Graphite volume percentage by asphalt concrete volume |

## TABLE OF CONTENTS


Page

ABSTRACT ..... ii

DEDICATION ..... iv

ACKNOWLEDGEMENTS ..... v

CONTRIBUTORS AND FUNDING SOURCES ..... vi

NOMENCLATURE ..... vii

TABLE OF CONTENTS ..... ix

LIST OF FIGURES ..... xii

LIST OF TABLES ..... xvii

1. INTRODUCTION ..... 1

    1.1 Background ..... 1
    1.2 Objectives ..... 7

2. LITERATURE REVIEW ..... 10

    2.1 Approaches to Impart Conductivity into Asphalt Concrete ..... 10
    2.2 Multifunctional Applications of Conductive Asphalt Concrete ..... 22
        2.2.1 Snow and Ice Removal Using Electric Heating ..... 23
        2.2.2 Promoting Self-Healing ..... 24
        2.2.3 Strain and Damage Self-Sensing ..... 24
    2.3 Multifunctional Applications of Conductive Cement Concrete ..... 26
        2.3.1 Conductivity of Cement-Based Composites ..... 27
        2.3.2 Self-Actuating Materials ..... 29

3. CONDUCTIVITY CONTROL OF ASPHALT CONCRETE USING CONDUCTIVE FILLERS ..... 34

    3.1 Introduction ..... 34
    3.2 Preliminary Research ..... 39
        3.2.1 Characterizations of Raw Materials ..... 39

Page


3.2.2 Electrical Conductivity of Asphalt Mastic ..... 48
3.3 Experimental Method ..... 58
3.3.1 Specimen Preparations ..... 58
3.4 Measurement Set-up ..... 61
3.4.1 Viscoelastic Properties of Asphalt Mastic ..... 61
3.4.2 Electrical Resistivity of Asphalt Concrete ..... 63
3.4.3 Indirect Tensile Strength of Asphalt Concrete ..... 63
3.5 Results and Discussions ..... 64
3.5.1 DSR Test ..... 64
3.5.2 Conductivity and Strength of Asphalt Concrete ..... 67
3.6 Conclusions ..... 72

4. ELECTRICAL CHARACTERIZATION WITH AC IMPEDANCE SPECTROSCOPY ..... 75

4.1 Introduction ..... 75
4.2 Technical Background ..... 77
4.2.1 AC Response ..... 77
4.2.2 Nyquist and Bode Diagram ..... 81
4.2.3 Electrical Equivalent Circuit ..... 83
4.3 Materials and Test Methods ..... 86
4.3.1 Physical Properties of Used Materials ..... 86
4.3.2 Sample Preparation ..... 87
4.4 Measurement Set-up ..... 91
4.5 Results and Discussions ..... 93
4.5.1 Electrical Characters of Conductive Asphalt Composites ..... 93
4.5.2 Effect of Temperature ..... 107
4.5.3 Effect of Moisture ..... 113
4.5.4 Size Effect ..... 117
4.6 Conclusions ..... 117

5. APPLICATION TO DAMAGE SELF-SENSING ..... 120

5.1 Introduction ..... 120
5.2 Materials and Test Methods ..... 121
5.2.1 Materials and Sample Preparation ..... 121
5.2.2 Test Method ..... 122
5.3 Results and Discussions ..... 123
5.3.1 Dry Condition ..... 124
5.3.2 Wet Condition ..... 130
5.4 Conclusions ..... 136

Page

6. APPLICATION TO SNOW AND ICE REMOVAL ..... 138

6.1 Introduction ..... 138
6.1.1 Background ..... 138
6.1.2 Research Objectives ..... 140
6.2 Literature Reviews ..... 141
6.3 Simulation of Deicing System for Airfield Application ..... 145
6.3.1 Description of Model ..... 145
6.3.2 Heat Transfer Model ..... 147
6.3.3 Simulation Result ..... 152
6.4 Experimental Program ..... 178
6.4.1 Characteristics of Graphite ..... 178
6.4.2 Conductive Asphalt Concrete ..... 178
6.4.3 Bench Scale Demonstration ..... 189
6.5 Life-Cycle Assessment ..... 193
6.5.1 Data Collection of Two Alternatives ..... 193
6.6 Interpretation of Environmental, Economic and Social Implications ..... 197
6.6.1 Economic Transaction ..... 197
6.6.2 Transportation Movement ..... 197
6.6.3 Land Use ..... 198
6.6.4 Global Warming Potential and Greenhouse Gases ..... 198
6.7 Conclusions ..... 200

7. CONCLUSION AND FUTURE WORK ..... 204

7.1 Conclusion ..... 204
7.2 Future Work ..... 208

REFERENCES ..... 210

## LIST OF FIGURES

Page

Figure 1. Research roadmap ..... 9

Figure 2. Effect of type of conductive additives on the electrical resistivity of asphalt concrete (Wu et al. 2005) ..... 12

Figure 3. Mechanical properties of HMA mixture with conductive additives (Huang et al. 2009) ..... 14

Figure 4. Schematic representation of volume resistivity versus conductive additive content (Garcia et al. 2009) ..... 15

Figure 5. Variation in electrical resistivity with sand-bitumen ratio (Garcia et al. 2009) ..... 16

Figure 6. Mechanical test results of conductive asphalt concrete (Wu et al. 2010) ..... 18

Figure 7. The indirect tensile strength on conductive porous asphalt concrete (Liu et al. 2010b) ..... 19

Figure 8. Possible applications and benefits of electrically conductive asphalt concrete ..... 36

Figure 9. Components of high-performance conductive asphalt concrete. ..... 36

Figure 10. Electrical resistivity transition curve ..... 39

Figure 11. SEM images of graphite powders ..... 42

Figure 12. Experimental set-up for measuring electrical property ..... 51

Page

Figure 13. Electrical resistivity of asphalt mastics containing various graphite types ....53

Figure 14. Asphalt concrete specimens ....60

Figure 15. Experimental set-up for measuring viscoelastic property....62

Figure 16. Indirect tension test set-up ....64

Figure 17. Variation of complex modulus with graphite contents ....65

Figure 18. Variation of phase angle with graphite contents....66

Figure 19. Variation of $|G^*| \cdot \sin\delta$ (KPa) with graphite contents....66

Figure 20. Variation of $G^* / \sin\delta$ (KPa) with graphite contents ....67

Figure 21. Volume resistivity versus F146 content for conductive asphalt concrete....70

Figure 22. Volume resistivity versus F516 content for conductive asphalt concrete....70

Figure 23. Comparing IDT strength of F146 and F516 ....72

Figure 24. Linear current response to a sinusoidal voltage excitation of small amplitude around a constant value $V_c$ ....78

Figure 25. (a) Nyquist diagram and (b) Bode diagram ....82

Figure 26. Schematic representation of a resistor (a), a capacitor (b), and an inductor (c) ....83

Figure 27. Asphalt composite specimens (a) Asphalt mastic (b) Asphalt concrete ....91

Page

Figure 28. Resistivity measurement set-up: Phase gain/phase analyzer .....92

Figure 29. Bode Diagram of Asphalt mastic specimens including different graphite contents.....94

Figure 30. Phase angle of asphalt mastic specimens including different graphite contents.....96

Figure 31. Nyquist diagram of asphalt mastic specimens including different graphite contents .....98

Figure 32. Electrical Equivalent Circuits of Asphalt Composite Containing Graphite.....101

Figure 33. Bode Diagram of Asphalt concrete specimens including different graphite contents .....102

Figure 34. Phase Angle of Asphalt concrete specimens including different graphite contents.....104

Figure 35. Nyquist diagram of asphalt concrete specimens including different graphite contents .....105

Figure 36. Temperature effect of Asphalt concrete specimens $V_{GC}$ = 2.99% ($V_{GM}$ = 16.40%) .....109

Figure 37. Temperature effect of Asphalt concrete specimens $V_{GC}$ = 2.99% ($V_{GM}$ = 16.40%) .....110

Figure 38. Wet condition of asphalt concrete specimens.....114

Figure 39. Impedance variation with time in wet condition of asphalt concrete specimens .....115

Page

Figure 40. Moisture effect of Asphalt concrete specimens ($V_{GC}$ = 2.99%) .....116

Figure 41. Experiment specimens .....123

Figure 42. AC Impedance spectroscopy with different damage contents for conductive asphalt concrete (Dry condition).....127

Figure 43. Conductive asphalt concrete in a wet condition .....131

Figure 44. AC Impedance spectroscopy with different damage contents for conductive asphalt concrete (Wet condition) .....133

Figure 45. Structural design of perpetual pavement containing electrically conductive asphalt layer .....146

Figure 46. Simulation model of airport runway.....146

Figure 47. Computational pavement model .....149

Figure 48. Pavement simulation flow chart (Xijun 2014).....151

Figure 49. 24-hour temperature variation during winter.....153

Figure 50. Temperature distribution of pavement with conductive sub-layer .....153

Figure 51. Effects of the location of the conductive sub-layer .....155

Figure 52. Effects of the thickness of the conductive sub-layer .....160

Figure 53. Effects of the thickness of the conductive sub-layer .....167

Figure 54. Comparison of electric energy and cost.....175

Page

Figure 55. Sieve analysis of D-5 mix ..... 180

Figure 56. Air voids versus % binder content of D-5 mixture ..... 180

Figure 57. VMA versus % binder content of D-5 mixture ..... 181

Figure 58. VFA versus % binder content of D-5 mixture ..... 181

Figure 59. Experimental set-up for measuring electrical heating (DC) ..... 183

Figure 60. Temperature variation of conductive asphalt concrete specimens for electrical heating (DC) ..... 183

Figure 61. Comparison of temperature variation between experimental result and theoretical calculation ..... 186

Figure 62. Comparison of electrical resistivity of specimen with temperature variation ..... 188

Figure 63. Layout of the conductive asphalt concrete slab specimen ..... 189

Figure 64. Experimental set-up for deicing ..... 190

Figure 65. Experimental result of deicing test by using DC power supply ..... 192

Figure 66. Experimental result of deicing test in a freezer ..... 192

Figure 67. Main framework of EIO-LCA model ..... 194

Figure 68. Environmental, economic, and social impacts of two alternatives ..... 199

Figure 69. Research strategy including future works ..... 209

## LIST OF TABLES

Page

Table 1. Summary of previous research on conductive asphalt composites ..... 21

Table 2. Properties of graphite used for the research (Asbury Carbons Inc.) ..... 41

Table 3. Materials used for the research ..... 47

Table 4. Aggregate gradation ..... 58

Table 5. Volumetric properties of the mixture ..... 69

Table 6. Properties of other materials used for the research ..... 88

Table 7. Aggregate gradation ..... 90

Table 8. Values of All Impedance Components with Various Temperatures ..... 112

Table 9. Recent novel methods of pavement deicing ..... 144

Table 10. Thermal properties of the pavement ..... 148

Table 11. Aggregate gradation of D-5 mixture ..... 179

Table 12. Temperature variation of specimens with time under fixed 30V DC ..... 185

Table 13. Quantity takeoffs and EIO-LCA input values ..... 195

Table 14. EIO-LCA analysis results for two alternatives ..... 196

# 1. INTRODUCTION

## 1.1 Background

Multifunctional materials have simultaneous abilities to exhibit non-structural functions as well as their regular structural functions (Gibson 2010; Baur and Silverman 2011; Ye et al. 2005; Chou et al. 2010). By rendering a material multifunctional, the electrical, magnetic, thermal, and other functionalities can be integrated with structural properties (e.g., strength and stiffness). Materials of this kind have a tremendous potential for various smart applications. Among the listed non-structural properties, the use of electrical conductivity has been actively studied because of its various applications (Qiu et al. 2007; Kalaitzidou et al. 2007; Cebeci et al. 2009; Sandler et al. 2003; Li et al. 2007; Thostenson et al. 2009; Baeza et al. 2013; Jang et al. 2017).

Asphalt concrete is a composite material that is heavily used in the construction of highway, runways, and parking lots. Riding comfort, durability, reliability, and water resistance are the advantages making asphalt concrete the most preferred choice in the pavement industry. Asphalt concrete is a non-conductive composite material by nature, but its conductivity can be improved by using conductive additives (Wu et al. 2005; Huang et al. 2009; García et al. 2009; Pan et al. 2015; Wang et al. 2016).

The concept of electrically conductive asphalt concrete was initiated by Minsk (1968) in 1960s, and this topic has gained interest in the last decade resulting in increasing numbers of publications. These efforts have largely been motivated by various potential multifunctional applications utilizing electrical properties of asphalt composites. For

instance, the electrical heating applications using the conductive pavements have been studied to remove snow and ice (Blackburn 2004; Chen et al. 2012; Singla et al. 2013; Gomis et al. 2015). Electric heating of the conductive asphalt pavements is also expected to promote self-healing by reducing the rest period (Garcia 2012; Norambuena-Contreras and Garcia 2016; Norambuena-Contreras and Garcia 2017). In addition, piezoresistivity of the conductive asphalt, which refers to change in electrical resistivity with applied mechanical pressure, can be used for self-sensing of strain (Wen and Chung 2007a; Wu et al. 2006; Liu and Wu 2009; Han et al. 2015; D'Alessandro et al. 2016). Self-sensing of damage in pavement structures is possible if the relationship between the electrical property and internal damage is provided (Chung and Wang 2003; Galao et al. 2014; Hallaji and Pour-Ghaz 2014; Providakis et al.2014). Moreover, conductive fibers and some type of conductive fillers are known to improve the strength and durability of asphalt concrete (Park 2012; Park et al. 2014; Park et al. 2015). While the conductive asphalt concrete has the various potential applications listed above, the practical use of the multifunction requires further investigations. One of the problems is the poor understanding about the electrical properties of the conductive composites. Most of the previous investigators have focused on a single electrical parameter – static resistance measured with direct current (DC). In composite materials, the static resistance represents only an electrical state of the materials under a specific condition, and may vary with the environmental factors such as moisture and temperature. In general, the electrical properties can be described with capacitance and inductance as well as resistance, and a

method of measuring these parameters is needed to properly characterize conductive composites.

Alternating current impedance spectroscopy (ACIS) is a powerful technique to characterize the electrical properties of materials and their interface to electrodes in complex electrical system (Barsoukov and Macdonald 2005; Girault 2004). Impedance plays a vital role to show the characteristics of an electrical system, and is defined as the resistance to the flow of alternating current (AC). Through the measurement of ACIS, an equivalent electrical circuit that has the same electrical properties to the material can be constructed. The equivalent electrical circuit allows to predict the electrochemical behavior of electrode and electrolyte materials. ACIS also has been widely used to prove the physical characteristic of material structure and various chemical phenomena such as diffusion and corrosion in chemical science area. In civil engineering, the first application of ACIS were tried by McCarter et al. (1988) for cement pastes. In this study, ACIS has been used to monitor the hydration process of cement pastes with the frequency range from 100 Hz to 300 kHz. Since then, many studies using ACIS have concentrated on the mechanism of hydration of cement based composites during the last three decades (Campo et al. 2002; Gu et al. 1992; Gu et al. 1993; McCarter et al. 2009). Gu et al. (1993) stated that ACIS is a convenient method of characterizing microstructural development in hydrating cement or concrete systems. Gu et al. (1993) investigated the microstructure of the transition zone between aggregate and cement paste, and the effect of silica fume, slag, and fly ash using ACIS. The application of ACIS for damage monitoring of electrically conductive cement composites has been tried by Peled et al. (2001). They investigated the

correlation between electrical and mechanical properties of cement composites with conductive carbon fibers. The equivalent electrical circuit, constructed by the frequency dependent electrical properties, is useful to evaluate the damage of conductive cement concrete. On the other hand, ACIS has not been applied to asphalt concrete, and this is the first study that uses ACIS for the conductive asphalt concrete.

Self-sensing of damage is one of the plausible multifunctional applications in the conductive asphalt concrete. Potential drop method is a traditional method for monitoring fatigue crack growth of metallic materials in mechanical and aerospace engineering (ASTM E647 2013; Doremus et al. 2015; Zhu and Joyce 2012). This method evaluates the crack size by measuring the change of electrical resistance due to the crack growth in highly conductive materials. The sensitivity of detecting the damage depended significantly on the positions of electrodes and frequency range of the electrical source. Generally, the potential drop method requires point probes to increase the sensitivity of measurement and exact electrical calibration equations (Johnson 1965; Clark and Knott 1975). Thus, so far, the utilization of the potential drop method has been limited to metallic materials to prevent the problems related to electrodes and the conductivity of specimens (i.e., capacitance and inductance is negligible). Among the civil engineering materials, cement concrete was investigated in limited researches for measuring the damage content by using the potential drop method. Cement concrete is a well-known non-conductive material in dry condition, but its conductivity increases due to the ionic conduction when the cement concrete contains a sufficient amount of water (Wen and Chung 2006). Bontea et al. (2000) and Chung and Wang (2003) showed that a dry cement concrete containing

conductive additives (e.g., carbon fibers) had damage self-sensing capability. Lataste et al. (2003) introduced a numerical approach to assess crack depth in concrete members, and compared with experiment data using the potential drop method. Although these existing studies have proven that the electrical resistance increases with the damage growth, there are some limitations in measuring the extent of the damage in civil composite materials with the potential drop method (Le et al. 2014). In addition to the variation of concrete conductivity with the moisture content, the direct current (DC) resistance measurement used in the traditional potential drop method causes electric polarization due to the cumulative ion movement in water. The polarization brings about the increase of the measured resistance. (Wen and Chung 2001c; Cao and Chung 2004). Since the moisture condition in civil structures varies with the environment, the application of this method is limited to the laboratory, at where the moisture condition can be controlled. While the potential drop method used only the static resistance value measured with DC to figure out the crack size, ACIS with AC frequency sweep has various benefits in examining the microstructural changes of materials by utilizing various electrical properties, such as the resistance, dielectric constant, and phase angle. Under alternating current (AC), the ions move back and forth because the polarity of the input voltage repeatedly changed. Thus, the effect of polarization, which makes the difficulty to measure accurately the resistance, can be minimized by using AC (Wen and Chung 2007a). The potential drop method has not been used and studied for asphalt concrete due to their non-conductive nature.

Another potential application of conductive infrastructure materials is the removal of snow and ice on roads. In the regions of cold climate, snow and ice on pavement

surfaces cause a great number of traffic problems. Considering the traffic accidents and human injuries due to the loss of skid resistance, deicing is a critical safety issue on roads. Kuemmel (1994) estimated that the direct cost is $11 billion (manpower, materials, and equipment), and the indirect cost is $21 billion (environmental effects due to the use of chemical agents) for removing snow from the 75 mile long highway around Lake Tahoe for 25 years. The use of deicing agents and mechanical method (snow plowing) are traditional ways of removing ice and snow on roads, but those methods are not perfect solutions. Chemical deicing agents bring corrosion of vehicles, destruction of the vegetation, and pollution of ground and water (Jones and Jeffrey 1992; Williams et al. 2000; Wang et al. 2006). In addition, the chemical agents have a limitation in the applicable temperature range. For example, sodium chloride does not effective below -3.9°C (Löfgren 2001; Sanzo and Hecnar 2006). The mechanical methods, such as vehicle with large plow or shovel, require high maintenance costs and cause traffic delays. Moreover, the mechanical methods do not completely remove the snow and ice, and cause damage on the pavement surface (Nixon 1993).

As an alternative solution, thermal deicing, called heated pavement, is considered to be an effective and green method. Installations of heating pipes (Lee et al. 1984) or electrical coils (Lee 2012) below a surface layer of pavements have been tried by some countries to melt snow and ice. However, their widespread use is hindered by expensive installation cost and short service life - the electric coils are easily broken under repeated traffic loads. According to Lee (2012), installation cost for the electric coil is $160,000 for 300 m road. Some recent studies tried to use conductive carbon fiber tapes (Yang et al.

2012), infrared heat lamp (Zenewitz 1977), microwave (Hopstock 2003), and conductive paving materials (Yehia and Tuan 2000; Wu et al. 2012).

In order to resolve the problems of the coil or pipe heating system, the idea proposed herein is to make the paving material itself to be electrically conductive. Recent studies (Wu et al. 2003; García et al. 2009; Park 2012) show that the poor electrical conductivity of asphalt can be remarkably improved by adding conductive fibers and/or fillers. Such conductive additives are cheaper than the coil or pipe installation, and do not lose its conductivity at damaged conditions.

## 1.2 Objectives

The overall objective of the research is to investigate the feasibility of multifunctional applications of the conductive asphalt concrete. In the first phase, the method of imparting and controlling conductivity of asphalt concrete is investigated with various particle type conductive additives. Then, the electrical characteristics of the conductive asphalt concrete are investigated by using ACIS. Among the various multifunctional applications, damage self-sensing and heated pavement are selected, and their feasibilities are investigated using ACIS and inductive heating. Figure 1 illustrates the roadmap of this research. The specific objectives that will be achieved through the course of this research are listed below:

1) Conductivity Control:
    - To control electrical conductivity of asphalt concrete with the most efficient graphite types.

- To investigate the viscoelasticity properties of asphalt mastic (asphalt binder + conductive filler) containing various conductive additives.
- To investigate the effect of the conductive additives on the mechanical properties of conductive asphalt concrete.

2) Electrical Characterization with Alternating Current Impedance Spectroscopy:
   - To characterize the electrical properties of conductive asphalt concrete with various conductive additive contents using ACIS.
   - To construct the equivalent electrical circuit for conductive asphalt concrete with various conductivity.
3) Application to Damage Self-sensing of Conductive Asphalt Concrete:
   - To investigate the feasibility of damage evaluation and monitoring of conductive asphalt concrete using ACIS.
   - To investigate the effects of various factors including conductive additive content on the sensitivity of ACIS parameters for damage evaluation.
   - To develop an electrical behavior prediction model using electrical equivalent circuits analysis for damage evaluation.
4) Application to Snow and Ice Removal on Conductive Pavement:
   - To evaluate the feasibility of heated pavement system using conductive asphalt concrete.
   - To estimate the energy consumption of the heated pavement.
   - To verify heating capability of the snow/ice removal system consisted of multiple HMA layers including a conductive layer.

- To conduct the LCA that the snow removal and deicing alternatives are compared from the economic, social, and environmental standpoints through EIO-LCA.

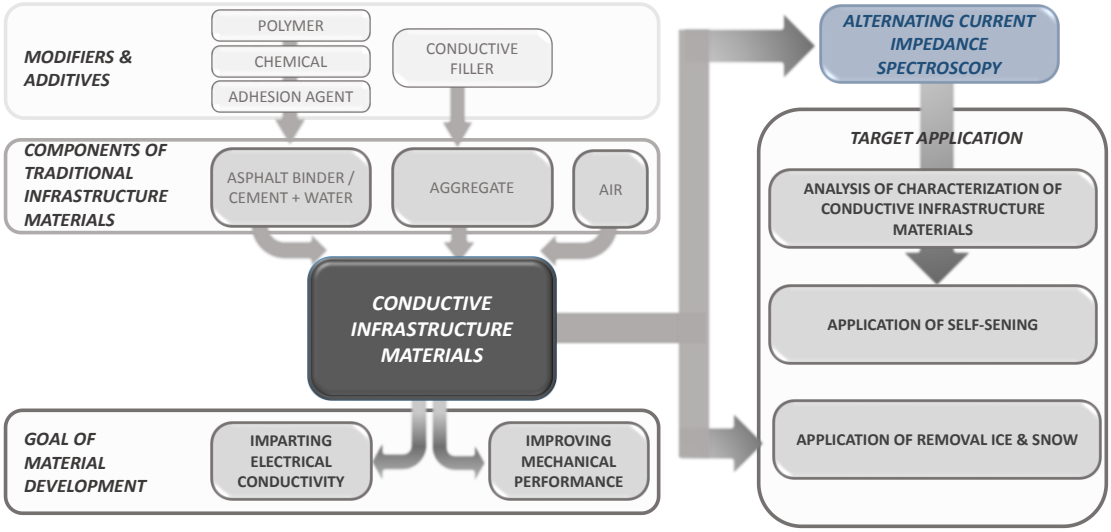


**Figure 1. Research roadmap**

# 2. LITERATURE REVIEW

A review of literatures on imparting and controlling conductivity in asphalt concrete and the various possible multifunctional applications are summarized in the this section.

## 2.1 Approaches to Impart Conductivity into Asphalt Concrete

The interest in imparting electrical properties into asphalt concrete dates back to 1970s. Minsk (1971) patented "Electrically conductive asphaltic concrete" using graphite as a conductive medium for the purpose of melting snow and ice on roadway surfaces by electrical heating. Stratfull (1974) and Fromm (1976) used coke-breeze from steel industry to produce conductive hot-mix asphalt (HMA) for cathodic protection of steel rebars in concrete bridges. Zaleski et al. (1998) patented a pavement system containing electrically conductive layer for de-icing purpose. They utilized graphite and coke as conductive additives. Parallel to asphalt concrete, extensive study on electrically conductive Portland cement concrete have been published. Barnard (1965) patented electrically conductive cementitious concrete, and since then, various efforts were reported on the widened applications of conductive concrete (Chung 2003).

Findings from numerous research studies in the past have shown that the electrical conductivity of asphalt concrete can be improved with the addition of conductive fillers and/or fibers. Wu et al. (2003) showed that the inclusion of graphite beyond a critical content decreases the resistivity of asphalt-based composites. In this paper, the authors focused mainly on the self-sensing ability of conductive asphalt. In 2005, electrical

conductivity of asphalt concrete with other additives such as carbon black (CB), graphite (G) and carbon fibers (CF) were investigated (Wu et al. 2005). It was found that pure carbon fiber modified asphalt concrete showed the best performance in conductivity followed by graphite and carbon black as illustrated in Figure 2. In the figure, the content of conductive additive is presented as volume percentage of the binder phase of the mixture. The electrical resistivity was found to decline rapidly when specific amounts of conductive additives were added, which is percolation threshold. Previous investigators (Wu et al. 2005; Huang et al. 2006) explained that a three-dimensional conductive network is established at percolation threshold, and hence improvement in conductivity is not significant after this point. Wu et al. (2005) thus concluded that the desired electrical resistivity can be obtained by keeping the content of conductive additives slightly above the optimum (percolation) level, but making sure that it should not go beyond to minimize the influence on mechanical properties of asphalt concrete.

Similar studies were carried out by a research team at University of Tennessee. Huang et al. (2006) investigated the different options for producing electrically conductive asphalt. Micro-scale steel fibers (8 μm in diameter and 6 mm in length), aluminum chips (passing 0.10 mm sieve), and graphite (passing 0.075 mm sieve) were examined for their ability in imparting conductivity. It was observed that the aluminum chips are not effective in increasing electrical conductivity of the mixture in spite of their excellent conductivity.

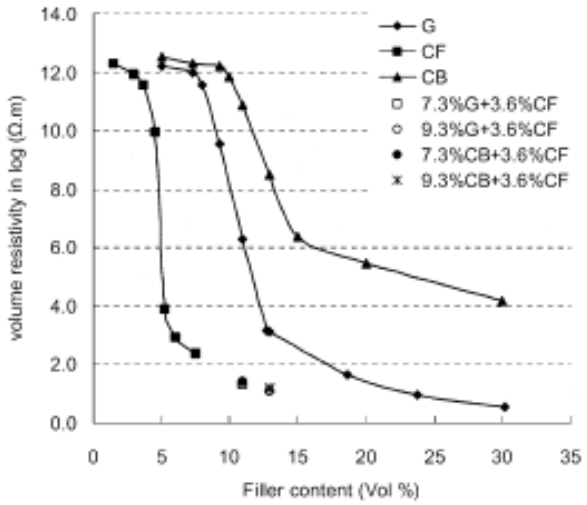


**Figure 2. Effect of type of conductive additives on the electrical resistivity of asphalt concrete (Wu et al. 2005)**

The reason was that aluminum gets easily oxidized in air forming aluminum oxide, which has low conductivity. While aluminum is not the right choice for practical purpose, the mixtures with micro-scale steel fibers and graphite exhibited good electrical conductivity. Resistivity in order of $10^3\Omega$.m was reached with the addition of 0.33% steel fibers by volume of asphalt binder. Approximately 2.3% graphite by volume of asphalt binder was needed to obtain the similar resistivity level. Variation in electrical conductivity during fatigue evolution was also studied through indirect tensile test (IDT) and beam fatigue tests.

Huang et al. (2009) extended their investigation to the mechanical performance of conductive asphalt composites. Dynamic Shear Rheometer (DSR) test was conducted to

study the effect of conductive additives, i.e., micro-scale steel fibers, carbon fibers and graphite; on the viscoelastic properties of asphalt mastic (mixture of asphalt binder and conductive additives). The results show that with increase in the content of the conductive additives, the complex shear modulus, G*, increases. This implies that the conductive additives can stiffen asphalt binder. High contents of graphite were required to achieve sufficiently low resistivity, and hence the stiffness of the mastic was improved to a great extent. The mechanical performances of conductive HMA mixtures were investigated through IDT and dynamic modulus tests. Though graphite reduces the IDT strength of the mixtures, it improves the dynamic modulus. On the other hand, the fracture energy of the mixtures with carbon or steel fibers was slightly improved due to the reinforcing effect of the fibers. Figure 3 depicts the IDT strength and dynamic modulus of asphalt concrete containing various additives.

A comprehensive study was conducted by Garcia et al. (2009). The effect of fiber content, sand–bitumen ratio and the combination of fillers and fibers (graphite and steel wool) on the resistivity of asphalt mortar were examined. The authors divided the changes in the resistivity with volume percentages of conductive additive into four different phases: the insulated phase, transition phase, conductive phase, and excess of fibers phase. The insulated phase is where the fibers are not connected with one another and the resistivity is approximately equal to that of plain asphalt concrete. The transition phase is where the percolation path of fibers forms and the resistivity drops rapidly leading to the next phase called the conduction phase. Beyond the conductive phase, named as the excess of fibers phase, the reduction in length of conductive paths is not significant any more, and

electrical resistivity of the composite decreases slightly with increase in fiber content. In addition, it becomes difficult to mix when clusters of fibers start forming with large proportions of fibers. Figure 4 shows the schematic of the conductivity variation.

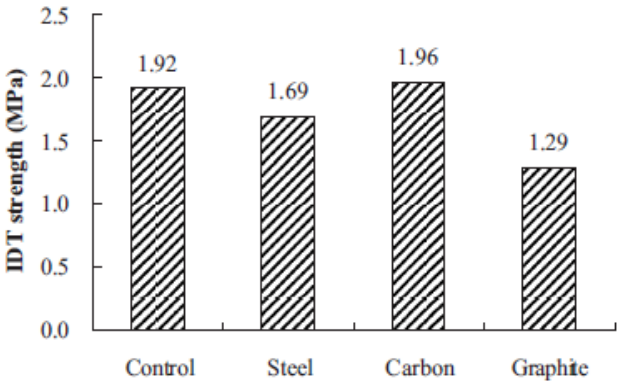


(a) IDT strength for various additives

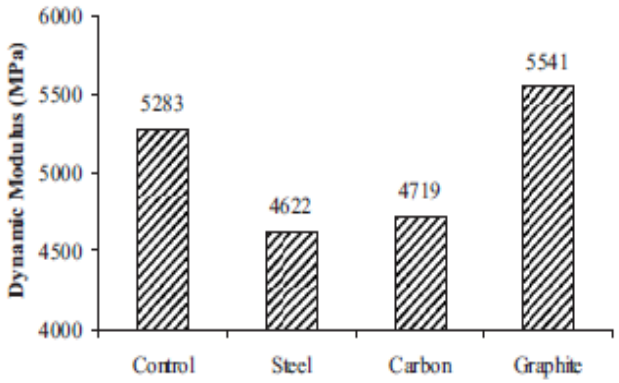


(b) Dynamic Modulus at 10 Hz

**Figure 3. Mechanical properties of HMA mixture with conductive additives (Huang et al. 2009)**

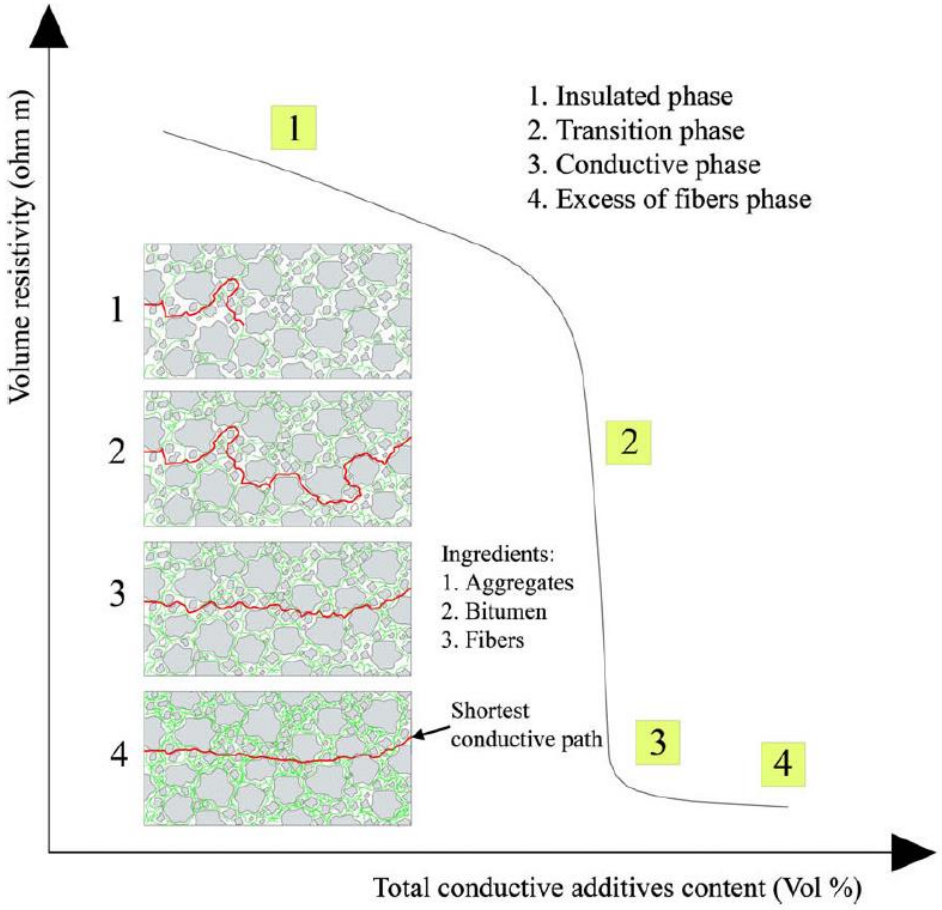


**Figure 4. Schematic representation of volume resistivity versus conductive additive content (Garcia et al. 2009)**

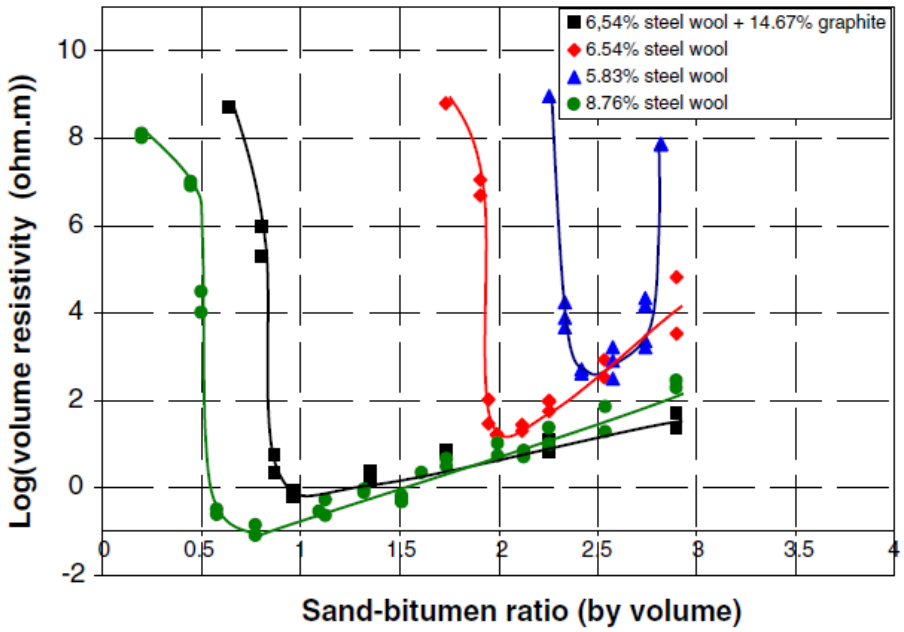


**Figure 5. Variation in electrical resistivity with sand-bitumen ratio (Garcia et al. 2009)**

According to Garcia et al. (2009), the resistivity of the composite material varied not only with the content of conductive additives, but also with sand-bitumen ratio. It was observed that there exists an optimum conductive particles-bitumen ratio for each sand-bitumen ratio where the resistivity of the mixture reached a minimum. Figure 5 shows the optimum sand-bitumen ratios for different amount of conductive additives. It should be noted that graphite significantly reduces the optimum sand-bitumen ratio when it is combined with steel wool.

In addition, Liu et al. (2008a) and Liu and Wu (2009) investigated the piezoresistivity of conductive asphalt concrete. Piezoresistivity is an electrical property that the electrical resistivity of a material changes due to applied stress or strain. It reflects the microstructural change in the material on application of load. This phenomenon was observed in conductive asphalt, and it implies that conductive asphalt has a possibility of being utilized as a self-sensing material. The relationship between electrical property and mechanical condition broadens the possible multifunctional application of conductive asphalt.

The mechanical characteristics of the conductive asphalt concrete using graphite and carbon fiber were investigated by Wu et al. (2010). They studied the indirect tensile strength, indirect tensile resilient modulus, and indirect tensile fatigue life of the conductive asphalt concrete containing carbon fibers and graphite. The results indicated that conductive asphalt concrete has higher tensile strength than regular asphalt concrete in dry condition, but has lower wet tensile strength and tensile strength ratio (TSR). This means the conductive asphalt concrete has relatively lower resistance to water, but fortunately the ratio is higher than the minimum required value. The indirect tensile resilient modulus increases with the addition of conductive components. The effect of carbon fibers on indirect resilient modulus is more prominent than that of graphite. The results of the indirect tensile fatigue test show that the fatigue life of conductive asphalt concrete at higher stress levels is greatly enhanced when it is compared to regular asphalt concrete. Figure 6 summarizes the findings of Wu et al. (2010).

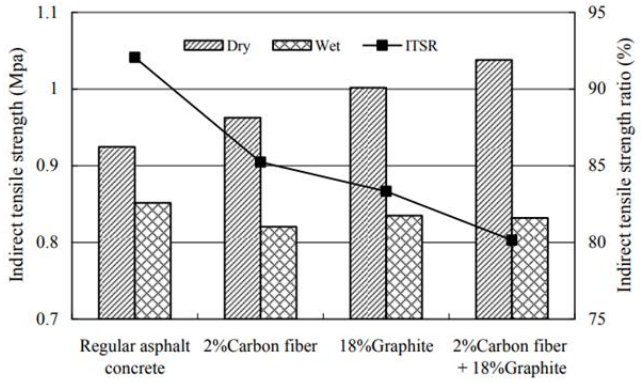


(a) Indirect tensile strength results for regular and conductive asphalt

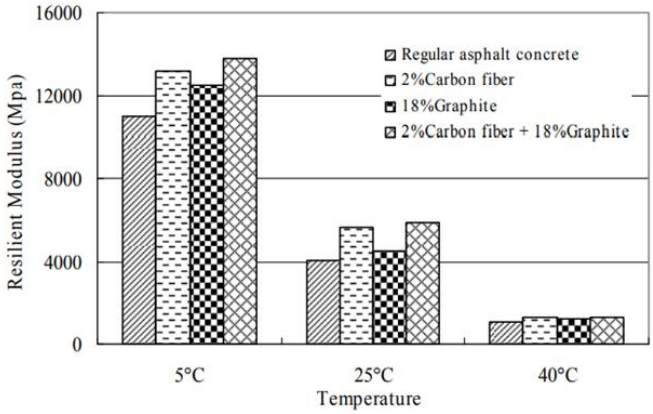


(b) Indirect tensile resilient modulus results at different temperatures

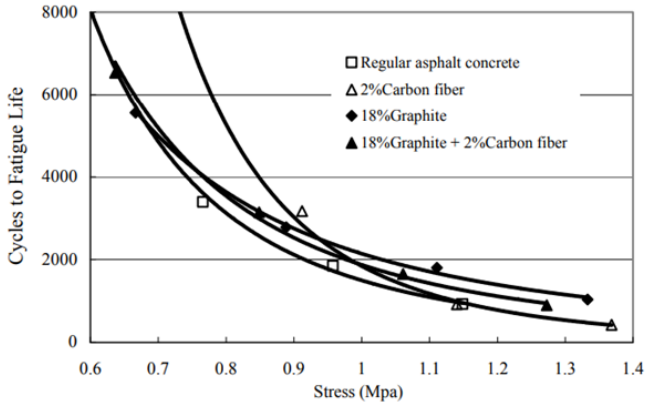


(c) Indirect tensile fatigue life graph for regular and conductive asphalt composites

**Figure 6. Mechanical test results of conductive asphalt concrete (Wu et al. 2010)**

Similar study on the IDT strength of porous asphalt concrete with steel fibers was conducted by Liu et al. (2010b). It was observed that the IDT strength of the mixture increases with the increase of steel fibers until a certain content. Beyond that, more addition of fibers reduces the thickness of mastic film around the aggregates leading to poor adhesion. This reduces the IDT strength of porous asphalt concrete. Figure 7 shows the results of IDT test on conductive porous asphalt concrete.

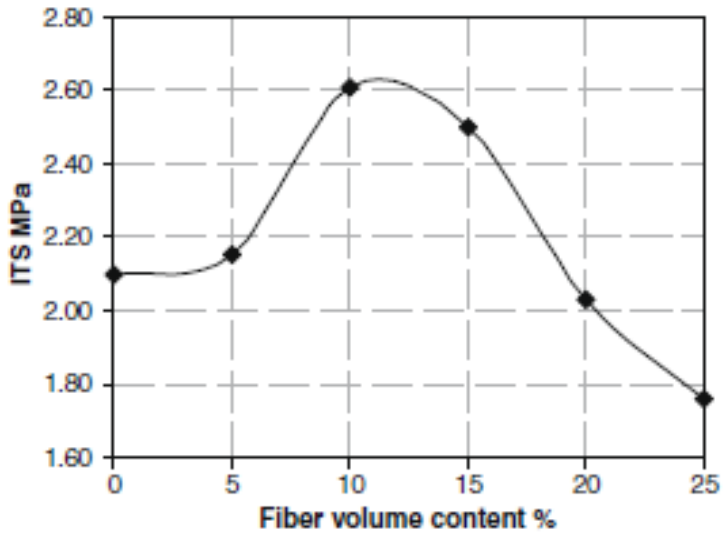


**Figure 7. The indirect tensile strength on conductive porous asphalt concrete (Liu et al. 2010b)**

Liu and Wu (2011a) investigated the variation of Marshall Stability, resilient modulus, and dynamic stability of graphite and carbon fiber modified asphalt concrete.

According to Liu and Wu (2011a), the addition of graphite did not considerably enhance the mechanical strength of asphalt concrete. They concluded that graphite can be a good conductive filler, but its lubricating property caused by weak bond between plain hexagonal crystal structures of graphite might impair the mechanical properties of asphalt concrete.

Park (2012) studied the effect of graphite powders on imparting electrical conductivity in asphalt mastic and showed that the electrical resistivity significantly varied with the types (shape and size) of graphite.

**Table 1. Summary of previous research on conductive asphalt composites**

| Authors | Conductive Fillers Used | Percentage of additives to attain resistivity of $10^3$ Ω.cm (% vol. by binder) | Purpose |
|---|---|---|---|
| Minsk (1968) | Graphite (G) | G- 17% and 21% | Snow and ice removal |
| Stratfull (1974) | Coke-breeze | --- | Cathodic protection of steel rebars in concrete bridges |
| Fromm (1976) | Coke-breeze | --- | Cathodic protection of concrete bridge decks |
| Zaleski et al. (1998) | Graphite and coke | --- | De-icing purpose |
| Wu et al. (2003) | Graphite | G- 26% | Self-sensing applications |
| Wu et al. (2005) | Carbon black (CB), graphite, carbon fibers (CF) | CB- 13%, CF- 6% or G- 30% | Imparting conductivity CF>G>CB |
| Huang et al. (2006) | Micro-scale steel fibers (SF), aluminum chips and graphite | SF -0.75% or G-11% | Study conductivity, IDT and beam fatigue test |
| Huang et al. (2009) | Micro-scale steel fiber, carbon fiber and graphite | SF- 0.99%, CF- 5% or G- 18% | IDT strength, IDT fracture energy, Dynamic modulus, Flow number, APA rut depth |
| Garcia et al. (2009) | Graphite and steel wool (SW) | SW- 6% or G- beyond 30% | Sand-bitumen ratio, effect of fiber content |
| Liu and Wu (2009) | Graphite and carbon fiber | G-12% | Piezo-resistivity |
| Wu et al. (2010) | Graphite and carbon fiber | G-22% or CF- beyond 8% | IDT, indirect tensile fatigue life |
| Liu and Wu (2011a) | Graphite and carbon fiber | G-15% | Marshall stability, resilient modulus and dynamic stability |
| Park (2012) | Graphite | G -21% | Electrical conductivity of different types of graphite |

Another type of the conductive additive is proposed by Zhang et al. (2011). Polyaniline (PANI) is a conductive polymer, and Zhang et al. (2011) tried to impart electrical conductivity into stone matrix asphalt using self-made PANI/PP (polypropylene) compound. The conductivity increased by 6 orders of magnitude and the percolation threshold was 1%.

As reviewed above, electrically conductive asphalt concrete has become popular during last ten years. Table 1 summarizes the previous research on conductive asphalt. As compared in the Table 1, the amount of conductive additives required for specific resistivity varies significantly with the investigators. For example, volume percentage of graphite at $10^3$ Ω.cm ranges from 11% to 30%. Therefore, the causes of this variability and the factors affecting conductivity of asphalt mixtures should be clarified for the precise conductivity control.

## 2.2 Multifunctional Applications of Conductive Asphalt Concrete

Multifunctional materials are considered to be smart and innovative materials due to their widespread technological impact and ability to respond to external stimuli in an environment friendly manner. The technology necessary to build the next-generation devices like autonomous robots, smart homes, intelligent sensors, structural health monitoring, and smart transportation system is expected to be centered on multifunctional materials.

The concept of developing multifunctional materials stems from the need to accomplish multiple applications and performances in a single system. The sought-after

characteristics of these materials include energy efficient non-structural functions, such as self-sensing, self-healing, and electromagnetic properties, in addition to traditional structural functions resisting to external forces. Hence, the research and development involved in multifunctional materials faces a great technological challenge with various applications. Interdisciplinary investigations have been carried out for the molecular structure and non-structural properties of various materials to explore multifunctional possibilities and to extend their use across different disciplines.

In case of the conductive asphalt concrete, the potential multifunctional applications include electrical heating, sensing, and energy harvesting. These features are discussed below for a more thorough understanding of the benefits.

### 2.2.1 Snow and Ice Removal Using Electric Heating

One of the major issues in the society was to improve the transportation safety under freezing and/or snowy weather. Removing snow and ice, especially on highway and bridge surfaces, is a crucial step to enhance transportation safety. Deicing agents such as salt or sand can be used to remove ice from pavement (Blackburn 2004). Salt is most popular deicing agent because it is inexpensive and efficient. However, deicing chemicals have obvious negative impacts including the concrete corrosion and environmental pollution. These problems are paid much attention by International Energy Agency (IEA) and World Health Organization (WHO) (Lofgren 2001; Sanzo and Hecnar 2006). Snow and ice on the conductive asphalt pavement can be removed by electric heating, which is

a process of converting electric energy to heat (Chen et al. 2012). This method ensures reliable deicing and reduced pollution.

### 2.2.2 Promoting Self-Healing

Asphalt concrete is a self-healing material (Bommavaram 2009). Once the load causing microcracks is removed, the molecules on either side of each crack starts diffusing to the other end, and the microcracks are healed with time. The time required for this healing process is called rest period. The challenge arises when the traffic flow is too heavy to allow sufficient rest period for self-healing. One of the solutions is to increase the temperature of asphalt concrete because the healing can be accelerated with the increase of temperature (Bonnaure et al. 1982; Daniel and Kim 2001). Liu et al. (2010a; 2010b; 2010c), Garcia (2012), Garcia et al. (2011a; 2011b) showed the possibility of promoting self-healing by induction electrical energy into conductive asphalt concrete. Garcia et al. (2011a; 2011b) and Liu et al. (2010a; 2010b; 2010c) suggested a non-contact electric heating technique using electromagnetic field. The induced current dissipates heat in the specimen by the Eddy current effect.

### 2.2.3 Strain and Damage Self-Sensing

A self-sensing material can monitor its own strain and damage without an external sensor. Thus, compared to structural health monitoring system based on the attached sensor network (extrinsic), self-sensing structural materials are intrinsically smart. The intrinsically smart structures have possible advantages than extrinsically smart structures

due to their low cost, good durability, large sensing volume, and absence of mechanical property degradation due to the embedding of sensors (Chung and Wang 2003).

The contact resistance between the conductive filler governs the resistivity of the asphalt or cementitious composites. Upon application of an external compressive load, the filler particles get closer resulting in decreased resistivity (Wen and Chung 2007a). Such a change in resistivity with application of mechanical stresses is referred as piezoresistivity (Wu et al. 2006). This is the mechanism by which conductive asphalt pavements sense their own structural health. Liu et al. (2008a; 2009; 2011a; 2011b) proposed a series-wound model to explain the piezoresistivity of conductive asphalt concrete by experimental studies. The number of electron carriers (conductive path) in the interior of the conductive asphalt concrete influences the electrical property and the number of carriers is varied with different loading conditions. The relationship between number of carriers and electrical resistivity is inversely proportional. In other words, the resistance reduces in increase compressive stress during loading and it increases during unloading until the stress reaches a certain value. Under compression, the contact resistance between graphite particles is reduced and insulating gaps between graphite particles are decreased, developing new conductive paths. Another reason mentioned is the ability of microcracks to destroy the conductive network due to the large width gap of microcracks preventing electron hopping. The third effect is the dislocation of conductive path which results from the large vertical deformation originated from the shear stress between aggregates. In addition, Liu et al (2008b) studied the engineering properties and electrical property of asphalt concrete with different graphite and carbon fiber content. The filler was 5% by

weight and 4.5% for asphalt. Graphite of 150 μm and carbon fiber of 10 μm diameter and 5 mm length were used. The results from the indirect tensile test indicate that the mechanical properties of asphalt mixture are influenced by the addition of conductive filler like graphite and carbon fiber. The resilient modulus all increased when a combination of graphite and carbon fibers was used while smaller increases were observed with the use of solely carbon fiber or graphite.

### 2.3 Multifunctional Applications of Conductive Cement Concrete

Concrete is the most widely used construction material nowadays and has a huge impact on the construction industry. Concrete by itself has strong structural properties, but is a poor electrical conductor. Incorporation of electrically conductive materials in the cement matrix enhances the smart function of concrete for various multifunctional applications. The typical conductive additives are steel/carbon fibers and graphite powders. More recently, attempts to use carbon nanotubes have been made. The promising multifunctional applications include self-sensing, self-heating, self-healing, electromagnetic shielding, and more recently, energy harvesting.

The factors affecting the conductivity of cement-based composites are volume fraction of fibers, length of fibers, temperature, chloride content, compressive, tensile or flexure load, sand/cement ratio, relative humidity, and curing age. The average length of carbon fibers found in literature is between 5 and 10 mm, and the average diameter is 10-15 μm. The typical volume fraction of fibers is ranged from 0.2 to 1.5%. Carbon fibers are considered to be most effective for strain sensing while steel fibers are most effective for

thermal sensing and deicing purposes. Silica fume is a useful additive for enhancing fiber dispersion. Carbon fibers are strong, durable and not dense whereas the one drawback of carbon fibers is their high cost (Chung 1997; 1999; 2000; 2002; 2003; 2012).

### 2.3.1 Conductivity of Cement-Based Composites

Various previous investigators verified that conductivity of concrete increases with the increase of fiber volume fraction. Chacko and Banthia (2007) showed that 5% fiber volume fraction produced hardly any increase in resistivity over time. In fact, samples with 3% fibers or less showed significant increases in resistivity over time. Chiarello and Zinno (2004) showed that longer fibers produced higher conductivity effects in concrete. 6 mm fibers yielded higher conductivity than 3 mm or shorter fibers. Conductivity was shown by several to be independent of specimen age. Chen et al (2004) also showed the effect of fiber length on electric conductivity. She declared a volume fraction around 0.3-0.4% to be the percolation threshold.

Chacko and Banthia (2007) examined the effect of various parameters on the resistivity of concrete. The electrical resistivity of carbon fiber reinforced cement composites increases dramatically over time. The increase is due to the microstructure change in hydration of concrete. There was a considerable decrease in conductivity of concrete when exposed to chloride ions present a dilemma with their high corrosive nature. On direct compressive loading, the resistivity decreased during the elastic regime, when fibers were coming in contact. The resistivity flattened out until the first crack was encountered, where it increased suddenly, further supporting the notion of self-sensing

capability in concrete. The electrical resistivity decreased with temperature and vice versa. The w/cm ratio did not affect the conductivity at high volume fractions where the carbon fibers seem to provide most of the conductivity, so moisture/humidity levels don't play a major role in controlling resistivity of cement materials; however, a w/cm ratio of 0.3 seemed to provide the least resistivity in low fiber content composites. Wen and Chung (2001c) studied the effect of carbon fibers on dielectric constant. Carbon fibers were found to be most effective in increasing dielectric constant. Wen and Chung (2004) summarized and showed the trends that different fillers and additives exhibited on the resistivity and thermoelectric power of concrete. Resistivity decreases with increasing fiber volume fraction. Carbon fiber is more effective in decreasing resistivity than carbon filament or graphite powder at large contents. Carbon filaments were found more effective in conductivity than coke powder but less inferior in EMI shielding. A material stronger in thermoelectricity or electromagnetic shielding is not necessarily stronger in conductivity. Hong and Song (2006) studied the effect of graphite slurry infiltrated with steel fibers on resistivity of fiber concrete. With a w/cm of 0.5 and 1:1 sand cement ratio, resistivity decreased with increasing graphite content and more importantly, showed less resistance magnitudes with longer steel fibers. In post-threshold zone, the resistivity decrease slowed down. With the addition of fiber, unconnected steel fibers were connected by graphite particles, forming a graphite bridge and lowering the resistivity. Vaidya (2011) attempted to impart electric conductivity in fly-ash based composite. Replacing Portland cement with fly ash proved more effective than only Portland cement in lowering resistivity with higher carbon fiber volume fractions. A fiber percentage of 0.1% is the required value to establish

electric percolation. This was attributed to the increase in alkali content in supplementary cementitious materials which contribute to higher ionic conduction.

### 2.3.2 Self-Actuating Materials

Self-actuating capability allows material to respond to what has been sensed. The structural material provides strain or stress in response to an input such as an electric field or a magnetic field. The phenomenon known as reverse piezoelectric effect or electrostriction is responsible for this behavior. Short carbon fiber reinforced cement has been observed to exhibit such behavior.

#### *Self-Sensing Cement Matrix Composites*

Self-sensing refers to the ability of a material to sense its own condition such as strain, stress, damage and temperature. Some applications of self-sensing include structural vibration control, traffic monitoring, weighing, building facility management, and structural health monitoring. Sensing is achieved by electrical resistance measurements. With temperature, thermocouples made from structural materials have been achieved. Development of cement-based materials containing short carbon fibers is opening new possibilities in the research field of multifunctional structural materials. The effects of numerous modes of loading on the piezoresistive phenomenon have been investigated including flexure, tension, compression, impact, strain amplitude and moisture.

The electrical resistance of self-sensing concrete varies with stress or strain. To measure the surface electrical resistance, the four probe method was used in which the

outer two contacts are for passing current and the inner two contacts are for voltage measurement. The two probe method give less effective results. The gage factor, the fractional change in resistance per unit strain, is up to 700 for compression or tension. The resistance increase reversibly with tension and decreases with compression, due to fiber pull-out upon micro crack opening. Chung (1997) reported concrete can contain as low as 0.2% carbon fiber content to exhibit piezoresistive capabilities. Fractional changes in longitudinal resistance during repeated uniaxial compressive loading at a series of various strain amplitudes. Resistivity at the peak of the strain varies linearly with peak strain, allowing strain sensing by resistance measurement. Gage factor for cementitious composites approaches 300, compared to a value of 2 that is typical of metal strain gages. The gage factor does however decrease with increasing strain amplitude.

Azhari and Banthia (2012) attempted to study the effects of carbon nanotubes on the piezoresistivity. The combined use of carbon nanotubes and carbon fiber gives superior sensing than the use of carbon nanotube as the sole conductive admixture. However, the high cost of carbon nanotube compared to carbon fiber is a significant disadvantage in view of the cost-conscious concrete industry. Carbon black is even less expensive than short carbon fiber, but its gives low values of the gage factor, so it is a useless material for controlling conductivity. Replacing 50% cement by carbon black maintains conductivity and electromagnetic shielding, but reduces strain sensing. Although research has emphasized cement in the form of Portland cement, sulfoaluminate cement has been shown to be an effective cement matrix for providing piezoresistivity in the presence of short carbon fibers as filler.

### *Damage Sensing*

Damage sensing has also been investigated in which damage causes some breakage of the brittle carbon fibers, resulting in an irreversible increase in resistivity. The resistivity in both stress direction and transverse direction increases upon tension, because of fiber pull-out that accompanies crack opening and decreases upon compression, as a result of fiber push in. Piezoresistivity allows the use of AC or DC electrical resistance to monitor the strain of cement-based materials. The damage can be monitored by measuring the DC electrical resistivity via a four probe method. Damage was found to increase the electrical resistivity and in the case of major damage, this resistivity increase is irreversible because the strain never returned to zero, and it was found that fiber fracture controls the damage. Various resistance measurements used throughout the field include volume resistance for measuring the damage of a volume, surface resistance for damaging the damage of a surface and contact resistance for measuring the damage of an interface.

### *Temperature Sensing*

In regards to temperature sensing, cement based materials have been developed into thermistors and thermocouples. Each thermocouple takes the form of a cement-based pn-junction. The thermoelectric effect of cement-based materials has been observed in which electricity is generated by a temperature gradient. Wang and Chung showed the thermistor effect where electrical resistivity decreases with increasing temperature. The effect is attributed to the jump of electrons from one lamina to another across the inter-laminar surface. Steel fiber was found very effective in use for heat resistance. Wen and Chung (2004) reported that carbon fibers and graphite are less effective in heat sensing

due to a higher voltage requirement and electrical resistivity. The use of steel fibers instead of carbon fibers results in highly positive thermoelectric power values as steel fibers provide electron conduction whereas carbon fibers involve hole conduction. Steel fibers were found to give a better thermoelectric material than carbon fiber. The thermoelectric effect is the bases for thermocouples for temperature measurement. The resistivity decreases upon heating and the effect is quite reversible upon cooling. That the resistivity is slightly increased after a heating and cooling cycle is probably due to thermal degradation of the material. Chung (2004) found that a cement–matrix composite containing 0.7 vol% steel fibers (8 μm diameter) and a mat of discontinuous uncoated carbon fibers for use as an interlayer are effective for self-heating. However, the effectiveness is low compared to flexible graphite, which is not a structural material.

***Electromagnetic Shielding***

Mainly due to their high reflectivity, carbon materials are effective for shielding too. The EMI shielding effectiveness of flexible graphite (made by the compression of exfoliated graphite in the absence of a binder) reaches 130 dB (at 1 GHz) which is higher than or comparable to all EMI shielding materials, including carbon and non-carbon materials. The high effectiveness of flexible graphite is due to the high electrical conductivity and high surface area, which is valuable due to the skin effect. Flexible graphite has the additional advantages of resiliency (needed for EMI gaskets, which are particularly challenging due to the requirement of resiliency), low density, low thermal expansion, thermal conductivity (which helps microelectronic heat dissipation), and chemical resistance.

### *Percolation Theory*

The percolation theory describes the behavior of concrete reinforced with conductive carbon fibers. The conductivity changes significantly at a critical fiber content, which is found to be independent of the matrix. This refers to the volume fraction above which the fibers touch one another to form a continuous electrical path. Longer fibers were found to decrease the threshold where the threshold is between 0.5 to 1.0% fiber volume fractions. Wen and Chung (2007b) observed double percolation in cement-based composites where one percolation threshold was attributed to the fiber percolation and the other to cement percolation. Triple percolation was also observed by Alicante and Chung.

# 3. CONDUCTIVITY CONTROL OF ASPHALT CONCRETE USING CONDUCTIVE FILLERS[*]

## 3.1 Introduction

Asphalt concrete is a composite material that is heavily used in the construction of highway, runways and parking lots. Riding comfort, durability, reliability, and water resistance are some of the driving mechanical characteristics making it the most preferred choice in the pavement industry. With the increasing emphasis on the long term well-being of individuals and environmental conservation, sustainability is becoming a key goal in planning and constructing civil infrastructures.

Multifunctional materials have the simultaneous ability to exhibit non-structural functions apart from their regular structural functions (Gibson 2010). Mechanical properties such as strength and stiffness are the primary functions of structural materials. However, by manipulating electrical, magnetic, optical, and other non-structural properties, the material can exhibit advantages beyond the sum of the individual capabilities. Materials of this kind have tremendous potential for a wide range of real-life applications that can improve the efficiency and safety of daily lives. Asphalt concrete, by nature, is a non-conductive composite material, but its electrical conductivity can be improved by using conductive additives. Various non-structural applications can be developed by controlling the conductivity, and the multifunctional asphalt concrete has

[*] Reprinted with permission from "Electrical and mechanical properties of asphaltic composites containing carbon based fillers" by Younho Rew, Aishwarya Baranikumar, Albert V. Taashausky, Sherif El-Tawil, and Philip Park, 2017, Construction and Building Materials, vol. 135, pp394-404, Copyright 2017 by ELSEVIER.

strong potential that can lead to a breakthrough in sustainable pavement systems. The concept of electrically conductive asphalt concrete was initiated by Minsk in 1968, and this topic has gained immense interest in the last decade resulting in an increased number of publications. These efforts have largely been motivated by the potential benefits of utilizing electrical properties of asphalt composites. For instance, the electrical heating applications of conductive pavements have been studied to remove snow and ice (Xiangyang and Yuxing 2010). The electric heating is also expected to promote self-healing by reducing the rest period. In addition, piezoresistivity of conductive asphalt, which refers to change in electrical resistivity with applied mechanical pressure, can be used for self-sensing of strain (Liu and Wu 2009). Self-sensing of damage for evaluating pavement distress is possible if the relationship between the electrical property and internal damage is provided. Moreover, some conductive additives may improve the durability of asphalt concrete, thereby increasing the service life of the pavement systems (Park 2012).

Figure 8 shows the possible non-structural functions and their benefits of the conductive asphalt concrete, and Figure 9 summarizes the components of the high-performance conductive asphalt concrete.

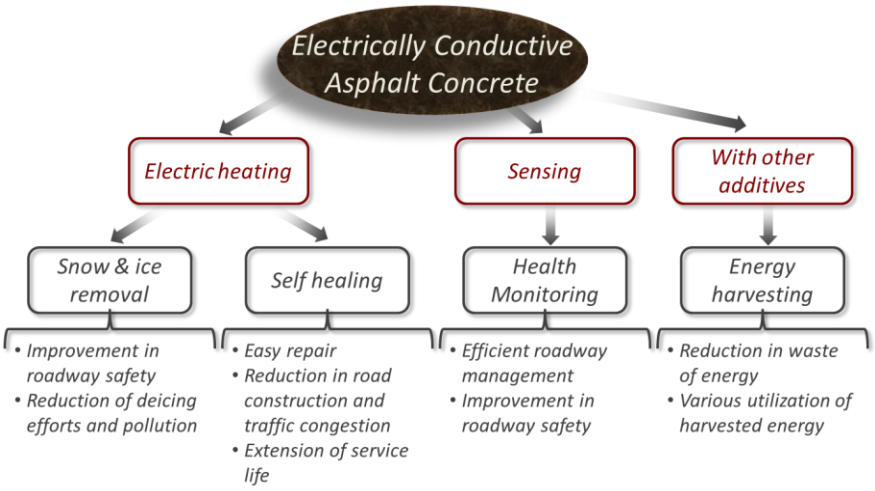


**Figure 8. Possible applications and benefits of electrically conductive asphalt concrete**

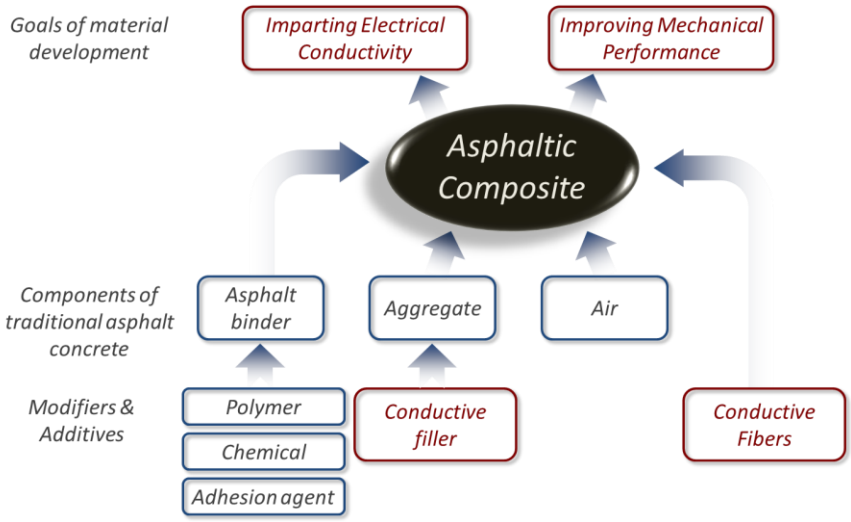


**Figure 9. Components of high-performance conductive asphalt concrete.**

In order to utilize the full spectrum of applications of electrically conductive asphalt composites, a precise control of the volume resistivity is needed. Previous investigators have tested various conductive fillers and fibers including micro-steel fibers (Huang et al. 2006; Serin et al. 2012), carbon fibers (Wu et al. 2005), steel wool (Garcia et al. 2009), carbon black (Wu et al. 2005), and graphite powder (Wu et al. 2005; Garcia et al. 2009) to impart electrical conductivity into asphalt concrete. Most of the previous investigators selected the fiber type additives as their primary conductive additives rather than powder types because relatively smaller amount of fibers are needed to improve conductivity than graphite or carbon black (Huang et al. 2006). Fibers have larger lengths, which can facilitate the flow of electrons easier than powder type additives. On the other hand, the asphalt concrete containing conductive fibers has a phenomenon called percolation threshold, which hinders the precise control of the electrical conductivity.

Percolation threshold is a sudden transition from the insulated to the conductive phase (Wu et al. 2005; Garcia et al. 2009). The dotted line in Figure 10 shows a typical relationship between the electrical resistivity and the content of conductive additive reported from the previous investigators. The transition between insulated phase and conductive phase can be characterized by a sudden drop in electrical resistivity at a specific content of conductive additive, the percolation threshold. According to Huang et al. (2006), the electrical conductivity of the asphalt composite comes from the formation of continuous conductive path through the contacts between the conductive additives. By narrowing the adjustable volume resistivity range of conductive asphalt, the percolation threshold introduces limitations for developing various multifunctional applications. To

enable precise manipulation of electrical resistivity over a wide range, a gradual resistance change with increase of conductive additive is favorable as illustrated to be a solid line in Figure 10. Another limitation in using discrete fiber type additives is the dispersion and clumping of fibers during mixing (Abtahi et al. 2010). It is known that the clumping of discrete fibers becoming severe as the increase of the fiber length to thickness ratio, which is called aspect ratio.

Graphite is one of the powder type conductive additives used as a supplementary material by some investigators (Huang et al. 2006; Garcia et al. 2009; Liu and Wu 2011b). While the percolation threshold is prevalent with fiber type conductive additives, the use of graphite powder ensures relatively easy mixing and uniform dispersion. More importantly, the percolation threshold might be mitigated by using graphite powder even though larger quantities of graphite rather than conductive fibers are needed to reduce the electrical resistivity (Huang et al. 2009; Mo et al. 2005). On the other hand, the efficiency of graphite in imparting conductivity is not consistent in the previous publications. According to Park (2012), this is due to the use of different types of graphite, but no other investigators has not focused on the effect of graphite types including shape, size, and origin of the graphite powders. Motivated by this observation, this study investigated the effect of various graphite types on imparting conductivity, and identified the most efficient graphite type that ensures the smooth resistivity transition.

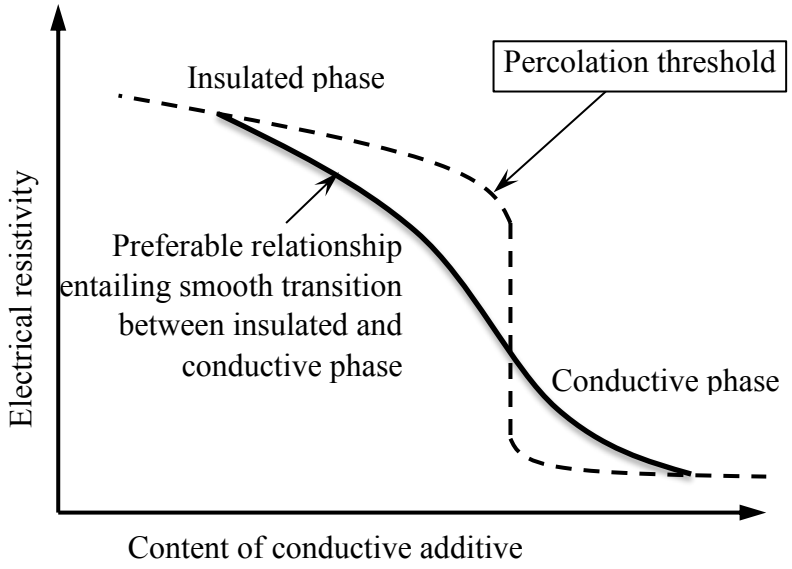


**Figure 10. Electrical resistivity transition curve**

## 3.2 Preliminary Research

### 3.2.1 Characterizations of Raw Materials

This section introduces physical properties of the materials used in the previous research (Baranikumar 2013). The properties of graphite including density, particle size, and surface area play a major role in deciding the electrical resistivity, mixing, and compaction difficulties of the conductive asphalt concrete. Scanning electron microscope images of the graphite provide an explanation on the observed conductivity variation with the graphite types. In addition, the physical properties of other materials used in this research, such as aggregate, binders, fillers, wood stick, silver paste, and copper tapes are investigated.

*Types of Graphite*

Eight different types of graphite and a carbon black produced from Asbury Carbons Inc. were selected to study their effect on imparting conductivity into asphalt concrete. Graphite has two-dimensional hexagonal crystal structure, and hence, the ideal shape of graphite particles is hexagonal plate. However, the shape and size of the particles vary with the source and manufacturing process. The graphite types are classified into three flake types (F146, F516 and F3204), two amorphous types (505 and 508), one artificial type (A99), and two types with ultra-high surface area (SA4827 and TC307). Although the graphite 505 and 508 is called amorphous type because of the particle shape, they are crystalline materials. On the other hand, carbon black is a genuine amorphous material, which does not have a long range order in their atomic structure. The properties of these graphite and carbon black are presented in Table 2.

*Scanning Electron Microscope Analysis*

SEM images of the graphite powders were taken to investigate the shape of the graphite particles.

Figure 11 (a)-(i) shows the SEM images of the nine conductive powders. The magnification scale was 2000 for all images. As shown in Figure 11 (a), (b), and (c), the flake graphite particles have thin plate shapes. On the other hand, the amorphous and artificial graphite types have irregular shapes as seen in the other figures. It is known that the graphite has super conductivity along the flat surface while the conductivity through the plate is significantly lower, and hence, the difference in the particle shapes may lead difference in conductivity. Particle size and shape can affect mixture properties. For

instance, particle size of TC307 is small resulting in very high surface area (352 $m^2/g$). This implies that TC307 will require more binder to coat its surface than other graphite.

**Table 2**. **Properties of graphite used for the research (Asbury Carbons Inc.)**

| Asbury ID | % Carbon | Typical Size (μm) | True Density | Surface area ($m_2/g$) | Typical Resistivity (Ω·cm) | TL Price ($/lb) | Note |
|---|---|---|---|---|---|---|---|
| F146 | 96.86 | 20 (< 44) | 2.25 | 6.35 | 0.03-0.05 | $1.27 | Flake type |
| F3204 | 97.05 | 15 (< 44) | 2.25 | 7.41 | 0.03-0.05 | $1.18 | Flake type |
| F516 | 95.45 | - (< 212) | 2.26 | 5.0 | 0.03-0.05 | $1.66 | Flake type |
| 505 | 84.50 | 35 (< 75) | 2.30 | 22 | 0.13 | $0.55 | Amorphous type |
| 508 | 81.77 | 20 (97%< 44) | 2.30 | 21 | 0.13 | $0.59 | Amorphous type |
| A99 | 99.68 | 20 | 2.23 | 8.47 | 0.047 | $1.01 | Artificial type |
| SA4827 | 99.66 | <1 um | 2.20 | 248.92 | 0.184 | $4.15 | Artificial Graphite nanoplatelet |
| TC307 | 99.92 | < 1 um | 2.20 | 352 | 0.289 | $4.58 | Artificial Graphite nanoplatelet |
| CB5303 | 99.90 | 0.03 | 1.8 | 254 | 0.341 | $7.87 | Carbon black |

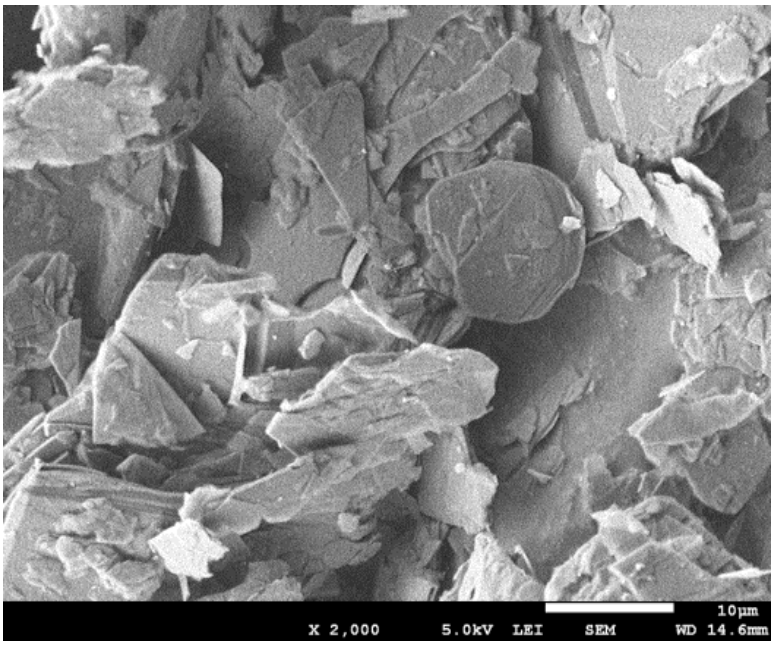


(a) Flake Graphite F146

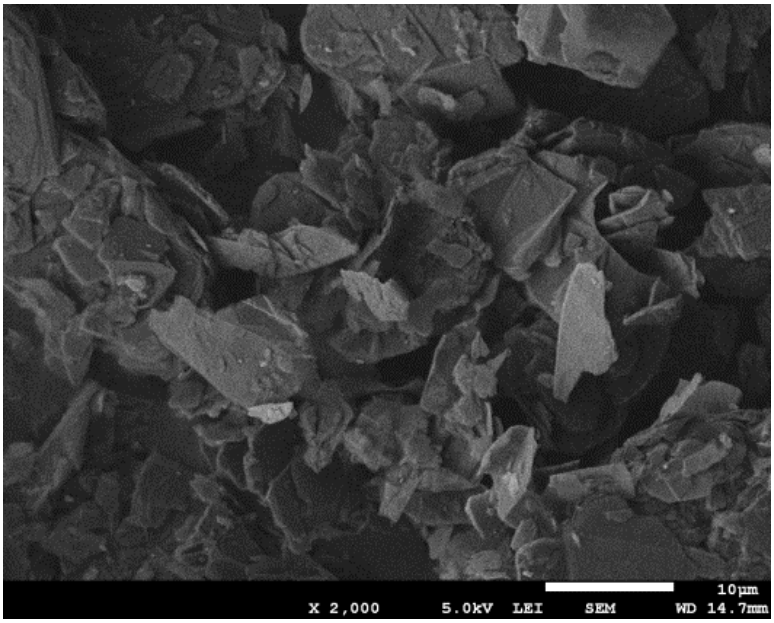


(b) Flake Graphite F3204

**Figure 11. SEM images of graphite powders**

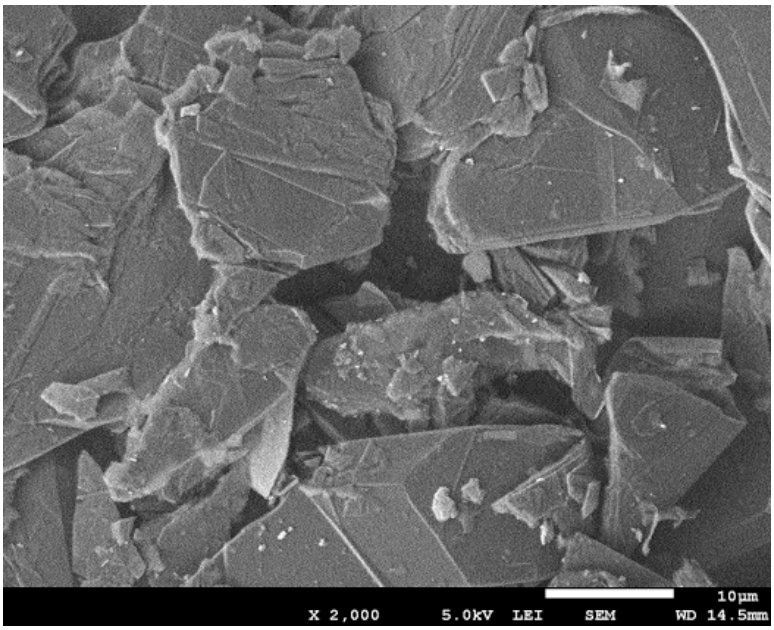


(c) Flake Graphite F516

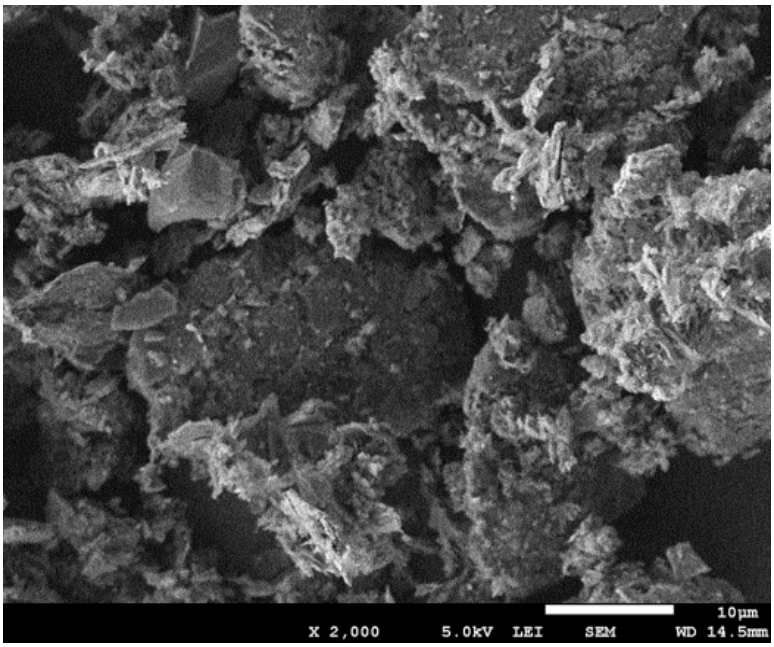


(d) Amorphous Graphite 505

**Figure 11. Continued**

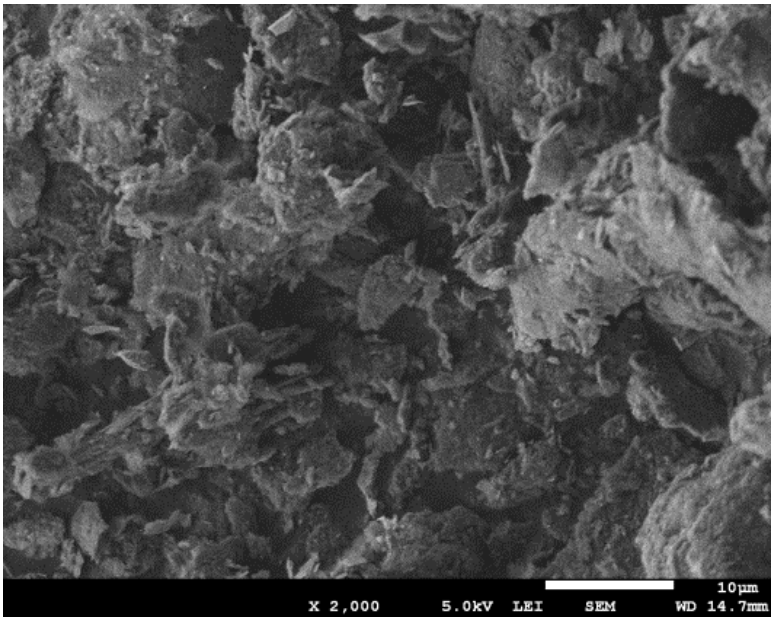


(e) Amorphous Graphite 508

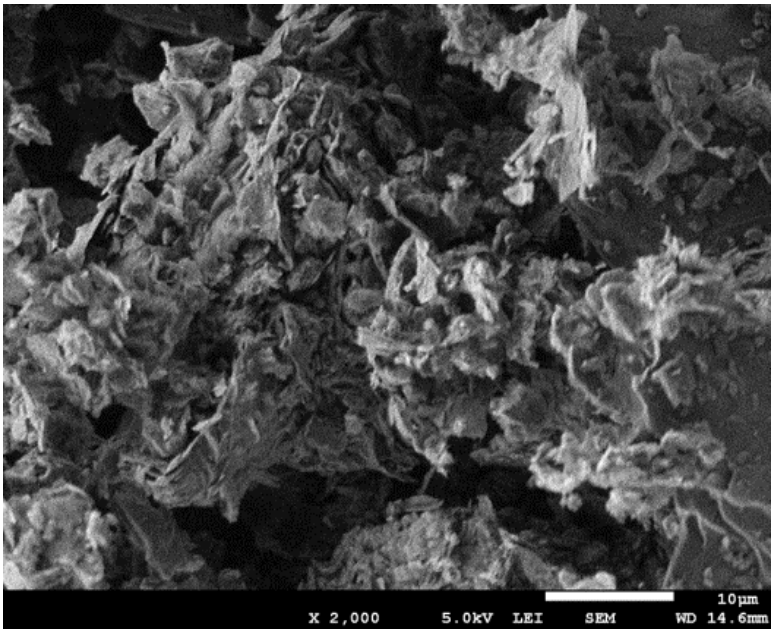


(f) Artificial Graphite A99

**Figure 11. Continued**

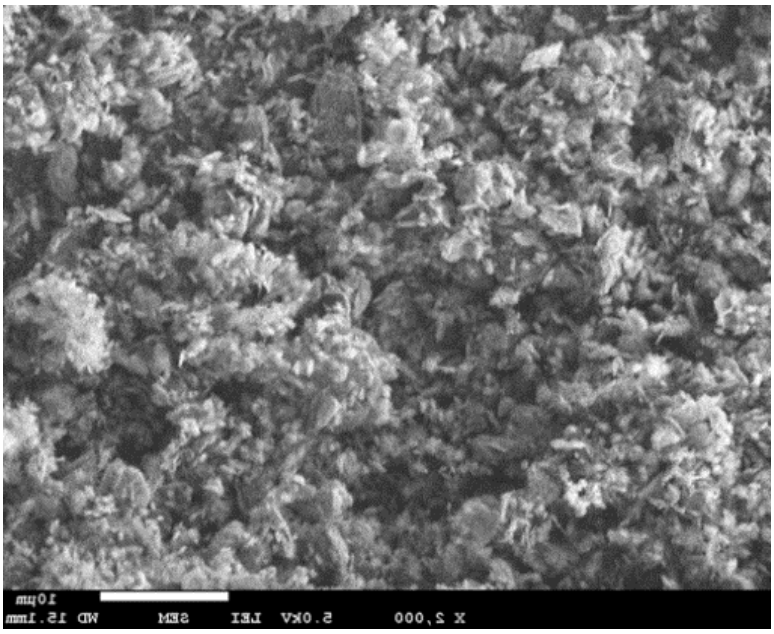

(g) Ultra-High Surface area Graphite SA4827

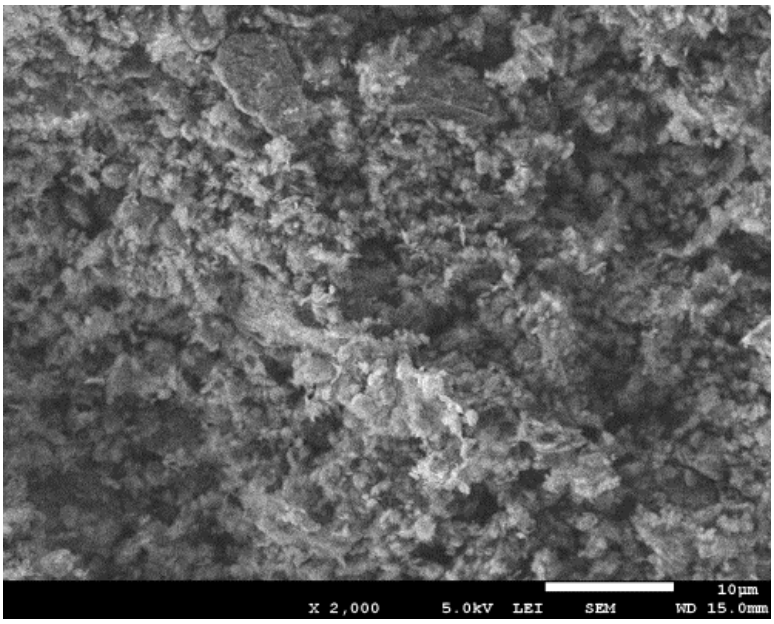


(h) High-Surface area Graphite TC307

**Figure 11. Continued**

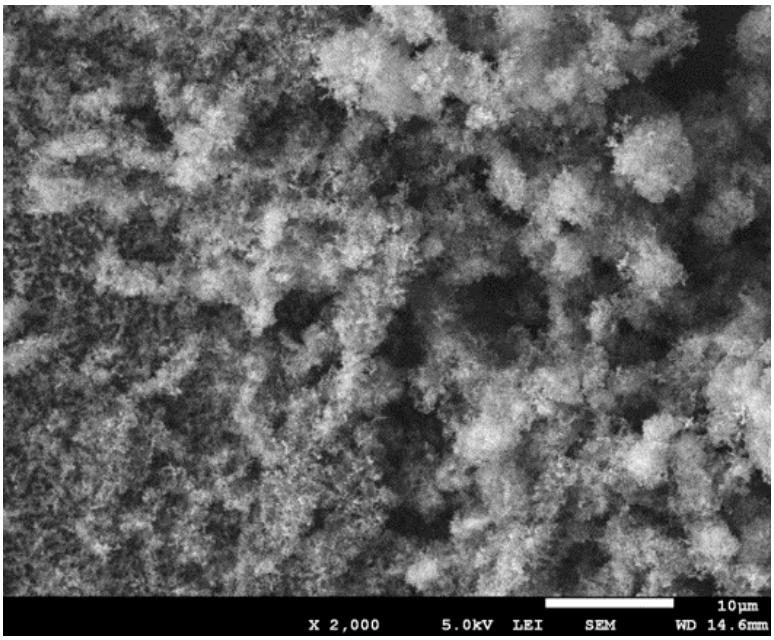


(i) Carbon Back CB5303

**Figure 11. Continued**

*Physical Properties of Other Materials*

Several materials were used for the experiment, and their properties are investigated. For fixing asphalt mastic specimens in a thin film form, wood sticks were used as a non-conductive base. The electrical volume resistivity of pine wood ranges from $10^{14}$ to $10^{16}$ ($\Omega \cdot m$), and varies with the moisture content. The wood base were heated in the oven for 24 hours to remove moisture. Asphalt concrete is a mixture of coarse aggregate, fine aggregate, filler, and binder. In this study, the conductive additives are considered to replace traditional fillers to minimize the effect on the skeleton structure of asphalt concrete. As the traditional filler for manufacturing the control specimens, Type II Portland cement was used. Silver paste and copper tape were used as the electrodes for measuring the electrical resistivity.

Three different performance grade binders: PG70-22, PG64-22, and PG58-22 were selected to investigate the effects of binder grade on electrical resistivity. The three performance grade binders used are: 70-22, 64-22, and 58-22 grades. PG 64-22 and PG 58-22 are produced from the different crude oils, while PG 70-22 is a modified binder of PG 64-22. The modifiers used for PG 70-22 are 2% SBS and 0.5% sulfur. Table 3 lists the physical properties of the materials used in the research.

**Table 3. Materials used for the research**

| Material | Typical Size | Density | Thermal Conductivity (W/mK) | Electrical Resistivity (Ω·m) | Note |
|---|---|---|---|---|---|
| Coarse Aggregate | 4.75mm-25mm | Specific Gravity 2.57 g/cc | 1.25-1.75 | $10^9$ | |
| Fine Aggregate | 0.075mm-4.75mm | Specific Gravity 2.63 g/cc | 1.25-1.75 | $10^9$ | |
| Fillers | <0.075mm | Specific Gravity 3.15 g/cc | 0.29 | $10^9$ | Type 2 Portland Cement |
| Binder | Liquid | 1.032 g/cm$^3$ | | | Jebro, INC. PG70, 64, 58-22 |
| Wood Stick | 1”x2”x8’ | 400-420 kg/m$^3$ | 0.12 | $10^{14}$-$10^{16}$ | Radiata Pine Claymark, INC. |
| Silver paste | Particle size: 0.4-1.0μm | Specific Gravity 2.25g/cc$^3$ | - | Sheet Resistance 0.02 - 0.05 ohms/sq/mil (25μm) | Ted Pella, INC. |
| Copper tapes | W: 6.3mm L: 16.46m T: 2.4 mils (66μm) | 8.94 kg/cm$^3$ | - | Sheet Resistance (ohms/sq): 0.001 | Ted Pella, INC. |

### 3.2.2 Electrical Conductivity of Asphalt Mastic

Steel wool, steel fibers, carbon fibers, and some anonymous types of graphite have been used as the conductive additives to impart conductivity. Among those additives, the graphite showed the possibility for precise conductivity control – gradual drop in resistivity with increasing graphite contents. The previous study focused on the effect of various types of graphite on controlling conductivity of asphalt composites. In this section, the test procedure, specimen preparation, and their test results for asphalt mastic were presented. In addition, mixing difficulties observed in certain graphite types were discussed.

*Materials and Experiment*

The asphalt mastic specimens were prepared using PG70-22 asphalt binder (ASTM 2007a) and various combinations of conductive and non-conductive fillers. The density of binder is 1.032 g/cm$^3$.

The asphalt mastics are composed of 50% asphalt binder and 50% filler by weight. This proportion was kept constant throughout the experiment. Type II Portland cement was used as the non-conductive traditional filler. Graphite or carbon black, replace part of cement filler in the mastic specimens ranged from 10% to 50% by weight of the mastic. For example, when the graphite content is 20%, cement content is 30% to maintain the 50% of filler content in the mastic.

The mastic specimens were prepared in thin film shape as shown in Figure 12 (a). Dry pine wood was used as a base for spreading asphalt mastic. The wooden base blocks

were coated with heat resistant epoxy to prevent the absorption of asphalt binder. The wood, binder, and filler were conditioned at 150 ºC for 2 hours in the oven before mixing. Once the materials were heated, the binder and filler (combination of cement and graphite with various proportions) were mixed manually by hand for 3-5 minutes to ensure uniform and complete dispersion of the filler in the mastic. The mastic was then spread on the epoxy-coated wooden blocks. The average thickness of mastic was measured by reading the weight of the wooden block before and after spreading the mastic. Once the weight of mastic on the wooden block was found, it was divided by the density of mastic and the spread area to obtain its average thickness. The density of the mastic was estimated using the individual densities of the binder, cement, and graphite and their respective weight proportions in the mastic. For each type and content of graphite, three mastic specimens were prepared to improve reliability of the results.

The mastic specimens were conditioned at room temperature for 8 hours before testing. Copper tapes were installed at every 50 mm distance and were used as electrodes (Figure 12 (a)). Silver paste was painted between the mastic and copper tapes to ensure full contact between them. Two-point sensing method was used to measure impedance of the mastic specimens. The copper tapes at various locations on the specimen enabled to select different combinations of electrodes, i.e., distance between electrodes can be 50 mm, 100 mm, or 200 mm, to observe the impedance change with distance.

Solartron 1260A and 1296 (Impedance/Gain Phase Analyzer, Figure 12 (b)) were used to measure the resistance of the specimens. Solartron 1260A can measure resistance only up to 100 MΩ. To extend the measurable range up to 100 TΩ, Solartron 1296 was

combined with 1260A. Electrical impedances of the specimens were measured at 0.1V with AC frequency sweep ranged from 0.01 Hz to 1000 Hz. Once the resistances were obtained, the volume resistivity was calculated using the equation (1) below:

$$\rho = R\frac{A}{L} \tag{1}$$

Where, ρ is the volume resistivity measured in Ω-cm; $R$ is the resistance in Ω obtained from the experiment; $A$ is the cross-sectional area of the mastic in $cm^2$; and $L$ is the distance between the electrodes in cm. The electric field is assumed to be constant and the end effect is assumed to be negligible.

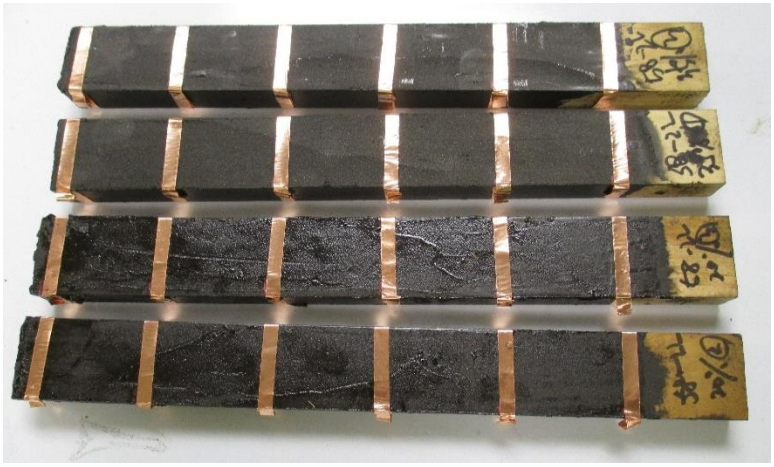

(a) Mastic specimens

(b) Resistivity measurement set-up: Solartron 1296 & 1260A

**Figure 12. Experimental set-up for measuring electrical property**

*Result- Effect of Graphite Types on Electrical Conductivity*

Figure 13 from (a) to (i) compare the variations of electrical resistivities with the contents of conductive additives for the eight different graphite types and carbon black. Approximately 24 readings were obtained for each mastic specimen. It is clear from the figure that the mastic resistance varies with the types of graphite. The specimens with the flake type graphite: F516, F3204, and F146, display the lowest conductivity, whereas the mastics with amorphous graphite: 505 and 508, still remain non-conductive at 40% content. These results can be compared with the particle shape of graphite observed from the SEM analysis. The thin plate shape of the flake type graphite particles is similar to the ideal crystal structure of graphite, and allows super-conductivity along with the flat surface. On the other hand, the irregular shapes of the amorphous graphite particles seem to work as a barrier against the flow of electrons, leading to poor conductivity. These graphs demonstrate the importance of selecting the proper type of graphite for imparting conductivity.

As shown in Figure 13 (a) - (c), the resistance gradually decreases with the increase of the graphite contents. A relatively rapid drop in resistivity exists between 13-16% (F146 and F3204) or 10-13% (F516) by the mastic volume, and after that point, the resistivity drops gradually from $10^5$ Ω·cm and reaches the resistivity about $10^2$ Ω·cm. This implies that the electrical resistivity can be controlled within the range of $10^2 – 10^5$ Ω·cm, and sufficiently low conductivity ($10^{-2}$ /Ω·cm) can be obtained only by using graphite.

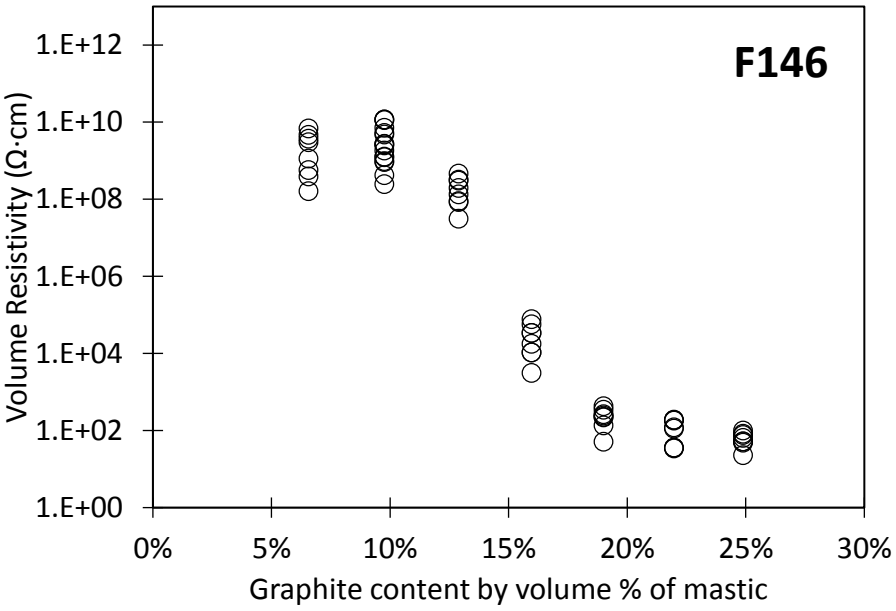


(a) Flake Graphite F146

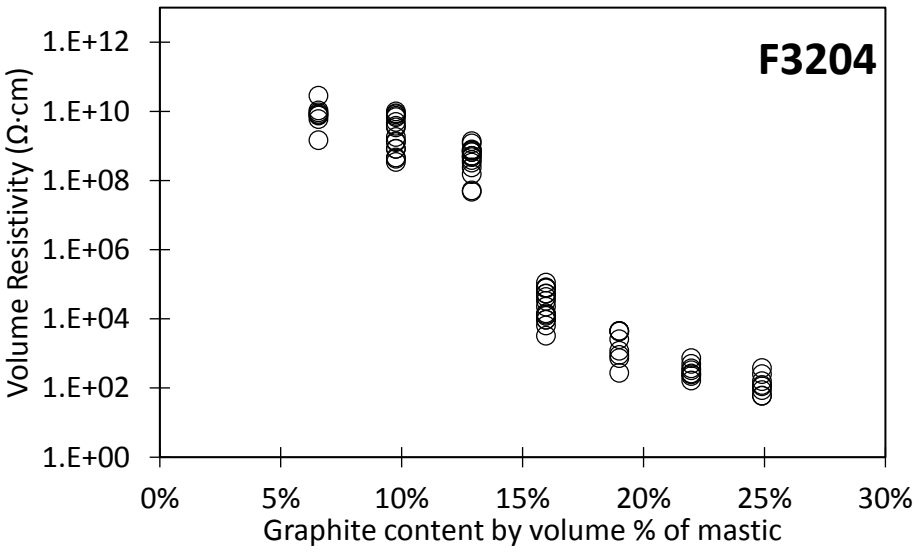


(b) Flake Graphite F3204

**Figure 13. Electrical resistivity of asphalt mastics containing various graphite types**

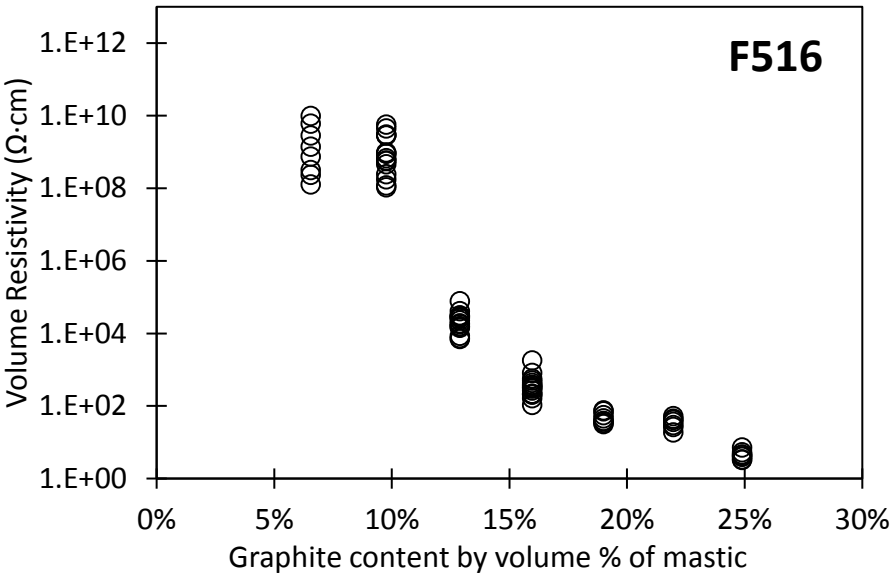


(c) Flake Graphite F516

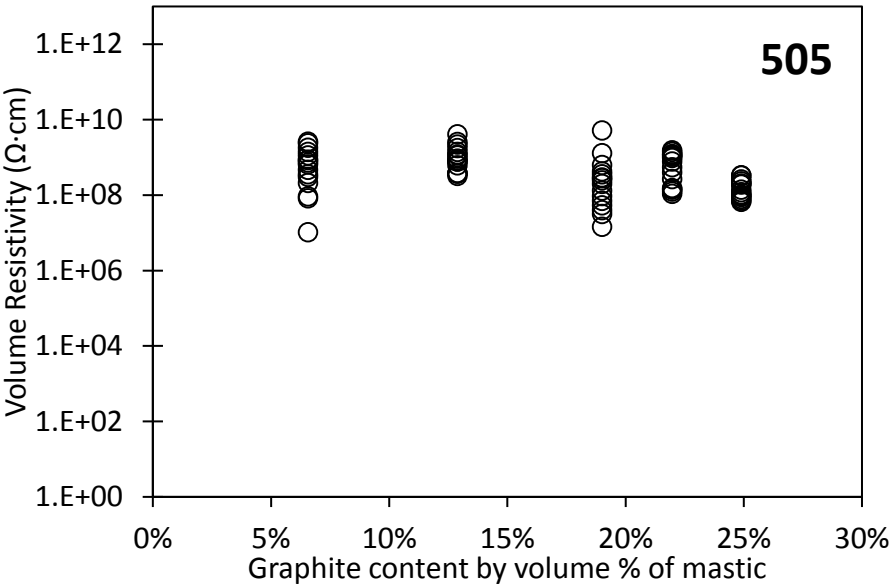


(d) Amorphous Graphite 505

**Figure 13. Continued**

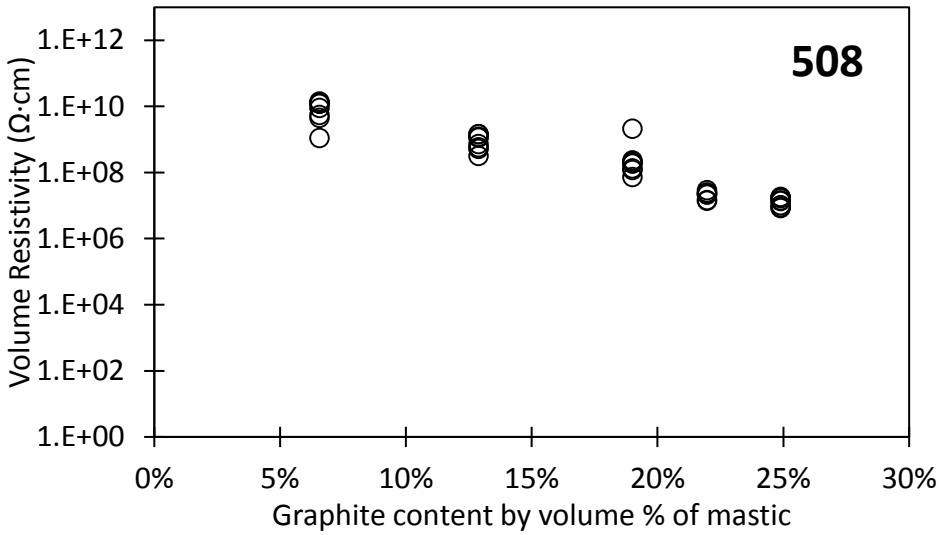


(e) Amorphous Graphite 508

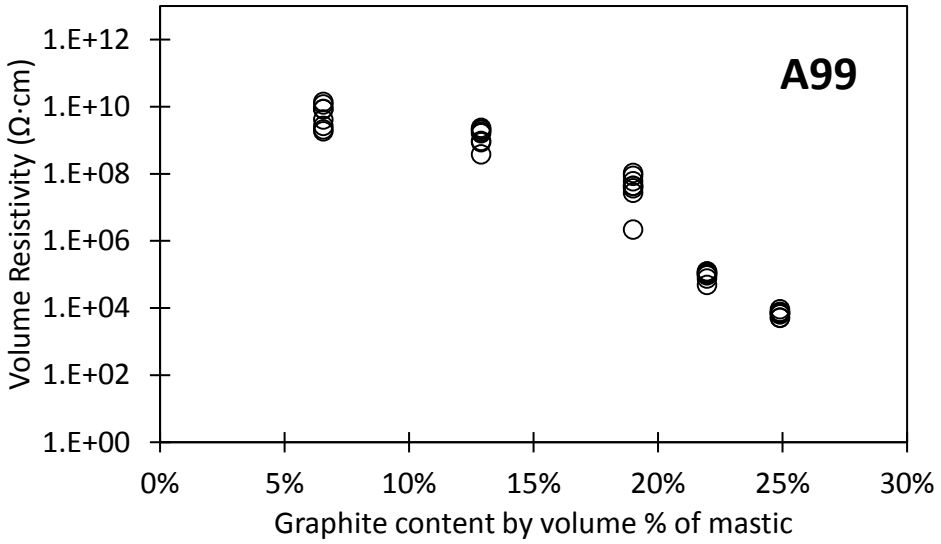


(f) Artificial Graphite A99

**Figure 13. Continued**

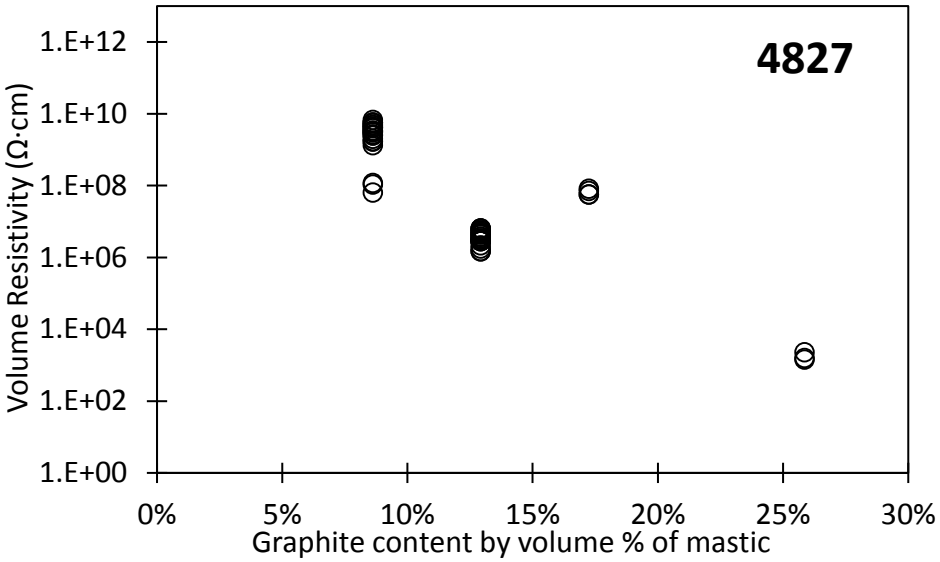


(g) Ultra-High Surface area Graphite SA4827

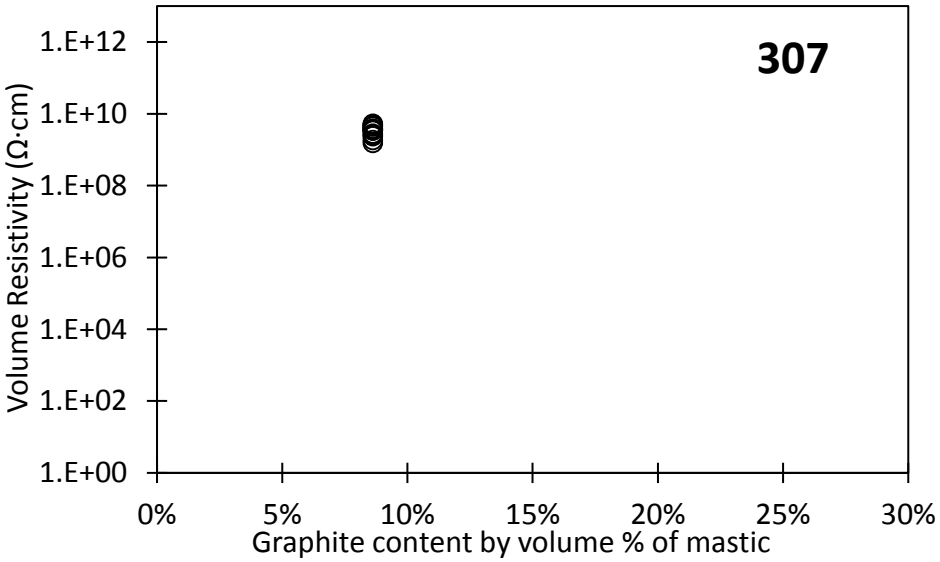


(h) High-Surface area Graphite TC307

**Figure 13. Continued**

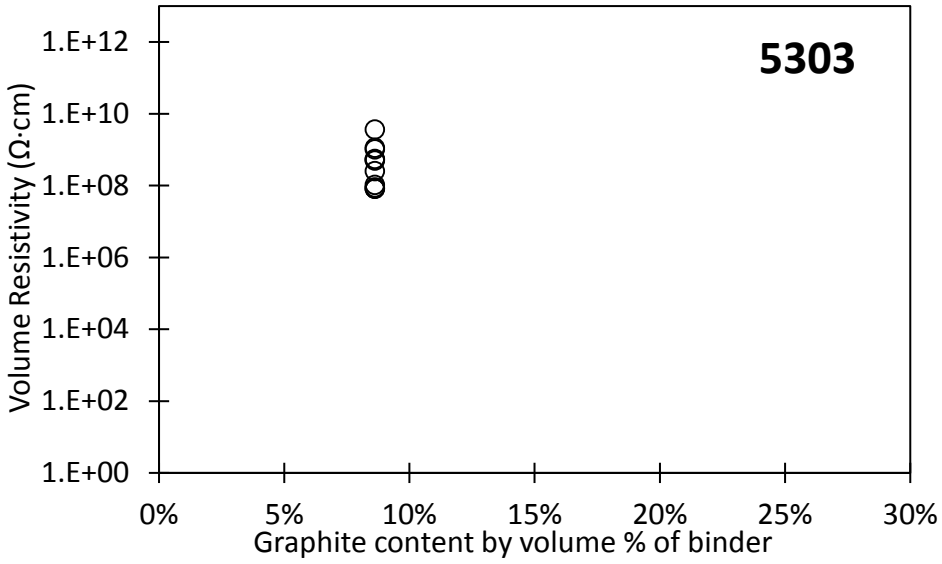


(i) Carbon Back 5303

**Figure 13. Continued**

## 3.3 Experimental Method

### 3.3.1 Specimen Preparations

*Asphalt Concrete Specimens*

Asphalt concrete is a mixture of coarse aggregate, fine aggregate, filler, and binder. Based on the asphalt mastic test results that will be discussed later, the natural flake graphite F146 and F516 are selected for fabricating cylindrical asphalt concrete specimens. The asphalt concrete specimens were prepared in accordance with the Superpave mixture design method using a PG70-22 asphalt binder (density 1.032 g/cc). The specific gravities of coarse aggregate, fine aggregate, and traditional filler were measured as 2.57 g/cc, 2.63 g/cc, and 3.15 g/cc, respectively. D6 mixture with 12.5 mm of maximum aggregate size was selected, and the proportion of coarse and fine aggregates was determined to satisfy mixture requirements specified in ASTM D3515 (2001).

The aggregate gradation used in this study are shown in Table 4. The optimum binder content for the mixture was 5.3% by weight of the total mixture by the Superpave method. The variation of the mixture conductivity with graphite content was investigated.

**Table 4. Aggregate gradation**

| Sieve size (mm) | 37.5 | 25 | 19 | 12.5 | 9.5 | 4.75 | 2.36 | 1.18 | 0.6 | 0.3 | 0.15 | 0.075 |
|---|---|---|---|---|---|---|---|---|---|---|---|---|
| D-6 % passing | 100 | 100 | 100 | 99.9 | 95.3 | 68.1 | 50.8 | 35.3 | 21.0 | 11.5 | 7.2 | 6.1 |

The aggregates and fillers were heated at 150 ºC for at least 24 hours to eliminate moisture, and the binder was heated for 2 hours at the same temperature prior to mixing. The heated filler and aggregates were mixed first, and then the binder was added. A mechanical mixer was used to mix the materials until the aggregates and fillers were well coated with the binder. The mixture was then conditioned in the oven at the compaction temperature (135 ºC).

A Superpave gyratory compactor was employed to compact the specimens. Cylindrical specimens with a 150 mm diameter and 95 mm height were compacted by gyration until the 4% percent air void was reached. For each test case, four cylindrical specimens were prepared: three for measuring indirect tensile strength and one for measuring the electrical conductivity. The specimen for electrical conductivity was drilled to make three core samples out of it. The rough top and bottom surface of the specimen were cut to make a smooth surface. This cutting eliminates the error in the conductivity measurement by removing the conductive mastic at the sides of the specimens. As shown in Figure 14, copper tapes were installed as electrodes at the top and bottom of the core-cut specimens. A highly conductive silver paste was applied on the top and bottom surfaces of the specimen to maintain full contact between the specimen and copper tape.

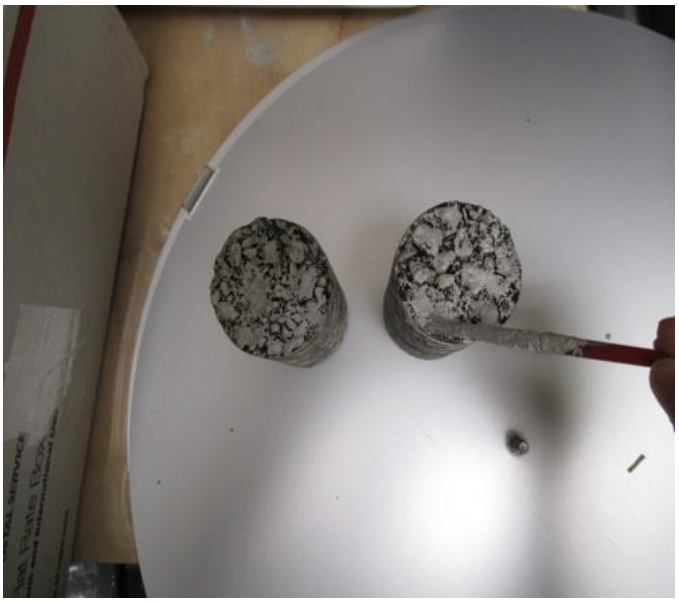

(a) Painting silver paste on top and bottom surfaces of specimens

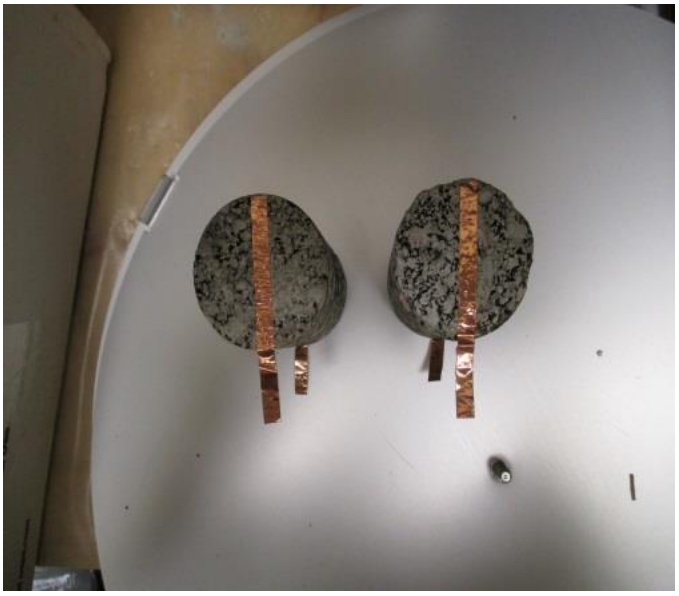

(b) Installing copper tapes as electrodes

**Figure 14. Asphalt concrete specimens**

## 3.4 Measurement Set-up

### 3.4.1 Viscoelastic Properties of Asphalt Mastic

A direct shear rheometer (DSR, Figure 15) is used to obtain the rheological parameters of the mastics at intermediate and high temperatures. The tests are conducted in accordance with ASSHTO T315, and complex shear modulus (|G*|) and phase angle of binder (δ) are obtained. |G*| represent stiffness of a binder that include contribution of elastic property and viscous property of an asphalt. δ represent contribution elastic property to viscous property. The more value of δ indicates that asphalt behave like a viscous liquid. In DSR test, asphalt specimen is placed between two plates as shown in Figure 15 (a). The bottom plate is fixed while the top one is oscillating with a frequency of 10 radians per second. The diameter of the mastic sample is 25 mm.

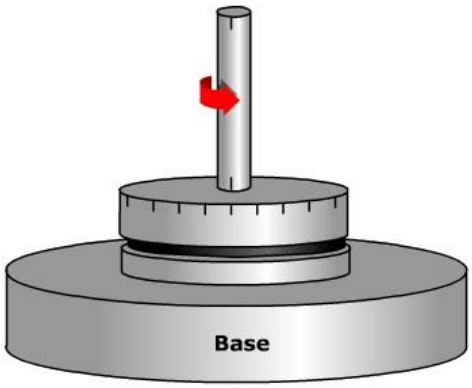


(a) DSR plates


(b) DSR test equipment

**Figure 15. Experimental set-up for measuring viscoelastic property**

### 3.4.2 Electrical Resistivity of Asphalt Concrete

As explained in Chapter 3.2.1, Copper tapes were installed as electrodes at the top and bottom of the core-cut specimens. The rough top and bottom surface of the specimen were cut. A highly conductive silver paste was applied on the specimen surface to maintain the full contact between the specimen and copper tape. Solartron 1260A and 1296 (Impedance/Gain Phase Analyzer, Figure 12) were used to measure the resistance of the specimens. The measured resistance was then converted to volume resistivity corresponding to the dimensions of the specimen. The specimens and measurement set-up are shown in Figure 12 and Figure 14.

### 3.4.3 Indirect Tensile Strength of Asphalt Concrete

Indirect tensile strengths were measured to investigate the effects of adding graphite on the mechanical properties of the conductive asphalt concrete. For each case, three compacted specimens were conditioned at room temperature (25 ºC) before testing. An electromechanical materials testing system, Instron 5583, was used for performing the indirect tension (IDT) test. During the IDT test, a monotonic compressive load was applied on the specimen at a constant displacement rate of 50.8 mm/min (2 inch/min) until fracture. The load and displacement were recorded. The IDT strength was computed as follows:

$$S_T = \frac{2 \text{ x } P}{\pi \text{ x } t \text{ x } D} \quad (2)$$

Where, S is the IDT strength in MPa, P is the maximum load in N, t is the specimen height immediately before test in mm, and D is the specimen diameter in mm. The test

was performed in accordance with ASTM D6931 (2007). The IDT test set-up and the fractured specimen are shown in Figure 16.

**Figure 16. Indirect tension test set-up**

## 3.5 Results and Discussions

### 3.5.1 DSR Test

The complex shear modulus (|G*|) and phase angle (δ) of the mastics are measured by the DSR test. The mastics containing the traditional filler (cement) and F516 graphite with various proportions are tested at three different temperatures (64, 70, and 76 °C).

As shown in Figure 17, the complex modulus (|G*|) increases as the graphite content increases. On the other hand, of the phase angle (δ) of the mastic does not affected significantly as |G*| does. δ drops slightly at high graphite contents (22-25 % by volume, Figure 18). Correspondingly, |G*| · Sinδ (Figure 19) and |G*| / Sinδ (Figure 20) showed the similar trend with Figure 17. This implies that the graphite can improve rutting resistance, but may reduce fatigue resistance.

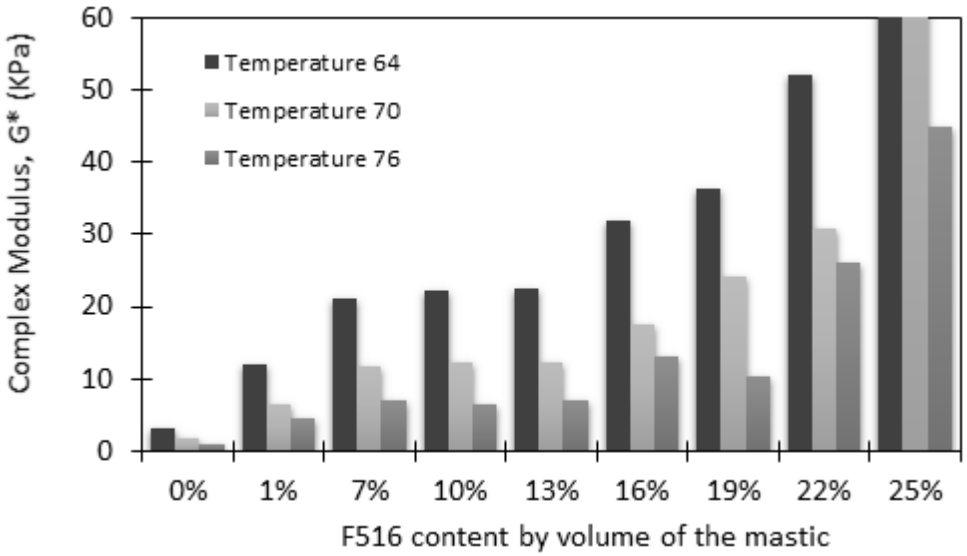


**Figure 17. Variation of complex modulus with graphite contents**

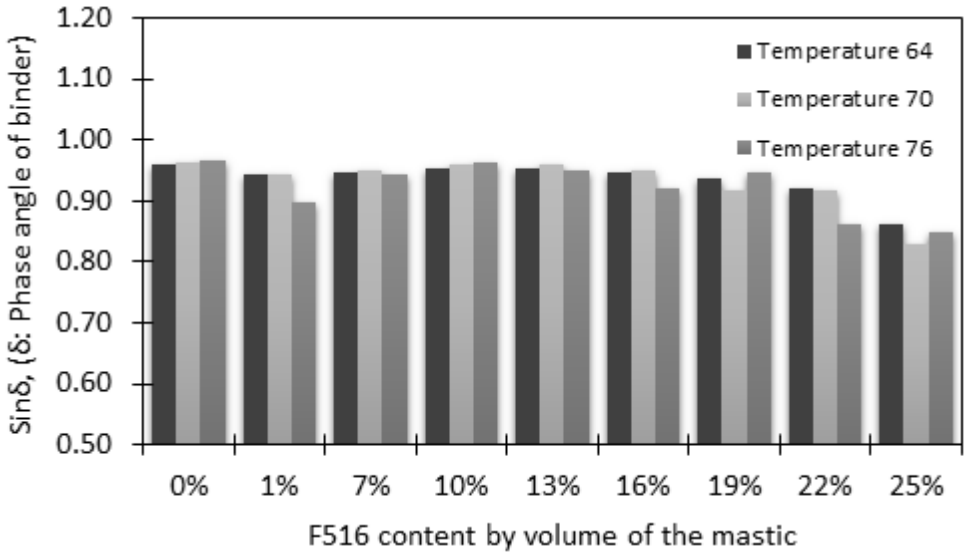


**Figure 18. Variation of phase angle with graphite contents**

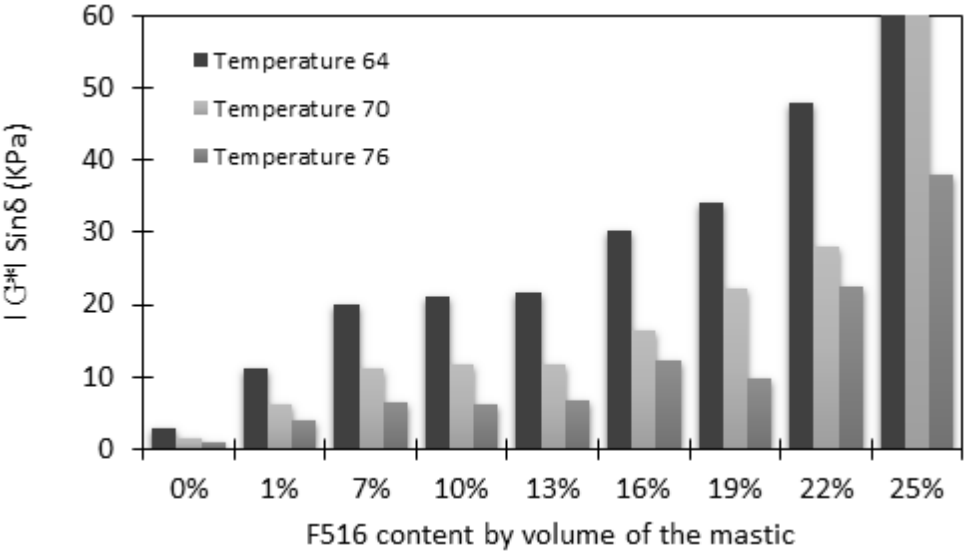


**Figure 19. Variation of |G*| · sinδ (KPa) with graphite contents**

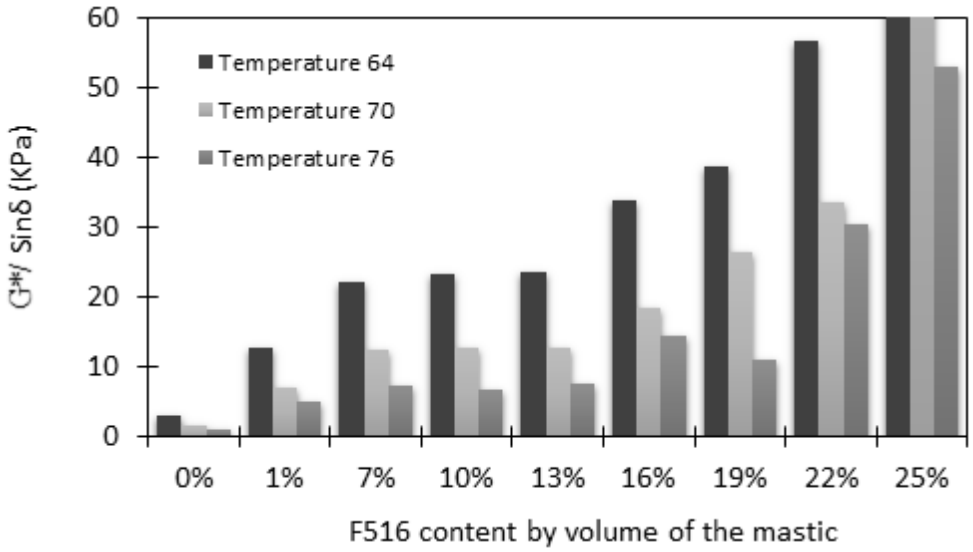


**Figure 20. Variation of G* / sinδ (KPa) with graphite contents**

### 3.5.2 Conductivity and Strength of Asphalt Concrete

*Volumetrics of Asphalt Concrete*

A volumetric analysis for the asphalt concrete containing flake graphite (F516 and F146) was conducted in accordance with ASTM standards: ASTM D2041 (2003), ASTM D3203 (2005), ASTM C136 (2006), and ASTM D1188 (2007). Four specimens for each case were prepared, and their volumetric properties were evaluated. Table 5 shows the average values of the volumetric properties. Based on the D6 mixture design (Table 4), 6.1% filler content and 5.3% binder content by weight were kept constant, but the proportion of the graphite and traditional filler varied. The graphite contents were 7%, 10%, 13%, 16%, 19%, 22%, and 25% by volume of the asphalt mastic, which are 1.20%,

1.80%, 2.41%, 3.00%, 3.60%, 4.19% and 4.78% by volume of the asphalt mixture, respectively.

The target air void was 4.0%, and most of the specimens had an air-void (AV) in the range of 4±0.5%. The specific gravity of aggregates (coarse aggregate + fine aggregate + filler), $G_{sb}$, slightly decreased with an increase of graphite content because the density of graphite is smaller than that of cement. $G_{mm}$ and $G_{mb}$ are the theoretical maximum specific gravity (excluding air voids) and bulk specific gravity (including air voids) of the mixture, respectively. The VMA and VFA are calculated from the following Equations:

$$VMA = 100 - \frac{G_{mb} \times P_s}{G_{sb}} \tag{3}$$

$$VFA = 100 \times \frac{VMA - AV}{VMA} \tag{4}$$

Where, Ps is the percentage of aggregates in the total mixture, and AV is a percent air voids. Table 5 also shows the number of gyrations needed to obtain 4 % target air voids for the specimens with various graphite contents. The control mixture has 56 gyrations, and the number of gyrations increases with increasing graphite content. As shown in the mastic DSR test, adding graphite causes an increase in the |G*| value, and results in additional compaction efforts. This implies that the mixtures with graphite require extra care in compaction. The mixtures with F516 (bigger particles) require fewer gyrations to achieve the target air voids than the mixtures with F146 when same amount of graphite is added.

**Table 5. Volumetric properties of the mixture**

| Specimens | OBC (%) | Gsb(g/cc) | Gmm | Gmb | Air Voids (%) | VMA | VFA |
|---|---|---|---|---|---|---|---|
| Control Mix | 5.3 | 2.642 | 2.428 | 2.329 | 4.09 | 16.52 | 75.27 |
| F146-20% | 5.3 | 2.625 | 2.394 | 2.298 | 4.01 | 17.09 | 76.57 |
| F146-25% | 5.3 | 2.621 | 2.411 | 2.311 | 4.14 | 16.50 | 74.92 |
| F146-30% | 5.3 | 2.617 | 2.427 | 2.315 | 4.60 | 16.22 | 71.65 |
| F516-20% | 5.3 | 2.624 | 2.389 | 2.285 | 4.38 | 17.55 | 75.01 |
| F516-25% | 5.3 | 2.620 | 2.402 | 2.302 | 4.19 | 16.79 | 75.07 |
| F516-30% | 5.3 | 2.615 | 2.386 | 2.288 | 4.10 | 17.14 | 76.09 |
| D-3 Gradation | 4.0 | 2.604 | 2.454 | 2.358 | 4.02 | 15.02 | 73.24 |
| D-5 Gradation | 4.8 | 2.602 | 2.425 | 2.325 | 4.03 | 16.83 | 76.18 |
| D-6 Gradation | 4.9 | 2.670 | 2.479 | 2.364 | 4.04 | 15.52 | 74.21 |
| D-6_25% Gradation | 3.9 | 2.574 | 2.431 | 2.335 | 4.00 | 15.74 | 75.05 |

*Electrical Resistivity of Asphalt Concrete*

Electrical resistivity of the asphalt concrete specimens is compared to the resistivity of asphalt mastics. The solid lines in Figure 21 indicate the average volume resistivity of the asphalt mastic specimens and the symbols are the resistivity measured from the asphalt concrete. The volume resistivity of the control specimens (no graphite) is $1.03 \times 10^{13} \Omega.cm$. The asphalt concrete with the two types of conductive graphite show similar trends to the mastic test results (Figure 21and Figure 22) – resistivity decreases with an increase in graphite content. The scatter range of the resistivity data obtained from asphalt concrete is smaller than that from asphalt mastic. It is presumed that the higher

consistency in resistivity is caused by the bigger size of the asphalt concrete specimens than the asphalt mastic specimens. In addition, this implies the graphite particles are well dispersed over the specimen by the standard mixing and compaction process.

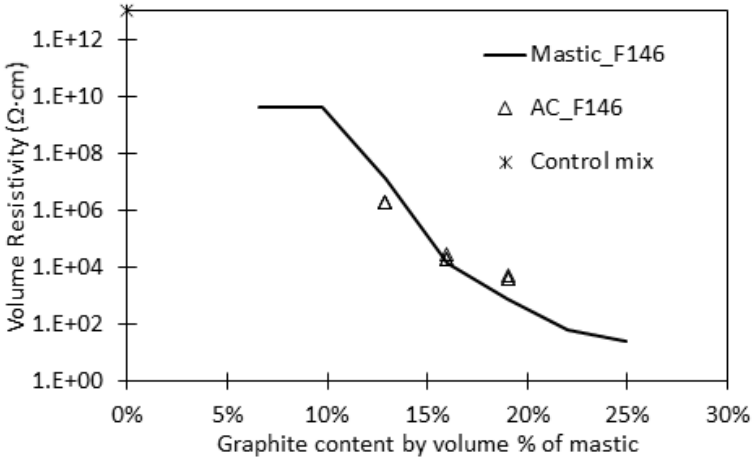


**Figure 21. Volume resistivity versus F146 content for conductive asphalt concrete**

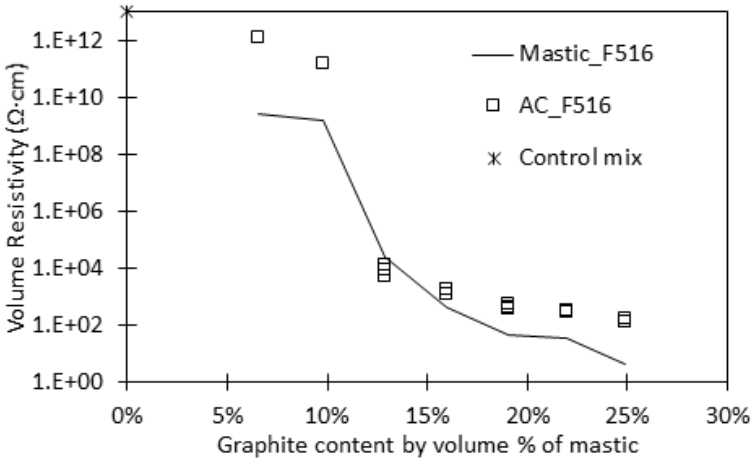


**Figure 22. Volume resistivity versus F516 content for conductive asphalt concrete**

*Indirect Tensile Strength of Conductive Asphalt Concrete*

IDT strengths were measured to investigate the effects of adding graphite on the mechanical properties of the conductive asphalt concrete. Figure 23 shows the IDT strengths obtained from three specimens for each case (except for 7% and 10%). The average IDT strength of the control specimens was 1.12 MPa. The strength of the specimens containing 13%, 16%, and 19% graphite by volume of mastic (equivalent to 2.2%, 2.7%, and 3.2% graphite by volume of the asphalt concrete) were higher than others including the control specimens. The maximum improvement in IDT strength was 41% for the specimens containing 2.7% graphite by volume of the asphalt concrete. Addition of the higher amount of graphite to the asphalt concrete results in a decrease of IDT strength. Thus, the addition of 2.7% (by volume of asphalt concrete) of F516 to asphalt concrete had sufficiently low electrical resistivity ($1.6x10^3$ Ω.cm) and also improved the mechanical strength. The improvement in IDT strength is an unexpected and interesting benign effect of adding graphite. Since the total filler contents are kept constant, the results indicate that graphite has an attribute to improve the bonding between binder and aggregate when it is compared with conventional filler. The authors presume that the hydrophobic nature of graphite provides a stronger adhesion to the hydrophobic asphalt binder than the hydrophilic traditional fillers. Considering both the efficiency in imparting conductivity and mechanical performance, it can be concluded that flake type F516 graphite is the best graphite for multifunctional applications.

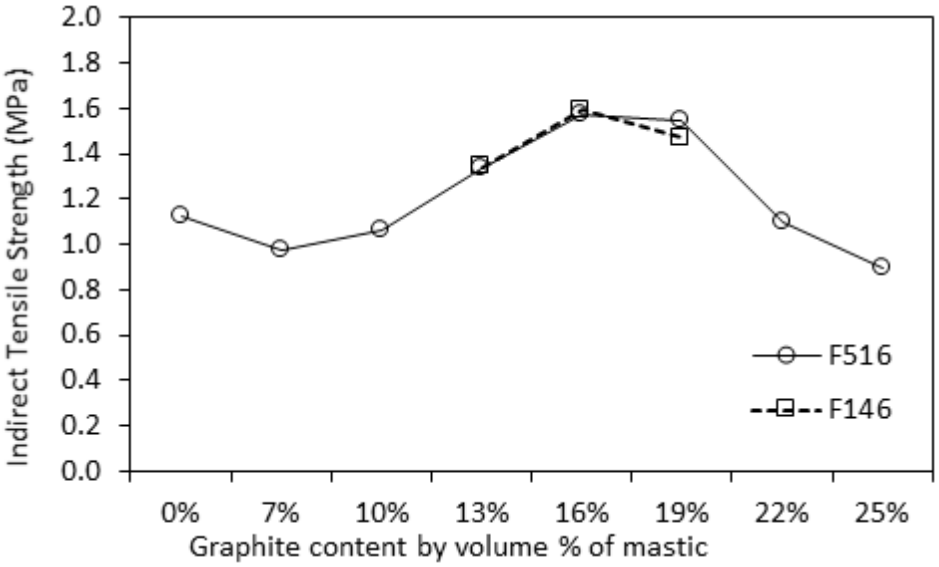


**Figure 23. Comparing IDT strength of F146 and F516**

## 3.6 Conclusions

The effects of graphite as a conductive additive on controlling electrical conductivity and mechanical properties of asphalt concrete are investigated in this study. Electrical volume resistivity of the mastic specimens containing various types and contents of graphite is examined, and the physical explanations for their resistivity variation are suggested based on the SEM analysis for the graphite particles. From the mastic test results, two graphite types are selected and added into asphalt concrete, and the conductivity of the asphalt concrete are compared with that of asphalt mastics. The effect of aggregate gradation is also investigated.

Major findings from the study are listed as follows:

- A sudden change in electrical resistivity from no conduction to conduction, i.e. the so-called percolation threshold, is observed in specimen containing steel fibers. Achieving this threshold implies that the steel fibers form conductive paths and it is therefore impossible to manipulate its resistivity
- Electrical conductivity of asphalt mastics varies significantly with the type of conductive fillers. It turned out that natural flake graphite powder is the most efficient in imparting conductivity into asphalt. Sufficiently low electrical resistivity can be obtained by replacing a part of the fillers by the flake type graphite powder in asphalt mastics.
- The volume resistivity of asphalt mastic and asphalt concrete containing natural flake graphite powder varies widely with the amount of the graphite powder mixed in the mastic. This implies that the resistivity of asphaltic composite can be manipulated over a wide range of conditions thereby various multifunctional applications. The graphite does not completely eliminate the percolation threshold, but substantially mitigates it.
- The different binder types do not have significant influence on electrical conductivity of asphalt mastics, but binder modifiers may reduce electrical conductivity.
- When the fixed amount of graphite is added to the mixture, less amount of fine aggregate and binder results in higher electrical conductivity.

- The conductive asphalt concrete containing the flake type graphite has improved ITS when compared to control asphalt concrete. DSR tests for asphalt mastic show that the flake type graphite additives increase complex modulus. This implies that adding graphite is beneficial for improving rutting resistance.

Flake graphite exhibits good electrical conductivity along with mechanical performance. The stepwise decrease in electrical resistivity of this conductive asphalt concrete can be utilized for various multifunctional applications as discussed in the previous chapters.

# 4. ELECTRICAL CHARACTERIZATION WITH AC IMPEDANCE SPECTROSCOPY

## 4.1 Introduction

Multifunctional materials have simultaneous abilities to exhibit non-structural functions as well as their regular structural functions (Gibson 2010; Baur and Silverman 2011; Ye et al. 2005; Chou et al. 2010). By rendering a material multifunctional, the electrical, magnetic, thermal, and other functionalities can be integrated with structural properties (e.g., strength and stiffness). Materials of this kind have a tremendous potential for various smart applications. Among the listed non-structural properties, the use of electrical conductivity has been actively studied because of its various applications (Qiu et al. 2007; Kalaitzidou et al. 2007; Cebeci et al. 2009; Sandler et al. 2003; Li et al. 2007; Thostenson et al. 2009).

Asphalt concrete is a composite material that is heavily used in the construction of highway, runways, and parking lots. Riding comfort, durability, reliability, and water resistance are the advantages making asphalt concrete the most preferred choice in the pavement industry. Asphalt concrete is a non-conductive composite material by nature, but its conductivity can be improved by using conductive additives (Wu et al. 2005; Huang et al. 2009; García et al. 2009).

Alternating current impedance spectroscopy (ACIS) is a powerful technique to characterize the electrical properties of materials and their interface with electrodes in complex electrical system (Barsoukov and Macdonald 2005; Girault 2004). Impedance plays a vital role in showing the characteristics of an electrical system, and is defined as

an obstacle to the flow of alternating current (AC). Through the measurement of ACIS, an equivalent electrical circuit that has the same electrical properties as the material can be constructed. The equivalent electrical circuit allows the prediction of the electrochemical behavior of the electrodes and electrolyte materials such as a battery (Cho et al. 2015). ACIS also has been widely used to prove the physical characteristic of material structures and various chemical phenomena such as diffusion and corrosion (Cubides and Castaneda 2016). In civil engineering, the first impedance spectroscopy for cement pastes was tried by McCarter et al. (1988). In this study, ACIS has been used to monitor the hydration process of cement pastes with the frequency range from 100 Hz to 300 kHz. Since then, many studies using ACIS have concentrated on the mechanism of hydration of cement based composites during the last three decades (Campo et al. 2002; Gu et al. 1992; Gu et al. 1993; McCarter et al. 2009). Gu et al. (1993) stated that ACIS is a convenient method of characterizing microstructural development in hydrating cement or concrete systems. Gu et al. (1993) investigated the microstructure of the transition zone between aggregate and cement paste, and the effect of silica fume, slag, and fly ash using ACIS. McCarter and Garvin (1989) also illustrated that the sensitivity of electrical properties of cement based materials to moisture content was shown by ACIS. This research showed that impedance spectroscopy can be employed for monitoring moisture effect in various composite materials (Wandowski et al. 2016).

The conductive civil materials were studied as the application of electrical techniques for monitoring their characteristics. The conductive cement composites were investigated as a thermistor, which is a thermometric device consisting of conductive

additives whose electrical resistivity decrease as the temperature increases by previous researchers (Wen and Chung 2004; McCarter et al. 2005). The opposite phenomenon, on the other hand, was observed in the conductive asphalt concrete that the electrical resistivity increased as the temperature increased (Wu et al. 2012; Pan et al. 2015). When the temperature increases, some existed electrical pathways is destroyed due to the volume expansion of asphalt. Therefore, this implies that conductive asphalt composites can be utilized as a thermistor along with conductive cement composites.

This study aims to characterize the electrical properties of conductive asphalt composite with added graphite by using ACIS and constructing the equivalent electrical circuit for the composite with various levels of conductivity to understand the relationship between components and investigate the feasibility of multifunctional applications.

## 4.2 Technical Background

### 4.2.1 AC Response

The basic theory of ACIS has been widely used in material science engineering and summarized by many researchers (Barsoukov and Macdonald 2005; Girault 2004). The application of ACIS to electrically conductive asphalt composites is a new approach that can be used as a damage-sensing tool instead of the potential drop method. Impedances and phase angle measurements are obtained over a broad range of frequencies by ACIS. Imaginary and real impedances, plotted on graphs, which are called Nyquist diagrams, can subsequently be investigated in terms of electrical equivalent circuit parameters: resistors, capacitors, and inductors, to represent the characteristics of electrically conductive asphalt composites.

In the ACIS for this research, a sinusoidal voltage with small amplitude is applied to specimens as input data. Electrical conductive asphalt concrete system can be considered as linear response of the current against small voltage perturbations as shown in Figure 24. Equation (5) is used to describe input voltage including a sinusoidal excitation of an AC voltage. The resulting steady state current, moreover, is measured as output data. Equation represents the output function as an electrical current reacting to a sinusoidal voltage.

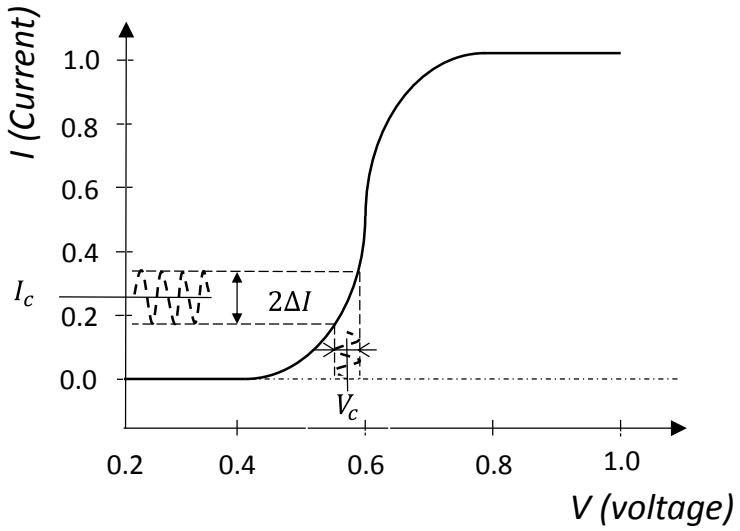


**Figure 24. Linear current response to a sinusoidal voltage excitation of small amplitude around a constant value $V_c$**

$$V(t) = V_c + \Delta V \sin \omega t \tag{5}$$

Where, $V_c$ is the constant voltage value, $\Delta V$ is an amplitude of sinusoidal voltage excitation, $\omega$ is the angular frequency, and $t$ is time domain.

$$I(t) = I_c + \Delta I \sin(\omega t + \theta) \tag{6}$$

Where, $I_c$ is the constant current value, $\Delta I$ is an amplitude of sinusoidal current response, and $\theta$ is the phase angle between the two signals.

The relationship between properties of system and reaction to sinusoidal excitation is complex in the time domain because of the differential equations required in an analysis of a system comprised of capacitive and inductive elements. Equations (7) and (8) show the response of a capacitor and an inductor, respectively.

$$I(t) = \frac{dV(t)}{dt} C \tag{7}$$

$$V(t) = \frac{dI(t)}{dt} L \tag{8}$$

Where, $I(t)$ is sinusoidal excitation of input current, $V(t)$ is sinusoidal excitation of output voltage, $C$ is a capacitance, and $L$ is an inductance.

A Laplace transformation is used to simplify the mathematical treatment of this system. The Laplace transformation of a function $F(t)$ defined by Equation (9) can be defined by considering the variable in the Laplace plane, $s$, as a complex number.

$$\bar{F}(s) = L\{F(t)\} = \int_0^\infty F(t) e^{-st} dt = \int_0^\infty F(t) e^{-(\sigma + j\omega)t} dt \tag{9}$$

$$s = \sigma + j\omega \tag{10}$$

Time domain equations, which are Equation (5) and (6), can be transformed into Equations (11) and (12) to present the input and the output functions of ACIS with various frequency ranges by Laplace.

$$\Delta \bar{V}(s) = \Delta V \frac{\omega}{(s^2 + \omega^2)} \tag{11}$$

$$\Delta \bar{I}(s) = \Delta I \frac{\omega}{(s^2 + \omega^2)} = \Delta V \frac{Y(s) \cdot \omega}{(s^2 + \omega^2)} \tag{12}$$

$$Y(s) = \frac{\Delta \bar{I}(s)}{\Delta \bar{V}(s)} \tag{13}$$

The transfer function of electrically conductive asphalt concrete system, which is the admittance ($Y$), is defined as the ratio of the Laplace transforms of the variations of the output to the input data as shown in Equation (13).

In view of the complex number of $s$, it is useful to distinguish what we can call the frequency domain, which depends on the angular frequency $\omega$, and which consists of taking $s = j\omega$ in the Laplace transform. Thus, in the inverse transformation of the equation, the frequency domain corresponds to the sinusoidal part of the output function, as can be seen in Equation(14).

$$\Delta I(t) = \Delta V \left| Y(\omega) \right| \sin(\omega t + \theta) \tag{14}$$

To make an electric circuit to examine the characteristics of electrically conductive asphalt composites, the transfer function from the voltage (input function) to the current (output function) is called the admittance to the system and has the symbol $Y$. In the frequency domain, it is defined by Equation (15).

$$\Delta \bar{I}(\omega) = Y(\omega) \Delta \bar{V}(\omega) \tag{15}$$

In the same way, the transfer function from the current to the voltage is called the impedance of the system and has the symbol Z in Equation (16). Clearly, the admittance is the inverse of the impedance.

$$\Delta\bar{V}(\omega) = Z(\omega)\Delta\bar{I}(\omega) \tag{16}$$

### 4.2.2 Nyquist and Bode Diagram

The transfer function, which is the impedance in electrically conductive asphalt concrete system, in the frequency domain consisted with a complex number. Nyquist diagram is useful to represent the impedance by plotting the imaginary part as a function of the real part, as shown in Figure 25 (a) and Equation (17).

$$Z(\omega) = ReZ(\omega) + j\ ImZ(\omega) \tag{17}$$

$|Z(\omega)|$ is the modulus of $Z(\omega)$ defined as a function of the real part $ReZ(\omega)$ and the imaginary part $ImZ(\omega)$ of Equation (18).

$$\left|Z(\omega)\right| = \sqrt{\left[Re\ Z(\omega)\right]^2 + \left[Im\ Z(\omega)\right]^2} \tag{18}$$

$\theta$ is the phase angle (difference) between the voltage and the current defined by Equation (19).

$$\theta = Phase\,angle\left[Z(\omega)\right] = arctan\left|\frac{Im\ Z(\omega)}{Re\ Z(\omega)}\right| \tag{19}$$

In electrochemical systems, in fact, it is more customary to trace $-ImZ(\omega)$ as a function of $ReZ(\omega)$ for explaining various physical and chemical phenomena. The graph obtained by doing this is called a Nyquist diagram and is shown in Figure 25 (a). The Nyquist diagram illustrates a semi-circle going from the point at coordinates $(K, 0)$ where

the angular frequency tends to zero, and finishing at the origin where the angular frequency tends to infinity. Another graph representing a complex number is called a Bode diagram, shown in Figure 25 (b). The graph plots the modulus, which is the magnitude of an impedance (Z) or an admittance (Y), as a function of the angular frequency. These diagrams are significant roles to measure and analyze many complex materials variables such as defects, microstructure, dielectric properties, and compositional influence on the conductance of solids material in this research.

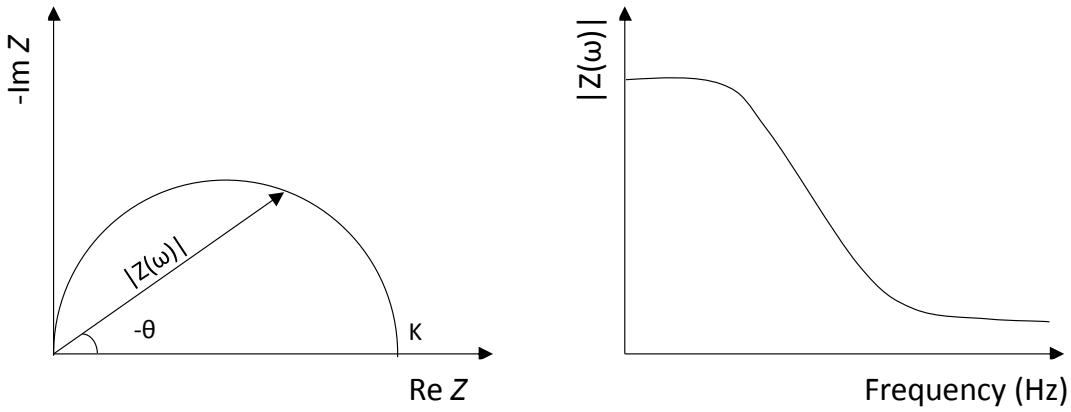


(a) (b)

**Figure 25. (a) Nyquist diagram and (b) Bode diagram**

### 4.2.3 Electrical Equivalent Circuit

Electrical equivalent circuit based on ACIS is useful for analyzing the microstructure of the composite materials and accounting for numerous chemical and physical phenomena. This electrical equivalent circuit is comprised of pure resistors, capacitors, inductors, and other various circuit components. In general, three elements, which are resistor, capacitor, and inductor, are utilized in electrical equivalent circuits to evaluate the system. These elements are shown as symbols in Figure 26.

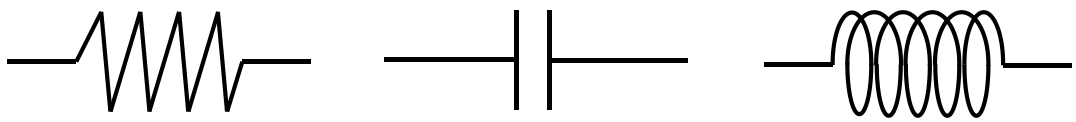

(a) (b) (c)

**Figure 26. Schematic representation of a resistor (a), a capacitor (b), and an inductor (c)**

*Resistor*

The voltage difference at the terminals of a resistor is given by Ohm's law, as shown in Equation (20).

$$\Delta V(t) = R\Delta I(t) \tag{20}$$

Where, $\Delta V(t)$ is a voltage in time domain, $\Delta I(t)$ is a current in time domain, and $R$ is a resistor. And Equation (21) is transformed simply by the Laplace.

$$\Delta\bar{I}(\omega) = R^{-1}\Delta\bar{V}(\omega) \tag{21}$$

Where, $\Delta\bar{I}(\omega)$ is a Laplace transformation of $\Delta I(t)$, and $\Delta\bar{V}(\omega)$ is a Laplace transformation of $\Delta V(t)$. The admittance $(Y)$ of a resistor, therefore, is illustrated in Equation (22).

$$Y(\omega) = \frac{\Delta\bar{I}(\omega)}{\Delta\bar{V}(\omega)} = R^{-1} \tag{22}$$

If the alternating voltage is written as Equation (23),

$$\Delta V(t) = \Delta V \sin \omega t \tag{23}$$

The inverse transform of Equation (21) in the frequency domain is given by Equations (18) and (19). Thus, the alternating current $I_{ac}$ is

$$I_{ac} = \Delta I(t) = \Delta V\left|Y(\omega)\right|\sin\left(\omega t + \arctan(0)\right) = \frac{\Delta V}{R}\sin \omega t \tag{24}$$

Thus, Equation (20) is verified with Equation (24). A resistor does not introduce dephasing, and Ohm's law applies equally to alternating currents and potentials.

*Capacitor*

The potential difference at the terminals of a capacitor is proportional to its charge

$$Q(t) = C\ V(t) \tag{25}$$

Where, $Q(t)$ is the charge amount of the capacitor. The current is defined as the variation in the charge with time

$$I(t) = \frac{dQ(t)}{dt} = \frac{CdV(t)}{dt} \tag{26}$$

And therefore the Laplace transform is given by

$$\Delta\bar{I}(s) = Cs\Delta\bar{V}(s) \tag{27}$$

The admittance in the frequency domain is obtained by taking $s = j\omega$

$$Y(\omega) = \frac{\Delta\bar{I}(\omega)}{\Delta\bar{V}(\omega)} = jC\omega \tag{28}$$

If the potential is given by Equation (23), then the inverse transform of Equation (28) from Equations (18) and (19) gives

$$I_{ac} = \Delta I(t) = \Delta V\left|Y(\omega)\right|\sin\left(\omega t + \arctan(\infty)\right) = \Delta VC\omega\sin\left(\omega t + \frac{\pi}{2}\right) = \Delta VC\omega\cos(\omega t) \tag{29}$$

Unlike a resistor, the current at the capacitor component is dephased by 90°, compared to its input potential.

*Inductor*

The potential difference at the terminals of an inductor is proportional to its charge

$$V(t) = L\,S(t) \tag{30}$$

Where, $L$ is the inductor, and $S(t) = \frac{di}{dt}$. The current is defined as the variation of the charge with time

$$I(t) = \int S(t)\,dt = \frac{1}{L}\int V(t)\,dt \tag{31}$$

And therefore the Laplace transform is given by

$$\Delta\bar{V}(s) = Ls\Delta\bar{I}(s) \tag{32}$$

The admittance in the frequency domain is obtained by taking $s = j\omega$

$$Y(\omega) = \frac{\Delta\bar{I}(\omega)}{\Delta\bar{V}(\omega)} = (jL\omega)^{-1} \tag{33}$$

If the potential is given by Equation (23), then the inverse transform of Equation (33) from Equations (18) and (19) gives

$$I_{ac} = \Delta I(t) = \Delta V\left|Y(\omega)\right|\sin\left(\omega t + \arctan(\infty)\right) = \frac{\Delta V}{L\omega}\sin\left(\omega t + \frac{\pi}{2}\right) = \frac{\Delta V}{L\omega}\cos(\omega t) \tag{34}$$

Unlike a resistor, the current at the inductor component is dephased by 90°, compared with its input potential.

## 4.3 Materials and Test Methods

### 4.3.1 Physical Properties of Used Materials

The conductive additives are selected within the filler size (<75μm) conductive particles. The traditional asphalt concrete contains up to 6% fillers by total mixture volume. In this study, a part of traditional fillers is replaced the conductive fillers. The flake type of graphite (F516) produced from Asbury Carbons Inc. is selected to study its characterization of electrical conductivity into asphalt concrete (Rew et al. 2017). Graphite has two-dimensional hexagonal crystal structure, and hence, the ideal shape of graphite particles is hexagonal plate.

Several materials are used for the experiment, and their properties are investigated. For fixing asphalt mastic specimens in a thin film form, wood sticks were used as a non-

conductive base. The electrical volume resistivity of pine wood ranges from $10^{14}$ to $10^{16}$ ($\Omega \cdot m$), and varies with the moisture content. The wood base were heated in the oven for 24 hours to remove moisture. Asphalt concrete is a mixture of coarse aggregate, fine aggregate, filler, and binder. In this study, the conductive additives are considered to replace traditional fillers to minimize the effect on the skeleton structure of asphalt concrete. As the traditional filler for manufacturing the control specimens, Type II Portland cement was used. Silver paste and copper tape were used as the electrodes for measuring the electrical resistivity. Table 6 summarizes physical properties of materials used in this research.

### 4.3.2 Sample Preparation

*Asphalt Mastic Specimens*

The asphalt mastic specimens were prepared using PG64-22 asphalt binder (ASTM D1073-07) and various combinations of conductive and non-conductive fillers. The density of binder is 1.032 g/cm3. The asphalt mastics are composed of 50% asphalt binder and 50% filler by weight. This proportion is kept constant throughout the experiment. Type II Portland cement is used as the non-conductive traditional filler. Graphite replaces a part of cement filler in the mastic specimens ranged from 10% to 50% by weight of the mastic. For example, when the graphite content is 20%, cement content is 30% to maintain the 50% of filler content in the mastic.

**Table 6. Properties of other materials used for the research**

| Asbury ID | % Carbon | Typical Size (µm) | True Density | Surface area ($m_2/g$) | Typical Resistivity (Ω·cm) | Note |
|---|---|---|---|---|---|---|
| F516 | 95.45 | - (< 212) | 2.26 | 5.0 | 0.03-0.05 | Flake type |
| **Material** | **Typical Size** | **Density** | **Thermal Conductivity (W/mK)** | **Electrical Resistivity (Ω·m)** | | **Note** |
| Coarse Aggregate | 4.75mm-25mm | Specific Gravity 2.57 g/cc | 1.25-1.75 | $10^9$ | | |
| Fine Aggregate | 0.075mm-4.75mm | Specific Gravity 2.63 g/cc | 1.25-1.75 | $10^9$ | | |
| Fillers | <0.075mm | Specific Gravity 3.15 g/cc | 0.29 | $10^9$ | | Type 2 Portland Cement |
| Binder | Liquid | 1.032 $g/cm^3$ | | | | Jebro, INC. PG64-22 |
| Silver paste | Particle size: 0.4-1.0µm | Specific Gravity 2.25$g/cc^3$ | - | Sheet Resistance 0.02 - 0.05 ohms/sq/mil (25µm) | | Ted Pella, INC. |
| Copper tape | W: 6.3mm L: 16.46m T: 2.4 mils (66µm) | 8.94 $kg/cm^3$ | - | Sheet Resistance (ohms/sq): 0.001 | | Ted Pella, INC. |

The mastic specimens are prepared in thin film shape as shown in Figure 27 (a). Dry pine wood is used as a base for spreading asphalt mastic. The wooden base blocks are coated with heat resistant epoxy to prevent the absorption of asphalt binder. The wood, binder, and filler are conditioned at 150 ºC for 2 hours in the oven before mixing. Once the materials were heated, the binder and filler (combination of cement and graphite with various proportions) are mixed manually by hand for 3-5 minutes to ensure uniform and complete dispersion of the filler in the mastic. The mastic is then spread on the epoxy-coated wooden blocks. The average thickness of mastic is measured by reading the weight of the wooden block before and after spreading the mastic. Once the weight of mastic on

the wooden block is found, it is divided by the density of mastic and the spread area to obtain its average thickness. The density of the mastic is estimated using the individual densities of the binder, cement, and graphite and their respective weight proportions in the mastic. For each type and content of graphite, three mastic specimens are prepared to improve reliability of the results.

The mastic specimens are conditioned at room temperature for 8 hours before testing. Copper tapes are installed at every 50 mm distance and are used as electrodes (Figure 27 (a)). Silver paste is painted between the mastic and copper tapes to ensure full contact between them. Two-point sensing method is used to measure impedance of the mastic specimens.

*Asphalt Concrete Specimens*

Asphalt concrete is a mixture of coarse aggregate, fine aggregate, filler, and binder. The asphalt concrete specimens are prepared in accordance with the Superpave mixture design method using a PG64-22 asphalt binder (density 1.032 g/cc). The specific gravities of coarse aggregate, fine aggregate, and traditional filler were measured as 2.57 g/cc, 2.63 g/cc, and 3.15 g/cc, respectively. D6 mixture with 12.5 mm of maximum aggregate size is selected, and the proportion of coarse and fine aggregates is determined to satisfy mixture requirements specified in ASTM D3515 (2001).

The aggregate gradation used in this study are shown in Table 7. The optimum binder content for the mixture was 5.3% by weight of the total mixture by the Superpave method. The variation of the mixture conductivity with graphite content was investigated.

**Table 7. Aggregate gradation**

| Sieve size (mm) | 37.5 | 25 | 19 | 12.5 | 9.5 | 4.75 | 2.36 | 1.18 | 0.6 | 0.3 | 0.15 | 0.075 |
|---|---|---|---|---|---|---|---|---|---|---|---|---|
| D-6 % passing | 100 | 100 | 100 | 99.9 | 95.3 | 68.1 | 50.8 | 35.3 | 21.0 | 11.5 | 7.2 | 6.1 |

The aggregates and fillers are heated at 150 ºC for at least 24 hours to eliminate moisture, and the binder is heated for 2 hours at the same temperature prior to mixing. The heated filler and aggregates are mixed first, and then the binder was added. A mechanical mixer is used to mix the materials until the aggregates and fillers are well coated with the binder. The mixture is then conditioned in the oven at the compaction temperature (135 ºC).

A Superpave gyratory compactor is employed to compact the specimens. Cylindrical specimens with a 150 mm diameter and 95 mm height are compacted by gyration until the 4% percent air void is reached. For each test case, four fan shaped specimens are cut for determining the electrical characterization of conductive asphalt concrete with various graphite contents, the temperature effect, and the moisture effect in ACIS analysis. The small specimens for detecting size effect are drilled to make three core samples out of it. Their size is 25 mm diameter and 80 mm height. The rough top and bottom surface of the specimen were cut to make a smooth surface. This cutting eliminates the error in the conductivity measurement by removing the conductive mastic at the sides of the specimens. As shown in Figure 27 (b), copper tapes are installed as electrodes at the top and bottom of specimens. A highly conductive silver paste is applied on the top and

bottom surfaces of the specimen to maintain full contact between the specimen and copper tape.

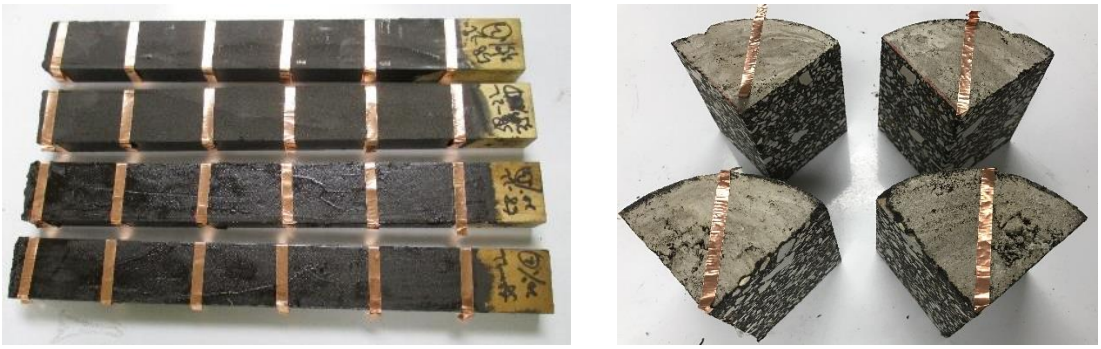

(a) Mastic specimens with various graphite contents for determining electrical characteristics

(b) Asphalt concrete samples with various graphite contents for determining electrical characteristics

**Figure 27. Asphalt composite specimens (a) Asphalt mastic (b) Asphalt concrete**

## 4.4 Measurement Set-up

Impedance/Gain Phase Analyzer (Solartron 1260A and 1296, Figure 28) is used to measure the electrical impedance of the specimens. Solartron 1260A can measure resistance only up to 100 MΩ. To extend the measurable range up to 100 TΩ, Solartron 1296 is combined with 1260A. Electrical impedances of the specimens are obtained at 0.1V with AC frequency sweep ranged from 1 Hz to 10MHz. The non-conductive asphalt mastic specimens, on the other hand, are conducted with different frequency ranges from

$10^{-4}$ Hz to 10 Hz due to available scope to measure the impedance in Impedance/Gain Phase Analyzer.

Electrical impedance is measured at room temperature (25˚C). Volume impedance can be calculated from the measured impedances as shown in Equation (35).

$$\text{Volume impedance} = Z\frac{A}{l} \tag{35}$$

Where, A and l are the cross sectional area ($cm^2$) and the length (cm) of the specimen.

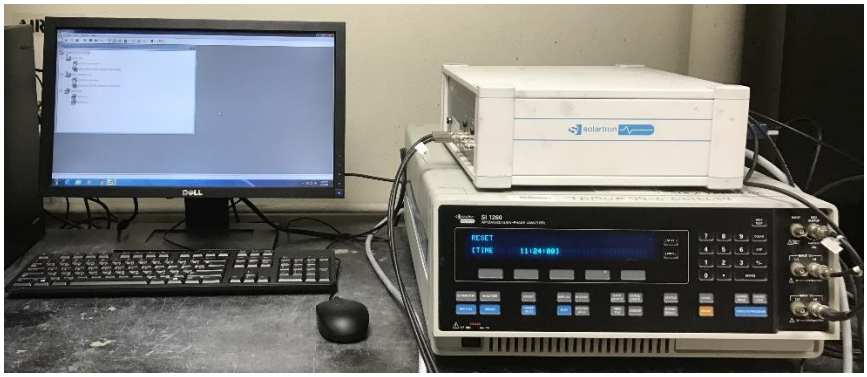


**Figure 28. Resistivity measurement set-up: Phase gain/phase analyzer (Solartron 1296 & 1260A)**

## 4.5 Results and Discussions

### 4.5.1 Electrical Characters of Conductive Asphalt Composites

*Asphalt Mastic Specimens*

The electrical characteristics of the conductive asphalt composite containing various graphite contents were investigated by AC impedance spectroscopy. Figure 29 shows the variations of volume impedance magnitude with the contents of graphite additives by a Bode diagram. The figures clearly show that electrical conductive paths are existed or not according to graphite contents. As shown in Figure 29 (a) and (b), the mastics containing low graphite contents ($V_{GM}$ = 6.75% ~ 13.24%) have higher volume impedance magnitude beyond $10^8$ Ω·cm, whereas the mastics with high graphite contents ($V_{GM}$ = 16.40% ~ 22.5%) are electrically conductive with low volume impedance magnitude (less than $10^4$ Ω·cm). The volume impedance magnitude of mastics containing the graphite gradually decreases with the increase of the graphite content. In non-conductive asphalt mastics, the lower frequency range is required to obtain the steady state of volume impedance magnitude related to the electrical resistivity. Conductive specimens, on the other hand, need high frequency range for measuring the steady volume impedance magnitude. This implies that measuring time of the electrical resistivity can be shorter in conductive specimens than one in non-conductive specimens.

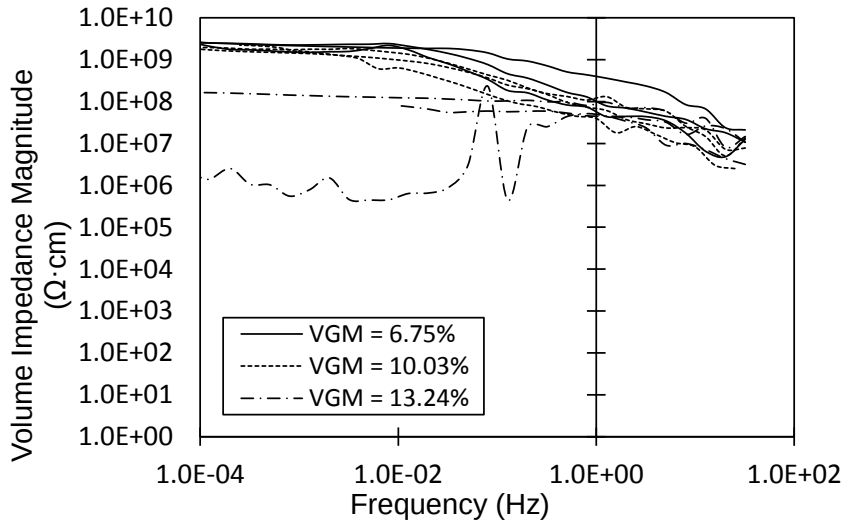


(a) Bode diagram of non-conductive mastic

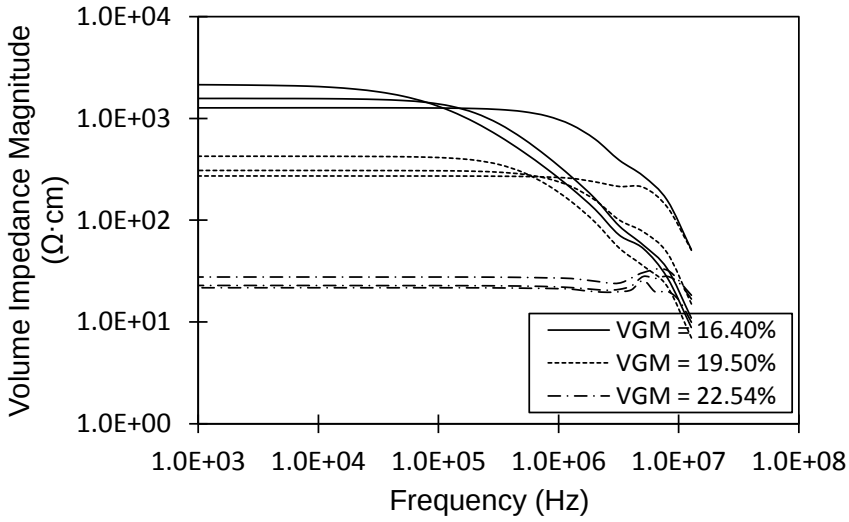


(b) Bode diagram of conductive mastic

**Figure 29. Bode Diagram of Asphalt mastic specimens including different graphite contents**

The values of impedance phase angle in asphalt mastics adding various graphite content are compared in Figure 30 (a) and (b). This comparison confirms that the clear difference exists between non-conductive and conductive asphalt mastics. As shown in Figure 30 (a), a considerable change of the phase angle is occurred with overall frequency scope of ACIS in non-conductive asphalt. Lower frequency range causes the decrease of fluctuation in impedance phase angle but small change is existed in non-conductive state. Addition of the higher amount of graphite results in a steady state of impedance phase angle, which has a zero-value, at approximately $10^4$ frequency. The observations for Figure 29 and Figure 30 reveal that impedance phase angle affects the tendency of volume impedance magnitude with various graphite contents. In addition, as shown in Figure 30 (b), the value of impedance phase angle reaches zero at higher frequency as higher graphite content.

Figure 31 shows the Nyquist diagrams of asphalt mastics containing various graphite amounts as another result of the ACIS. The non-conductive asphalt mastics show atypical trend in Figure 31 (a)-(c), while the conductive asphalt mastics have regular shape of curves in Figure 31 (d)-(f). The graphite content is significant to determine the curve trend of Nyquist diagrams. In the proximity of the phase transference from non-conductive to conductive ($V_{GM}$ = 16.40% ~ 19.50%), the Nyquist diagram shows the exact semi-circle shape as illustrated in Figure 31 (d). From semi-circle curves, the equivalent circuit can be expressed in Figure 32 (b). The ACIS indicates that the semi-circle shape is expressed the parallel relationship between a resistor and a capacitor. The circle diameter of Nyquist diagrams is related to the value of the electrical resistivity of the bulk specimen. The

distribution of dots in curves, in addition, can relate to the value of a capacitance in interface between the conductive particles.

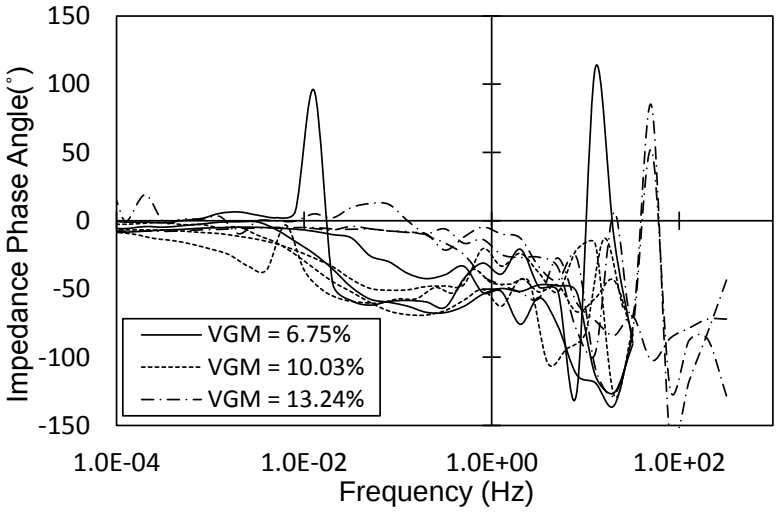


(a) Phase angle of non-conductive mastic

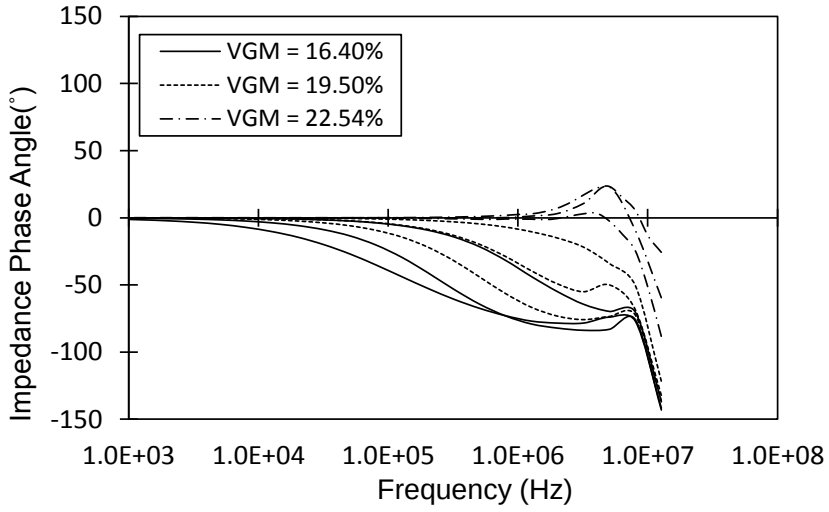


(b) Phase angle of conductive mastic

**Figure 30. Phase angle of asphalt mastic specimens including different graphite contents**

Figure 31 (f) shows the Nyquist diagram for the ACIS of specimens containing 22.54% graphite by volume. In the case of a high graphite content, the Nyquist diagram and the equivalent circuit from the ACIS are obtained differently because of low impedance, which consists of many internal conduction connections. The inductance component is existed in the electrical equivalent circuit as shown in Figure 32 (c). The equivalent circuit of specimens containing high graphite content can be formed as the series between two parallel relationships (a resistor-a capacitor and a resistor-an inductor). The curve section above zero imaginary impedance can be represented by the parallel network of a resistance and an inductance at a high frequency range. The semi-circle below zero imaginary impedance, on the other hand, is related to the parallel connection of a resistance and a capacitance of conductive asphalt mastics at a low frequency area. As shown in Figure 32 (a)-(c), the graphite content in the specimen plays a significant role in determining the electrical components of the equivalent circuit. Comparing among Figure 31 (d)-(f), the data density of a plot can be different according to the graphite content. With low graphite content, the Nyquist diagram is distributed uniformly. High graphite content, however, causes the Nyquist diagram to be cornered at a specific local part, such as Figure 31 (f). Well-distributed impedances are more beneficial that multifunctional applications of conductive composite can be used by utilizing the whole frequency range of AC.

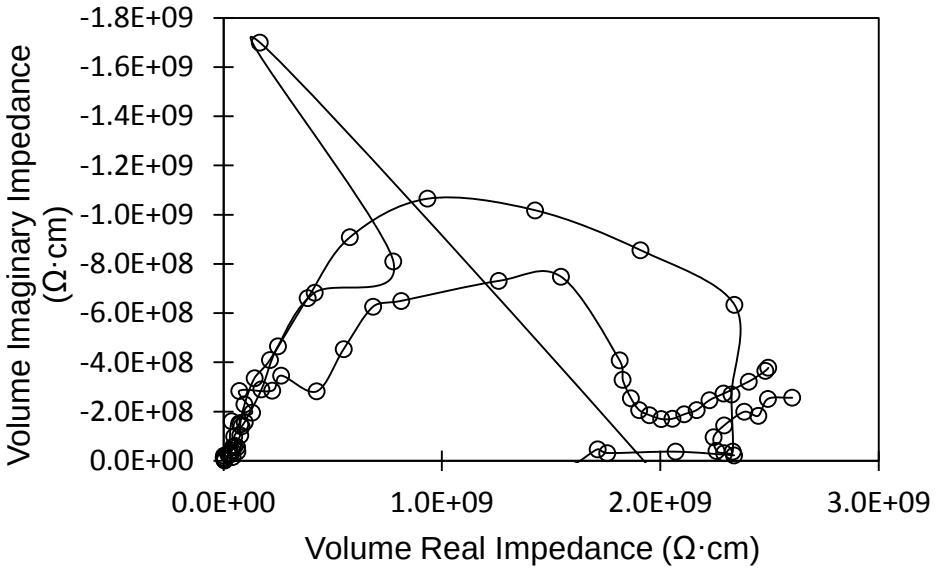


(a) $V_{GM}$ = 6.75%

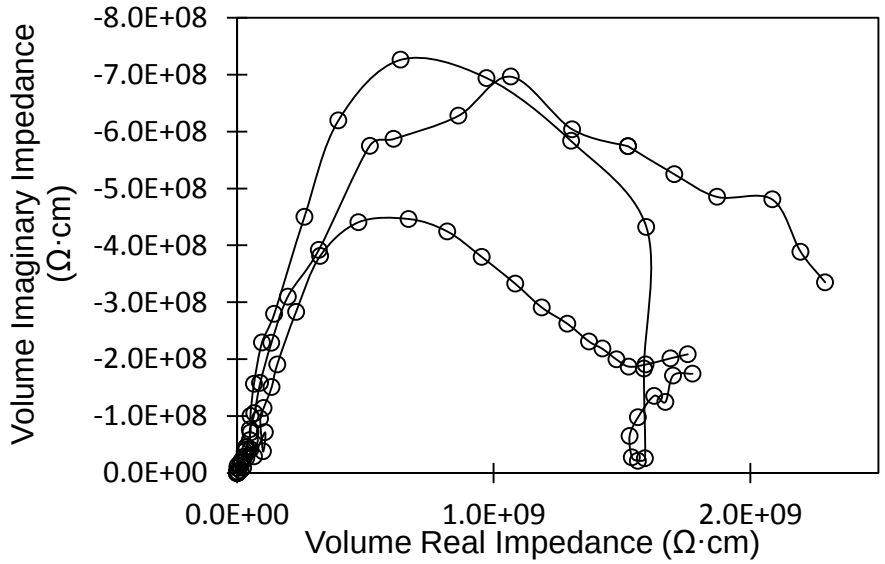


(b) $V_{GM}$ = 10.03%

**Figure 31. Nyquist diagram of asphalt mastic specimens including different graphite contents**

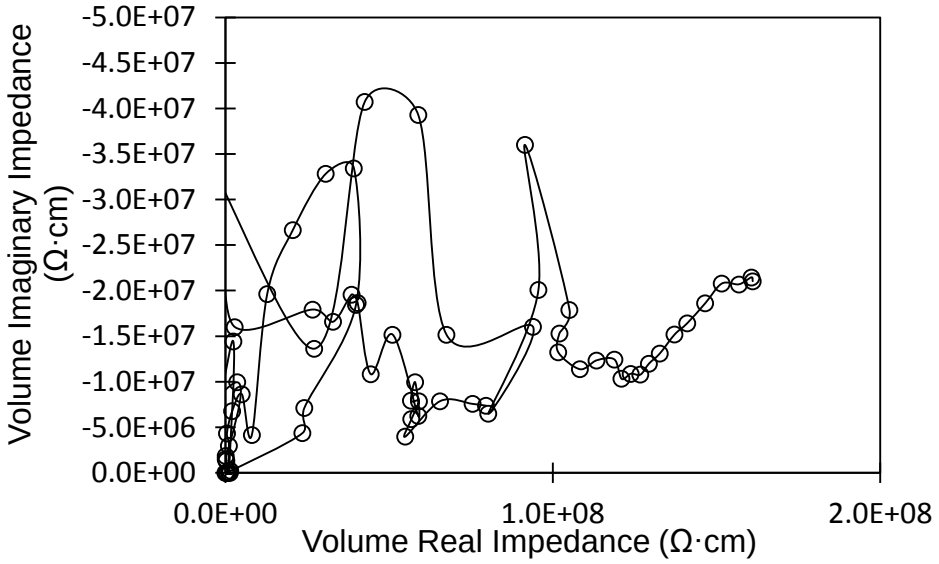


(c) $V_{GM}$ = 13.24%

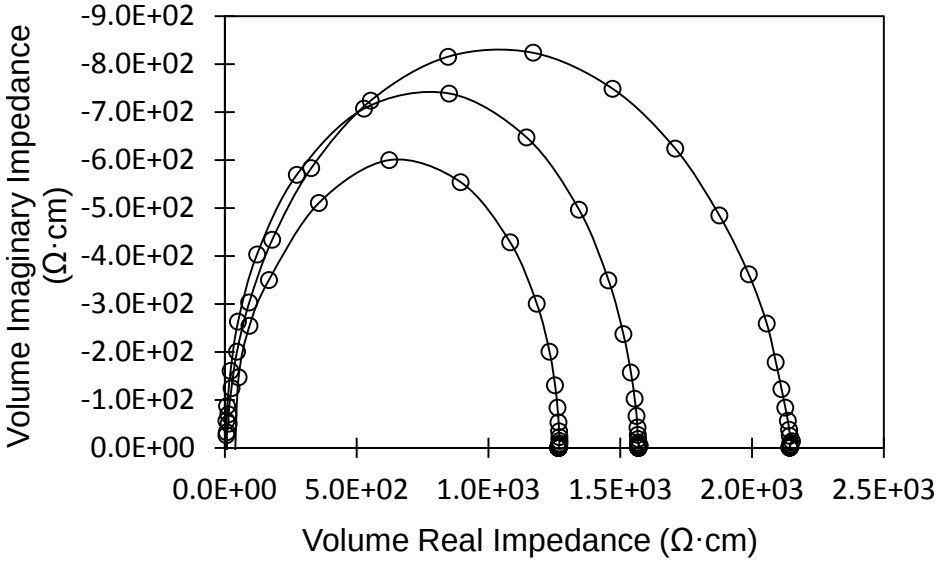


(d) $V_{GM}$ = 16.40%

**Figure 31. Continued**

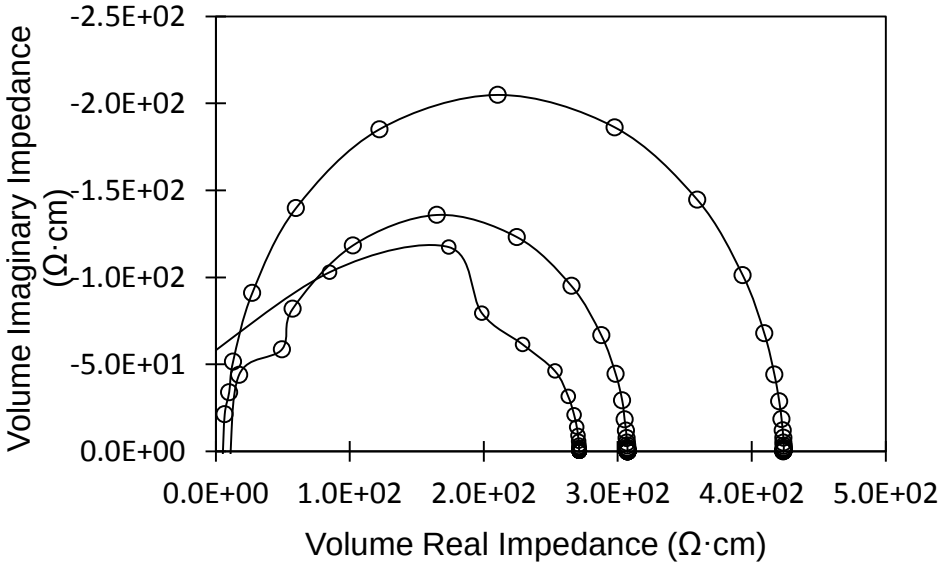


(e) $V_{GM}$ = 19.5%

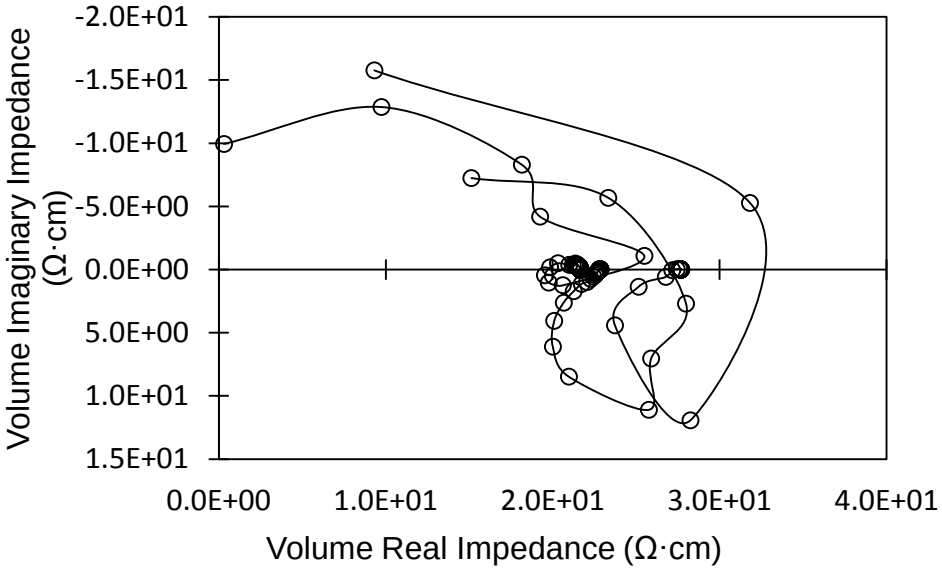


(f) $V_{GM}$ = 22.54%

**Figure 31. Continued**

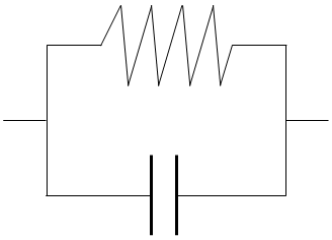

(a) Low Graphite Content ($V_{GM}$ =6.75%~13.24%)

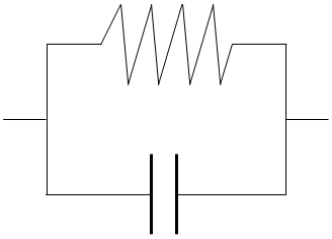

(b) Medium Graphite Content ($V_{GM}$ = 16.40%~19.50%)

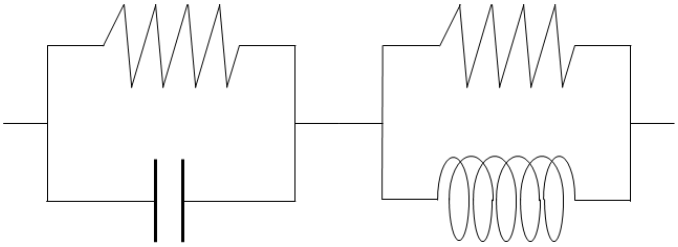

(c) High Graphite Content ($V_{GM} \geq$ 22.50%)

**Figure 32. Electrical Equivalent Circuits of Asphalt Composite Containing Graphite**

*Asphalt Concrete Specimens*

Volume electrical impedance magnitude of the asphalt concrete specimens is shown in Figure 33. Comparing between asphalt mastics and concretes, the results of volume impedance magnitude show similar trends. In the case of numerical values, however, asphalt concretes have higher volume impedance magnitude than asphalt

mastics. It is presumed that higher impedance is caused by fine aggregates of asphalt concrete specimens.

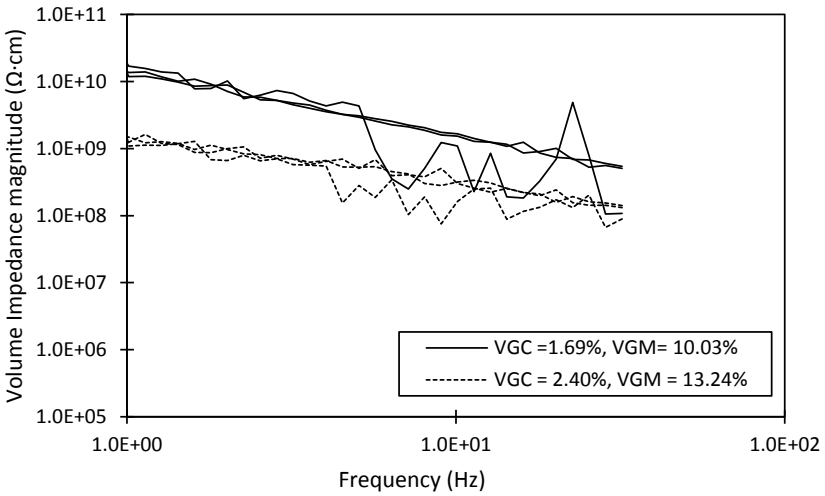


(a) Bode diagram of non-conductive concrete

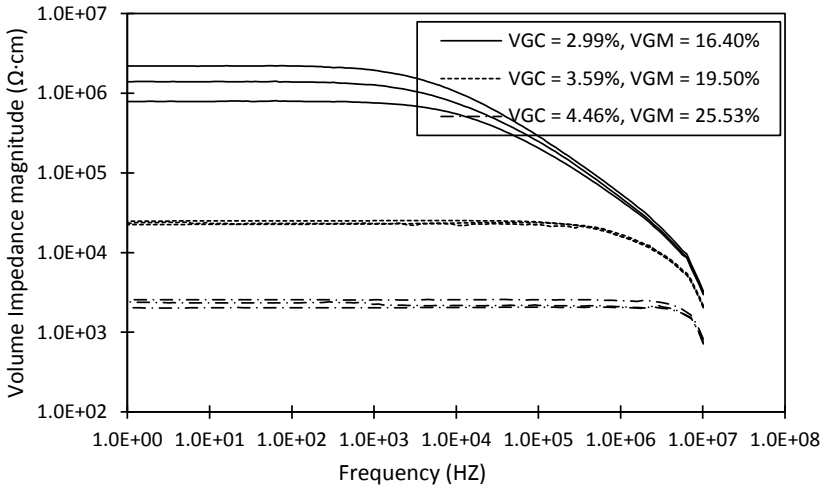


(b) Bode diagram of conductive concrete

**Figure 33. Bode Diagram of Asphalt concrete specimens including different graphite contents**

Figure 34 shows the impedance phase angle of asphalt concrete specimens. In common with asphalt mastics, low graphite contents have a considerable fluctuation, whereas higher graphite contents have a steady state at low frequency range. The phase angle of specimens containing 25.53% graphite by volume mastic has different feature, comparing with the result of asphalt mastic. As shown in Figure 30 (b), positive phase angle is measured at high frequency in highest graphite content of asphalt mastic specimen ($V_{GM}$ = 22.54%). Positive phase angle is not seen in highest graphite content of asphalt concrete specimen ($V_{GC}$ = 4.46%, $V_{GM}$ = 25.53%) in spite of more graphite content in $V_{GM}$ . This implies that aggregates affect the electrical impedance phase angle and magnitude. It also proved that positive phase angle is related to an inductor component in electrical equivalent circuit, comparing between Figure 31 (f) and Figure 35 (e). As higher conductive composites, an inductor component is seen generally in an equivalent circuit. This, moreover, demonstrates that the function of an inductor can be shown to adjust the change of an electrical current according to a current intensity.

Figure 35 shows the Nyquist diagrams of asphalt concretes containing various graphite amounts. Along with the results of asphalt mastics, the non-conductive asphalt concretes show irregular trend in Figure 35 (a)-(b), while the conductive asphalt concretes have relatively accurate shape of curves in Figure 35 (c)-(e). As explained the above, in asphalt concrete, positive imaginary impedance, which is related to an inductor component, is not existed in highest graphite content ($V_{GC}$ = 4.46%, $V_{GM}$ = 25.53%). The data density of a plot, also, is proved to have similar aspect with the result of asphalt mastic specimens.

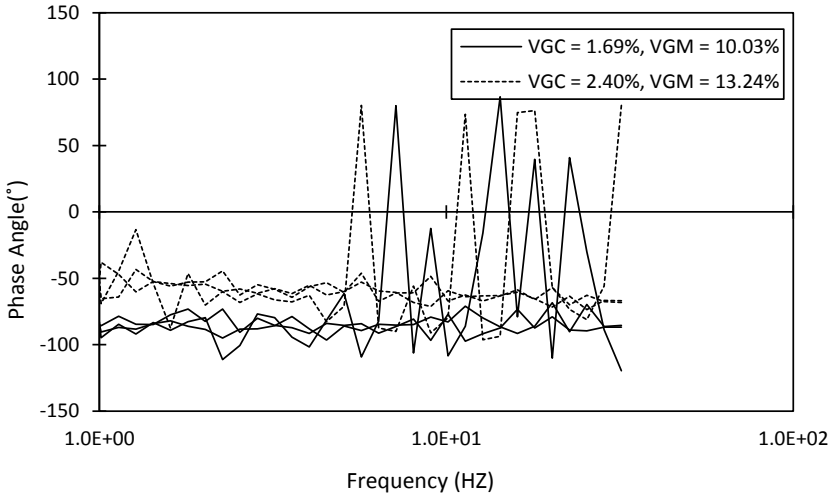


(a) Phase Angle of non-conductive concrete

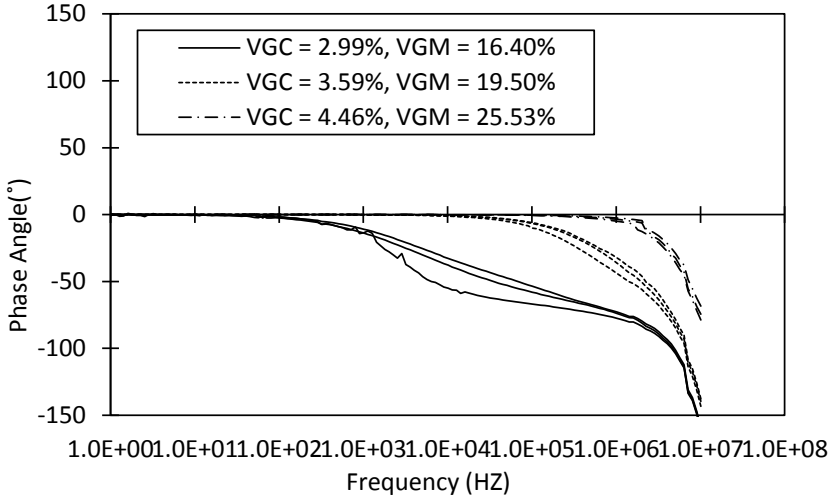


(b) Phase Angle of conductive concrete

**Figure 34. Phase Angle of Asphalt concrete specimens including different graphite contents**

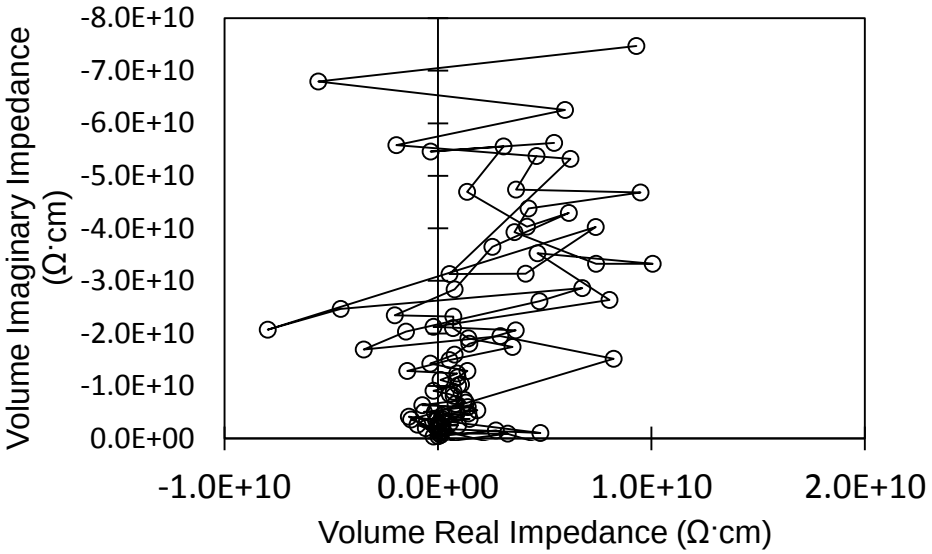


(a) $V_{GC}$ = 1.69% ($V_{GM}$ = 10.03%)

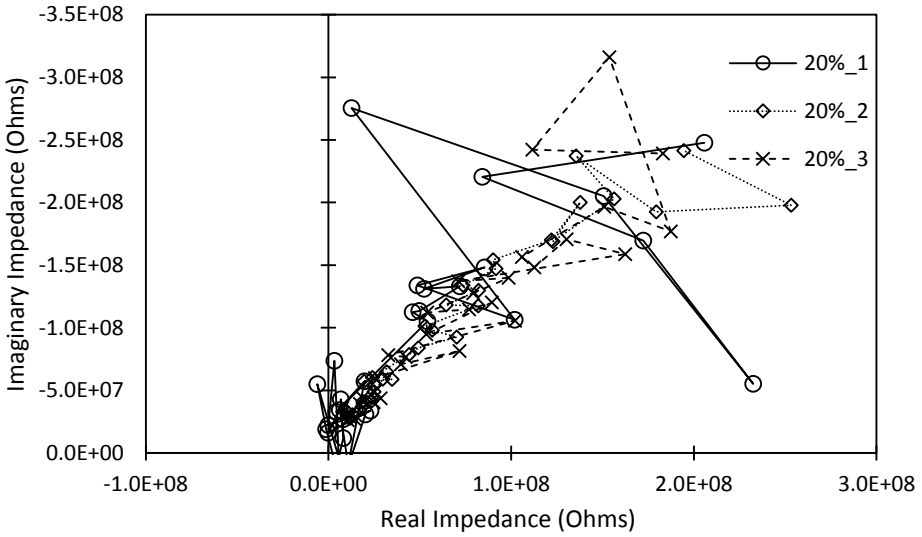


(b) $V_{GC}$ = 2.40% ($V_{GM}$ = 13.24%)

**Figure 35. Nyquist diagram of asphalt concrete specimens including different graphite contents**

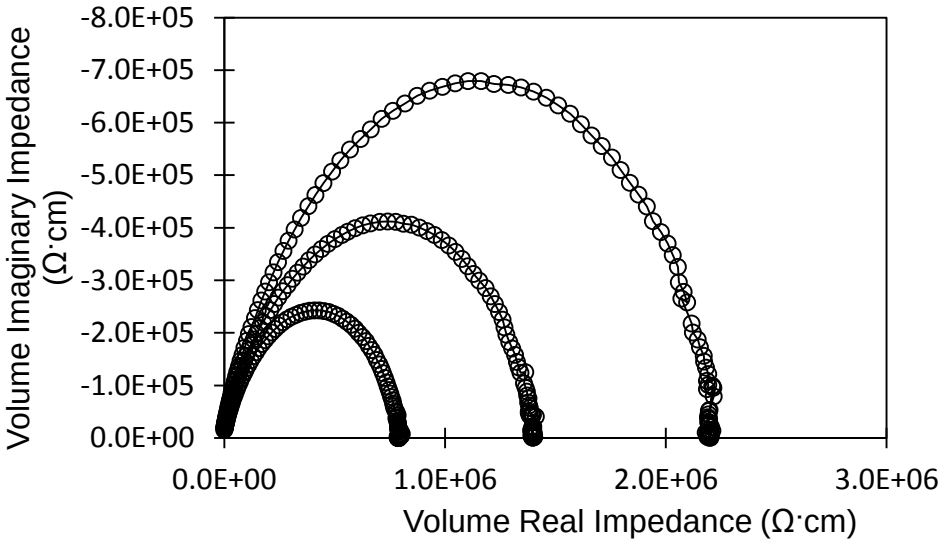


(c) $V_{GC}$ = 2.99% ($V_{GM}$ = 16.40%)

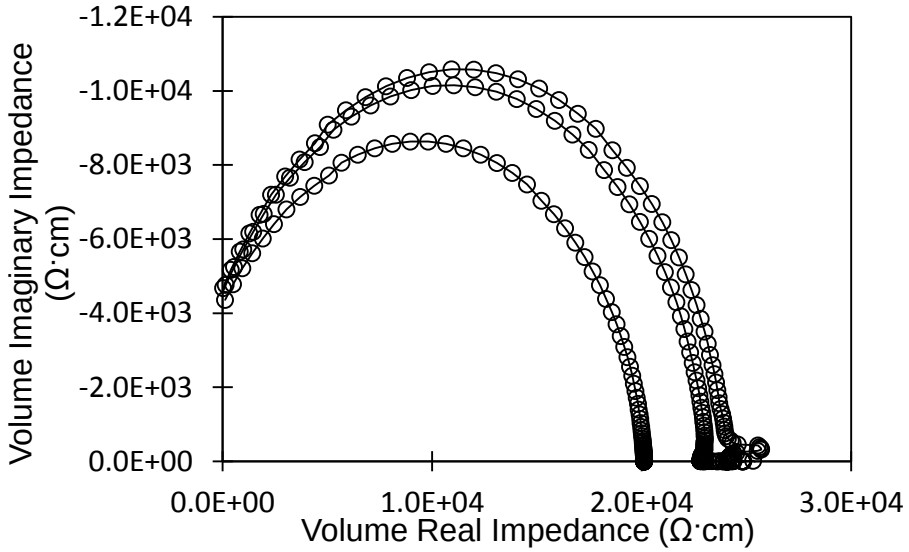


(d) $V_{GC}$ = 3.59% ($V_{GM}$ = 19.50%)

**Figure 35. Continued**

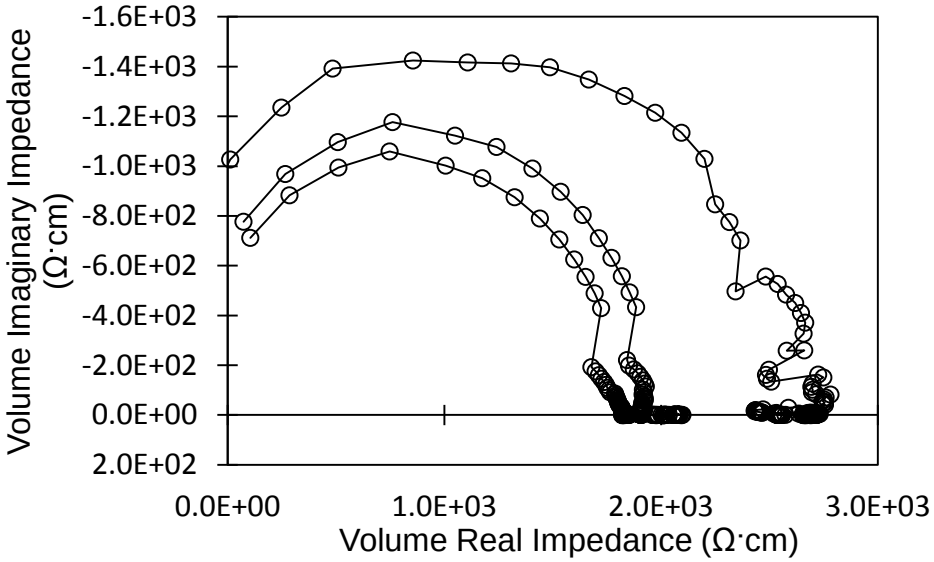


(e) $V_{GC}$ = 4.46% ($V_{GM}$ = 25.53%)

**Figure 35. Continued**

### 4.5.2 Effect of Temperature

Figure 36 shows the comparison among the experimental results of specimens with different temperatures. In the case of the graphite contents 2.99% by total mixture volume ($V_{GM}$ = 16.40%), the electrical impedances of conductive asphalt concretes increase as the temperature increase. By previous researchers, the opposite phenomenon was observed that the electrical resistivity of conductive cement concrete decreased as the temperature increased. Two causes of the alternation of the electrical resistivity depending on increasing of the temperature are existed: 1) as the temperature increases, the average distance between the conductive particles in the mixture increases because of thermal expansion of the mixture, and 2) as the temperature increases, the electrons movement in

the specimens are more energized in compliance with an electrical current. The first explanation indicates that the electrical resistivity of the mixture is sensitive to the volume change, implying the possibility of use the conductive asphalt composites for strain sensing. As shown in Figure 36, in the case of conductive asphalt concrete, the change of electrical impedance was affected by thermal expansion of the asphalt binder, whereas, in conductive cement concrete, it is presumed that the changes in the movement of electrons depending on different temperatures affect may be an important element to affect the electrical resistivity.

Figure 37 shows the change rate of electrical impedance components, which are volume real impedance, volume imaginary impedance, and volume impedance magnitude, depending on the increase of the temperature. As the temperature increases, relative values of all impedance components also increase as a logarithmic scale. Among the conductive asphalt composites, the specimens containing lower graphite content are more sensitive to the alternation of temperature than higher graphite content. This implies that the specimens beyond percolation threshold are beneficial to use a thermistor.

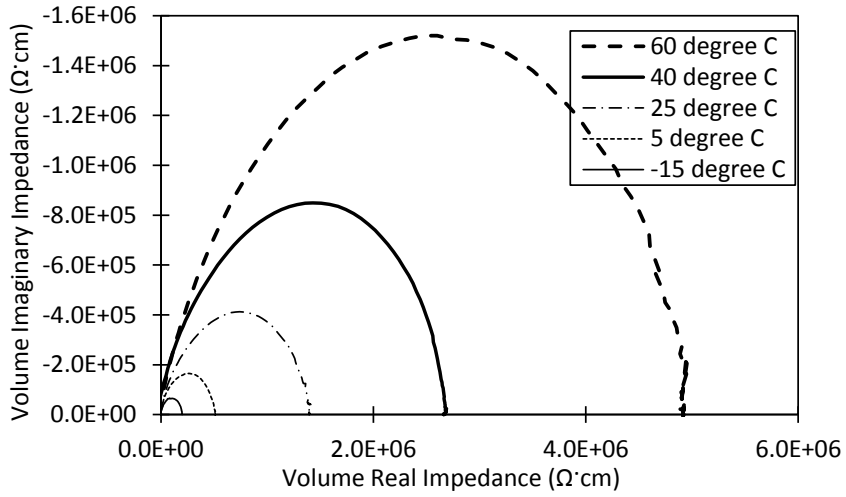


(a) Nyquist Diagram

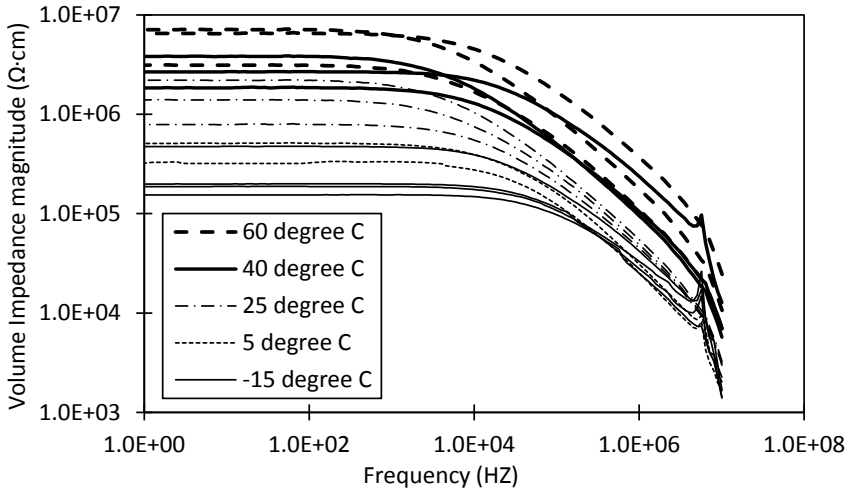


(b) Bode Diagram

**Figure 36. Temperature effect of Asphalt concrete specimens $V_{GC}$ = 2.99% ($V_{GM}$ = 16.40%)**

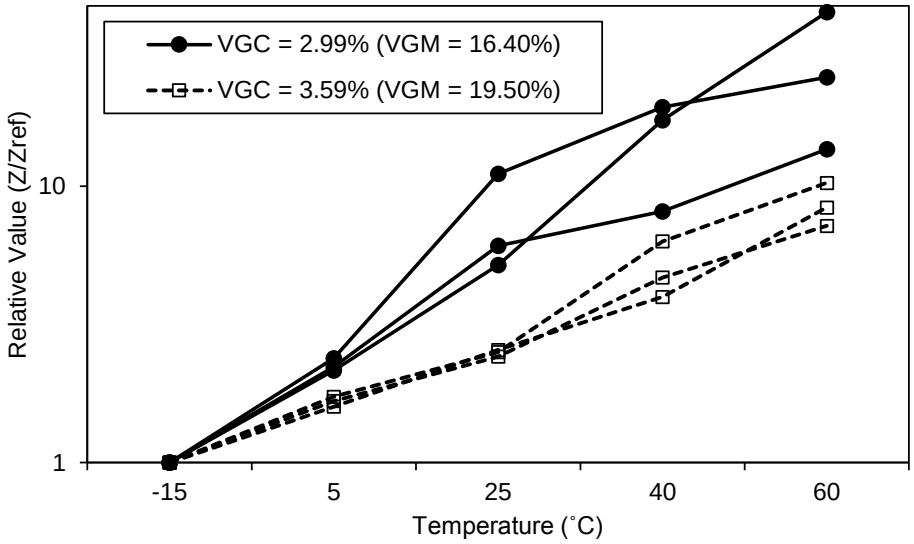


(a) Volume real impedance

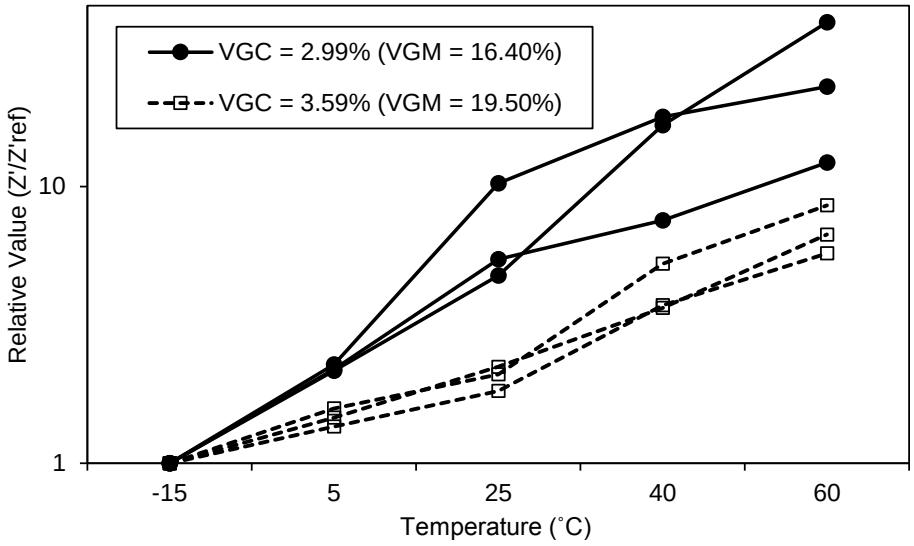


(b) Volume imaginary impedance

**Figure 37. Temperature effect of Asphalt concrete specimens $V_{GC}$ = 2.99% ($V_{GM}$ = 16.40%)**

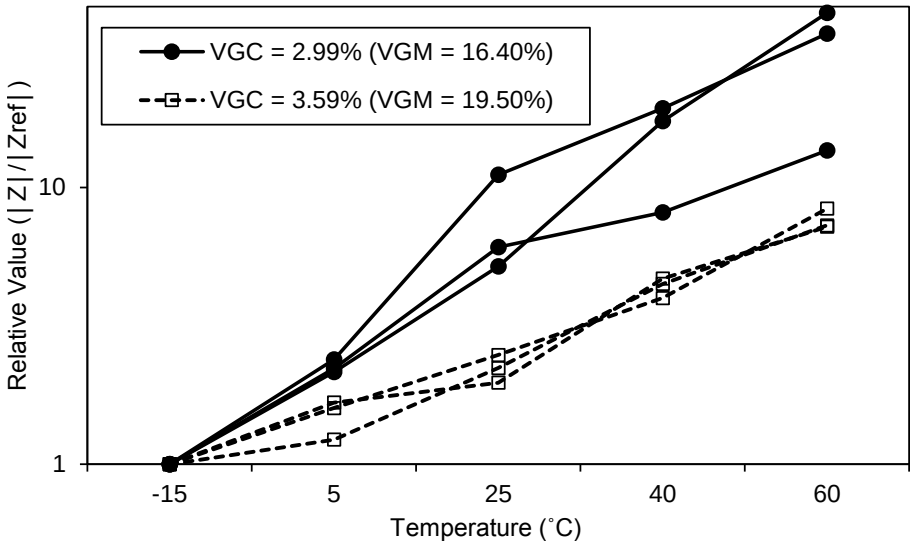


(c) Volume impedance magnitude

**Figure 37. Continued**

## Table 8. Values of All Impedance Components with Various Temperatures

| Temperature | Specimen | Graphite content | $V_{GC}$ = 2.99% ($V_{GM}$ = 16.40%) | | | | | | $V_{GC}$ = 3.59% ($V_{GM}$ = 19.50%) | | | | | |
|---|---|---|---|---|---|---|---|---|---|---|---|---|---|---|
| | | | Volume Real impedance (Ω·cm) | Relative value | Volume Imaginary impedance (Ω·cm) | Relative value | Volume Impedance magnitude (Ω·cm) | Relative value | Volume Real impedance (Ω·cm) | Relative value | Volume Imaginary impedance (Ω·cm) | Relative value | Volume Impedance magnitude (Ω·cm) | Relative value |
| 60 ˚C | 1 | | 3,156,155 | 13.62 | -921,500 | 12.22 | 3,157,461 | 13.63 | 87,218 | 7.20 | -35,347 | 5.73 | 87,412 | 7.21 |
| | 2 | | 4,956,877 | 24.84 | -1,519,444 | 22.95 | 7,178,001 | 35.97 | 81,448 | 8.38 | -30,519 | 6.71 | 81,454 | 8.38 |
| | 3 | | 6,619,510 | 42.73 | -2,001,178 | 39.24 | 6,619,805 | 42.73 | 82,358 | 10.28 | -35,269 | 8.56 | 82,494 | 7.29 |
| | Average | | 4,910,847 | 25.13 | -1,480,707 | 23.06 | 5,651,755 | 28.92 | 24,766 | 2.49 | -10,016 | 2.03 | 24,386 | 2.21 |
| 40 ˚C | 1 | | 1,880,657 | 8.12 | -568,551 | 7.54 | 1,880,740 | 8.12 | 56,669 | 4.68 | -22,966 | 3.72 | 56,794 | 4.69 |
| | 2 | | 3,856,802 | 19.33 | -1,182,235 | 17.86 | 3,859,260 | 19.34 | 38,673 | 3.98 | -16,562 | 3.64 | 38,737 | 3.99 |
| | 3 | | 2,688,615 | 17.36 | -849,211 | 16.65 | 2,688,718 | 17.36 | 50,597 | 6.32 | -21,668 | 5.26 | 50,681 | 4.48 |
| | Average | | 2,808,691 | 14.37 | -866,666 | 13.50 | 2,809,573 | 14.38 | 24,766 | 2.49 | -10,016 | 2.03 | 24,386 | 2.21 |
| 25 ˚C | 1 | | 1,411,329 | 6.09 | -412,065 | 5.46 | 1,411,913 | 6.09 | 29,324 | 2.42 | -11,256 | 1.83 | 23,868 | 1.97 |
| | 2 | | 2,216,553 | 11.11 | -679,445 | 10.26 | 2,217,965 | 11.11 | 24,850 | 2.56 | -10,157 | 2.23 | 24,120 | 2.48 |
| | 3 | | 803,699 | 5.19 | -242,970 | 4.76 | 803,735 | 5.19 | 20,123 | 2.51 | -8,635 | 2.10 | 25,169 | 2.23 |
| | Average | | 1,477,194 | 7.56 | -444,827 | 6.93 | 1,477,871 | 7.56 | 24,766 | 2.49 | -10,016 | 2.03 | 24,386 | 2.21 |
| 5 ˚C | 1 | | 514,840 | 2.22 | -164,879 | 2.19 | 514,849 | 2.22 | 20,251 | 1.67 | -8,372 | 1.36 | 20,251 | 1.67 |
| | 2 | | 476,705 | 2.39 | -150,569 | 2.27 | 476,723 | 2.39 | 15,501 | 1.60 | -6,647 | 1.46 | 15,501 | 1.59 |
| | 3 | | 334,132 | 2.16 | -110,070 | 2.16 | 334,152 | 2.16 | 13,882 | 1.73 | -6,504 | 1.58 | 13,882 | 1.23 |
| | Average | | 441,892 | 2.26 | -141,840 | 2.21 | 441,908 | 2.26 | 16,545 | 1.66 | -7,174 | 1.45 | 16,545 | 1.50 |
| -15 ˚C | 1 | | 231,739 | 1.00 | -75,416 | 1.00 | 231,739 | 1.00 | 12,120 | 1.00 | -6,166 | 1.00 | 12,120 | 1.00 |
| | 2 | | 199,561 | 1.00 | -66,208 | 1.00 | 199,569 | 1.00 | 9,715 | 1.00 | -4,549 | 1.00 | 9,719 | 1.00 |
| | 3 | | 154,909 | 1.00 | -50,997 | 1.00 | 154,914 | 1.00 | 8,009 | 1.00 | -4,121 | 1.00 | 11,310 | 1.00 |
| | Average | | 195,403 | 1.00 | -64,207 | 1.00 | 195,407 | 1.00 | 9,948 | 1.00 | -4,945 | 1.00 | 11,050 | 1.00 |

### 4.5.3 Effect of Moisture

In a wet condition, the surface of the specimens is dry but the inner portions are saturated with tap water. This condition is called saturated surface dry (SSD). The Nyquist diagram and the equivalent circuit in a wet condition, in contrast with dry condition tests, have a different pattern and elements in the circuit because of the water, as displayed in Figure 38 (a) and (b). This is a traditional response from a porous ionic conductor and is similar to previous researches studied on a cement paste. Figure 38 (a) shows that the Nyquist diagram is composed of a semi-circle arc and a straight line. A linear portion in low frequencies may be evaluated as the response from the specimen-electrode interface and a charging effect related to ions movement of water. The semi-circle in high frequencies represents the response from bulk specimens similar to the dry condition tests as Figure 35 (c). The equivalent circuit in Figure 38 (b) is made up of these two components. The resistance ($R_{st}$) is obtained from a measurement of ionic conduction effects through the continuously water-filled capillary pores between electrodes. This implied that the capacitance ($CPE_W$) is related to a charging effect of ion's movement in moisture of asphalt concrete specimens.

Figure 40 illustrates the differences of conductive asphalt concrete with two ambient conditions, which are dry condition and wet condition with salt water (3.5% salt by water weight). As explained the above and shown in Figure 38, the comparison confirms that moisture in specimens affects the results of ACIS. As well as the resistance and the capacitance in bulk specimens, another resistor and a capacitor, which are electrical components in water, provide the linear tail trend in low frequencies. In the case

of salt water, the principle ions in mature specimens will be Na+ and OH- the for charge balance. These elements influence significantly that the radius of semi-circle decrease dramatically because of sodium ions (Na+) and chlorine ions (Cl-).

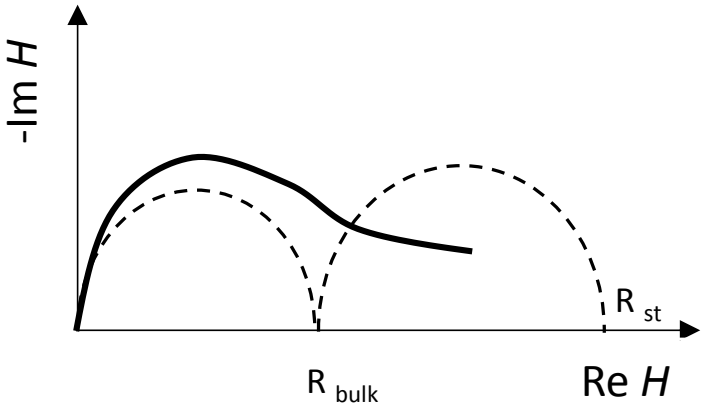


(a) Nyquist diagram in wet condition

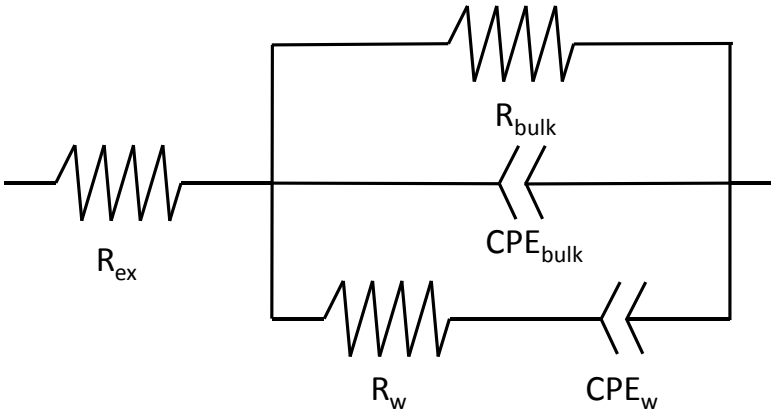


(b) Equivalent circuit in wet condition

**Figure 38. Wet condition of asphalt concrete specimens**

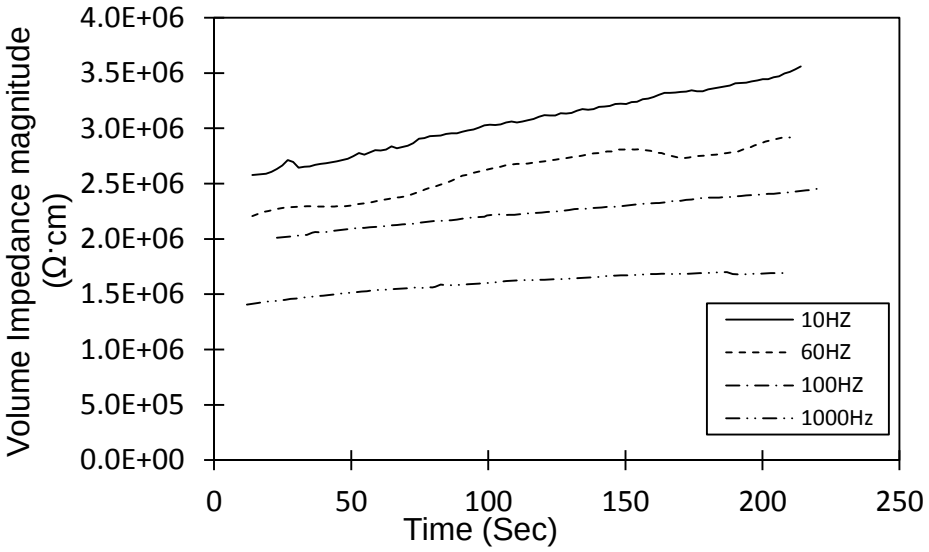


**Figure 39. Impedance variation with time in wet condition of asphalt concrete specimens**

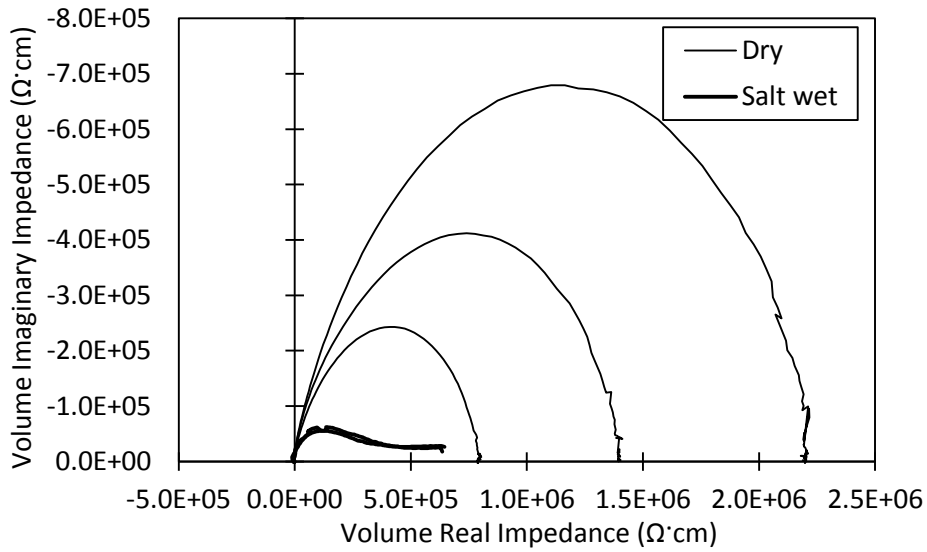


(a) Nyquist Diagram

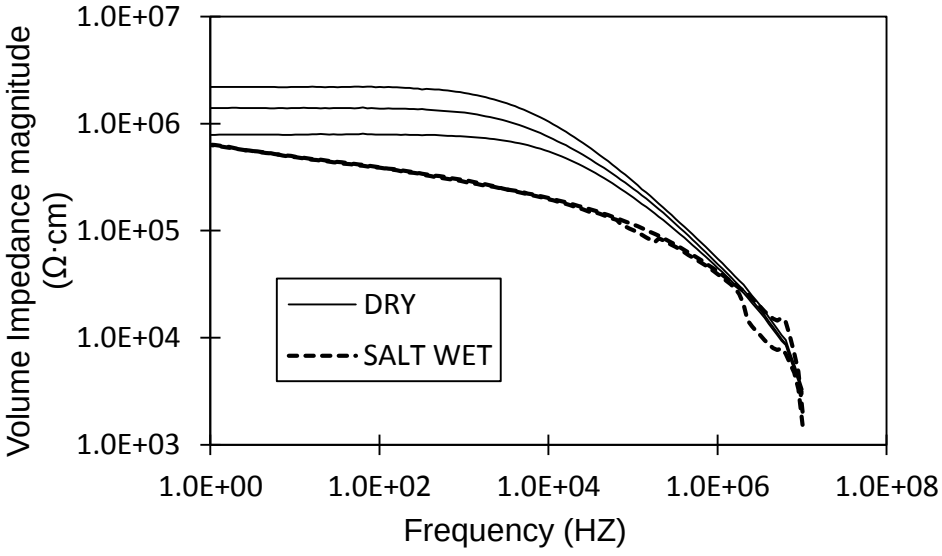


(b) Bode Diagram

**Figure 40. Moisture effect of Asphalt concrete specimens ($V_{GC}$ = 2.99%)**

### 4.5.4 Size Effect

Two size specimens were utilized to investigate the characterization of electrical properties in conductive asphalt concrete. The small cylindrical specimens with 2.54 cm diameter and 8 cm height were used to determine the electrical characters of the asphalt concrete adding various graphite contents and the effect of temperature. For making the bigger size specimens, cylindrical asphalt concrete with a 150 mm diameter and 95 mm height were compacted by gyration until 4% percent air void was reached. The test specimen was cut to make four samples with fan shape for investigating the effect of different graphite contents, the effect of various temperatures, and the effect of moisture. The size of specimens makes different patterns of Nyquist diagrams with an existence or nonexistence of negative real impedance. This implies that the more graphite contents and smaller specimens may have negative real impedance because of more conductive specimens. Therefore, the selection of the proper size of specimens can be important to gauge several effects, which are studied in previous chapters, in conductive asphalt concrete.

## 4.6 Conclusions

This research investigates the electrical characterization of conductive asphalt concretes containing various amounts of conductive additives, the effect of different temperature, the effect of moisture in test samples, and size effect in test samples. The electrical characteristics of the conductive asphalt concrete were evaluated through ACIS analysis. The findings of the study are summarized as follows:

- The mastic and concrete test results illustrate that electrical characterization of conductive asphalt composites influenced by the graphite contents. The Nyquist diagram, Bode diagram, and phase diagram show the different results according to graphite contents by ACIS. Based on these results, the electrical equivalent circuit is made by electrical components, which are a resistor, a capacitor, and an inductor, to understand the electrical characteristics in conductive asphalt composites.
- In Nyquist diagram, the data density in the diagram varies with the graphite content. With low graphite content, the Nyquist diagram is distributed uniformly. High graphite content, however, causes the Nyquist diagram to be cornered at a specific local part. Well-distributed impedances like proper content ($V_{GM}$ = 16.40%) are more beneficial that multifunctional applications of conductive composite can be used by utilizing the whole frequency range of AC.
- The alternation of the electrical resistivity depending on increasing of the temperature are existed. In the case of conductive asphalt concrete, the change of electrical impedance was affected by thermal expansion of the asphalt binder, whereas, in conductive cement concrete, it is presumed that the changes in the movement of electrons depending on different temperatures affect may be an important element to affect the electrical resistivity.

- The differences of conductive asphalt concrete with different ambient conditions, which are dry condition and wet condition with salt water (3.5% salt by water weight), are shown by the Nyquist diagrams. These results prove that the moisture and the salt are significant roles to change the components in electrical equivalent circuits.

These findings indicate that the electrical characterization of conductive asphalt composites can be determined by ACIS analysis. According to various graphite contents, the different equivalent circuits are obtained. The selection of a proper graphite content is critical in investigating the ACIS analysis of conductive asphalt composites. The findings of this research will provide fundamental knowledges for various applications of asphalt composites containing the electrical additives.

# 5. APPLICATION TO DAMAGE SELF-SENSING

## 5.1 Introduction

The application of ACIS for damage monitoring of electrically conductive cement composites has been tried by Peled et al. (2001). They investigated the correlation between electrical and mechanical properties of cement composites with conductive carbon fibers. The equivalent electrical circuit, constructed by the frequency dependent electrical properties, is useful to evaluate the damage of conductive cement concrete. While the potential drop method used only the static resistance value measured with DC to figure out the crack size, ACIS with AC frequency sweep has various benefits in examining the microstructural changes of materials by utilizing various electrical properties, such as the resistance, dielectric constant, and phase angle.

AC impedance spectroscopy has been widely used to detect micro cracks or damage in conducive composite materials. In the case of civil materials, the researches related to damage sensing by using impedance spectroscopy were limited for cement based composite material. The potential drop method is the primary method used to investigate the changes in the microstructure of cement composite materials. The change of only one parameter, resistance, was utilized and this limit indicated that the value of resistance increased during the test because of water polarization. The AC impedance spectroscopy may make up for the lack of methods that use DC resistance. This section investigates the feasibility of using AC impedance spectroscopy for damage sensing of asphalt concrete in various conditions or environments, such as specimens in dry and wet conditions.

This study aims at characterizing the characterize the electrical properties of conductive asphalt concrete with various conductive additive contents using ACIS and constructing the equivalent electrical circuit for conductive asphalt concrete with various conductivity for understanding the relationship between components and investigating the feasibility of multifunctional.

## 5.2 Materials and Test Methods

### 5.2.1 Materials and Sample Preparation

For the damage sensing tests, coarse aggregate, fine aggregate, and filler were used as before. Table 3 indicates the various physical properties of other materials which were used in the research.

The aggregate gradation used for the mixture is shown in Table 7 as before. The aggregate includes 35% crushed limestone (coarse aggregate), 60% river sand (fine aggregate) and 5% filler. The proportion of coarse and fine aggregates was selected to satisfy the mixture requirements specified in the ASTM 2001. The specific gravities of coarse aggregate, fine aggregates, and filler were measured as 2.57 g/cc, 2.63 g/cc, and 3.15 g/cc, respectively. The optimum binder content of the asphalt concrete was determined to be 4.8% by weight of the total mixture through the Superpave method. The specimen preparation and volumetric analysis were conducted in accordance with Superpave mixture design and ASTM standards. The aggregates and fillers were heated to 150 ºC for at least 24 hours to eliminate moisture, and the binder was heated for 2 hours to the same temperature prior to mixing. The fillers were combined with aggregates first, and then the binder was added. A mechanical mixer was used to stir the materials until the

aggregates and fillers were well-coated with the binder. The moisture was removed from the mixture in an oven at a compaction temperature of 135 ºC. For damage sensing tests, specimens with a 75 mm height, 500 mm width, and 500 mm length were made with a slab compactor. Slab samples, which had a 50 mm height, 50 mm width, and 200 mm length, were cut to investigate the changes in electrical properties caused by the increase in damages.

### 5.2.2 Test Method

The asphalt concrete specimens containing various graphite contents were conditioned at room temperature for 24 hours before testing. Damage sensing specimens consisted of a bulk sample with a crack and a surface electrode as shown in Figure 41 (a). Silver paste and copper tape were also used as electrodes. Various distances between two electrodes, long (200 mm), middle (130 mm), and short (65mm), were used to study the effects of the length sandwiched between them.

Complex impedance data were obtained in the range of 1 Hz – 32MHz by applying a small-amplitude, sinusoidal perturbation between the surface electrodes. Solartron 1260A and 1296 (Impedance/Gain Phase Analyzer) were used to operate a voltage input mode with a potential 0.1V held across the electrodes and the resulting displacement current was monitored. In a frequency sweep ranging from 1 Hz to 32,000,000 Hz, 20 spot data was gained per one decade (1 order).

(a) Asphalt concrete samples for damage sensing

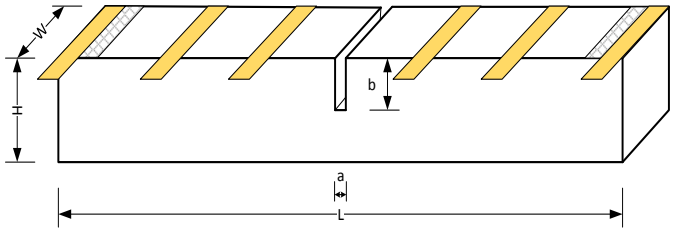


(b) Schematic drawing

**Figure 41. Experiment specimens**

## 5.3 Results and Discussions

AC impedance spectroscopy has been widely used to detect micro cracks or damage in conducive composite materials (Gu et al., 1993; Ozyurt et al., 2006; Park et al., 2006; Peled et al., 2001). In the case of civil materials, the researches related to damage sensing by using impedance spectroscopy were limited for cement based composite material. The potential drop method is the primary method used to investigate the changes in the microstructure of cement composite materials (ASTM International, 2011). The

change of only one parameter, resistance, was utilized and this limit indicated that the value of resistance increased during the test because of water polarization. The AC impedance spectroscopy may make up for the lack of methods that use DC resistance. This paper investigates how AC impedance spectroscopy may be significant in damage sensing in various conditions or environments, such as specimens in dry and wet conditions.

### 5.3.1 Dry Condition

As shown in Figure 41 (b), the damage sensing tests of conductive asphalt concrete were conducted by using rectangular specimens. Samples were tested with a number of damaged contents, within the range 0%-50% in a dry condition, and at a 25°C temperature. The resulting impedance plots are presented in Nyquist and Bode diagrams in Figure 25 (a) and (b). The data definitely show the damage dependence of the complex response over the considered damage content range. In general terms, increasing the damage results in a progressive displacement of the complex curve toward the end of x-axis as well as an increase in arc radii. The real and imaginary impedances are affected by damage contents at all frequency ranges to a greater or lesser extent. As shown in Figure 42 (a), there is a direct relationship between the AC impedance and damage contents. With an increase in the damage contents, the arc of the Nyquist diagram also increases because the conductive paths made by the graphite particles are reduced by the damage to the specimen. An increase in the resistance is observed on the specimen with more defects. The Nyquist diagram is not always an efficient way to display the resulting data related to the whole frequency range. In order to describe the response of the total frequency area, a Bode diagram is a proper way to explain the elements as a function of frequency as shown in

Figure 42 (b). In this diagram, resistive and capacitive parts are more easily recognized, as is frequency range, over which they dominate. To represent this point, the data in Figure 42 (a) are plotted in this form in Figure 42 (b), together with the modulus$|Z|$, which is defined as $\sqrt{R^2 + C^2}$. The frequency dependence of an impedance modulus over the seven decades of frequency is definitely obvious. In high frequency range (>100 kHz), an impedance modulus has difficulty in proving damage dependence according to a bulk resistance, whereas at lower frequencies, the damage dependence of an impedance modulus is attributable to a bulk resistance value.

In order to confirm the distance effect of electrodes, three distances for electrodes were applied to the same specimen as illustrated in Figure 41 (b). Figure 42 (c) indicates how the distance between electrodes results in an impedance value in a Nyquist diagram. Both the distance between electrodes and the damage content increase the diameter of an arc, that is, the growth of the resistance value of a bulk specimen. The longer the electrode distance, there is an increase of magnitude of the impedance response, and the area of the semi-circle is widened.

The characteristic of real impedance, $z'$, is plotted as a function of damage contents in Figure 42 (d). It is well known that the bulk resistance, $R_{bulk}$, can be related to its resistance with no damage. Compared to bulk resistance, the resistance value of damaged samples increases according to the growth of crack depth. Like a pattern of real impedance, the trend of imaginary impedance, $z"$, is designated as a function of damage contents in Figure 42 (e). Damage contents also influence the value of imaginary impedances across

the board. Imaginary impedance consists of resistance and capacitance as a parallel system and is defined by Equation (36).

$$Z = \frac{R}{1+\omega^2 R^2 C^2} - j\frac{\omega R^2 C}{1+\omega^2 R^2 C^2} \tag{36}$$

The capacitance becomes virtually independent of some damage contents (30, 40%), as shown in Figure 42 (f). In spite of that, the reason to increase an imaginary impedance is related to the square of a resistance. The capacitance value is governed by an interface between graphite particles rather than by a damage or a crack. The effect of the distance between electrodes is not clear, compared to a real impedance.

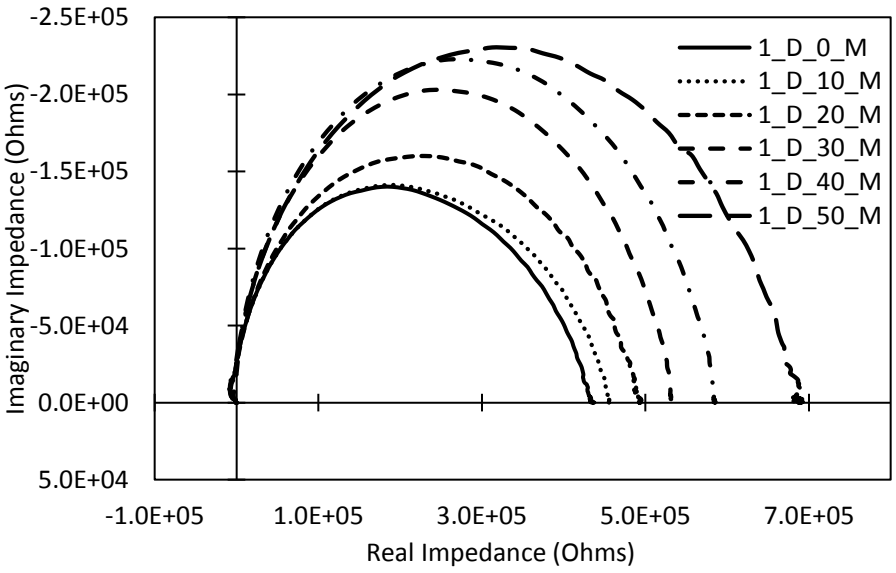


(a) Nyquist diagram (Middle distance between electrodes)

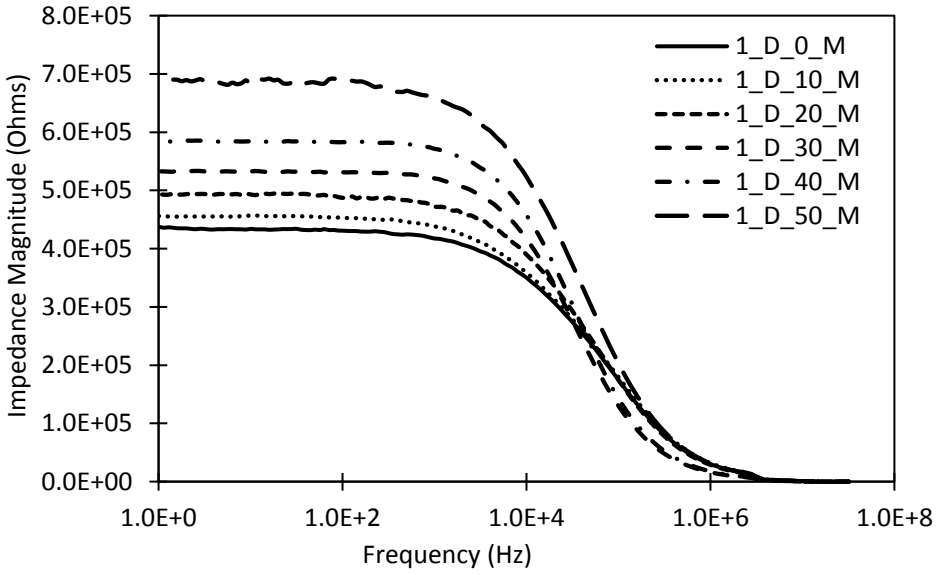


(b) Bode diagram (Middle distance between electrodes)

**Figure 42. AC Impedance spectroscopy with different damage contents for conductive asphalt concrete (Dry condition)**

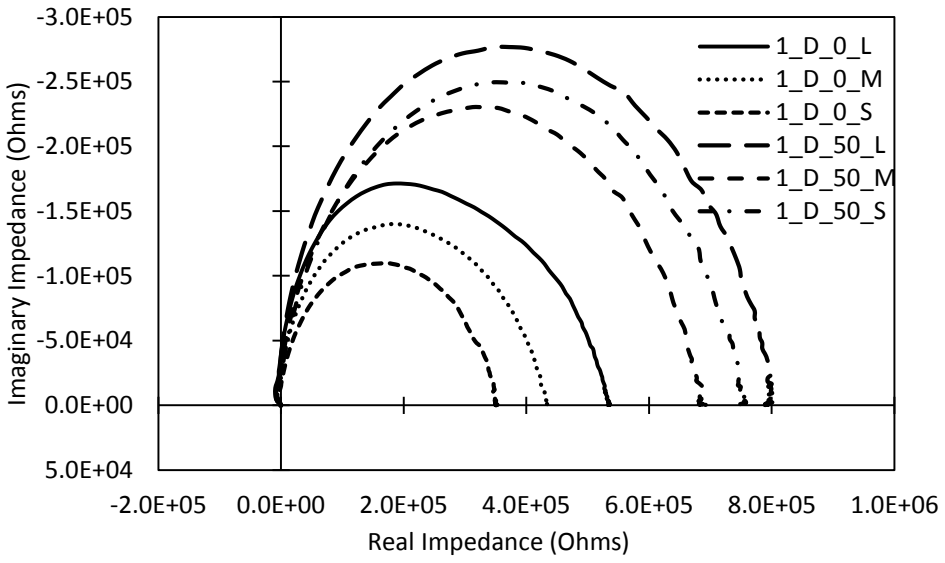


(c) Nyquist diagram (Short distance between electrodes)

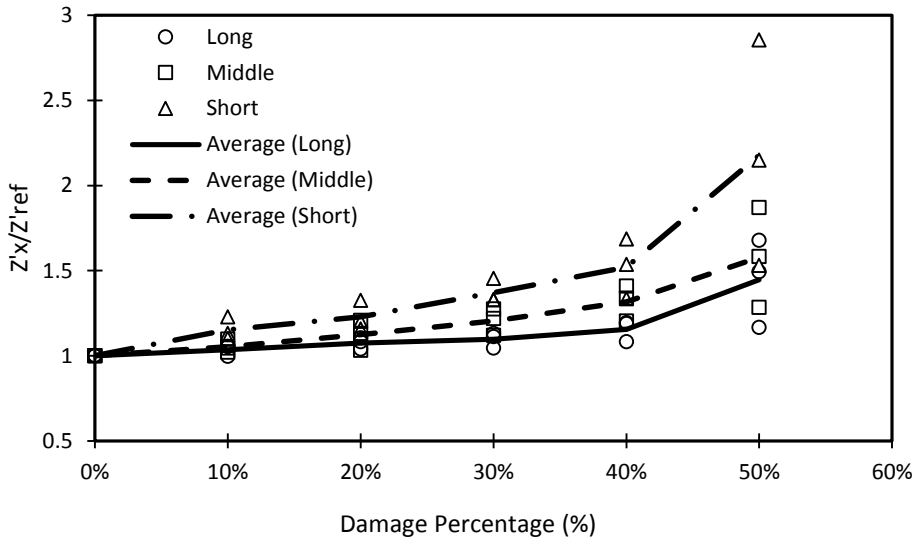


(d) Sensitivity of real impedance value

**Figure 42. Continued**

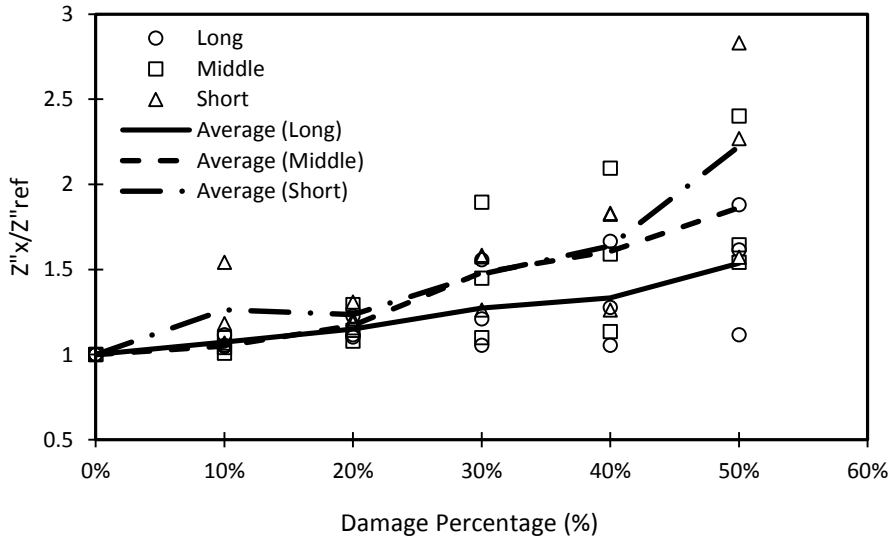


(e) Sensitivity of imaginary impedance value

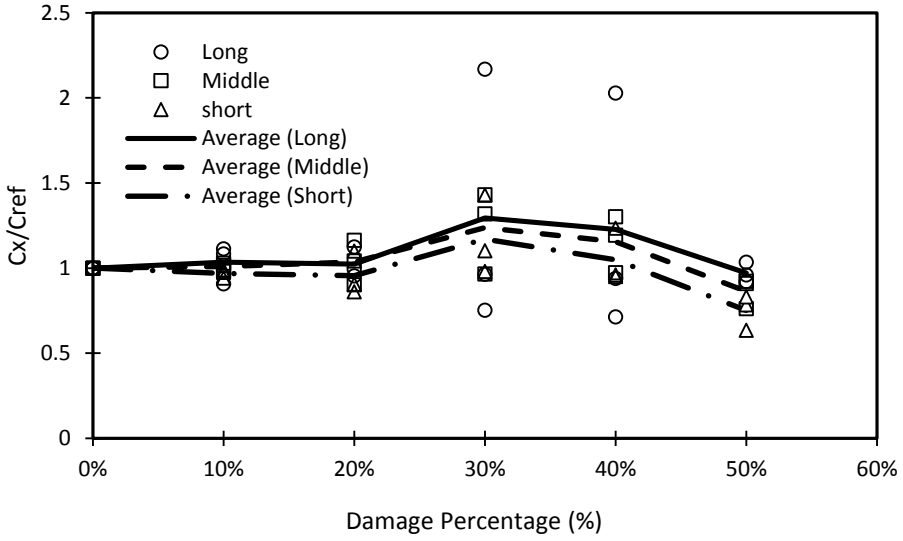


(f) Sensitivity of capacitance value

**Figure 42. Continued**

### 5.3.2 Wet Condition

In the case of the wet condition, like the dry condition tests, specimens were tested with a number of damaged contents and within the range 0%-50% in a dry condition at a 25°C temperature. In a wet condition, however, the surface of the specimens are dry but the inner portions are saturated with pure water. This condition is called saturated surface dry (SSD). The Nyquist diagram and the equivalent circuit in a wet condition, in contrast with dry condition tests, have a different pattern and elements in the circuit because of the water, as displayed in Figure 43 (a) and (b). This is a traditional response from a porous ionic conductor and is similar to previous researches done on a cement paste. Figure 43 (a) shows that the Nyquist diagram is composed of a semi-circle arc and a straight line. The low frequency linear portion is evaluated as that area of the response from the specimen-electrode interface and displays part of a much larger semi-circle at a low frequency range. The high frequency arc represents the response from bulk specimens similar to the dry condition tests. The equivalent circuit in Figure 43 (b) is made up of these two components. The low frequency resistance ($R_{st}$) is a measurement of ionic conduction effects through the continuously water-filled capillary pores between electrodes. In the case of salt water, the principle ions in mature specimens will be Na+ and OH- the for charge balance. The polarization is quantified by the capacitance of the specimen. In the case of asphalt concrete specimens, on the other hand, unlike conduction, the movement of charges is blocked or hindered because the water ions within isolated capillary cavities are blocked by asphalt binder or aggregates and the activated ions in pure water don’t move along the applied electric field.

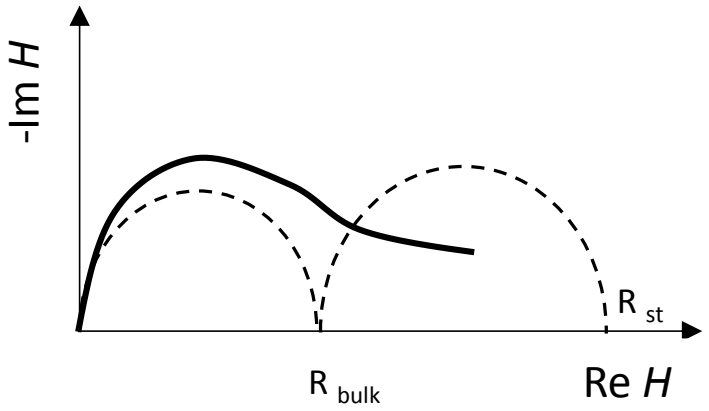


(a) Nyquist diagram

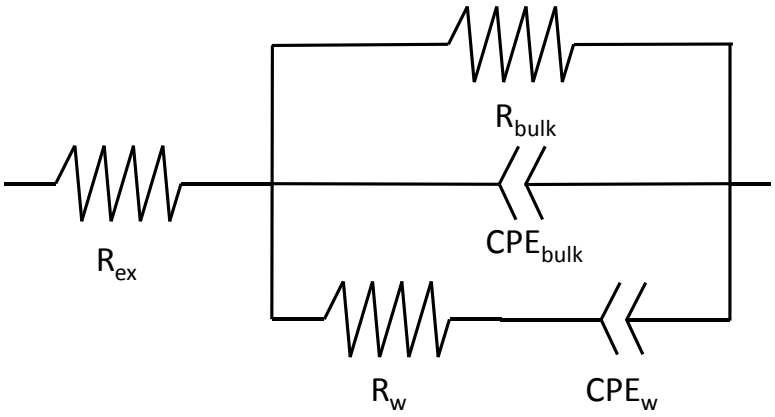


(b) Schematic representation of electrical equivalent circuit

**Figure 43. Conductive asphalt concrete in a wet condition**

The ionic conduction and polarization phenomena in wet condition tests are mostly determined by the water of the pores in the samples. These mechanisms show that increasing damage content results in the reduction of ionic conduction and an increase in the polarization effect as shown in Figure 44 (a) and (b). As confirmed in Figure 44 (a),

the real and imaginary impedance are affected by the damage at all frequency ranges to a greater extent, in a way similar to the dry condition tests. The low frequencies associated with the polarization effect increases as the depth of the damage increases and the high frequencies related to the bulk impedance response increase. The Bode diagram in Figure 44 (b) shows that an increase in the impedance modulus $|Z|$ indicates an increase in the crack depth and a decrease in the frequency. Compared to dry condition tests, the distance effect between the electrodes is displayed in Figure 44 (d), (e), and (f). As damage uniformly increases, however, there is a proportional increase in the ratio of real and imaginary impedance, as illustrated in Figure 44 (d) and (e). The capacitance is more independent in a dry condition because the presence of water may result in a uniform increase in the value of the capacitance in areas damaged by water. AC impedance spectroscopy, therefore, is more accurate for damage sensing in a real environment associated with wet conditions than in a laboratory associated with dry conditions.

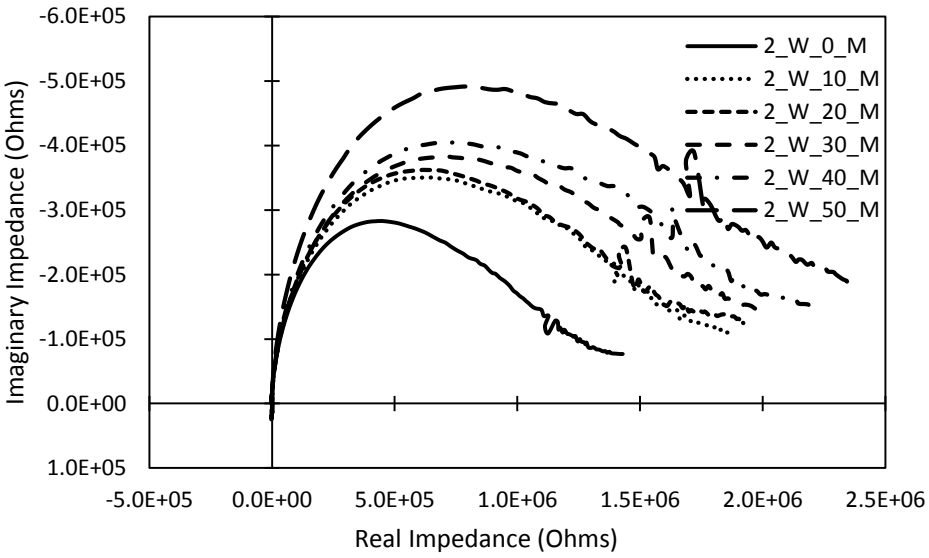


(a) Nyquist diagram (Middle distance between electrodes)

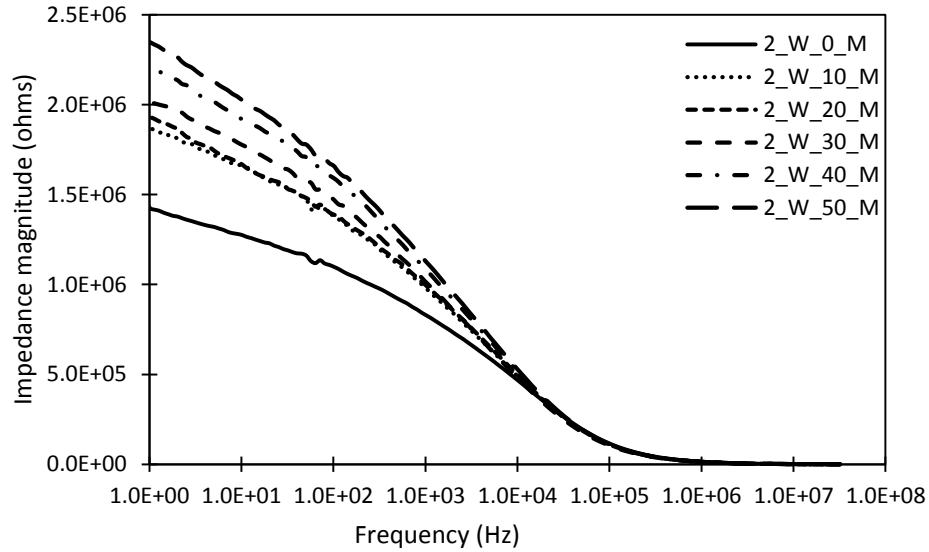


(b) Bode diagram (Middle distance between electrodes)

**Figure 44. AC Impedance spectroscopy with different damage contents for conductive asphalt concrete (Wet condition)**

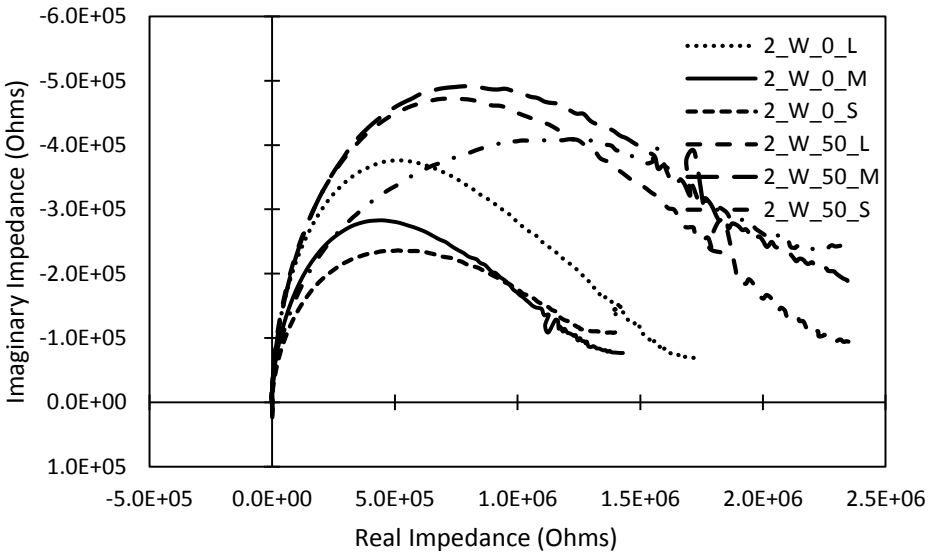


(c) Nyquist diagram (Short distance between electrodes)

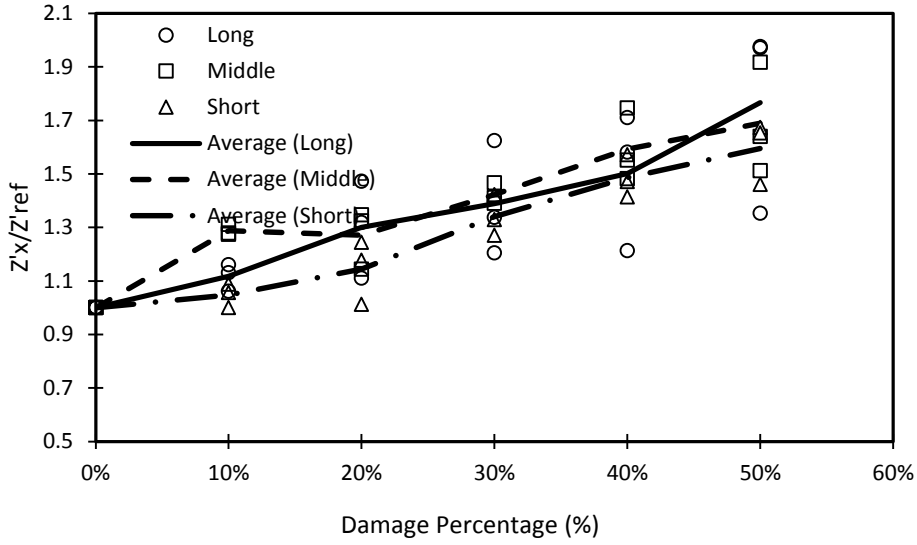


(d) Sensitivity of real impedance value

**Figure 44. Continued**

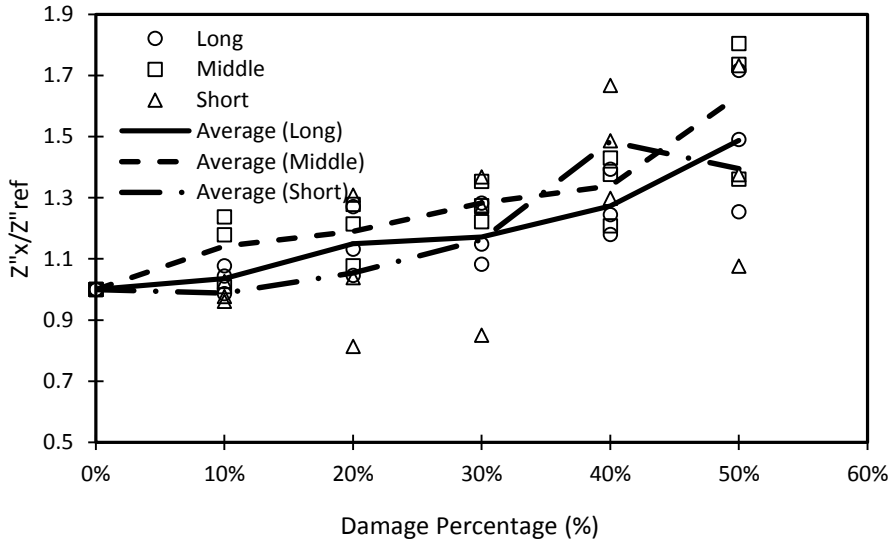


(e) Sensitivity of imaginary impedance value

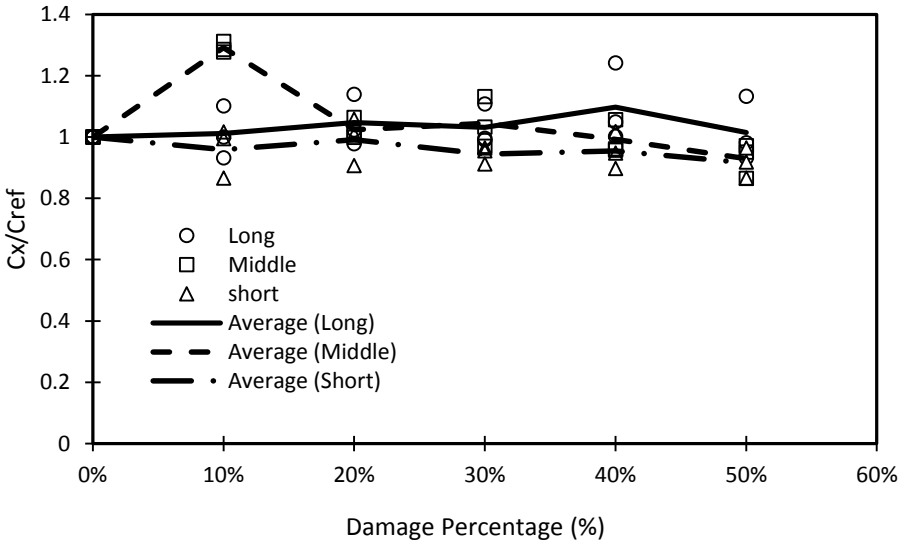


(f) Sensitivity of capacitance value

**Figure 44. Continued**

## 5.4 Conclusion

The effects of damage sensing on conductive asphalt concrete were investigated in this study by using AC Impedance spectroscopy (ACIS).

Major findings from the study are:

- For damage sensing tests, well-distributed data is more useful for distinguishing damage content through the whole frequency range. A 25% graphite by weight content was selected as the material with which to perform damage sensing tests on conductive asphalt concrete.
- In the case of a dry condition, as the damage in specimens increased, real impedance and imaginary impedance also increased. For the change in capacitance, however, there was no benefit in studying the damage content.
- The distance between electrodes can be important for measuring damage with ACIS. A dry condition, however, is more useful than a wet condition. It has been proven that humidity or environmental conditions affect the sensitivity of the length between electrodes as well as the change in impedance value.
- In a wet condition, the impedance response in various degrees of damage (0%-50%) was found to be more proportionally sensitive than the response in a dry condition and was affected by the polarization of water within isolated pores that hindered the movement of a charge or the mobility of ions.

AC impedance spectroscopy is an important way to determine the damage in asphalt concrete specimens in both dry and wet conditions. For damage sensing in a real

environment, AC impedance spectroscopy may be more accurate than is the potential drop method (DC resistance) that is widely used as the ASTM standard.

# 6. APPLICATION TO SNOW AND ICE REMOVAL

## 6.1 Introduction

### 6.1.1 Background

The primary function of animal skin is to protect organs and muscles, but it has additional functions such as self-sensing, self-healing, and temperature control. Inspired by biomaterials, the concept of multifunctional materials has attracted attention since 2000 with the increasing demand for sustainability in polymers (Gibson 2010) and cement concrete (Chung 2003). Multifunctional materials are structural materials that have nonstructural functions beyond traditional structural functions (Nemat-Nasser et al. 2005). Such nonstructural functions can be obtained by manipulating the thermal, electrical, and chemical properties of traditional materials. Multifunctional materials have enormous potential for a wide range of real-life applications that can improve the efficiency and safety of daily lives.

Asphalt mixture is a prevalent paving material that covers 94% of more than 4.2 million kilometers of paved roads in the United States (NAPA 2009). Asphalt mixture is a non-conductive composite material by nature, but its electrical conductivity can be improved by using conductive additives (Huang et al. 2009; Garcia et al. 2009; Wu et al. 2012; Rew et al. 2017). By controlling the conductivity, a number of non-structural inquiries can be developed. The multifunctional asphalt concrete has strong possibilities that can lead to sustainable pavement systems. The concept of electrically conductive asphalt concrete was initiated by Minsk (Minsk 1968; 1971), and this topic has gained attention in the last decade. Since then, various conductive additives, such as steel fiber,

carbon black, graphite powder, and carbon fiber, are used to impart electrical conductivity into asphalt concrete. The probable multifunctional applications of conductive asphalt concrete are deicing, self-healing, self- sensing, and so on (Park 2012; Park et al. 2014).

In the regions of cold climate, a great number of traffic problems occur due to snow and ice on pavements. Traffic accidents and human injuries due to the loss of skid resistance make the deicing a critical safety issue on roads. Kuemmel (1994) estimated the direct cost to be $11 billion (manpower, materials, and equipment) and the indirect cost to be $21 billion (environmental effects due to the use of chemical agents) for removing snow from the 75-mile-long highway around Lake Tahoe for 25 years. The use of deicing agents and mechanical method (snow plowing) are traditional ways of removing ice and snow on the roadway, but those methods are not perfect solutions. Chemical agents bring corrosion of vehicles, destruction of the vegetation, and pollution of ground and water (Williams et al. 2000; Wang et al. 2006). In addition, the chemical agents have a limit in the applicable temperature range, e.g. sodium chloride does not work well below -3.9°C (Löfgren 2001; Sanzo et al. 2006). The mechanical methods, such as vehicle with large plow or shovel, require high maintenance costs and cause traffic delays. Moreover, the mechanical methods do not completely remove the snow and ice, and cause damage on the pavement surface (Nixon 1993).

As one of the emerging solutions, the heated pavement gains attention in recent years. The heated pavement is a snowmelt system by heating the pavement. The heating system includes the pre-installed hydronic heating pipes (Lee et al. 1984; Chen et al. 2011; Lee et al. 2010), electrical coils (Henderson 1963; Lee 2012), conductive carbon fiber

tapes (Yang et al. 2012), infrared heat lamp (Zenewitz 1977), and microwave (Hopstock and Zanko 2005). As compared in Lee (2012), the heated pavement system is very effective in snow removal, free from traffic delays and pollution of ground water, and does not have a limitation in the applicable temperature range. However, their widespread use is hindered by expensive installation cost and short service life. According to Lee (2012), installation cost for the electric coil is $ 160,000 for 300 m road, and the electric coils are easily broken under repeated traffic loads. Alternative idea to overcome these shortages is to make the paving material itself to be electrically conductive and to use it as a heating layer. Recent studies on the multifunctional construction materials suggested to use conductive cement concrete (Yehia and Tuan 2000; Heymsfield et al. 2014) and conductive hot mix asphalt (Zaleski et al. 1998; Wu et al. 2012; Rew et al. 2017) as the heating layer. The conductive heating layer containing conductive fiber/filler are cheaper than the coil or pipe installation, and do not lose its conductivity at damaged conditions (Chen et al. 2012; Xiangyang and Yuxing 2010). Considering these previous investigations, it is obvious that the heated pavement is an effective and green way of snow removal, and the use of the conductive asphalt/concrete significantly reduces the cost of installation and maintenance. On the other hand, the comparative investigations for the operation cost, environmental impact, and design optimization have not been conducted yet.

### 6.1.2 Research Objectives

The objective of this study is to optimize the structural design of the heated layer through non-steady state heat transfer analysis and to evaluate environmental, economic,

and social impacts of the heated pavement system through the life-cycle assessment (LCA). In this study, flake type graphite powder is used as a conductive additive to impart conductivity into asphalt concrete. The electrical and thermal properties of the conductive asphalt concrete are evaluated, and a bench scale slab heating test is conducted to verify heating capability of the conductive asphalt concrete. Then, the variation of energy consumption with the structural design is investigated through non-steady state heat transfer simulation using the electrical and thermal properties measured from the material tests. The optimum location and thickness of the conductive layer are determined from the heat transfer simulation. The economic, social, and environmental impacts of the heated pavement are quantitatively evaluated through the LCA, and are compared to the traditional deicing method.

## 6.2 Literature Reviews

One of the major issues in modern societies was to improve the transportation safety under freezing and/or snowy weather. Removing snow and ice, especially on highway and bridge surfaces, is a crucial step to enhance transportation safety. Deicing agents such as salt or sand can be used to remove ice from pavement (Blackburn 2004). Both inorganic salts and organic compounds would chemically prevent water molecules from binding, therefore decreasing the freezing point. Among the various agents, sodium chloride (salt) is the most widely used around the world because it is inexpensive and efficient. However, deicing chemicals have negative impacts including metal corrosion and environmental pollution. These problems are paid much attention by International

Energy Agency (IEA) and World Health Organization (WHO) (Lofgren 2001; Sanzo and Hecnar 2006).

Zhao and Zhang (2011) added certain proportion of chloride into asphalt mixture, and created a chloride-stored asphalt concrete to help pavements to delay or even prevent from ice formation. According to their investigation, the stored chloride could be released effectively, and contribute to a better pavement anti-icing ability. Meanwhile, the mechanical performance of chloride asphalt concrete was also improved. However, the chloride salts accelerate metal corrosion and will cause damages to roads and bridges. Organic compounds do not cause corrosion and pollution, but their applications are limited because of the high prices, and sometimes they will cause refreezing phenomenon.

Porous asphalt pavement is an environmentally friendly choice to help with deicing. According to Houle et al. (2009), Porous asphalt pavement had a very good performance in northern climates. The porous pavement surface not only be faster to remove ice and snow, but also have a better friction resistance than conventional pavements.

Another interesting investigation was carried out in China by Chen and Li (2013). They used fracture mechanics theory to study ice layer failure. They assumed that the cracking of ice layer is initiated and propagated under repeated traffic load, and ice failure occurs when the cracking density reaches a certain limit. In their research, crumb rubber was added to decrease the modulus of asphalt concrete, and hence the pavement had a larger deformation under the same traffic loading. Both simulation and experiment results indicated that the ice layer is broken more easily under the larger deformation. Therefore,

the use of the crumb rubber in asphalt concrete improves the ability of ice and snow removal on the pavement.

Deicing by heating the pavement, which is called 'heated pavement', is one of the idea that is actively investigated in recent years. As was mentioned earlier, using of conductive asphalt concrete was suggested by Minsk (1968), and investigated by Zaleski et al. (1998), Xiangyang and Yuxing (2010), and Chen et al. (2012). A similar idea with cement concrete pavement was studied by Yehia and Tuan (2000), Ziegler (2013), and Heymsfield et al. (2014). Other methods of the heated pavement are using cable installation (Henderson 1963), Carbon tape (Yang et al. 2012), and pipe installation (Lee et al. 1984; Mallick et al. 2009; Lee and Correia 2010). A research team from China suggested a concept of asphalt solar collector (ASC) that would be beneficial for melting snow and ice on pavement surfaces during winter. Wu et al. (2008), Wu et al. (2009), and Chen et al. (2011) conducted a series of studies on ASC. They suggested to install pipes circuits below an asphalt pavement surface to absorb and transfer solar energy during summer. Graphite powder was utilized to improve thermal conductivity of the pavement. The stored energy is used not only to melt the snow and ice on the road, but also to provide heat to the adjacent buildings during winter time.

The recent novel approaches for pavement deicing are summarized in Table 9.

**Table 9. Recent novel methods of pavement deicing**

| Citation | Method | Major Conclusions |
|---|---|---|
| Zhao and Zhang (2011) | Create chloride-stored asphalt concrete | Stored chloride could be released effectively, contributing to better anti-icing ability. Mechanical performance was improved. |
| Houle et al. (2009) | Porous asphalt pavement | The pavement surface was faster to clear snow and ice. A better friction resistance was obtained. |
| Chen (2013) | Add crumb rubber | Decreased modulus resulted in larger deformation, which was conductive to ice layer failure. |
| Minsk (1968; 1971) Zaleski et al. (1998) Xiangyang and Yuxing (2010) Chen et al. (2012) | Conductive asphalt | Imparting electrical conductivity into asphalt pavement, and supplying electrical power to heat the pavement. |
| Yehia and Tuan (2000) Ziegler (2013) Heymsfield et al. (2014) | Conductive concrete | Imparting electrical conductivity into concrete pavement, and supplying electrical power to heat the pavement. |
| Yang et al. (2012) | Carbon tape | Installation of carbon tape below a pavement surface layer and supplying electrical power to heat the pavement. |
| Henderson (1963) | Electric coil installation | Installation of conductive coils below a pavement surface layer and supplying electrical power to heat the pavement. |
| Lee et al. (1984) Mallick et al. (2009) Lee and Correia (2010) Wu et al.(2008) Wu et al. (2009) Chen et al.(2011) | Pipe installation | Pipe circuits absorbed and transferred solar energy during summer and restored in winter Graphite powder increased thermal conductivity of pavement, improving efficiency of the asphalt collector |

## 6.3 Simulation of Deicing System for Airfield Application

This chapter investigated the effects of electric heating on the pavement temperature distribution. A numerical analysis based on a finite difference method of heat transfer was performed to estimate the amount of electrical power and corresponding cost for keeping an airfield runway above the freezing temperature.

### 6.3.1 Description of Model

The electric heating system using conductive asphalt is well suited with the concept of perpetual pavement having multiple hot-mix-asphalt layers. Perpetual pavement is a long life asphalt pavement, which has a structural life excess of 50 years with periodic replacement of thin surface layer. Usually, hot-mix- asphalt structure of perpetual pavement is consist of three layers: a rut resistant, impermeable, and wear resistant surface layer, a rut resistant and durable intermediate layer, and a fatigue resistant and durable bottom layer (Newcomb et al. 2001). As illustrated in Figure 45, the suggested study aims to install the conductive layer between the multiple layers to add anti-freezing function to the perpetual pavement.

A one-dimensional pavement heat transfer model was established to evaluate the effects of electric heating on the pavement daily temperature variation and temperature profile. An airport runway with a length of 3000m and a width of 46m was assumed. As a simple case, the pavement was considered as a full-depth asphalt pavement with 28 cm thick asphalt layer on top of 300 cm thick subgrade. An electrically conductive sub-layer modified by graphite (4.8 vol. %) was embedded in the middle of asphalt layer, and served

as a heating layer by supplying electrical power. Figure 46 displays the airport runway information for simulation model. The heat transfer simulation was conducted for a winter day having the highest and lowest air temperature are -1°C and -7°C, and the costs for electrical power were calculated for various thicknesses of the surface and conductive layers.

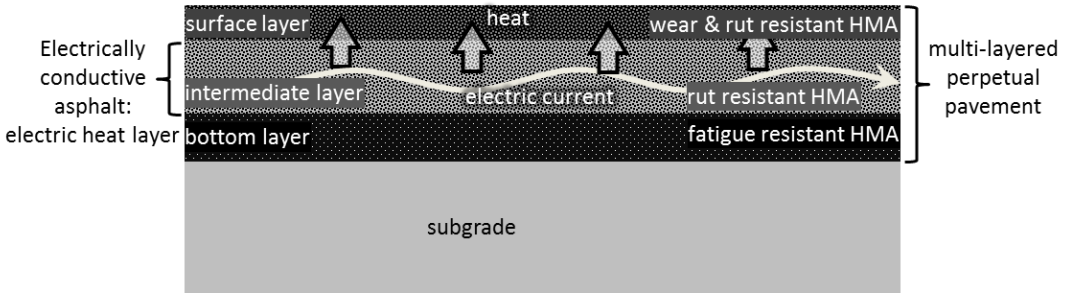


**Figure 45. Structural design of perpetual pavement containing electrically conductive asphalt layer**

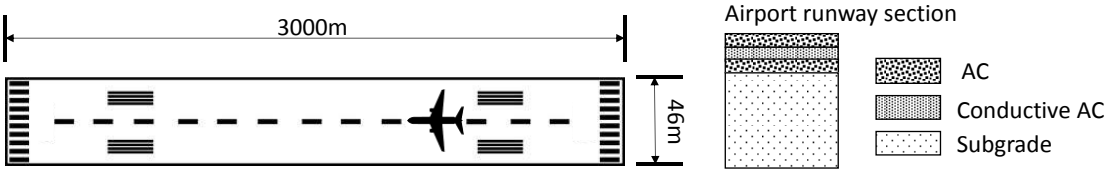


**Figure 46. Simulation model of airport runway**

### 6.3.2 Heat Transfer Model

The heat transfer model used finite difference approximation method to calculate the pavement temperature variations and temperature profile during 24-hours (from 0:00 to 24:00). The pavement is modeled as a semi-infinite solid, and heat conduction only occurs in vertical direction. Since electrical heating is a typical loss of electrical energy, all the electric energy are assumed to be converted into heat. The generated heat can be calculated by Joule's Law as shown in Equation (37).

$$\boldsymbol{P = UJ = \frac{U^2}{\rho}} \tag{37}$$

Within the pavement domain, the heat flows in non-steady state condition. Combining the electrical heating with the heat equation yields Equation (38);

$$\frac{\partial \boldsymbol{T}}{\partial \boldsymbol{t}} - \frac{\boldsymbol{k}}{\boldsymbol{C_v}}\left(\frac{\partial^2 \boldsymbol{T}}{\partial \boldsymbol{z}^2}\right) - \frac{\boldsymbol{P}}{\boldsymbol{C_v}} = 0 \tag{38}$$

Where,

P: Energy generated by the electric heat ($W/m^3$)

$C_v$: Volumetric Heat Capacity ($J/m^3 \cdot K$)

k: Thermal Conductivity ($W/m \cdot K$),

u: magnitude of the electric field (V/m)

$\rho$: Electrical resistivity ($\Omega \cdot m$)

J: magnitude of the current density ($A/m^2$), $J = \lim_{A \to 0} \frac{I(A)}{A}, J = \frac{U}{\rho}$

Figure 47 shows the pavement model for the heat transfer analysis. The boundary conditions on pavement surface include a solar radiation, heat convection, and emission.

The solar radiation is the major heat source of pavement system. A wind speed was a parameter to calculate the heat convection. The difference between the air temperature and pavement surface temperature is used to compute the heat convection and emitted radiation. At the bottom of the subgrade layer (328 cm from the pavement surface), a constant temperature is assumed during the analysis period (one day).

*Simulation Input*

In this model, the solar radiation, wind speed and air temperature at each hour are major climate inputs, which are obtained from the environment Canada Weather station in Fredericton, New Brunswick.

**Table 10. Thermal properties of the pavement**

| Layer | Thermal Conductivity ($\mathbf{W/m \times K}$) | Volumetric Heat Capacity ($\mathbf{MJ/m^3 \times K}$) | Other Properties |
|---|---|---|---|
| Plain Asphalt Concrete | 1.936 | 1.807 | Absorptivity:0.9<br>Emissivity:0.85 |
| Graphite Modified Asphalt Concrete | 2.768 | 1.895 | Electric Resistivity: 1.4726 Ω*m |
| Subgrade | 1.000 | 2.850 | |

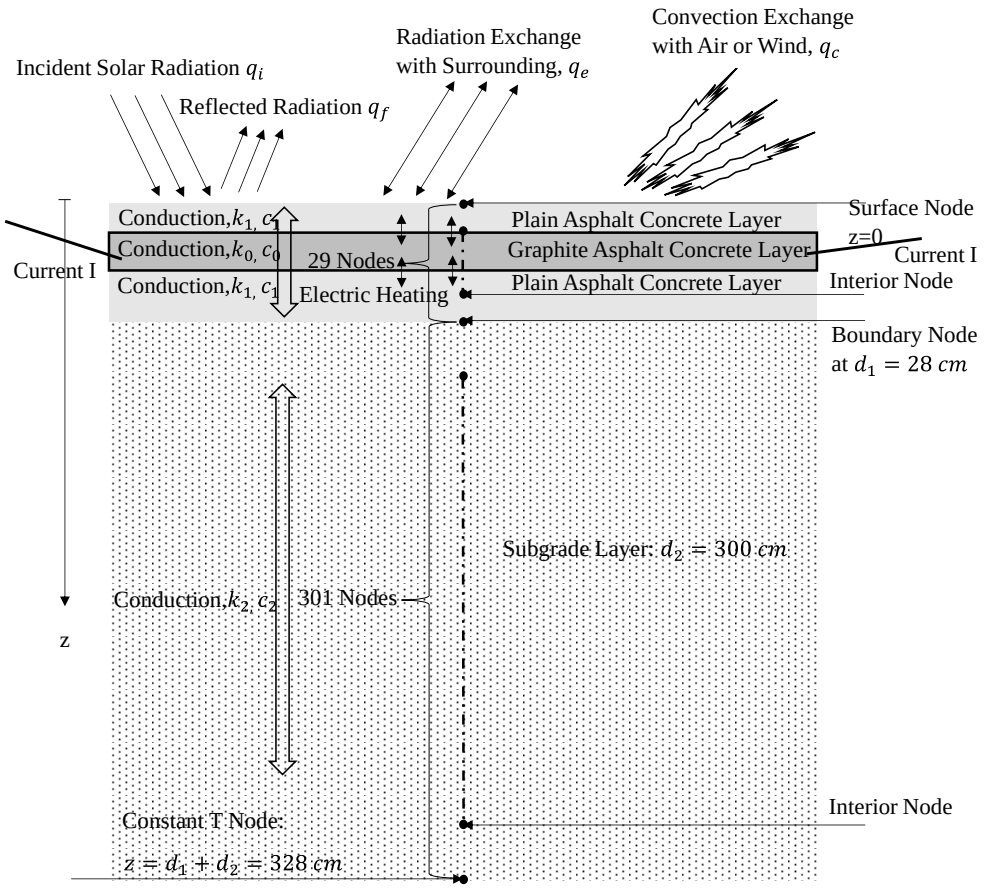


**Figure 47. Computational pavement model**

The required material properties for the heat transfer analysis are the absorptivity ($\alpha = 1 - \beta$) and emissivity (e) of the surface layer and thermal conductivity (k) and volumetric heat capacity (c) of all layers. The electrical resistivity of graphite modified asphalt concrete was obtained from the experiments conducted in this study (described in the next section). A summary of all the materials properties is listed in Table 10.

Because of the lacking of the field data, the initial temperature gradient for the simulation is assumed in reasonable manner after reviewing the temperature gradient data at other locations, and the constant temperature at the bottom of subgrade is assumed as 5.04°C.

The parameters to find a cost effective pavement structure containing the conductive layer are: thickness of the surface layer, thickness of the conductive layer, and electrical resistivity of the conductive layer.

*Prediction Procedure*

The numerical analysis was carried out using the finite discrete method (Hermansson 2001; Gui et al. 2007). The model was constructed in Matlab code, the flowchart of the simulation is shown in Figure 48. A 1 cm nodal intervals in z-direction of the pavement and a 12 second time increment was used in the simulation. All the results were obtained by running 10 iterations.

Because the major task for this simulation is to evaluate the costs for heating conductive layer for deicing, the pavement surface temperature is controlled to keep higher than a certain temperature T above freezing temperature (0°C) during the whole 24 hours. This is done by tracking the surface temperature and turning on/off the electric heating system, i.e., when the pavement surface temperature exceeds T, the electric heating stops, and when the surface temperature drops below T, the heating start.

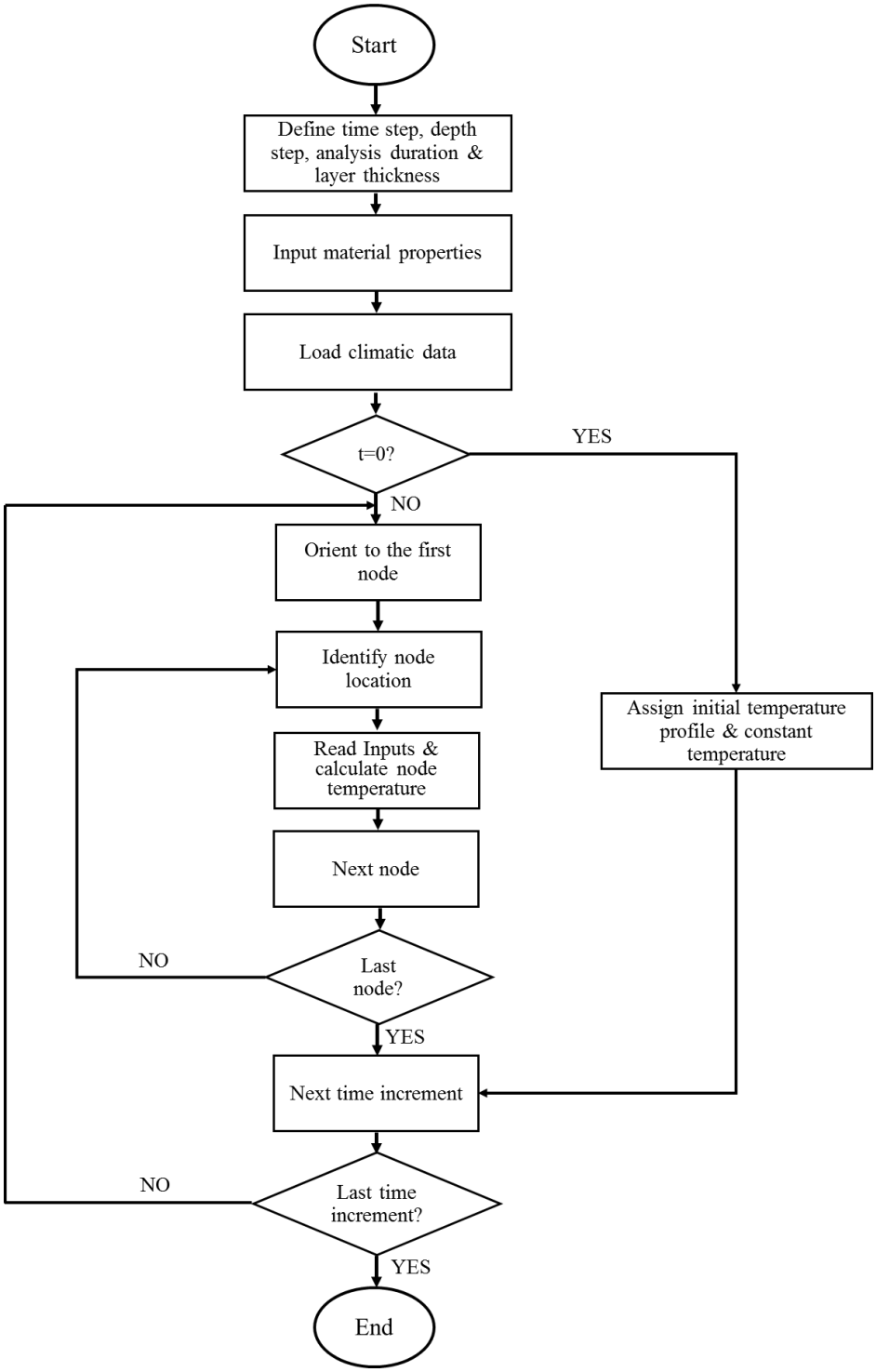


**Figure 48. Pavement simulation flow chart (Xijun 2014)**

### 6.3.3 Simulation Result

*Temperature distribution of pavement without conductive sub-layer*

As a control case, 24-hour temperature variations at surface, 5cm depth, and 20cm depth of the plain pavement (without conductive sub-layer) are calculated as shown in Figure 49. The temperature at pavement surface is more sensitive to the solar radiation (solar radiation) than the air temperature. The maximum pavement surface temperature is observed at 13:00pm while the minimum temperature occurred at 7:00am. The peak temperatures occur with delay as the depth increases. The solar radiation (sunlight) is strongest at 11:00 am. The pavement surface temperature starts increasing with the sunrise (7:00 am), and exceeds the freezing temperature from 10:00 am. The pavement surface temperature reaches the peak at 1:00 pm, and drops below 0°C at 5:00 pm. Assuming the melting point of the ice as 0°C, the electric heating is needed during 5:00 pm to 10:00 am.

The temperature profile (temperature gradient along the depth) of the plain pavement is plotted in Figure 50.

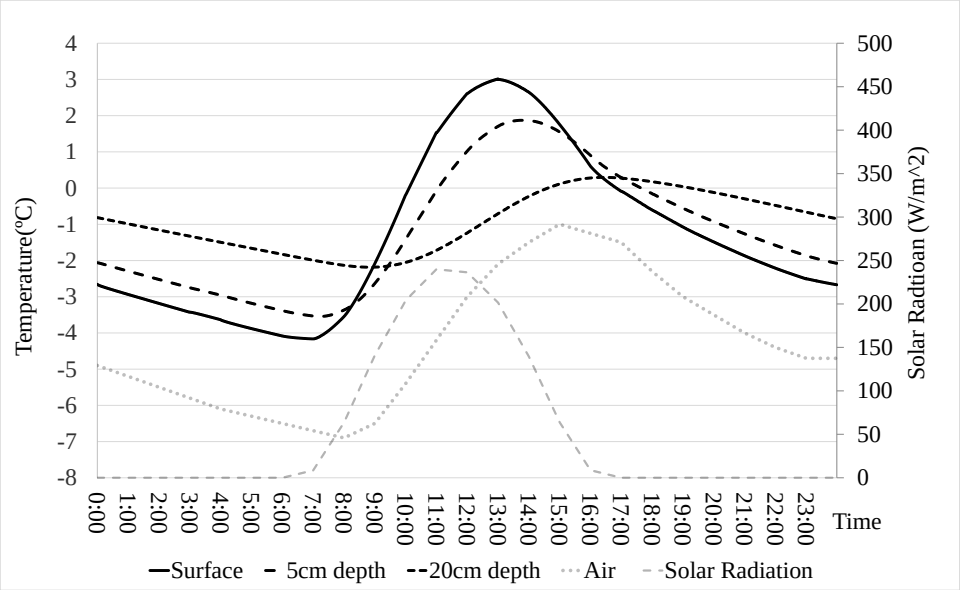


**Figure 49. 24-hour temperature variation during winter**

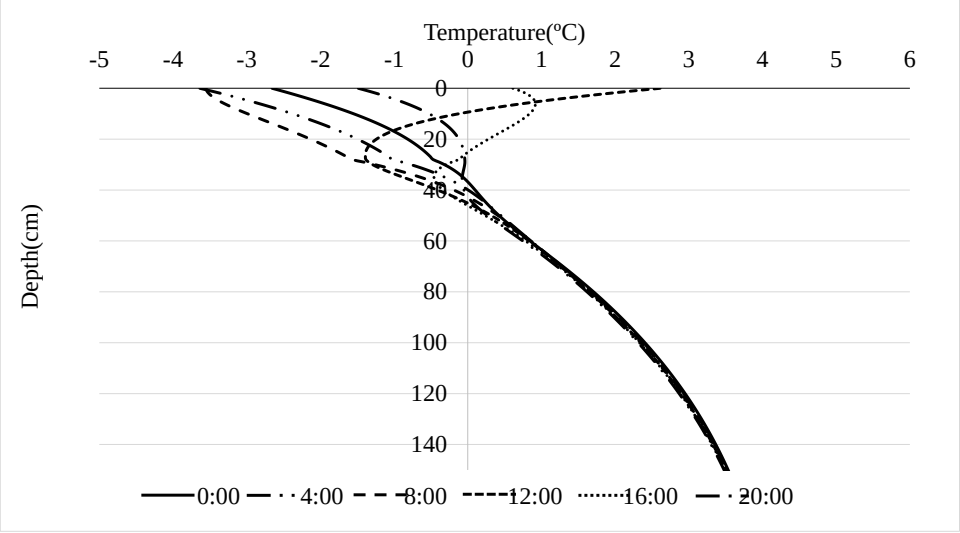


**Figure 50. Temperature distribution of pavement with conductive sub-layer**

*Effects of the surface layer thickness*

In the simulated model, the conductive sub-layer is installed below the non-conductive surface layer, and hence, the thickness of the surface layer is a depth where the conductive layer starts. The surface layer thickness is an important factor for the energy efficiency. Five different surface layer thicknesses: 0 cm (no-surface layer), 1cm, 2cm, 4cm, and 6cm are modeled and simulated, respectively. For these simulations, the conductive (heating) layer thickness is fixes as 2 cm, and the thickness of the bottom layer varies accordingly so that the total HMA layer thickness is 28 cm. An auto-control of the electric heating is utilized by setting the target pavement surface temperature as 0°C. A constant electric field of 100V/m is applied to the graphite modified asphalt concrete layer.

The simulated temperature variations are plotted in Figure 51(a), (c), (e), (g), and (i), and their corresponding temperature profiles along the depths are shown in Figure 51 (b), (d), (f), (h), and (j). By heating the conductive sub-layer, the temperatures of the whole HMA layer are maintained above 0°C or higher.

The results show that as the surface layer is thicker, the overall HMA layer temperature is higher. This implies that the more energy is needed to keep the surface temperature to be 0°C or higher. Pavement temperature profiles changed dramatically as well due to the electric heating. It is obvious that the domain nearby the conductive layer is heated up more rapidly.

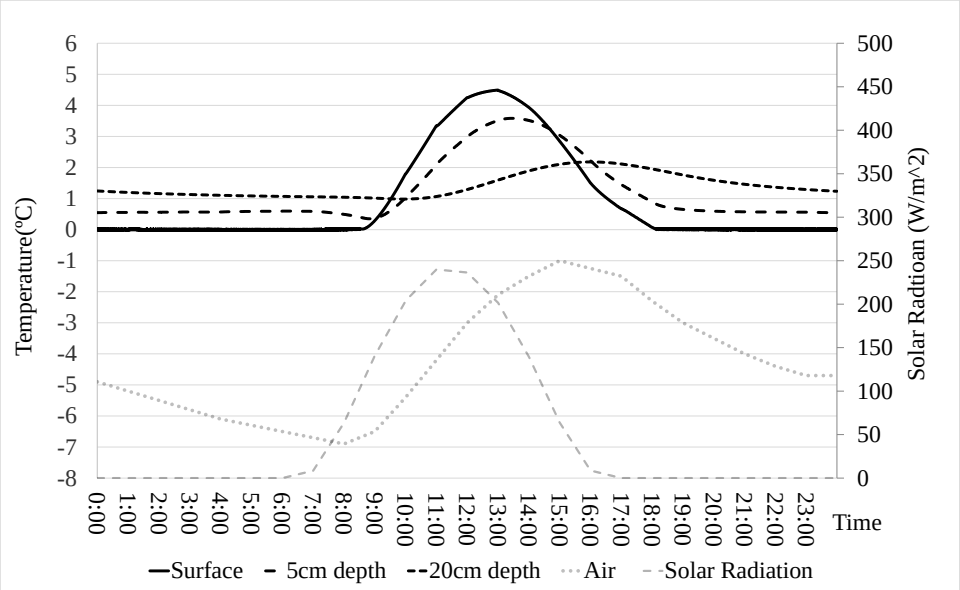


(a) 0cm~2cm conductive layer

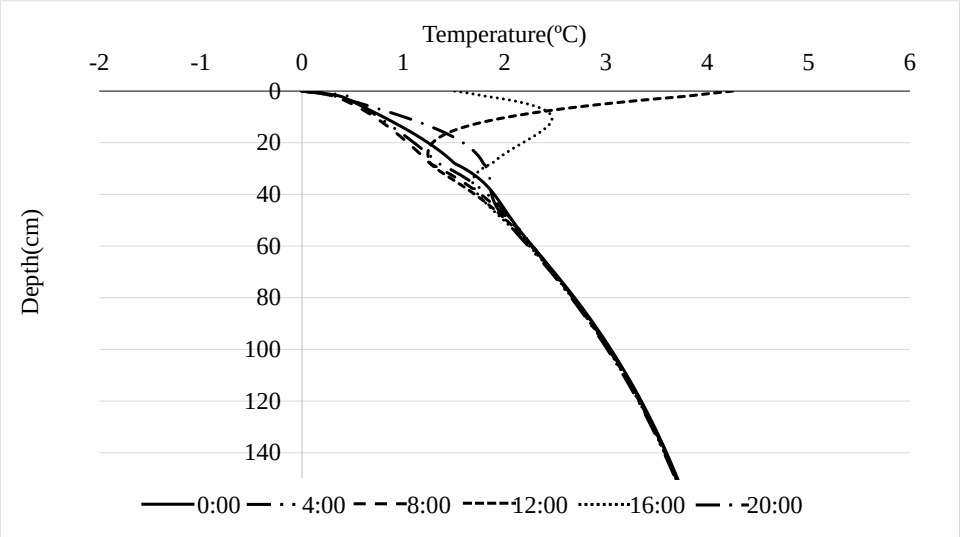


(b) Temperature profile along the depth related to (a)

**Figure 51. Effects of the location of the conductive sub-layer**

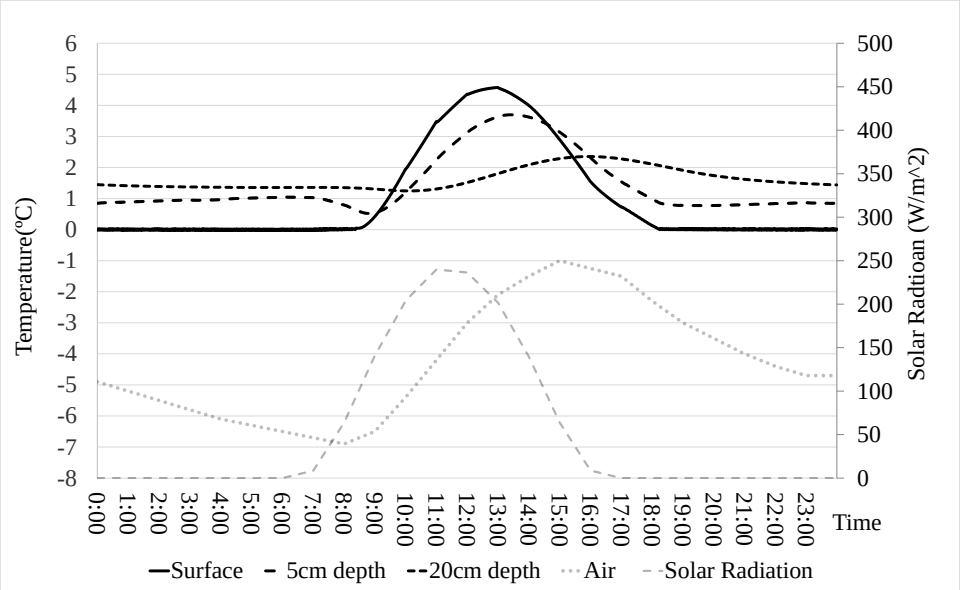


(c) 1cm~3cm conductive layer

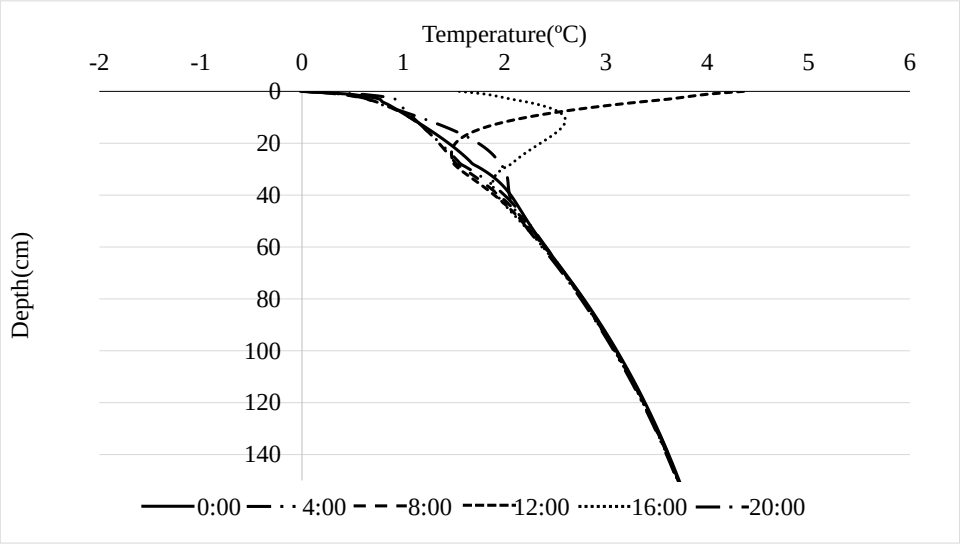


(d) Temperature profile along the depth related to (c)

**Figure 51. Continued**

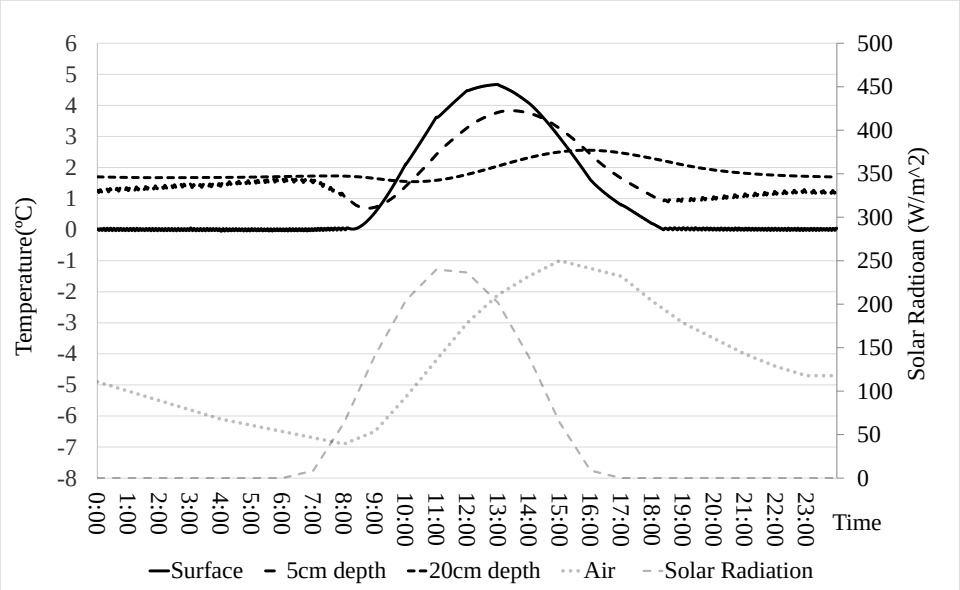


(e) 2cm~4cm conductive layer

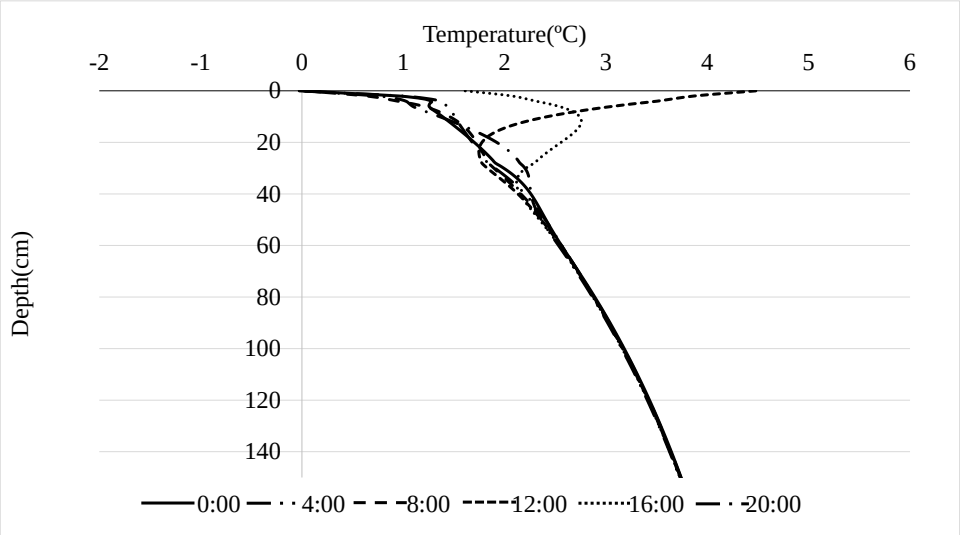


(f) Temperature profile along the depth related to (e)

**Figure 51. Continued**

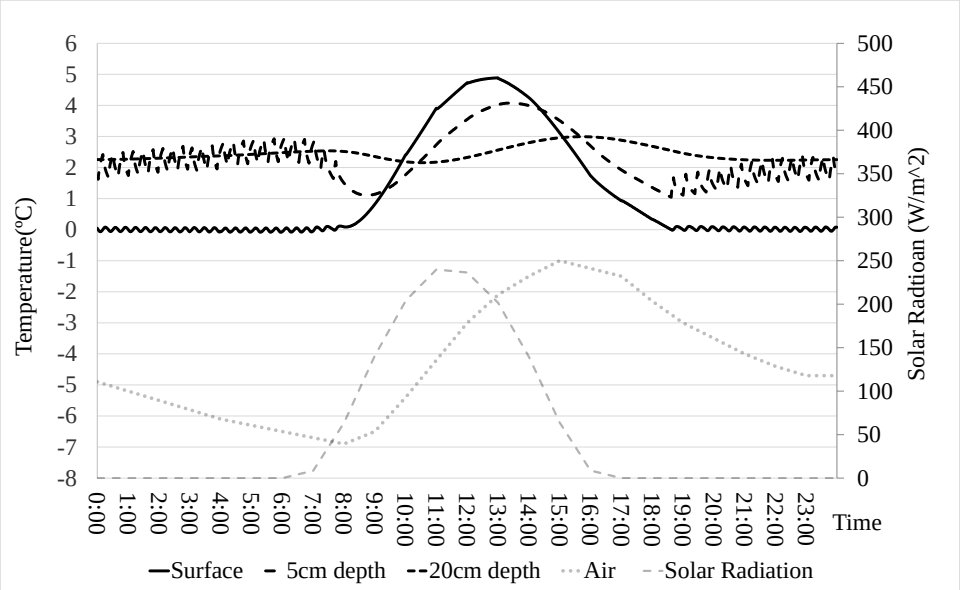


(g) 4cm~6cm conductive layer

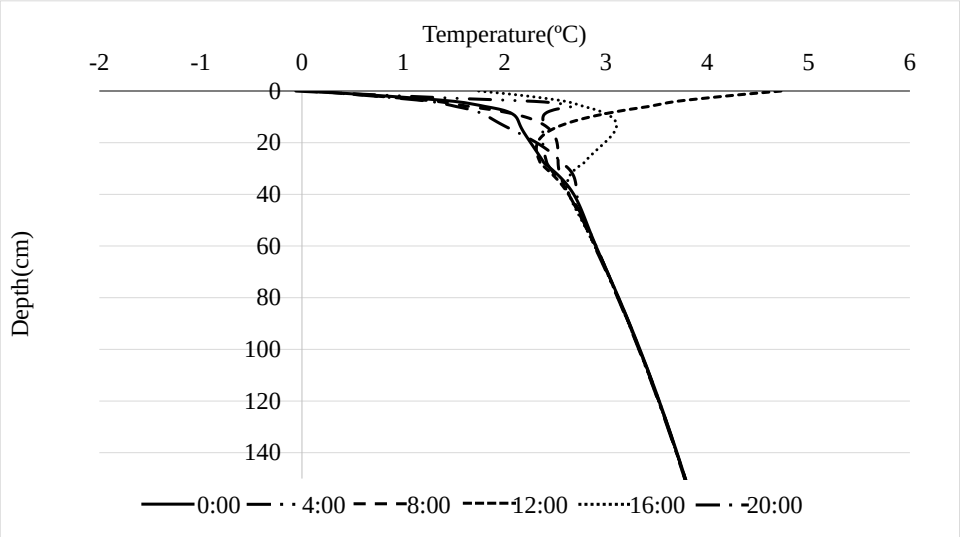


(h) Temperature profile along the depth related to (g)

**Figure 51. Continued**

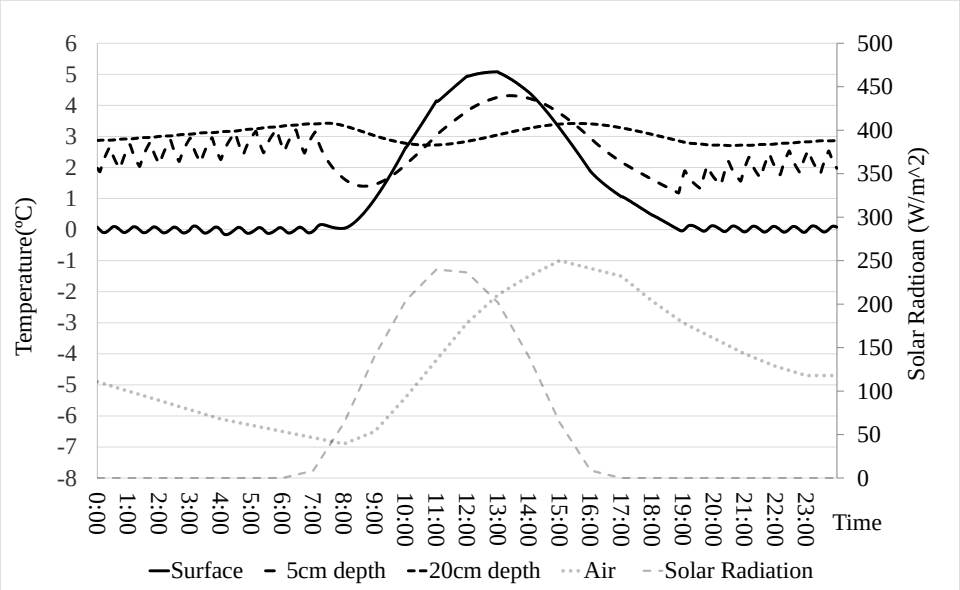


(i) 6cm~8cm conductive layer

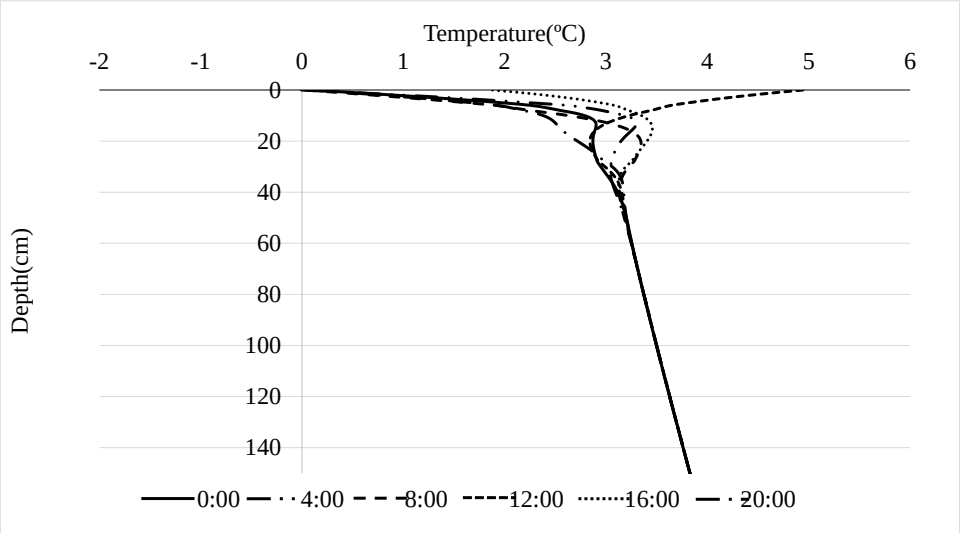


(j) Temperature profile along the depth related to (i)

**Figure 51. Continued**

*Effects of the conductive sub-layer thickness*

Pavements with a graphite modified sub-layer of various thickness were evaluated. In this set of the simulation, the thickness of the non-conductive surface layer is fixed to be 1 cm, which is the optimum conductive sub-layer location (discussed later), and their thickness varied as 2cm, 3cm, 4cm, 5cm, 9 cm and 19cm. The magnitude of electric field remains 100V/m for all the cases.

As shown in Figure 52 (a) to (l), the surface temperatures are successfully controlled to be 0°C or above in all cases. As the conductive layer becomes thicker, the overall HMA layer gets hotter with not doubt because of more heats generated. The temperature profiles plotted in Figure 52 (a) to (l) indicate the same phenomenon.

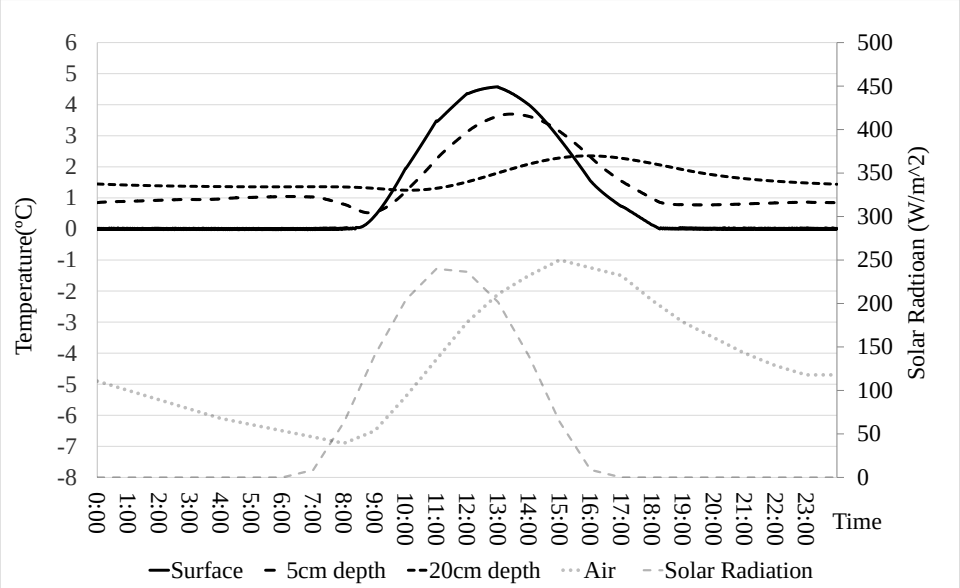


(a) 2cm thickness conductive layer

**Figure 52. Effects of the thickness of the conductive sub-layer**

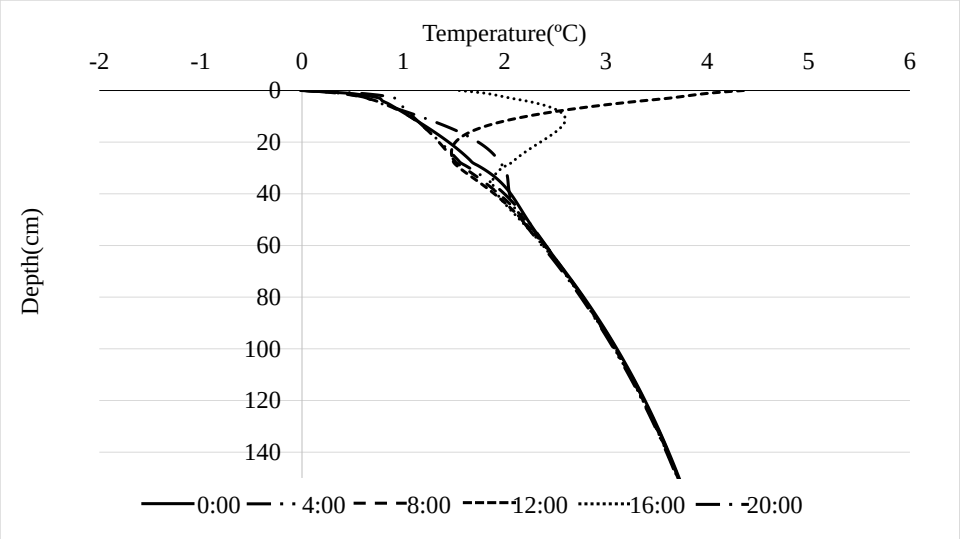


(b)Temperature profile along the depth related to (a)

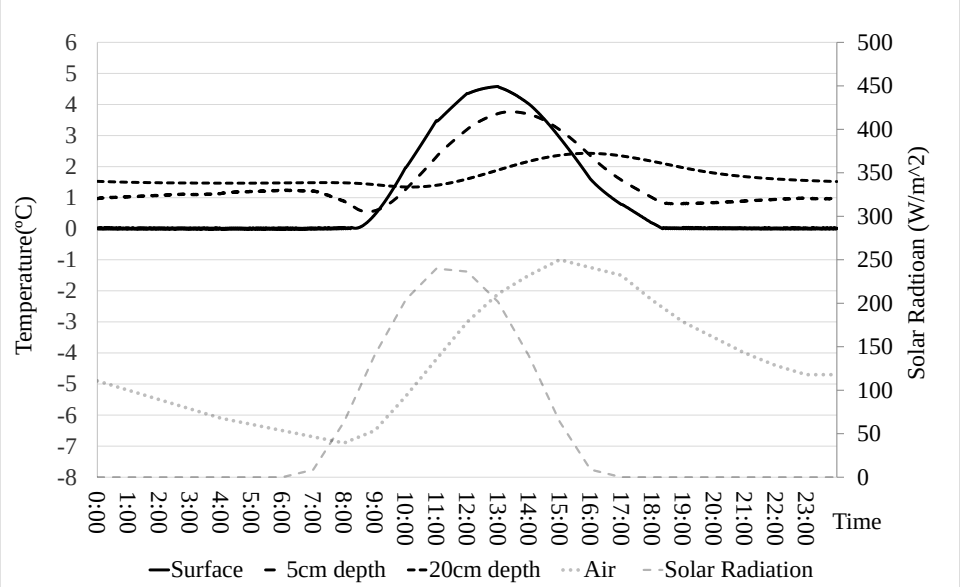


(c) 3cm thickness conductive layer

**Figure 52. Continued**

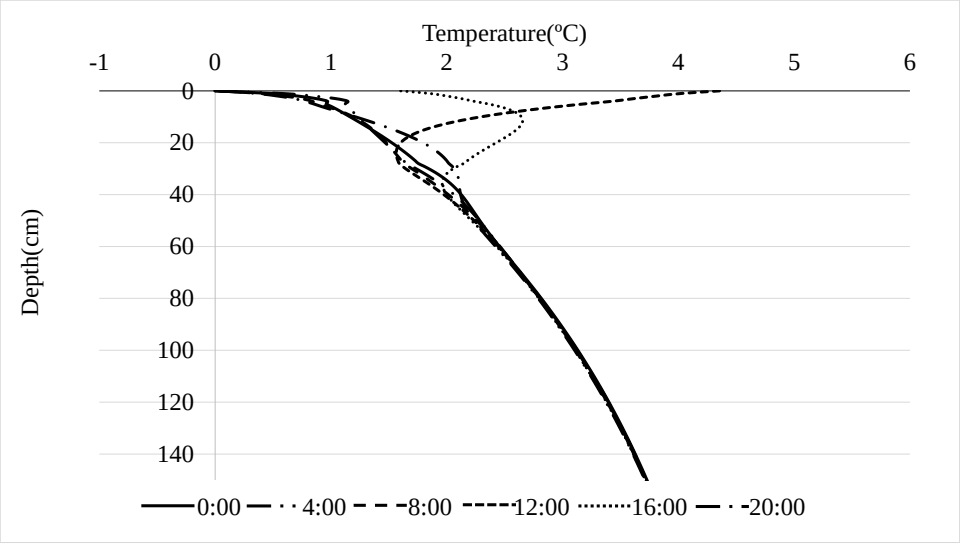


(d)Temperature profile along the depth related to (c)

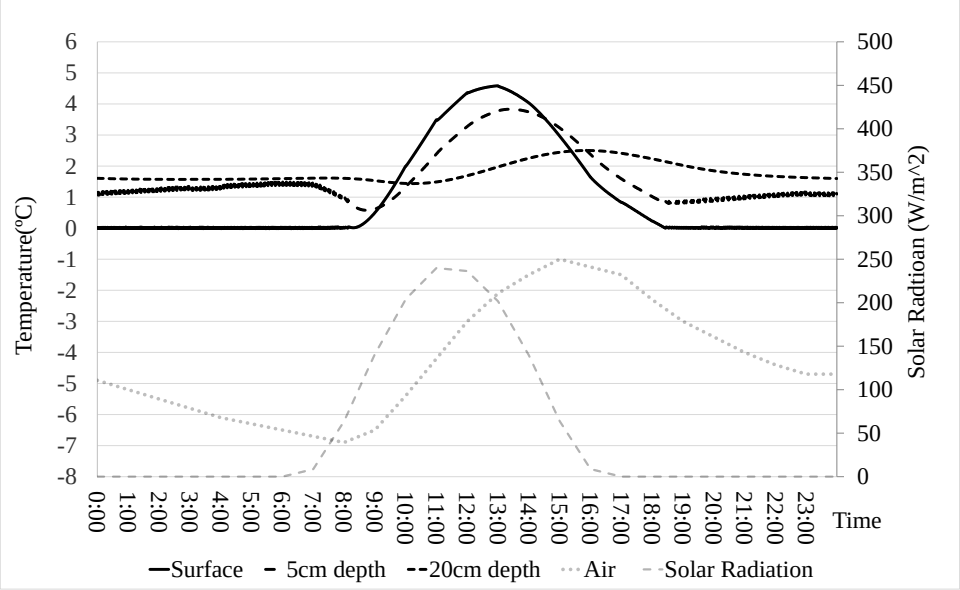


(e) 4cm thickness conductive layer

**Figure 52. Continued**

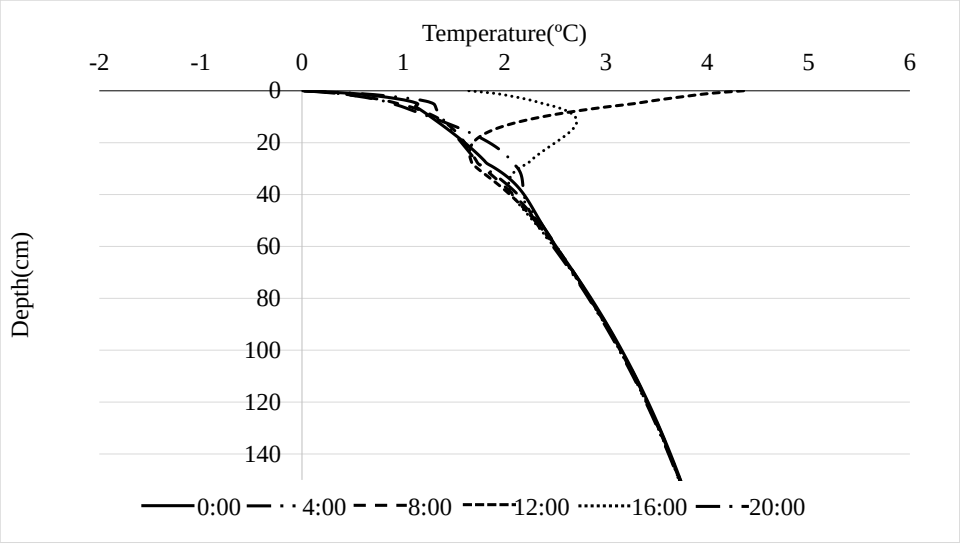


(f)Temperature profile along the depth related to (e)

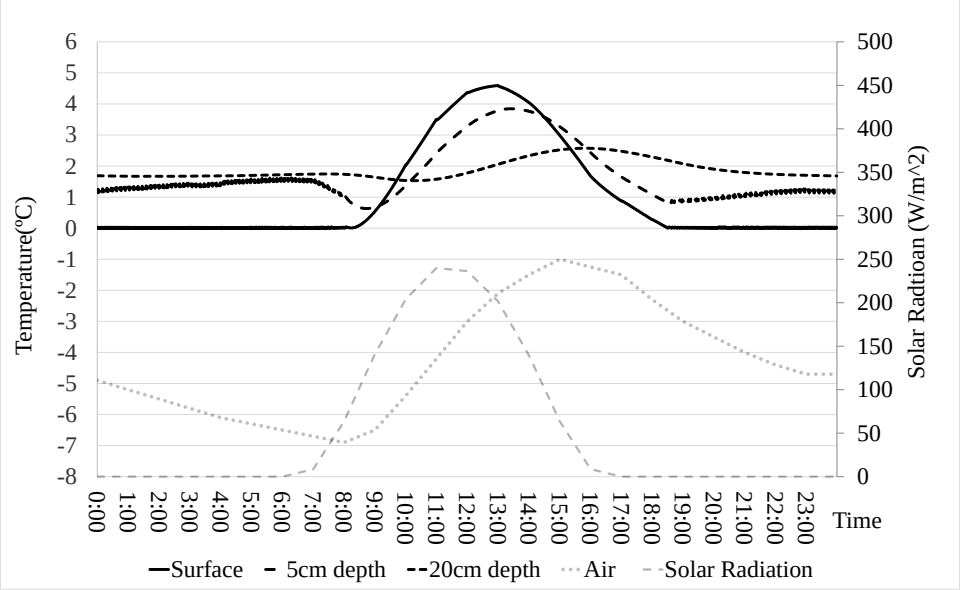


(g) 5cm thickness conductive layer

**Figure 52. Continued**

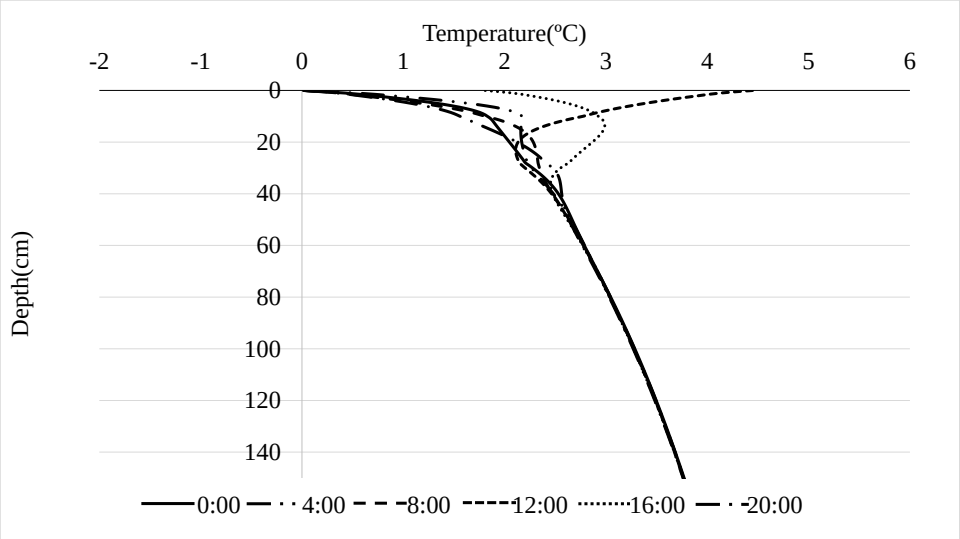


(h)Temperature profile along the depth related to (g)

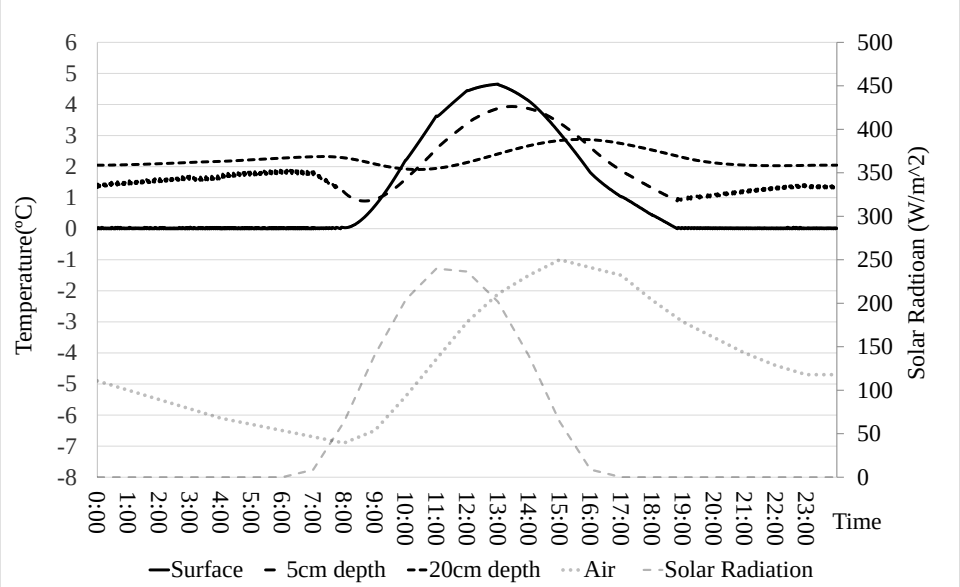


(i) 9cm thickness conductive layer

**Figure 52. Continued**

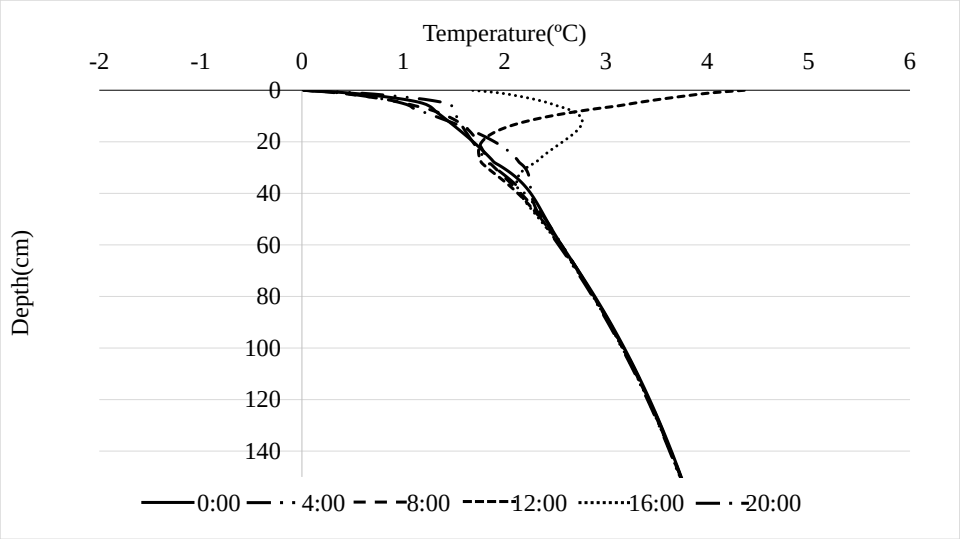


(j)Temperature profile along the depth related to (i)

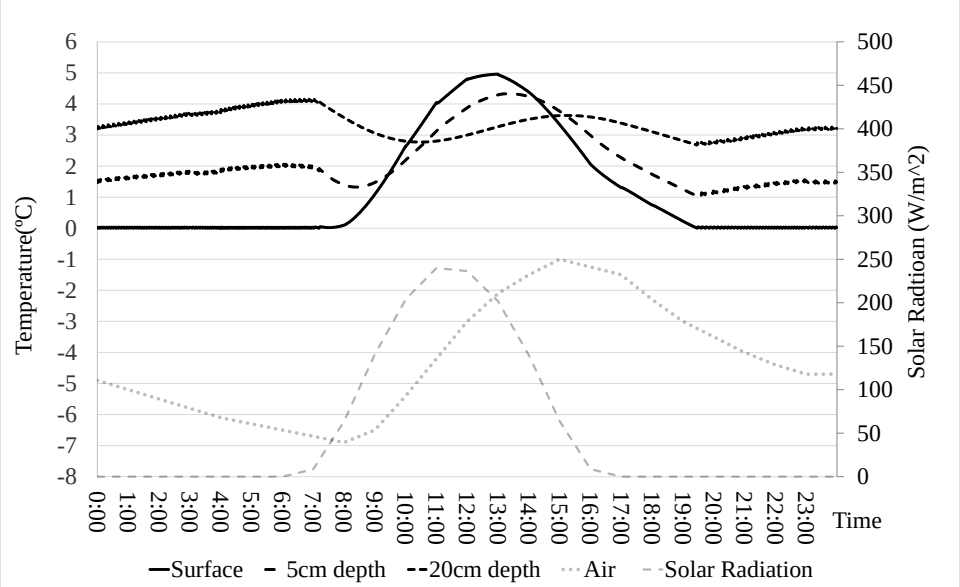


(k) 19cm thickness conductive layer

**Figure 52. Continued**

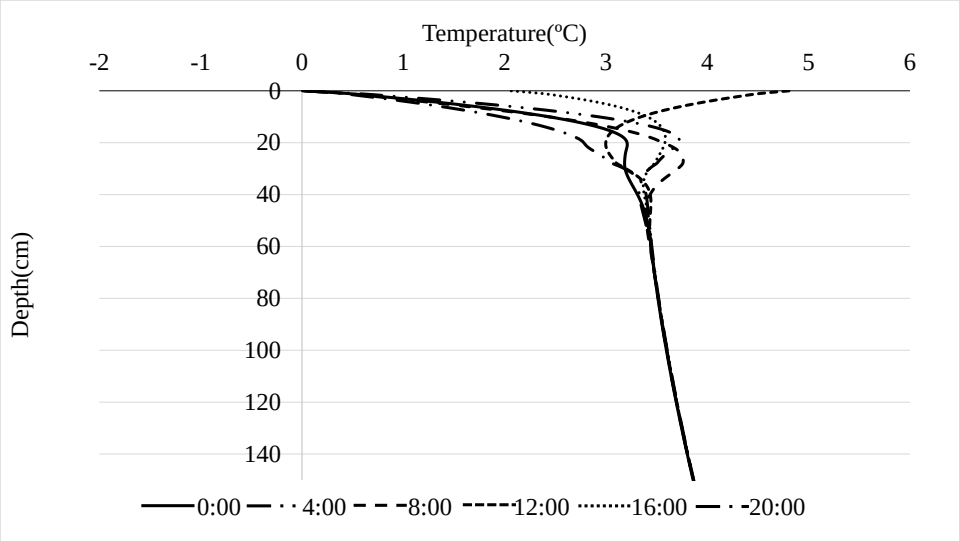


(l)Temperature profile along the depth related to (k)

**Figure 52. Continued**

*Effects of the conductive sub-layer thickness*

In the analysis described above, the resistivity of the conductive layer was assumed to be ρ=147.26 Ω*cm=1.4726 Ω*m, which is measured during the experiment. By using the same magnitude of electric field (100V/m) and conductive layer location (1cm~3cm), the effect of the resistivity of the conductive sub-layer is evaluated. However, not much differences on daily temperature variations or profiles are observed when the resistivity varies from 0.0001 Ω*m to 10 Ω*m, as shown in Figure 53 (a) to (l).

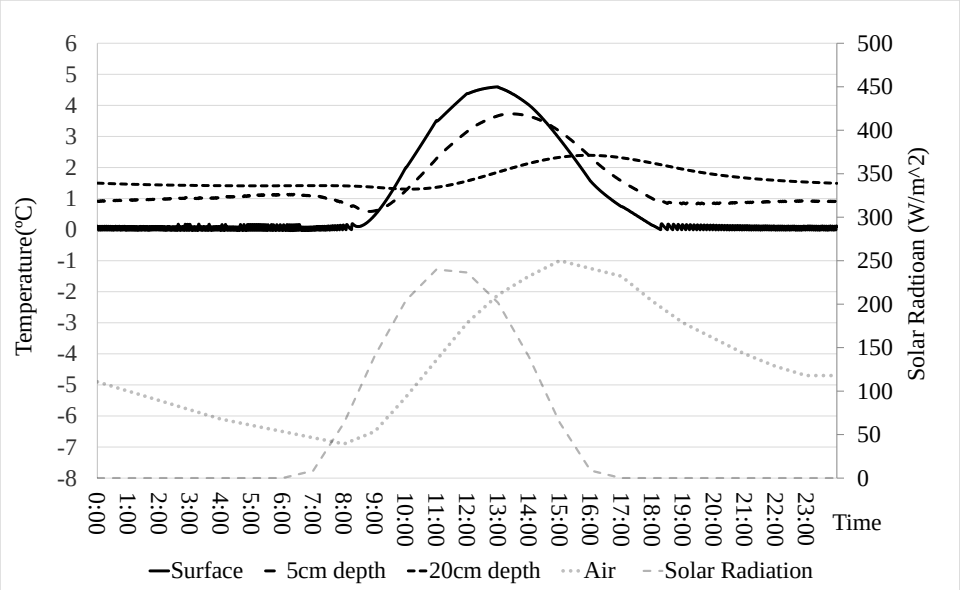


(a) $0.0001\ \Omega * \mathrm{m}$ resistivity of conductive layer

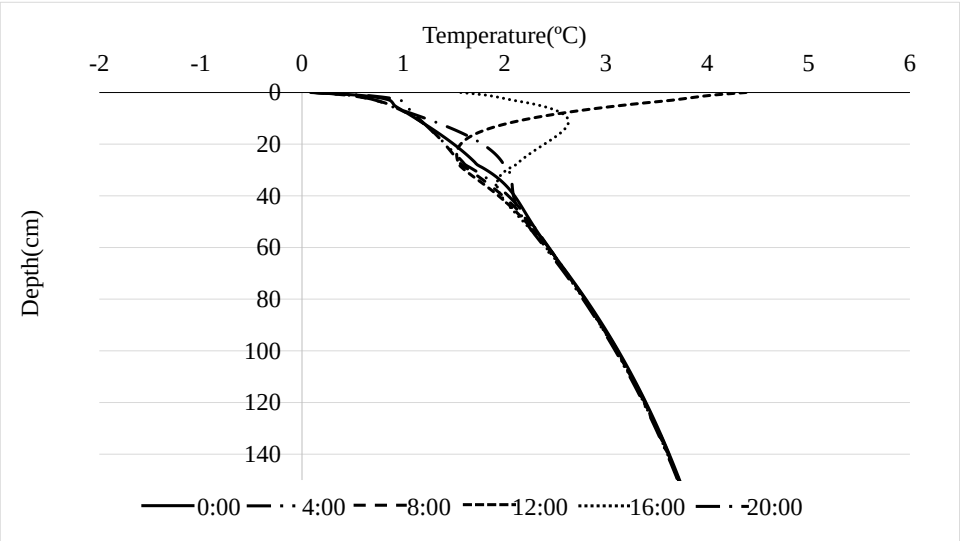


(b)Temperature profile along the depth related to (a)

**Figure 53. Effects of the thickness of the conductive sub-layer**

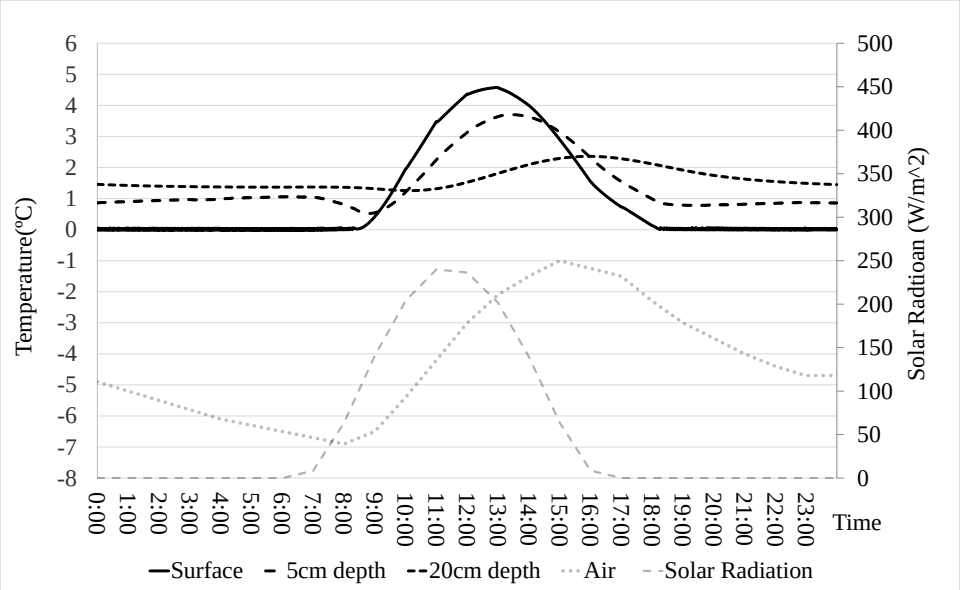


(c)$0.001\ \Omega * \mathrm{m}$ resistivity of conductive layer

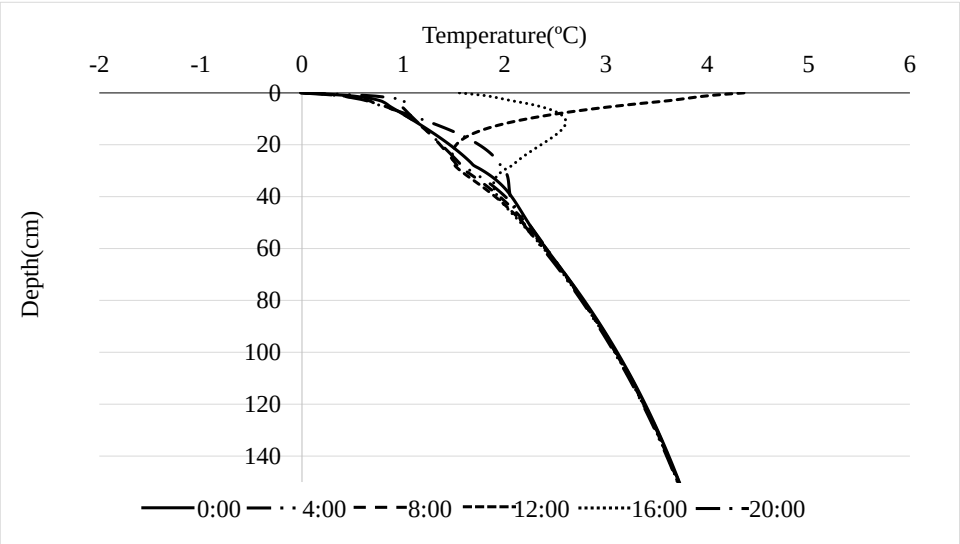


(d)Temperature profile along the depth related to (c)

**Figure 53. Continued**

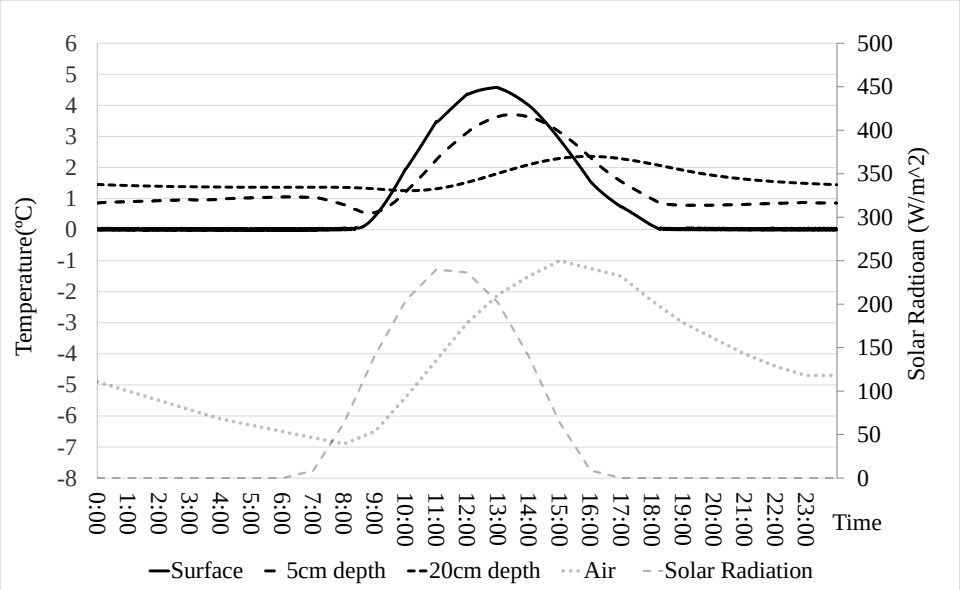


(e) $0.01\ \Omega * \mathrm{m}$ resistivity of conductive layer

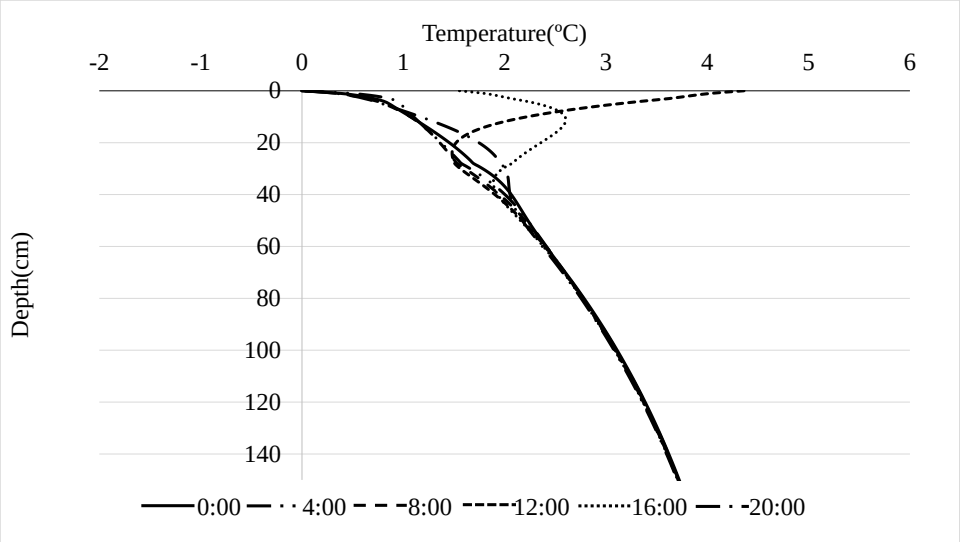


(f)Temperature profile along the depth related to (e)

**Figure 53. Continued**

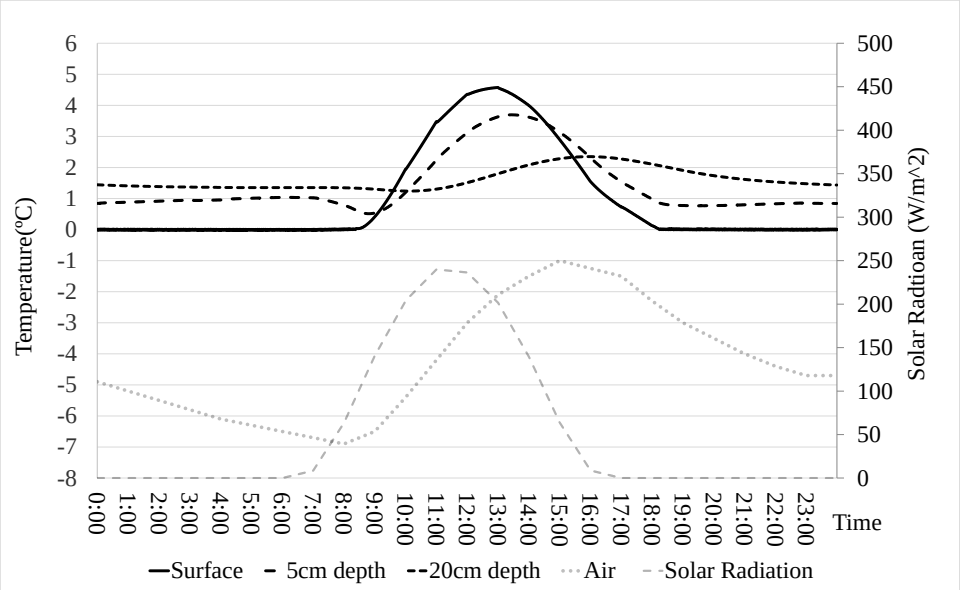


(g) $0.1\ \Omega * \mathrm{m}$ resistivity of conductive layer

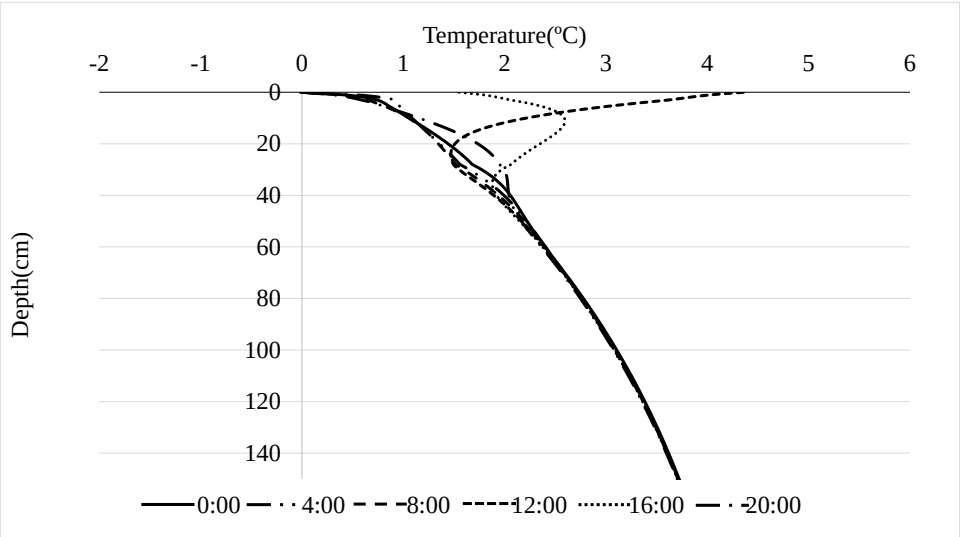


(h)Temperature profile along the depth related to (g)

**Figure 53. Continued**

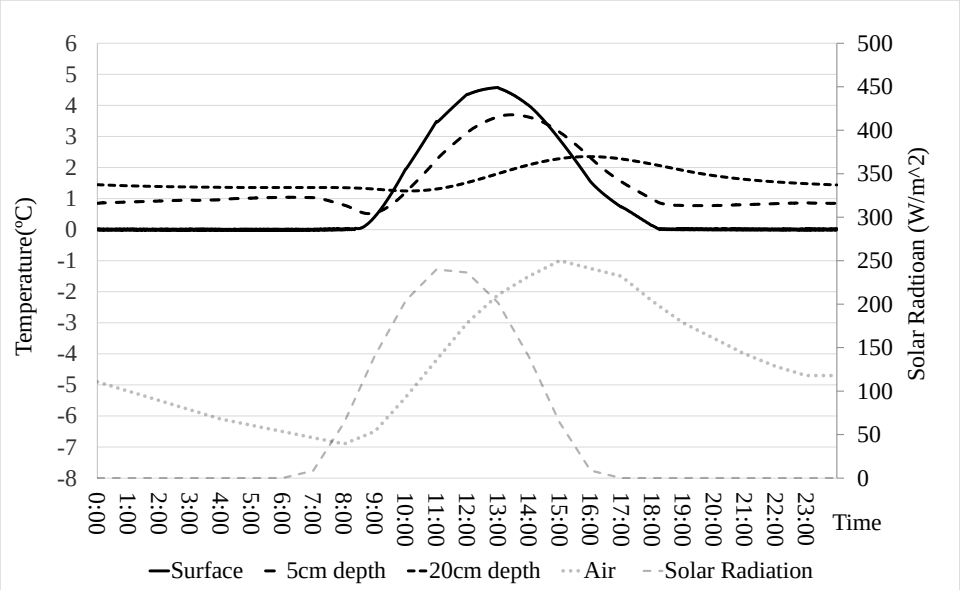


(i)1.0 Ω ∗ m resistivity of conductive layer

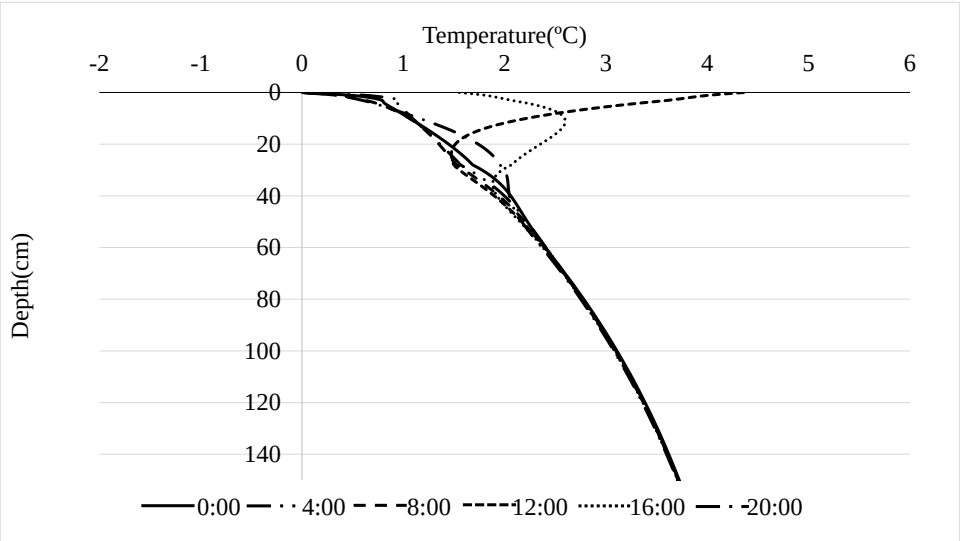


(j)Temperature profile along the depth related to (i)

**Figure 53. Continued**

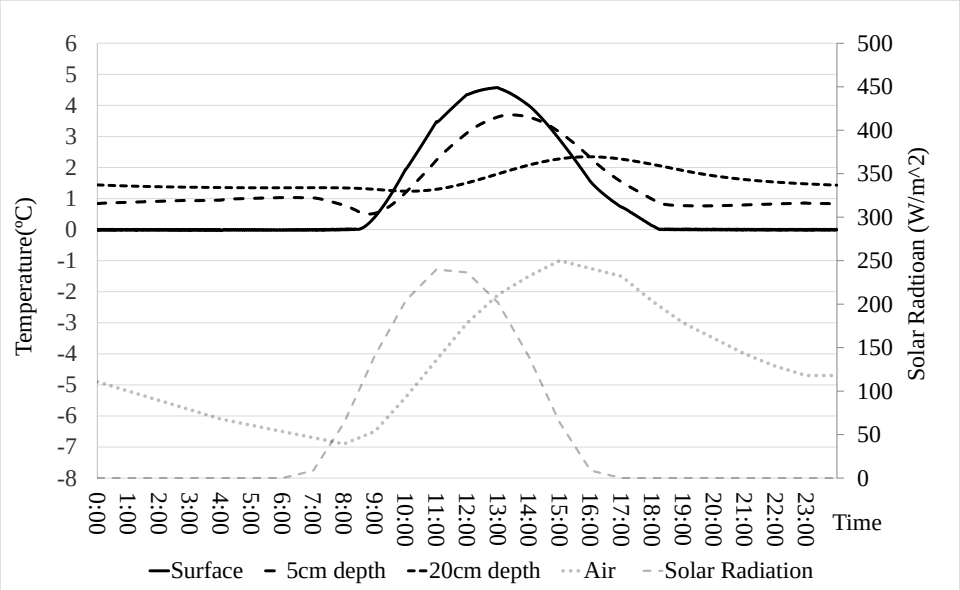


(k)10.0 Ω ∗ m resistivity of conductive layer

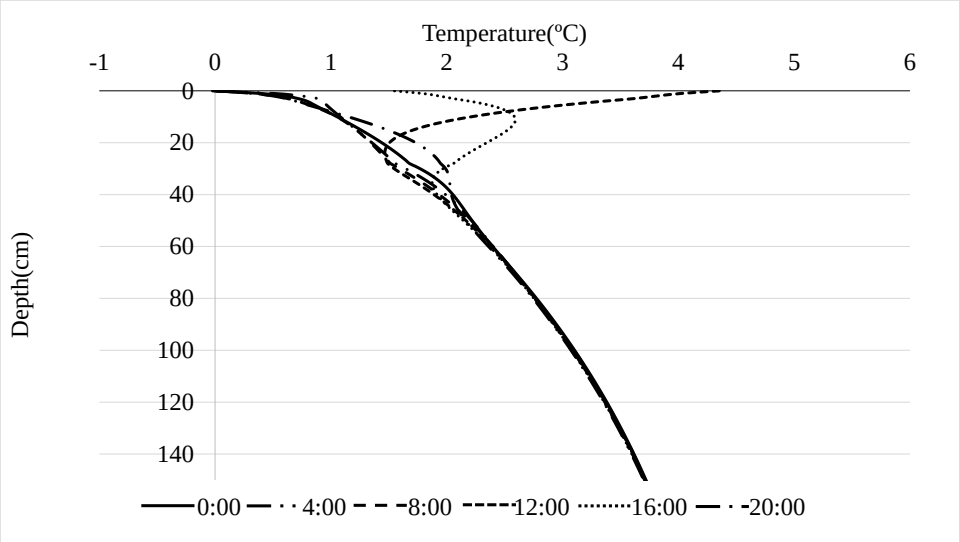


(l)Temperature profile along the depth related to (k)

**Figure 53. Continued**

*Effects of the magnitude of the electric field*

Five cases were simulated by selecting the magnitude of electric fields of 50v/m, 100V/m, 150V/m, 200V/m, and 250V/m. According to Ohm's law, the higher electric field provides higher electric current, and results in faster heating. The conductive sub-layer was assumed to be located between 1cm and 3cm deep. In this specific weather case, the pavement surface temperature can not maintain above 0°C when 50v/m because of the rate of heating is slower than the emitted energy. However, when the electric field is 100 V/m or higher, pavement surface temperature is successfully controlled, and all cases show the similar temperature distributions. Therefore, it is concluded that a minimum electric field is required to keep the surface temperature above a certain target value.

*Energy Consumption of Electric Heating for Deicing Purpose*

In addition to the technical issues, the amount of electrical power required to keep the pavement temperature above freezing temperature is one of the most important factor for practical application because it is directly proportional to the cost. The suggested deicing system using the conductive asphalt concrete has a significantly lower initial construction cost than the pipe or heating coil installations, but requires an operation cost for supplying electrical power. The amount of power and corresponding cost for heating the airfield runway (Figure 46, area=3000×46 $m^2$) on the specific weather (Figure 49, the air temperature varies from -7 to -1°C) is calculated for each simulation described above. The total daily consumption of electric energy is calculated by following Equation (39):

$$W=PDLt \tag{39}$$

Where,

W: Electric energy consumed daily

P: Energy generated by electric heating (W/m3)

D: Area of cross section of conductive asphalt concrete sub-layer (m2)

L: Pavement length (m)

t: Total daily heating time

To calculate the cost, the price of electricity is assumed as 0.1 USD/ KhW, which is within the range of residential electricity prices in the United States.

Figure 54 (a) compares the costs for the different surface layer thicknesses (depth of the conductive layer). Except for the case without the surface layer, the cost increases with the surface layer thickness. This indicates that the efficiency of the deicing system is higher when the non-conductive surface layer is thinner. However, the case without the surface layer consumes a high amount of power because convection and emission at the surface. The non-conductive surface layer serves as a heat insulator, preventing the heat loss from the pavement.

Figure 54 (b) shows the effect of the conductive sub-layer thickness on the cost. The cost gradually increases with the conductive layer thickness. This means that huge amount of electric energy is consumed to increase the temperature inside the asphalt concrete layer in addition to the pavement surface.

As shown in Figure 54 (c) and (d), the electrical resistivity of the conductive asphalt and the magnitude of electric field don't have significant influences on the energy efficiency. It should be noted that the electric field with 50V/m gives the lowest daily cost,

but it doesn't indicate magnitude is most cost effective. In fact, with this electric field, electric energy is not sufficient enough to maintain the surface temperature above 0°C.

The target controlled surface temperature plays a significant role in daily cost. The higher the target value, the higher the daily cost for electric energy. In the weather condition specified in this study, maintaining surface temperature above 4 °C is 2.4 times more expensive than 0 °C. As the melting point of ice is assumed as 0 °C, at least 10,260 USD needs to be spent to remove the ice layer on the surface potentially.

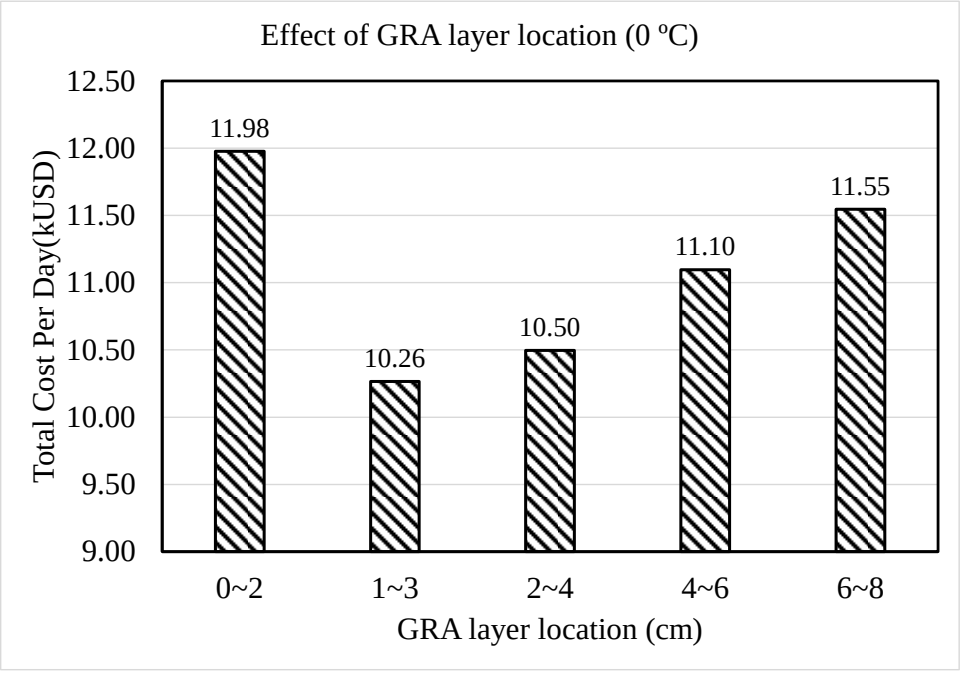


(a) Effect of GRA layer location

**Figure 54. Comparison of electric energy and cost**

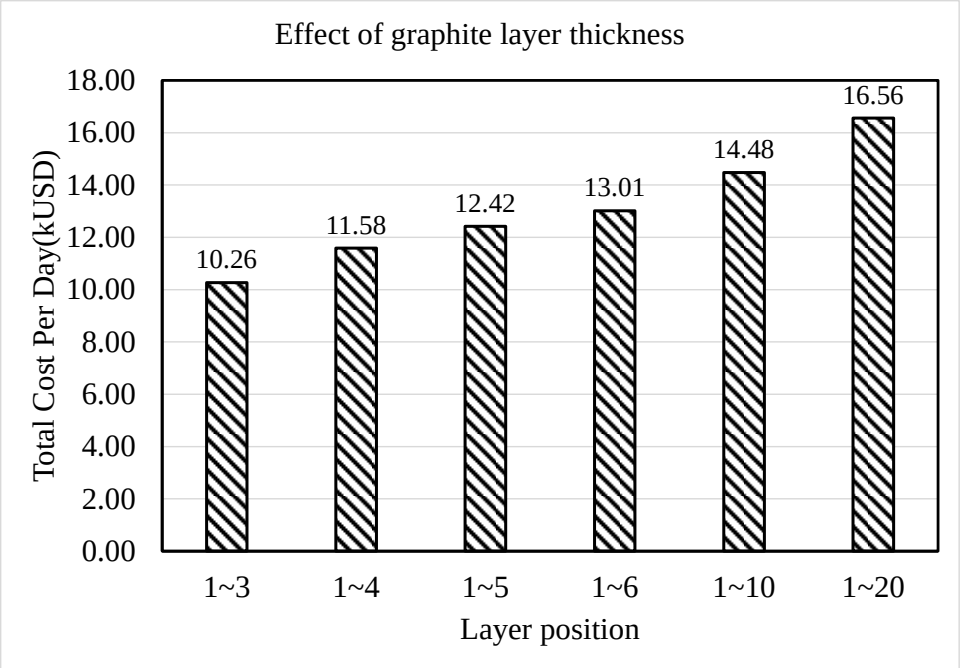


(b) Effect of graphite layer thickness

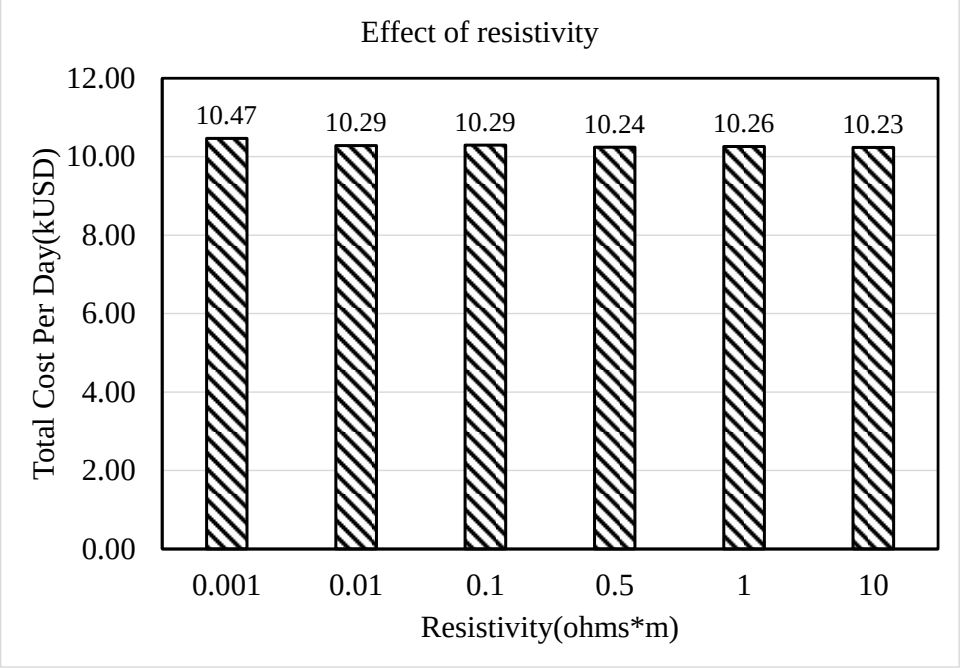


(c)Effect of resistivity

**Figure 54. Continued**

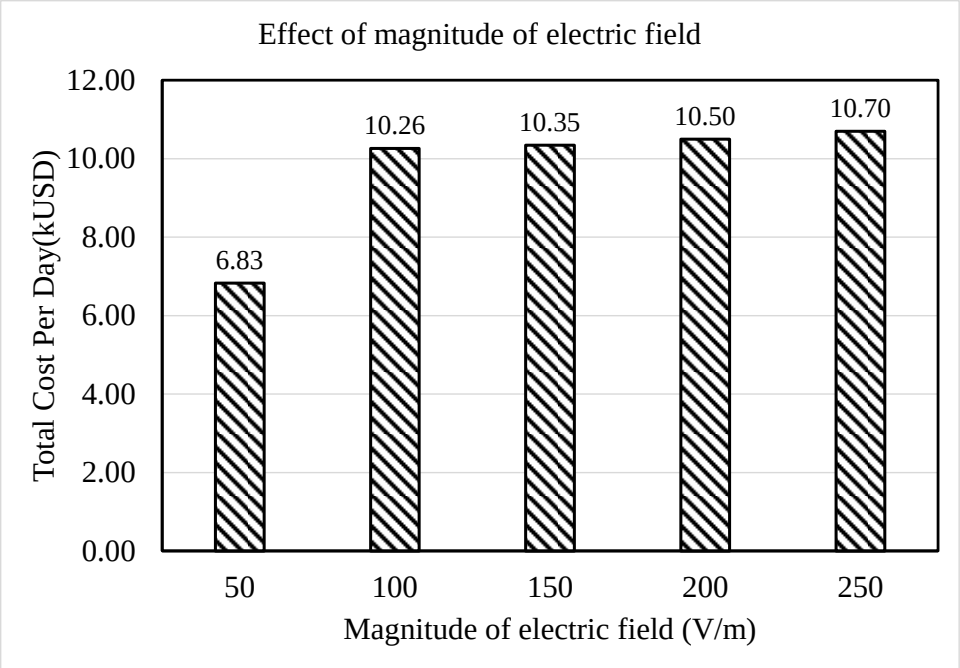


(d) Effect of magnitude of electric field

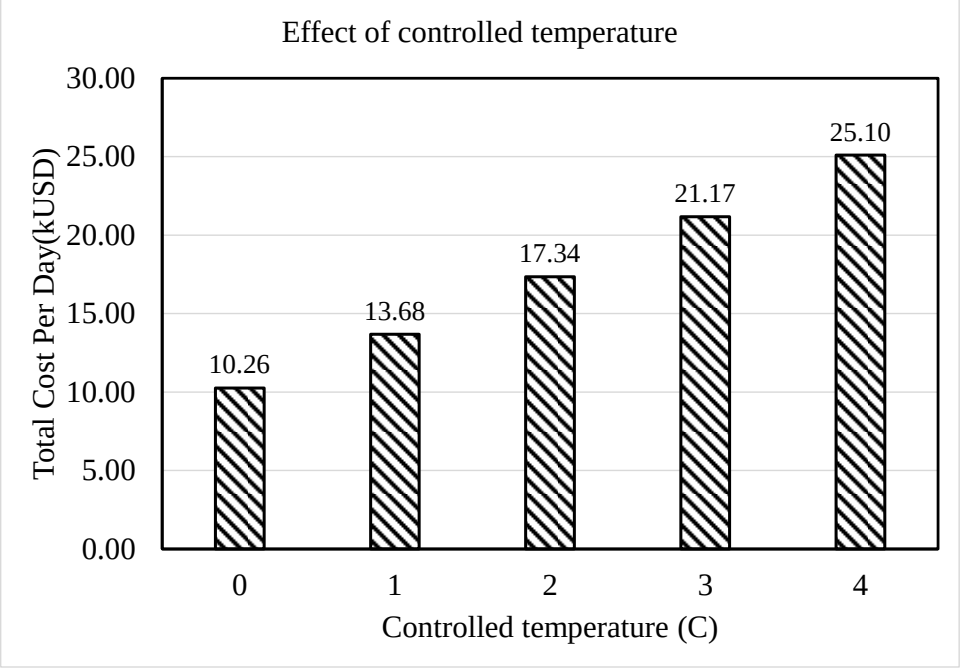


(e)Effect of controlled temperature

**Figure 54. Continued**

## 6.4 Experimental Program

### 6.4.1 Characteristics of Graphite

Based on the previous study by Park et al. (2014), flake type graphite F146 and F516 are selected to impart electrical conductivity into asphalt concrete. F146 and F516 are supported by Asbury Carbons Inc. The graphite powder has two-dimensional hexagonal crystal structure, and hence, the ideal shape of graphite particles is hexagonal plate. Park et al. (2014) reported that the shape and size of the particles vary with the source and manufacturing process, and the flake type shows the best performance in imparting conductivity.

Figure 11 shows Scanning Electron Microscope (SEM) images of the graphite powder. The SEM magnification scale was 2000 for all images. As shown in Figure 11, the flake graphite particles have thin plate shapes. The properties of these graphite are presented in Table 2.

### 6.4.2 Conductive Asphalt Concrete

This section presents the mix design, specimen preparation, test method, and test results of the conductive asphalt concrete.

*Materials and Mix Design*

A polymer modified asphalt binder PG70-22 (density 1.032 g/cc) was used for the specimen preparation. The specimens were prepared in accordance with the Superpave mixture design method. The specific gravities of coarse aggregate, fine aggregates, and filler are measured as 2.57 g/cc, 2.63 g/cc, and 3.15 g/cc, respectively. The proportion of

coarse and fine aggregates was selected to satisfy mixture requirements specified in ASTM D3515. In this study, D-5 gradation are used to know the effect of various graphite contents. Table 11 and Figure 55 show sieve analysis of D-5 gradation.

For D-5 gradation, the optimum binder content was determined to be 4.8% by weight of total mixture by Superpave method. The content of the filler is determined 5%. Portland cement is used as traditional filler, and the part of the filler is replaced with conductive graphite powder. The test data for those optimum binder contents can be found in Figure 56- Figure 58.

**Table 11. Aggregate gradation of D-5 mixture**

| ***Sieve size (mm)*** | ***% Passing Aggregate*** | ***% Remain Aggregate*** | ***Specification D-5 mix*** |
|---|---|---|---|
| 19 | 100 | 0 | 100 |
| 12.5 | 95 | 5 | 90-100 |
| 9.5 | 88 | 7 | |
| 4.75 | 65 | 23 | 44-74 |
| 2.36 | 40 | 25 | 28-58 |
| 1.18 | 20 | 20 | |
| 0.6 | 12 | 8 | |
| 0.3 | 8 | 4 | 5-21 |
| 0.15 | 5 | 3 | |
| 0.075 | 5 | 0 | 2-10 |

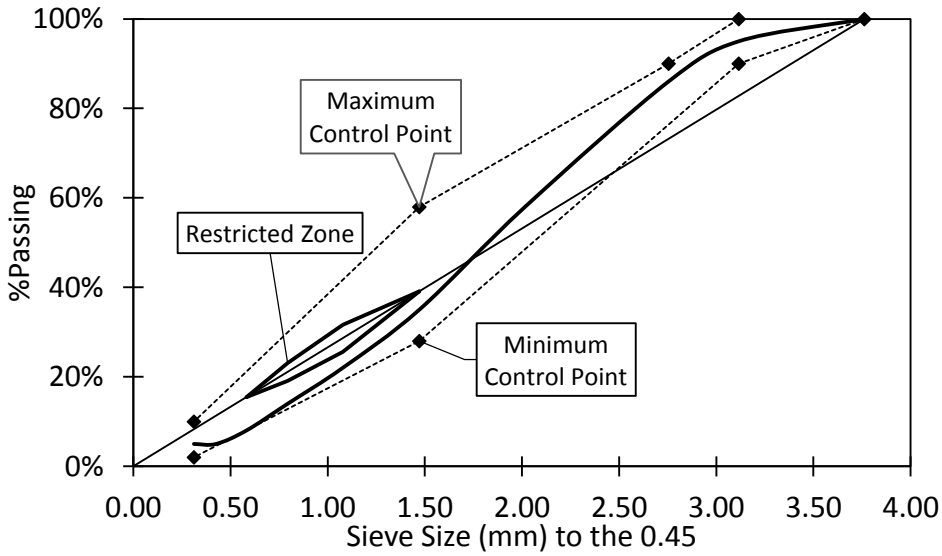


**Figure 55. Sieve analysis of D-5 mix**

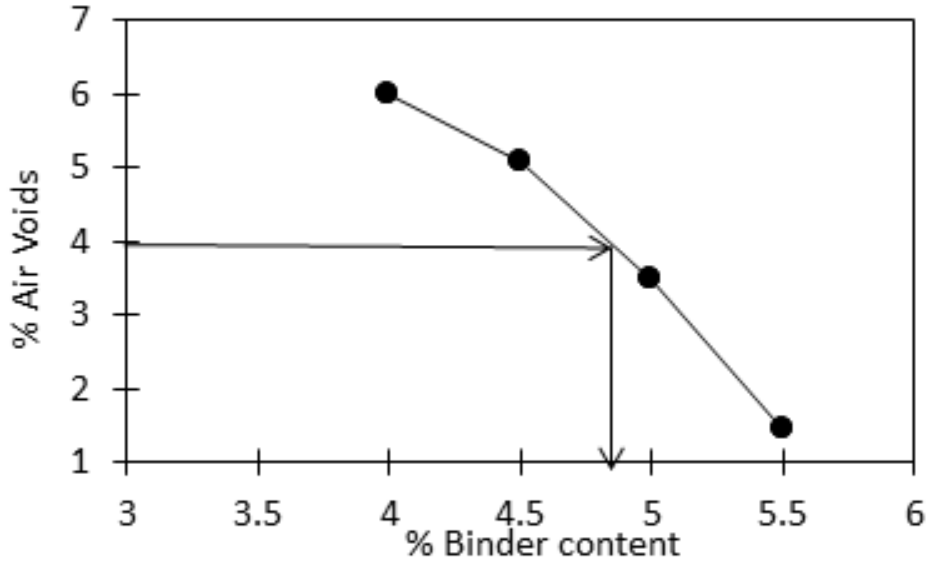


**Figure 56. Air voids versus % binder content of D-5 mixture**

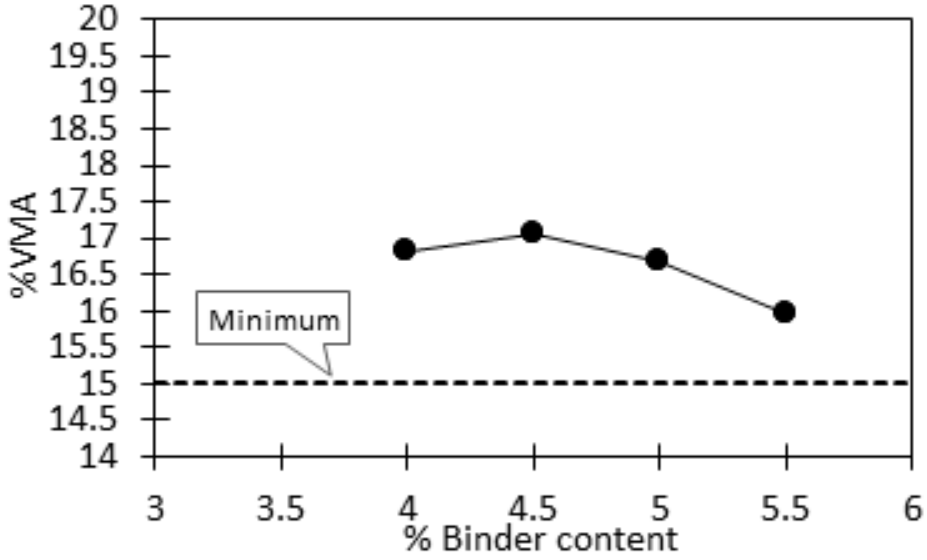


**Figure 57. VMA versus % binder content of D-5 mixture**

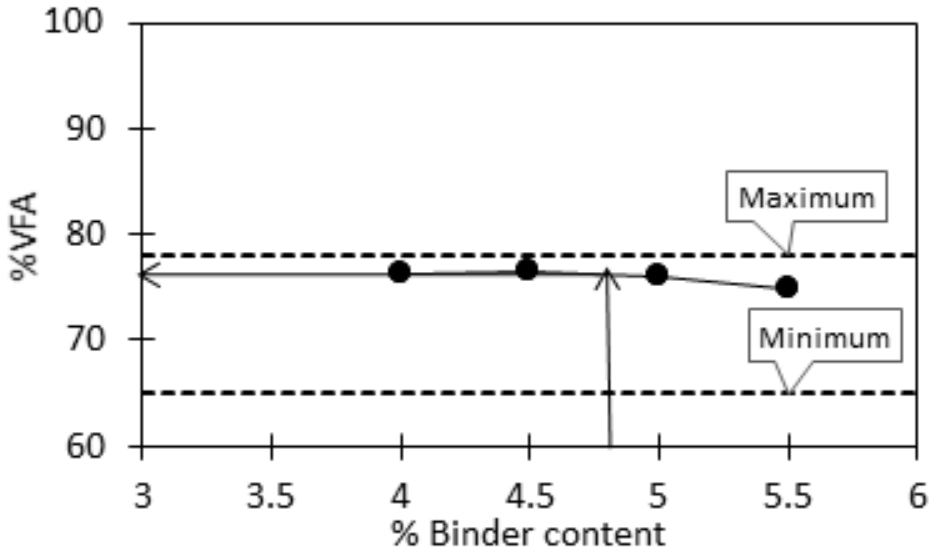


**Figure 58. VFA versus % binder content of D-5 mixture**

*Specimen Preparation*

The specimen preparation and volumetric analysis were conducted in accordance with Superpave mixture design and ASTM standards. The aggregates and fillers were heated at150 °C for at least 4 hours to eliminate moisture, and the binder was heated for 2 hours at the same temperature prior to mixing. The fillers including the graphite powder and Portland cement were mixed with aggregates first, and then binder was added. A mechanical mixer was used to mix the materials until the aggregates and fillers were coated well with the binder. The mixture was then conditioned in the oven at the compaction temperature (135 °C).

Superpave Gyratory compactor was utilized to compact the cylindrical specimens with 150 mm diameter and 95 mm height, which were compacted with gyrations until the 4% percent air void was reached. The cylindrical specimen was cored to make 2 inch diameter samples for measuring conductivity. This cutting will eliminate the error in conductivity measurement by removing the conductive mastic at the side of the specimens.

*Electrical Heating*

The electrical heating capacity of the conductive asphalt is tested using cored cylindrical specimens. A direct current (DC) power supplier (Instek GPR-3510HD) is used to supply electrical current, and the temperature is measured by a multi-meter. Figure 59 shows the experimental set-up.

**Figure 59. Experimental set-up for measuring electrical heating (DC)**

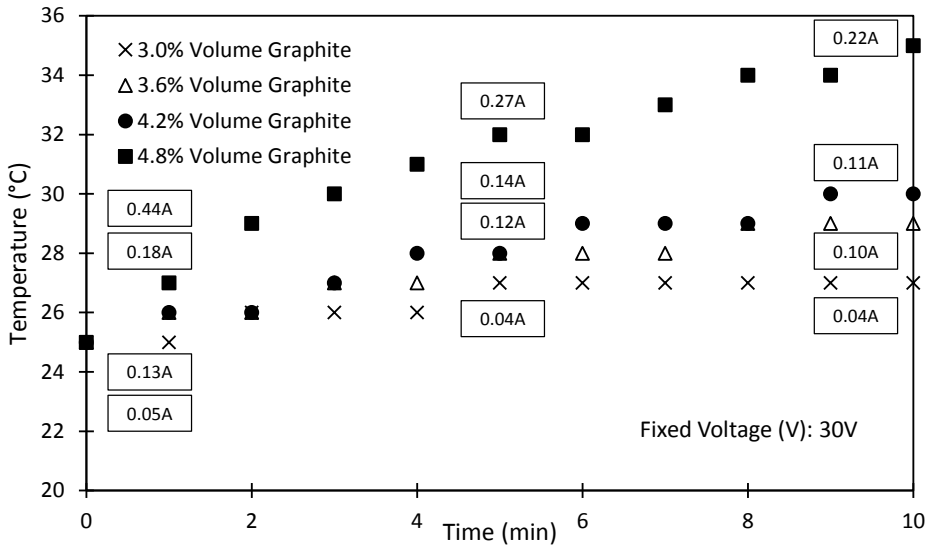


**Figure 60. Temperature variation of conductive asphalt concrete specimens for electrical heating (DC)**

Figure 60 illustrates the temperature variations of four cases (graphite content 3.0, 3.6, 4.2, and 4.8 % by volume) with heating time. At the beginning, the specimen temperature is 25°C. After 10 minutes of supplying 30V DC, the temperature of specimen with 4.8% volume graphite content increases around 10°C. The rate of heating is slower for the specimens with the lower graphite contents because of the lower conductivity. According to Ohm's law, the electrical current is proportional to the conductivity, and hence, the specimen with higher conductivity generates heat faster.

The heat generated from the conductive asphalt concrete can be theoretically calculated. The electrical power (energy per second) consumed by a material with an electrical resistance, R, can be calculated by Equation (40). By multiplying time (sec), the heat generated during a specific time can be obtained. The temperature of the material can be calculated from Equation (41). Table 12 shows the estimated temperatures by using these equations.

$$P = I^2 R = V^2 / R \tag{40}$$

Where, P=Power (Watt (J/sec)); I=Current (A); R=Resistivity (Ω); V=Voltage (V),

$$Q = cm\Delta T \tag{41}$$

Where, Q=Energy (J); C=Specific Heat Capacity (J/g·k); m=weight (g); $\Delta T = T_f - T_i$ (°C); $T_f$=Final temperature (°C); $T_i$=Initial Temperature (°C).

**Table 12. Temperature variation of specimens with time under fixed 30V DC**

| Graphite content (% volume by total mixture) | 3.00% | | 3.60% | | 4.20% | | 4.80% | |
|---|---|---|---|---|---|---|---|---|
| Time (minute) | Temperature(°C) | | Temperature(°C) | | Temperature(°C) | | Temperature(°C) | |
| | Equation | Test | Equation | Test | Equation | Test | Equation | Test |
| 0 | 25.00 | 25 | 25.00 | 25 | 25.00 | 25 | 25.00 | 25 |
| 1 | 25.21 | 25 | 25.77 | 26 | 26.14 | 26 | 27.34 | 27 |
| 2 | 25.43 | 26 | 26.54 | 26 | 27.28 | 26 | 29.67 | 29 |
| 3 | 25.64 | 26 | 27.30 | 27 | 28.42 | 27 | 32.01 | 30 |
| 4 | 25.86 | 26 | 28.07 | 27 | 29.56 | 28 | 34.35 | 31 |
| 5 | 26.07 | 27 | 28.84 | 28 | 30.71 | 28 | 36.68 | 32 |
| 6 | 26.29 | 27 | 29.61 | 28 | 31.85 | 29 | 39.02 | 32 |
| 7 | 26.50 | 27 | 30.38 | 28 | 32.99 | 29 | 41.35 | 33 |
| 8 | 26.71 | 27 | 31.15 | 29 | 34.13 | 29 | 43.69 | 34 |
| 9 | 26.93 | 27 | 31.91 | 29 | 35.27 | 30 | 46.03 | 34 |
| 10 | 27.14 | 27 | 32.68 | 29 | 36.41 | 30 | 48.36 | 35 |

Figure 61 shows the comparison between experimental results of DC electric heating and theoretical calculations. In the cases of the graphite contents 3.6, 4.2, and 4.8 %, the rates of heat decrease as the temperature increase. This was observed earlier by the previous investigators, and there are two reasons: 1) as the temperature increases, the average distance between the conductive particles in the mixture increases because of thermal expansion of the mixture, and 2) as the temperature difference between the specimen and ambient temperature increases, the specimen radiates heat faster. These explains the differences between theoretical values and test results. The first explanation indicates that the electrical resistivity of the mixture is sensitive to the volume change, implying the possibility of use the conductive asphalt for strain sensing.

Figure 62 shows that the changes in resistivity at different temperatures obtained from the specimen containing 4.8 % volume graphite content. In the case of -8°C in specimen temperature, its resistivity is about 80 ohms. Whereas, in 35°C, it has the resistivity with around 125 ohm.

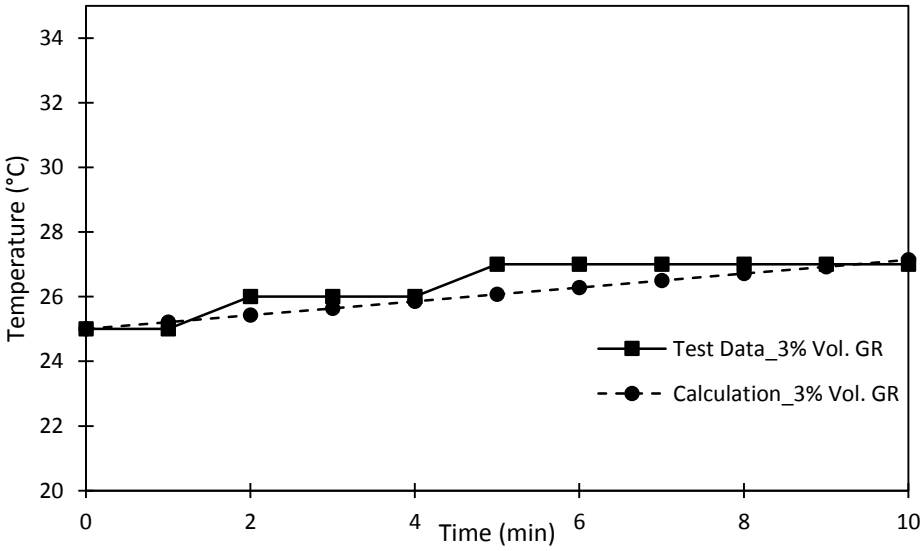


(a) 3.0% vol. graphite content

**Figure 61. Comparison of temperature variation between experimental result and theoretical calculation**

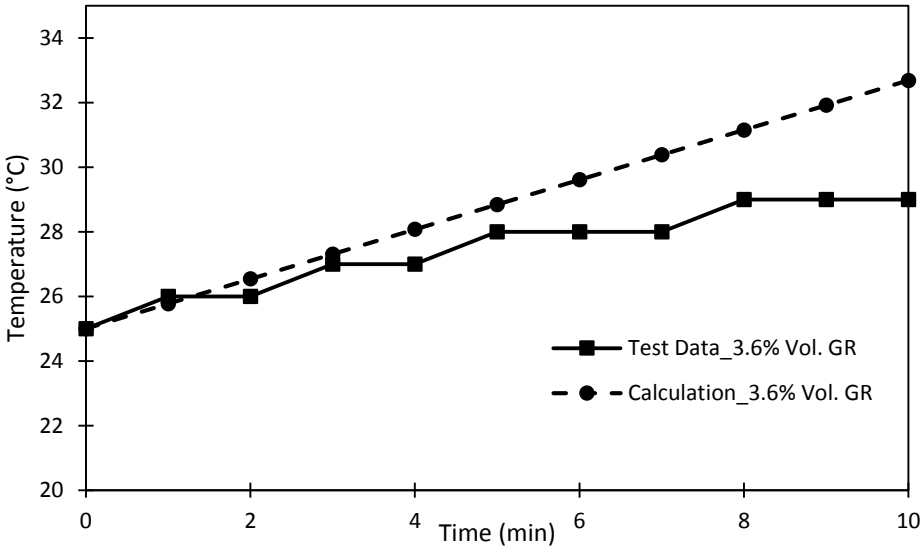


(b) 3.6% vol. graphite content

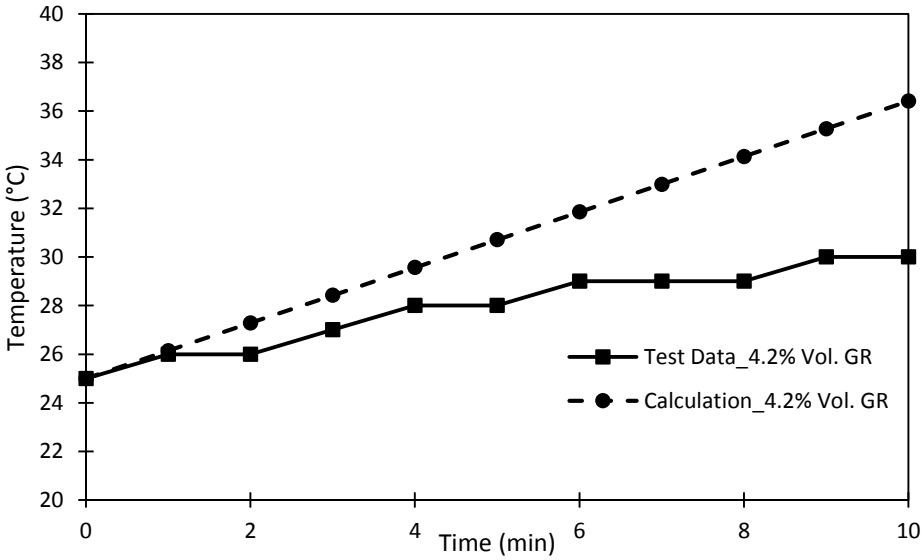


(c) 4.2% vol. graphite content

**Figure 61. Continued**

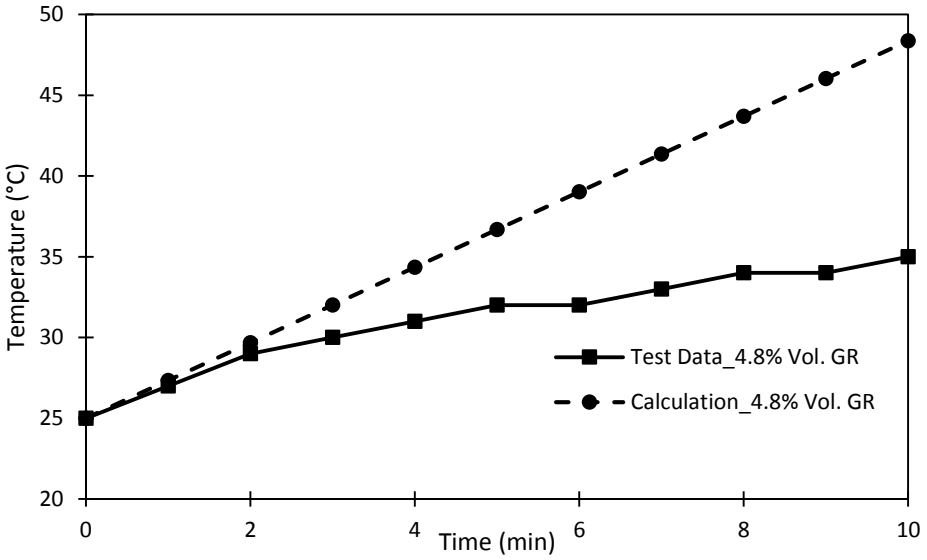


(d) 4.8% vol. graphite content

**Figure 61. Continued**

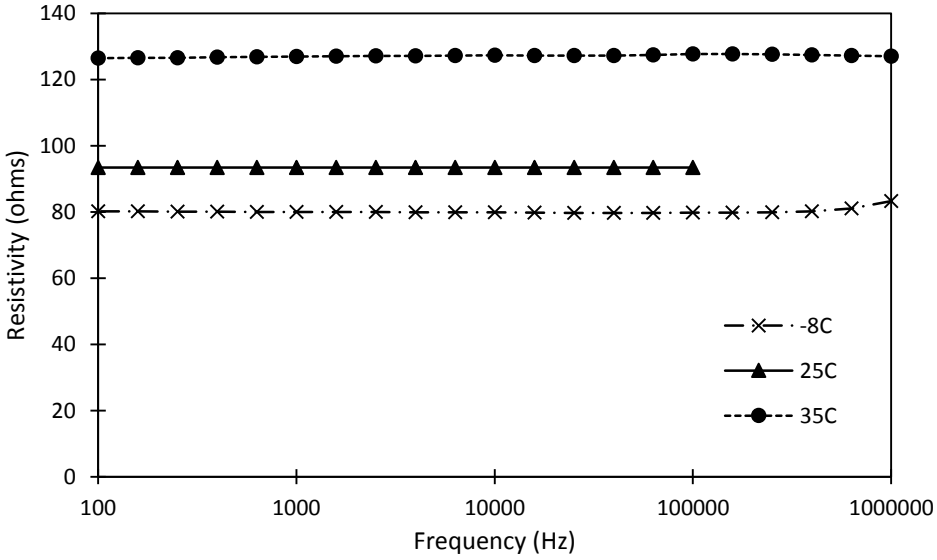


**Figure 62. Comparison of electrical resistivity of specimen with temperature variation**

### 6.4.3 Bench Scale Demonstration

A multi-layer asphalt concrete specimen containing a conductive layer in the middle is fabricated, and the heating capacity is demonstrated. Figure 63 shows the design of the multi-layer conductive asphalt slab. The slab specimen consists of three layers. Top and bottom layers are made of non-conductive traditional asphalt concrete, which is designed as insulator layers for energy efficiency and safety. The conductive layer is located between these non-conductive layers, and contains 4.8 % graphite by volume. The dimension of the slab is 20 in (width) x 20 in (length) x 3 in (thickness), and the thickness of each layer is 1 in. Silver paste was applied at the sides of the conductive layer (red shaded area in Figure 63 (a)), and copper tapes are attached on the silver paste as electrodes.

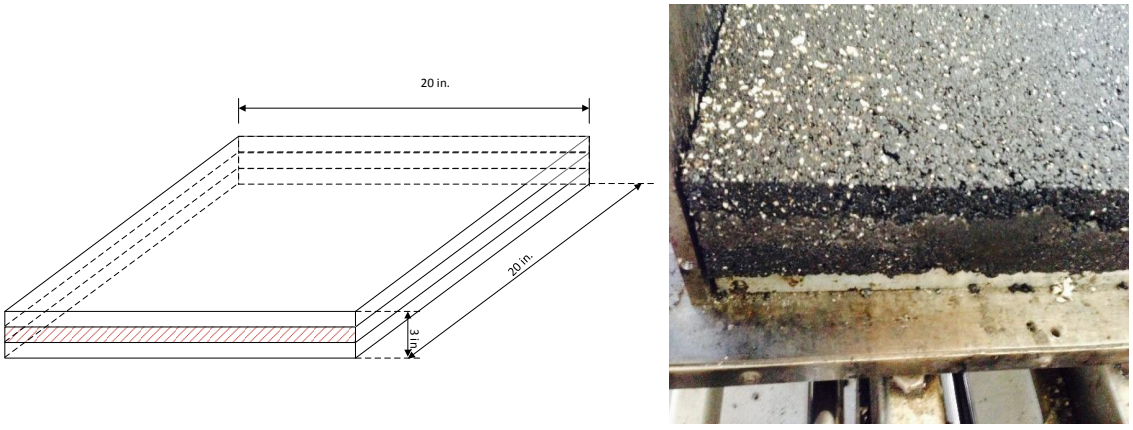


(a) Conductive slab layout (b) Conductive slab specimen

**Figure 63. Layout of the conductive asphalt concrete slab specimen**

In order to monitor the temperature of the conductive slab system at different locations, six thermal sensors are installed in the specimen as shown in Figure 64 (a). The three thermal sensors are located on the slab surface, and other three are embedded at the conductive layer. Figure 64 (b) displays the deicing experimental set-up including DC power supply, thermal sensors, and data acquisition system. 60V electrical potential is applied to heat the specimen.


(a) Distribution of thermocouples and thermal sensors

(b) Deicing experimental set-up

**Figure 64. Experimental set-up for deicing**

Figure 65 shows temperature variations of the six sensors with time tested at the room temperature. Starting temperature was 22.5°C, and the average temperature increases about 2°C after 12 hours of heating, which is slower than the results from the cylindrical specimen (5°C in 10 hours). Considering that the mixing and compaction process of the slab is different from the cylindrical specimen, this difference can be said

that in the acceptable range. The temperature is higher at the embedded sensors than the surface and at the center than the edge. The heating rate is slightly higher in the beginning, and slows down after three hours. The heating rate is very slow in this case, and the specimen needs to have faster heating rate for practical application. However, the observation from the cylindrical test implies that the heating rate can be faster when the temperature is lower (higher conductivity due to thermal contraction). Therefore, the same test is conducted in a freezer with the same specimen. As shown in Figure 66, the starting temperature was -7°C. Overall the heating rate is significantly faster, and most of the location except for the edge surface (the heat is emitted fastest), the temperatures are higher than the freezing temperature after 2-4 hours of heating. As was mentioned in the cylindrical specimen tests, the heating rate becomes slower as the temperature increases. The maximum heating rate at the center surface (at -7°C) is approximately 7°C per hour. After four hours of heating, the specimen temperatures are maintained above freezing temperature in the freezer of -10°C. This indicates that the slab with the 1 in. conductive layer containing 4.8 % graphite has the ability to deice at the weather of -10°C, but for a colder region, a layer with a higher conductivity (thicker conductive layer or lower electrical resistivity) will be needed.

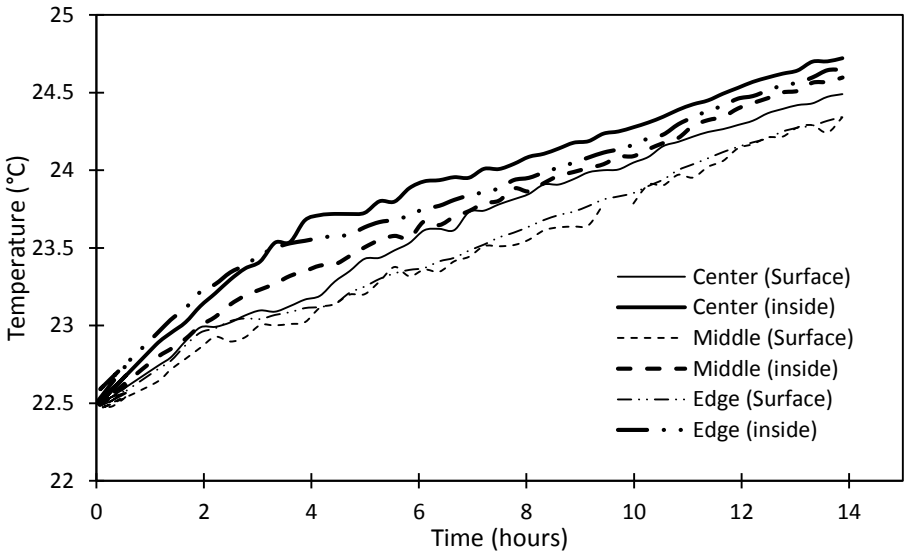


**Figure 65. Experimental result of deicing test by using DC power supply**

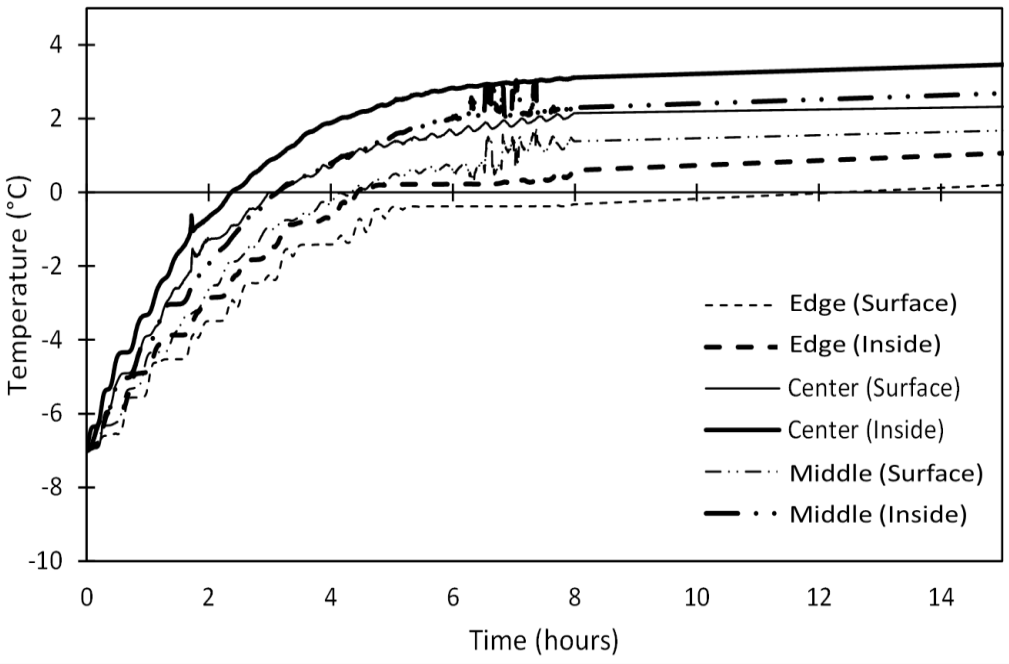


**Figure 66. Experimental result of deicing test in a freezer**

## 6.5 Life-Cycle Assessment

The chapter analyzes the environmental, economic, and social implications of the airport runway deicing choices through a product's life cycle from raw material extraction and production through construction and operation/ maintenance related to snow removal and deicing to the end of serviceable life. The conventional deicing method and the heated pavement system are compared and analyzed. This also aims to develop a systematic procedure to conduct an EIO-LCA (CMU 2011) of airport runway snow removal and deicing alternatives to support client who consider alternatives for airport runway maintenance. Understanding the environmental, economic and social impacts of each alternative can assist clients with selecting the most sustainable way, thus accounting for the implication their choices will have on future generations (Choi et al. 2015)

### 6.5.1 Data Collection of Two Alternatives

The main inputs to the EIO-LCA model for this study include other nonresidential structure for construction part and iron and nonresidential maintenance/repair for snow removal and deicing. Figure 67 shows the inputs and outputs of the EIO-LCA model.

In order to calculating the input data of EIO-LCA, the location of airport runway is assumed as Des Moines international airport in Iowa (Anand et al., 2014). The approximate area of the paved surface of the DSM airport is calculated as 6,224,503 $m^2$ and the size of a runway is 13,800$m^2$ like a condition of simulation research. In the case of a cost estimation for constructing the proposed deicing system, since the only difference between the conductive pavement and the non-conductive traditional pavement is the type of filler – traditional filler is replaced with graphite powder in the conductive pavement –

it is assumed that no additional process is required in the installation of the conductive pavement, i.e., only the material cost is added for the conductive pavement construction. The construction cost for the traditional HMA is assumed to be \$236.8/$m^2$, and the graphite price is \$3.652/kg (RS Means, 2002). When the weight fraction of the graphite powder is 3.18 %, the construction cost of the conductive pavement is 2.35% more expensive than the traditional pavement.

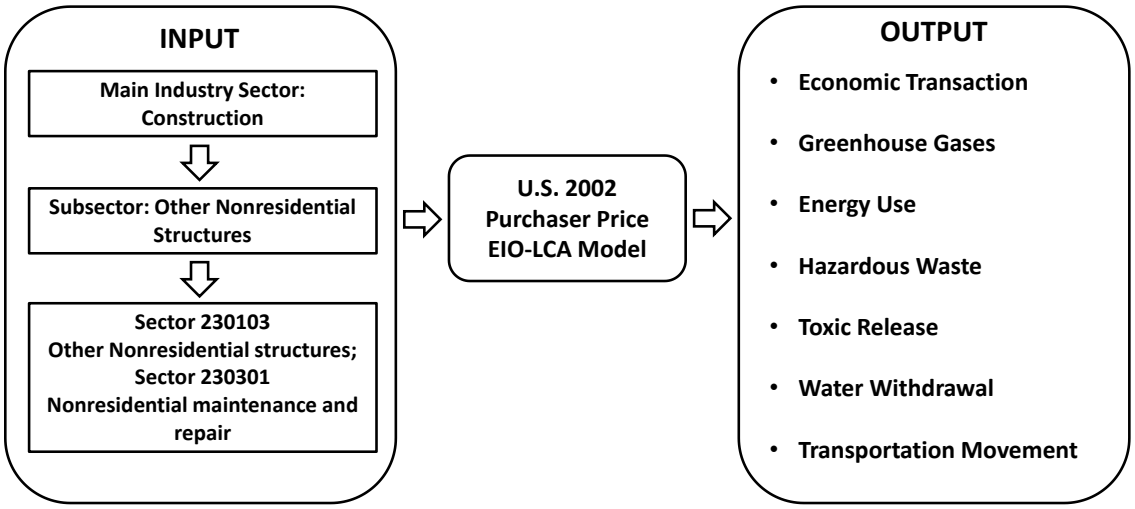


**Figure 67. Main framework of EIO-LCA model**

Conventional snow removal method includes machinery, deicing salts or chemicals, and labor. The input data consists of the initial cost (equipment purchase) and the recurring costs related to deicing that include the fuel cost, labor, and deicing chemical

(RF-11), a commonly used deicer at the DSM airport. RF-11 costs $25 per gallon and its recommended dosage is 3 gallons per 1,000 $ft^2$ for 1 inch of snowfall (Orison Marketing). The diesel price in Iowa is include as $3.65 per gallon (US Department of Energy). The labor cost involved in snow removal operations is estimated to be $25 per hour (U.S. Bureau of Labor Statistics 2013). To calculate the operation cost of heated pavement, the price of electricity is assumed as 0.1 USD/ KhW, which is within the range of residential electricity prices in the United States.

The values in Table 13 are used as the inputs to Sector 230103 (other nonresidential structure) and Sector 230301 (nonresidential maintenance and repair) for the two models.

**Table 13. Quantity takeoffs and EIO-LCA input values**

| Quantity and input | Item | Conventional snow removal and deicing | Heated pavement system |
|---|---|---|---|
| Quantity | construction | 13,800$m^3$ (Asphalt layer: 3000m length, 46m width, 10 cm depth) | 13,800$m^3$ (Plan asphalt layer: 3000m length, 46m width, 8 cm depth; Conductive asphalt layer: 2cm depth) |
| | Snow removal and deicing (Maintenance and repair) | 138,000$m^2$ (Asphalt layer: 3000m length, 46m width) | 138,000$m^2$ (Asphalt layer: 3000m length, 46m width) |
| Input values | Construction | $32,679,504.00 | $33,447,260.55 |
| | Snow removal and deicing (Maintenance and repair) | $13,814,554.79 | $268,931.63 |

**Table 14. EIO-LCA analysis results for two alternatives**

| Impact | Assessment | Unit | Type | Airport Runway Snow Removal Alternatives | |
|---|---|---|---|---|---|
| | | | | Conventional Snow Removal | Heated Pavement System |
| Economic impact | Year-of-expenditure dollars | $1 million in 2002 | Year of expenditure dollars | 88 | 65 |
| Social impact | Transportation movement | million t-km | Transportation movment | 110 | 81 |
| | Land use | Ha | Land use | 3,580 | 2,310 |
| Environmental impact | Global warming potential | $tCO_2e$ | Global warming potential | 28,600 | 20,600 |
| | Greenhouse gases emissions | $tCO_2e$ | $CO_2$ Fossil | 23,100 | 16,500 |
| | | | $CO_2$ process | 3,120 | 2,400 |
| | | | $CH_4$ | 1,750 | 1,290 |
| | | | $N_2O$ | 451 | 326 |
| | | | HFC/PFCs | 236 | 163 |
| | Energy use | TJ | Total energy | 390 | 279 |
| | | | Coal | 69 | 51 |
| | | | Natural Gases | 80 | 58 |
| | | | Petroleum-based fuel | 195 | 135 |
| | | | Biomass/waste fuel | 15 | 11 |
| | | | 31% non-fossil fuel electricity | 32 | 23 |
| | Hazardous waste | Short ton | Hazardous waste | 10,200,000 | 7,470,000 |
| | Toxic releases | kg | Fugitive air | 496 | 363 |
| | | | Total air | 2,880 | 2,110 |
| | | | Surface water | 464 | 343 |
| | | | Underground water | 416 | 291 |
| | | | Land | 4,880 | 3,450 |
| | | | Off-site | 2,060 | 1,520 |
| | Water withdrawals | kgal | Water withdrawals | 262,000 | 187,000 |

## 6.6 Interpretation of Environmental, Economic and Social Implications

As shown in Table 14, the environmental, economic, and social impacts of the selected snow removal alternatives are analyzed in the eight subcategories.

### 6.6.1 Economic Transaction

From the perspective of economic activity, "year-of-expenditure dollars" represents the complete economic supply chain of purchases needed to make the product. Figure 68 clearly shows that over the life cycle of 20 years, the heated pavement system has the least total and direct environmental, economic and social impact. This result conveys the fact that the heated pavement system can meet the equivalent design requirements (such as performance and functions) with 35.3% less economic cost to society than the conventional snow removal. The top three sectors contributing most to the economic transaction cost for the two alternatives are (1) other nonresidential structures, (2) architectural and engineering services, and (3) Wholesale trade.

### 6.6.2 Transportation Movement

The transportation movement category refers to movements in the eight types of transportation in ton-km, where 1 t-km refers to 1 t being transported for 1 km in distance. The eight types include air, oil pipe, gas pipe, rail, truck, water, international air, and international water. The conventional snow removal results in the most transportation movements, while the heated pavement system requires the least (Figure 68). The top three sectors contributing most to the transportation movement for the three pavement

alternatives are (1) other basic organic chemical manufacturing, (2) plate work and fabricated structural product manufacturing, and (3) paint and coating manufacturing.

### 6.6.3 Land Use

Transportation improvement projects have long lasting impacts on adjoining communities, business enterprises, and regional land use planning. The land use analysis performed in this paper examines the social impact of the two snow removal choices on land use. In this study, the results of the land use analysis were interpreted as spatial demand, taking no other controlling effects (e.g., soil quantity and land development activities) into account. Like transportation movement, the land use analysis clearly indicates that the conventional snow removal involves the larger land use, 54.9% more than the heated pavement system does (see the social impact category in Table 14). In the land use category, the top three sectors contributing most are: (1) logging, (2) forest nurseries, and (3) all other crop farming.

### 6.6.4 Global Warming Potential and Greenhouse Gases

Global warming potential (GWP) measures a relative amount of heat that is captured in the atmosphere by different types of greenhouse gases. The unit of GWP is metric tons of carbon dioxide (CO2) equivalent emissions (tCO2e). GWP includes CO2 fossil, CO2 process, methane (CH4), nitrous dioxide (N2O), and other high-GWP gases. In particular, the CO2 fossil and process gases represent the emissions of CO2 into the air from each sector's fossil fuel combustion and other sources. In the U.S., fossil fuels produce more than 90% of the greenhouse gas emissions due to heavy use of cars for

transportation (U.S. EPA 2011). For snow removal system, the analysis shows that other nonresidential structures is the most responsible sector, producing more than 30% of the tCO2e of the total GWP, followed by the power generation and cement manufacturing.

Figure 68 shows that the heated pavement system has 38.8% less GWP than the conventional snow removal. The results also indicate that CO2 fossil gas is mainly from chemical reactions, coal mining, and solid waste in cement manufacturing.

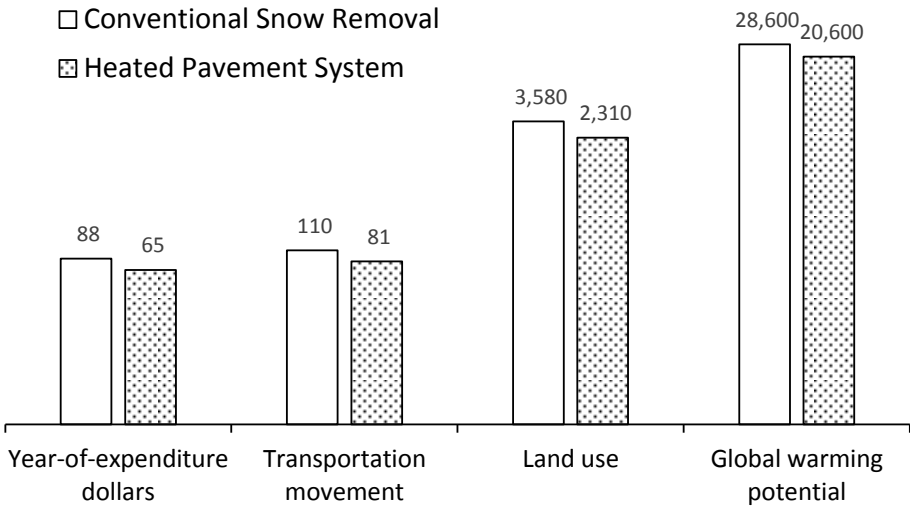


**Figure 68. Environmental, economic, and social impacts of two alternatives**

## 6.7 Conclusions

Sustainability of civil infrastructures, which considers social, environmental, and economical aspects, becomes a key-word for evaluating the merit of a technology. The proposed deicing system – direct electrical heating of pavement using conductive asphalt concrete – is expected to satisfy those three aspects of sustainability. Most importantly, the heating system is most effective way of eliminating safety threat due to snow/ice on the roadways (Lee 2012; Yehia and Tuan 2000). Mitigation of possible social impacts due to snow/ice on the pavement surface, such as traffic delay and other inconvenience, is the potential benefit of the proposed deicing system.

In the economic point of view, the installation of the conductive asphalt layer is cheaper than the heating system using electric coil or pipe. Since the proposed method replaces conventional filler with graphite, an additional process is not required to install the conductive layer. Considering that the volume fraction of graphite is 2-4% of the conductive mixture, and the price of graphite is around $2/kg, additional cost for 1 ton (covering 20 m2 when the conductive layer thickness is 1 inch) of conductive asphalt concrete might be $40-80 approximately. The additional cost for paving one kilometer of one lane road with the conductive asphalt concrete is estimated to be $14,400.

The cost for externally induced electric energy for heating can be another issue, and is compared with the cost of the deicing salt. For a day of ambient temperature ranged from -7°C to -1°C, the cost for electrical power is approximated to be $10,260 while the cost for four applications of deicing salt is $5,750 for an airport runway with 46 m wide and 3,000 m long. Besides, the proposed method can be considered as an environmentally

friendly technology. Melting snow/ice by heating will not generate polluted water and dust, which are byproducts of the chemical treatment.

The bench scale experiment using an asphalt concrete slab demonstrates the feasibility of the proposed deicing system. In a freezer of -10°C, the slab temperature is kept above the freezing temperature after three hours of electrical heating. The optimum depth and thickness of the conductive layer are suggested based on the non-steady state heat transfer analysis.

***Simulation Analysis***

- The closer the graphite modified asphalt concrete sub-layer to the surface, the less the cost. However, simply building a conductive sub-layer on the surface will consume more electric energy because of the direct heat emission from the surface. The thicker the graphite layer, the higher the cost, because more energy is required to heat the interior domain of the pavement.
- Changing resistivity of the conductive sub-layer or the magnitude of the electric field influence on the rate of heating. The higher conductivity (low resistivity) is able to heat the pavement faster, but the consumption of the electrical power is the same as long as the control temperature is constant.
- The higher the target surface temperature, the higher the cost.
- For a specific winter day of ambient temperature ranged from -7°C to -1°C, the cost for electrical power to heat the airport runway of 46 m width and 3,000 m long is approximated to be $10,260.

***Experimental Analysis***

- As a proof of concept, the direct electrical heating is tested with cylindrical specimen made of the conductive asphalt concrete. When 30V is applied for 10 minutes by using DC Power supplier, the temperature of the specimen containing 4.8% graphite increases around 10°C.
- The conductivity of the conductive HMA is sensitive to the temperature: the conductivity increases as the temperature decreases. While the temperature of the conductive mixture varies from -8°C to 35°C, the electrical resistance of the cylindrical specimen increases from 80Ω to 130Ω. Because of this conductivity drop, the heating rate of the specimen slowed down during the heating.
- For conductive slab experiment, the difference between inside and surface position makes that although surface temperature is average 0.7°C lower than inside, all thermal sensors in different locations have similar trend that it is increasing the temperature after DC power supplier turning on. In a freezer of -10°C, the slab temperature is kept above the freezing temperature after three hours of electrical heating.

***Additional advantages***

The proposed heating system has three additional benefits as follows:

- Fatigue cracking, which is a primary distress at cold temperature, can be reduced by keeping the pavement temperature higher than freezing temperature. For the same reason, rest period, which is the time required for asphalt self-healing, can be reduced as well. Eventually, extension of the pavement service life is expected.

- Heat conductivity will be improved with the increase of electrical conductivity. Improved heat conductivity may bring various benign effects on roadway pavement. For example, it may lead mitigation of heat island effect during the summer.

***Life-Cycle Assessment***

Sustainability of civil infrastructures, which considers social, environmental, and economical aspects, becomes a key-word for evaluating the merit of a technology. The proposed deicing system – direct electrical heating of pavement using conductive asphalt concrete – is expected to satisfy those three aspects of sustainability. The heating system is most effective way of eliminating safety threat due to snow/ice on the roadways. Mitigation of possible social impacts due to snow/ice on the pavement surface, such as traffic delay and other inconvenience, is the potential benefit of the proposed deicing system.

The result of LCA clearly indicate that the heated pavement system is much preferable to the conventional method for minimizing the negative environmental, economic and social impacts in all eight life-cycle assessments that are considered for a life cycle of 20 years.

# 7. CONCLUSION AND FUTURE WORK

## 7.1 Conclusion

**Section 3. Conductivity Control of Asphalt Concrete:** The experimental results for eight types of graphite and carbon black show that the conductivity of the asphalt mastic highly depends on the particle shape of graphite. Based on the mastic test results, two flake type graphite with different particle sizes were selected, and the effects of those on electrical conductivity and mechanical properties of asphalt concrete were investigated. The volume resistivity of asphalt concrete containing natural flake graphite powder showed similar trends to that of asphalt mastics. The results indicate that electrical conductivity of asphalt concrete can be controlled in a wide resistivity range by replacing a part of traditional filler with powder type carbon based additives, and even the improved mechanical properties can be obtained.

The conductive asphalt concrete containing the flake type graphite had improved indirect tensile strengths up to 40% when compared to the control asphalt concrete. On the other hand, the conductive asphalt concrete requires more compaction efforts to reach 4% target air voids.

The findings of the study will provide fundamental backgrounds for multifunctional applications of asphalt concrete.

**Section 4. Electrical Characterization with ACIS:** The electrical properties of the conductive asphalt concrete containing 20%, 25%, 30%, and 35% of the graphite by weight of total mastic were characterized by using ACIS. The electrical characteristics of the conductive asphalt are described with equivalent electrical circuits composed of

resistors, capacitors, and inductors. The equivalent circuits will be used to predict the electrical responses under the microstructural changes of composite materials, various electrochemical phases, and damage evolution.

The analysis of the measured data shows that the electrical characteristics of the composite vary with the graphite content, and consequently, the conductivity. This implies that a gradual change of conductivity with the conductive filler content is important for some multifunctional applications. A semi-circular shape Nyquist diagram is obtained from the asphalt concrete specimens containing 20~25% graphite by weight of mastic through ACIS measurement. The corresponding equivalent circuit can be expressed by a parallel connection of a resistor and a capacitor. The arc diameter is related to the resistance of the bulk specimen.

The Nyquist diagrams of specimens containing 30~35% graphite by weight of mastic show a different pattern because of low impedance. The corresponding equivalent circuit consists of multiple resistors, capacitors, and inductors. The inductance components appear in the equivalent circuit due to higher content of graphite. Nyquist diagram is also shown that the data density in the diagram varies with the graphite content. With low graphite content, the Nyquist diagram is distributed uniformly. High graphite content, however, causes the Nyquist diagram to be cornered at a specific local part.

The alternation of the electrical resistivity depending on increasing of the temperature are existed. In the case of conductive asphalt concrete, the change of electrical impedance was affected by thermal expansion of the asphalt binder, whereas, in conductive cement concrete, it is presumed that the changes in the movement of electrons

depending on different temperatures affect may be an important element to affect the electrical resistivity.

The differences of conductive asphalt concrete with various ambient conditions, which are dry condition, wet condition using tap water, and wet condition with salt water (3.5% salt by water weight), are shown by the Nyquist diagrams. These results prove that the moisture and the salt are significant roles to change the components in electrical equivalent circuits.

**Section 5. Application to Damage Self-Sensing:** The feasibility of damage self-sensing of conductive asphalt concrete was investigated in this section by using ACIS.

Major findings from the study are:

- For damage sensing tests, well-distributed data is more useful for distinguishing damage content through the whole frequency range. A 25% graphite by weight content is most suitable to perform damage self-sensing of conductive asphalt concrete.
- In the case of a dry condition, both the real and imaginary impedance increase with the increase of the damage in specimens. The capacitance value does not show a clear relationship with the damage evolution.
- In a wet condition, the impedance response is more sensitive and proportional to the damage evolution (0%-50%) than the response in a dry condition. The impedance response is affected by the polarization of water within isolated pores that hinder the movement of a charge or the mobility of ions.

- The distance between electrodes is important for measuring damage with ACIS. A dry condition is more useful for the damage evaluation than a wet condition. It has been proven that the impedance response is sensitive to the environmental conditions including humidity, the length between electrodes, and the change in impedance value.

ACIS is a useful tool to evaluate the damage in asphalt concrete in both dry and wet conditions. For damage sensing in a real environment, ACIS may be more accurate than the potential drop method (measuring DC resistance) that is widely used and standardized by ASTM.

**Section 6. Application to Snow and Ice Removal:** The electrical heating with the conductive asphalt concrete was tested as a cost effective and environmentally friendly method of snow and ice removal on pavements. The heat transfer analysis shows that the closer the graphite modified asphalt concrete sub-layer to the surface, the less the operation cost (consumption of electrical power). However, simply building a conductive sub-layer on the surface will consume more electric energy because of the direct heat emission from the surface. The optimum depth and thickness of the conductive layer are suggested based on the non-steady state heat transfer analysis.

The bench scale experiment using an asphalt concrete slab demonstrates the feasibility of the proposed deicing system. In a freezer of -10°C, the slab temperature is kept above the freezing temperature after three hours of electrical heating. When 30V is applied for 10 minutes by using DC Power supplier, the temperature of the specimen containing 4.8% graphite increases around 10°C.

The experimental data indicate that the conductivity of the conductive HMA is sensitive to the temperature: the conductivity increases as the temperature decreases. While the temperature of the conductive mixture varies from -8°C to 35°C, the electrical resistance of the cylindrical specimen increases from 80Ω to 130Ω. Because of this conductivity drop, the heating rate of the specimen slowed down during the heating. The average temperature measured at the non-conductive surface is 0.7°C lower than inside (conductive layer).

A life-cycle assessment for the proposed deicing system was conducted to compare the social, environmental, and economic impacts of the heated pavement with the conventional snow removal methods. The result of LCA clearly indicate that the heated pavement system is much preferable to the conventional method for minimizing the negative environmental, economic and social impacts in all eight life-cycle assessments that are considered for a life cycle of 20 years.

## 7.2 Future Work

Future works stemming from the results of this proposal are recommended as follows (Figure 69).

**Electrical Characteristics with AC Impedance Spectroscopy**

- To investigate the location of electrodes
- To know the microstructure related to percolation threshold of conductive asphalt composites
- To compare with ACIS of various kinds of graphite and carbon black

**Application to Damage Self-Sensing**

- To evaluate the effect of distance between electrodes
- To simulate the equivalent circuit with experimental results
- To find the efficient way to figure out the damage

**Application to Snow and Ice Removal**

- To investigate the temperature effect of variables (conductive layer thickness, electrical resistivity, the magnitude of the electric field)
- To study energy consumption of electric heating for deicing purpose

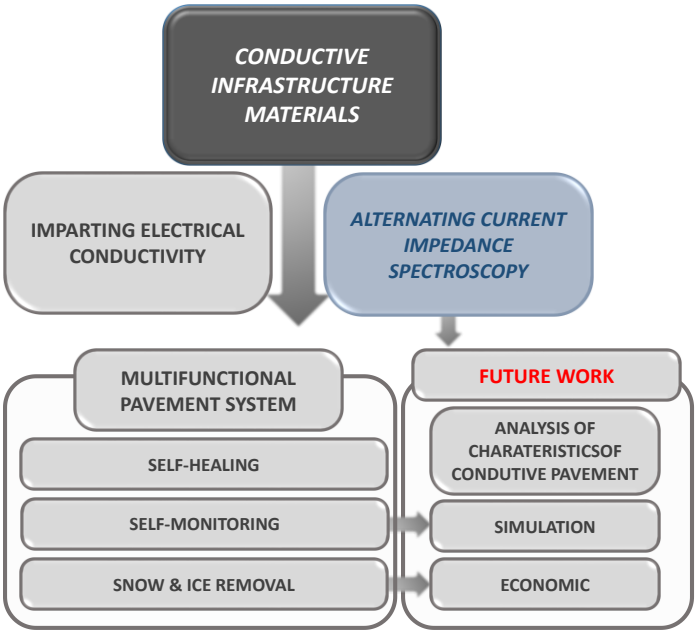


**Figure 69. Research strategy including future works**

## REFERENCES


Abtahi, S. M., Sheikhzadeh, M., and Hejazi, S. M. (2010). "Fiber-reinforced asphalt-concrete–a review." *Construction and Building Materials*, 24(6), 871-877.

Anand, P., Ceylan, H., Gkritza, K., Talor, P., Pyrialakou, V. D., Kim, S., and Gopalakrishnan, K. (2014). "Cost comparison of alternative airfield snow removal methodologies." *Civil, Construction and Environmental Engineering Conference Presentations and Proceedings*. Paper 9.

ASTM International. (2001). "Standard specification for hot-mixed, hot-laid bituminous paving mixtures." ASTM D3515–01, West Conshohocken, PA.

ASTM International. (2003). "Standard Test Method for Theoretical Maximum Specific Gravity and Density of Bituminous Paving Mixtures." ASTM D2041–03, West Conshohocken, PA.

ASTM International. (2005). "Standard Test Method for Percent Air Voids in Compacted Dense and Open Bituminous Paving Mixtures." ASTM D3203–05, West Conshohocken, PA.

ASTM International. (2006). "Standard Test Method for Sieve Analysis of Fine and Coarse Aggregates." ASTM C136–06, West Conshohocken, PA.

ASTM International. (2007). "Standard Test Method for Bulk Specific Gravity and Density of Compacted Bituminous Mixtures Using Coated Samples." ASTM D1188–07, West Conshohocken, PA.

ASTM International (2007). "Standard Specification for Fine Aggregate for Bituminous Paving Mixtures." ASTM D1073-07, West Conshohocken, PA.

ASTM International (2007). “Standard Test Method for Indirect Tensile (IDT) Strength of Bituminous Mixtures.” ASTM D6931-07, West Conshohocken, PA

ASTM International (2013). " Standard Test Method for Measurement of Fatigue Crack Growth Rates." ASTM E647, West Conshohocken, PA.

Azhari, F., and N. Banthia (2012). “Cement-Based Sensors with Carbon Fibers and Carbon Nanotubes for Piezoresistive Sensing.” *Cement and Concrete Composites*, 34 (7), pp. 866– 873.

Baeza, F. J., Galao, O., Zornoza, E., & Garcés, P. (2013). Multifunctional cement composites strain and damage sensors applied on reinforced concrete (RC) structural elements. *Materials*, 6(3), 841-855.

Barnard, E. H. (1965). “Electrically Conductive Concrete.” U.S. Patent 3,166,518.

Baranikumar, A. (2013). "IMPARTING ELECTRICAL CONDUCTIVITY INTO ASPHALT COMPOSITE USING GRAPHITE." Texas A&M University.

Barsoukov, E., and Macdonald, J. R. (2005). *Impedance spectroscopy: theory, experiment, and applications*, John Wiley & Sons.

Baur, J., and Silverman, E. (2011). "Challenges and Opportunities in Multifunctional Nanocomposite Structures for Aerospace Applications." *MRS Bulletin*, 32(04), 328-334.

Blackburn, R. R. (2004). *Snow and ice control: guidelines for materials and methods*, Transportation Research Board.

Bommavaram, R. R., A. Bhasin, and D. N. Little (2009). “Determining Intrinsic Healing Properties of Asphalt Binders.” *Transportation Research Record*, 2126 (1), pp. 47–54.

Bonnaure, F. P., A. H. Huibers, and A. Boonders (1982). “A Laboratory Investigation of the Influence of Rest Periods on the Fatigue Characteristics of Bituminous Mixes.” *Journal of the Association of Asphalt Paving Technologists,* 51, pp. 104–128.

Bontea, D.-M., Chung, D., and Lee, G. (2000). "Damage in carbon fiber-reinforced concrete, monitored by electrical resistance measurement." *Cement and Concrete Research*, 30(4), 651-659.

Campo, M., Woo, L., Mason, T. O., and Garboczi, E. (2002). "Frequency-dependent electrical mixing law behavior in spherical particle composites." *Journal of electroceramics*, 9(1), 49-56.

Cao, J., and Chung, D. D. L. (2004). "Electric polarization and depolarization in cement-based materials, studied by apparent electrical resistance measurement." *Cement and Concrete Research*, 34(3), 481-485.

Cebeci, H., Villoria, R. G. d., Hart, A. J., and Wardle, B. L. (2009). "Multifunctional properties of high volume fraction aligned carbon nanotube polymer composites with controlled morphology." *Composites Science and Technology*, 69(15-16), 2649-2656.

Chacko, R., and N. Banthia (2007). “Carbon Fiber Reinforced Cement Based Sensors.” *Canadian Journal of Civil Engineering*, 34 (3), pp. 284–290.

Chen, B., K. Wu, and W. Yao (2004). “Conductivity of Carbon Fiber Reinforced Cement-Based Composites.” *Cement and Concrete Composites,* 26 (4), pp. 291–297.

Chen, M., Wu, S., Wang, H., and Zhang, J. (2011). “Study of ice and snow melting process on 454 conductive asphalt solar collector.” *Solar Energy Materials and Solar Cells*, 95(12), 3241-455 3250.

Chen, F., Chen, M. Z., Wu, S. P., and Zhang, J. Z. (2012) "Research on pavement performance of steel slag conductive asphalt concrete for deicing and snow melting." *Proc., Key Engineering Materials*, Trans Tech Publ, 168-174.

CHEN, Y., and LI, Z. (2013). "Deicing mechanism for crumb rubber asphalt pavement." *Journal of Central South University (Science and Technology)*, 5, 049.

Chiarello, M., and R. Zinno (2004). “Electrical Conductivity of Self-Monitoring CFRC.” *Cement and Concrete Composites*, 27 (4), pp. 463–469.

Cho, S., Chen, C. F., and Mukherjee, P. P. (2015). "Influence of microstructure on impedance response in intercalation electrodes." *Journal of The Electrochemical Society*, 162(7), A1202-A1214.

Chou, T.-W., Gao, L., Thostenson, E. T., Zhang, Z., and Byun, J.-H. (2010). "An assessment of the science and technology of carbon nanotube-based fibers and composites." *Composites Science and Technology*, 70(1), 1-19.

Chung, D. D. L. (1997). “Self-Monitoring Structural Materials.” *Materials Science and Engineering*, 22 (2), pp. 57–78. 67

Chung, D. D. L. (1999). “Cement Reinforced with Short Carbon Fibers: A Multifunctional Material.” *Composites*, 31 (6), pp. 511–526.

Chung, D. D. L. (2000). “Cement-Matrix Composites for Smart Structures.” *Smart Materials and Structures*, 9 (4), pp. 389–401.

Chung, D. D. L. (2002). “Piezoresistive Cement-Based Materials for Strain Sensing.” *Journal of Intelligent Material Systems and Structures*, 13 (9), pp. 599–609.

Chung, D. D. L. (2003). Multifunctional Cement-Based Materials. *Marcel Dekker, Inc.*, New York, NY.

Chung, D. D. L. (2004). Self-heating structural materials. *Smart materials and structures*, 13(3), 562.

Chung, D. D. L. (2012). “Carbon Materials for Structural Self-Sensing, Electromagnetic Shielding and Thermal Interfacing.” *Carbon*, 50 (9), pp. 3342–3353.

Chung, D., and Wang, S. (2003). "Self-sensing of damage and strain in carbon fiber polymer-matrix structural composites by electrical resistance measurement." *Polymers and Polymer Composites*, 11(7), 515-525.

Choi, K., Lee, H. W., Mao, Z., Lavy, S., and Ryoo., B. Y. (2015). “Environmental, Economic, and 457 Social Implications of Highway Concrete Rehabilitation Alternatives.” *Journal of 458 Construction Engineering and Management*, 142(2), 04015079.

Clark, G., and Knott, J. (1975). "Measurement of fatigue cracks in notched specimens by means of theoretical electrical potential calibrations." *Journal of the Mechanics and Physics of Solids*, 23(4), 265-276.

CMU (Carnegie Mellon University). (2011). “EIO-LCA: Free, fast, easy life cycle assessment.” 461 ⟨http://www.eiolca.net⟩ (Dec. 2, 2011).

Cubides, Y., and Castaneda, H. (2016). "Corrosion protection mechanisms of carbon nanotube and zinc-rich epoxy primers on carbon steel in simulated concrete pore solutions in the presence of chloride ions." *Corrosion Science*, 109, 145-161.

Daniel, J. S., and Y. R. Kim (2001). “Laboratory Evaluation of Fatigue Healing of Asphalt Mixtures.” *Journal of Materials in Civil Engineering*, 13 (6), pp. 434–440.

D'Alessandro, A., Rallini, M., Ubertini, F., Materazzi, A. L., and Kenny, J. M. (2016). Investigations on scalable fabrication procedures for self-sensing carbon nanotube cement-matrix composites for SHM applications. *Cement and Concrete Composites*, 65, 200-213.

Doremus, L., Nadot, Y., Henaff, G., Mary, C., and Pierret, S. (2015). "Calibration of the potential drop method for monitoring small crack growth from surface anomalies – Crack front marking technique and finite element simulations." *International Journal of Fatigue*, 70, 178-185.

Fromm, H. J. (1976). “Electrically conductive asphalt mixes for the cathodic protection of concrete bridge decks.” *Asph. Paving Technol.*, 45, 382–399.

Galao, O., Baeza, F. J., Zornoza, E., and Garcés, P. (2014). Strain and damage sensing properties on multifunctional cement composites with CNF admixture. *Cement and concrete composites*, 46, 90-98.

García, Á. (2012). Self-healing of open cracks in asphalt mastic. *Fuel*, 93, 264-272.

García, Á., Schlangen, E., van de Ven, M., and Liu, Q. (2009). "Electrical conductivity of asphalt mortar containing conductive fibers and fillers." *Construction and Building Materials*, 23(10), 3175-3181.

García, Á., E. Schlangen, M. Van de Ven, and D. Van Vliet (2011a). "Crack Repair of Asphalt Concrete with Induction Energy." *Heron*, 56 (1/2), pp. 37–48.

García, Á., E. Schlangen, M. Van de Ven, and D. Van Vliet (2011b). "Induction Heating of Mastic Containing Conductive Fibers and Fillers." *Materials and Structure*, 44, pp. 499– 508.

Gibson, R. F. (2010). "A review of recent research on mechanics of multifunctional composite materials and structures." *Composite Structures*, 92(12), 2793-2810.

Girault, H. H. (2004). *Analytical and physical electrochemistry*, CRC Press.

Gomis, J., Galao, O., Gomis, V., Zornoza, E., & Garcés, P. (2015). Self-heating and deicing conductive cement. Experimental study and modeling. *Construction and Building Materials*, 75, 442-449.

Gu, P., Xie, P., Beaudoin, J. J., and Brousseau, R. (1992). "AC impedance spectroscopy (I): A new equivalent circuit model for hydrated Portland cement paste." *Cement and Concrete Research*, 22(5), 833-840.

Gu, P., Xie, P., and Beaudoin, J. (1993a). "Microstructural characterization of the transition zone in cement systems by means of AC impedance spectroscopy." *Cement and Concrete Research*, 23(3), 581-591.

Gu, P., Xie, P., Beaudoin, J. J., and Brousseau, R. (1993b). "AC impedance spectroscopy (II): Microstructural characterization of hydrating cement-silica fume systems." *Cement and Concrete Research*, 23(1), 157-168.

Gui, J., Phelan, P. E., Kaloushi, K. E., and Golden, J. S. (2007). "Impact of pavement thermophysical 468 properties on surface temperatures." *Journal of Materials in Civil Engineering*, 19 (8), 683-469 690.

Hallaji, M., and Pour-Ghaz, M. (2014). "A new sensing skin for qualitative damage detection in concrete elements: Rapid difference imaging with electrical resistance tomography." *NDT & E International*, 68, 13-21.

Han, B., Ding, S., and Yu, X. (2015). "Intrinsic self-sensing concrete and structures: A review." *Measurement*, 59, 110-128.

Henderson, D. (1963). "Experimental roadway heating project on a bridge approach/and discussion." *474 Highway Research Record*, 14, 14-23.

Hermansson, A. (2001). "Mathematical model for calculation of pavement temperatures: Comparison 478 of calculated and measured temperatures." *Transportation Research Record*, 1764, 180-188.

Heymsfield, E., Osweiler, A., Selvam, P., and Kuss, M. (2014). "Developing Anti-Icing Airfield 480 Runways Using Conductive Concrete with Renewable Energy." *Journal of Cold Region 481 Engineering*, DOI: 10.1061/(ASCE)CR.1943-5495.0000064.

Hong, L., and Song, Y. P. (2006). "Study on conductive properties of graphite slurry infiltrated fiber concrete." *Journal of Building Materials*, 9(6), 649-653.

Hopstock, D. (2003). "Microwave-absorbing road construction and repair material." *Final Report to NRRI on Idea Evaluation Subcontract*.

Hopstock, D. and Zanko, L. M. (2005). "Minnesota Taconite as a Microwave-Absorbing Road 483 Aggregate Material for Deicing and Pothole Patching Applications-Final Report." *Intelligent 484 Transportation Systems Institute Center for Transportation Studies*, Minneapolis, MN

Houle, K. M., Roseen, R. M., Ballestero, T. P., Briggs, J. F., and Houle, J. J. (2009). "Examinations of pervious concrete and porous asphalt pavements performance for storm water management in northern climates." *Paper presented at the World Environmental and Water Resources Congress 2009@ sGreat Rivers*, pp. 1105-1122.

Huang, B., J. Cao, X. Chen, X. Shu, and W. He (2006). "Laboratory Investigation into Electrically Conductive HMA Mixtures." *Journal of the Association of Asphalt Paving Technologists*, 75, pp. 1235–1253.

Huang, B., Chen, X., and Shu, X. (2009). "Effects of electrically conductive additives on laboratory-measured properties of asphalt mixtures." *Journal of Materials in Civil Engineering*, 21(10), 612-617.

Jang, S. H., Hochstein, D. P., Kawashima, S., and Yin, H. (2017). Experiments and micromechanical modeling of electrical conductivity of carbon nanotube/cement composites with moisture. *Cement and Concrete Composites*, 77, 49-59.

Johnson, H. (1965). "Calibrating the electric potential method for studying slow crack growth(Calibration of electric potential technique to study slow or steady crack

growth in high strength materials)." *Materials Research and Standards*, 5, 442-445.

Jones, P., and Jeffrey, B. (1992). *Environmental impact of road salting in chemical deicers and the environment*, Lewis Publishers, Boca Raton, FL.

Kalaitzidou, K., Fukushima, H., and Drzal, L. T. (2007). "Multifunctional polypropylene composites produced by incorporation of exfoliated graphite nanoplatelets." *Carbon*, 45(7), 1446-1452.

Kuemmel, D. E. (1994). "Managing roadway snow and ice control operations," NCHRP Synthesis 207, *489 Transportation Research Board*, National Academic Press, Washington, D. C.

Lataste, J. F., Sirieix, C., Breysse, D., and Frappa, M. (2003). "Electrical resistivity measurement applied to cracking assessment on reinforced concrete structures in civil engineering." *NDT & E International*, 36(6), 383-394.

Le, J.-L., Du, H., and Pang, S. D. (2014). "Use of 2D Graphene Nanoplatelets (GNP) in cement composites for structural health evaluation." *Composites Part B: Engineering*, 67, 555-563.

Lee, H. G. (2012). “Electric coil installed road melting snow, good idea but…” News article from SBS, 491 Seoul, South Korea, http://media.daum.net/v/20121206210309052.

Lee, K. W. W. and Correia, A. J. (2010). "A Pilot Study for Investigation of Novel Methods to Harvest 493 Solar Energy from Asphalt Pavements." *KICT Report*, Seoul, South Korea. 494

Lee, R. C., Sackos, J., Nydahl, J., and Pell, K. (1984). “Bridge heating using ground-source heat pipes.” *495 Transportation Research Record*, 962, 51-56.

Li, J., Ma, P. C., Chow, W. S., To, C. K., Tang, B. Z., and Kim, J. K. (2007). "Correlations between Percolation Threshold, Dispersion State, and Aspect Ratio of Carbon Nanotubes." *Advanced Functional Materials*, 17(16), 3207-3215.

Liu, X., S. Wu, L. Ning, and G. Bo (2008a). “Self-Monitoring Application of Asphalt Concrete Containing Graphite and Carbon Fibers.” *Materials Science Edition*, 23 (2), pp. 268–271.

Liu, X., S. Wu, Y. Qunshan, Q. Jian, and L. Bo (2008b). “Properties Evaluation of Asphalt Based Composites with Graphite and Mine Powders.” *Construction and Building Materials*, 22, pp. 121–126.

Liu, X., and Wu, S. (2009). "Research on the conductive asphalt concrete’s piezoresistivity effect and its mechanism." *Construction and Building Materials*, 23(8), 2752-2756.

Liu, X., and S. Wu (2011a). “Study on the Graphite and Carbon Fiber Modified Asphalt Concrete.” *Construction and Building Materials*, 25, pp. 1807–1811.

Liu, X., and S. Wu (2011b). “Study on the Piezoresistivity Character of Electrically Conductive Asphalt Concrete.” *Advanced Materials Research*, Vol. 233–235, pp. 1756–1761.

Liu, Q., E. Schlangen, M. Ven, and M. Poot (2010a). “Optimization of Steel Fiber Used for Induction Heating in Porous Asphalt Concrete.” *Proceedings of the Seventh*

*International Conference on Traffic and Transportation Studies*, ASCE, Kunming, China, August 3–5, pp. 1320–1330.

Liu, Q., E. Schlangen, A. García, and M. Ven (2010b). "Induction Heating of Electrically Conductive Porous Asphalt Concrete." *Construction and Building Materials*, 24 (7), pp. 1207–1213.

Liu, Q., E. Schlangen, M. Ven, and A. Garcia (2010c). "Healing of Porous Asphalt Concrete via Induction Heating." *Road Materials and Pavement Design*, 11 (S1), pp. 527–542.

Löfgren, S. (2001). "The chemical effects of deicing salt on soil and stream water of five catchments in southeast Sweden." *Water, Air, and Soil Pollution*, 130(1-4), 863-868.

Mallick, R. B., Chen, B. L., Bhowmick, S. (2009). "Harvesting energy from asphalt pavements and reducing the heat island effect." *International Journal of Sustainable Engineering*, 2(3), 214-228.

McCarter, W., Garvin, S., and Bouzid, N. (1988). "Impedance measurements on cement paste." *Journal of materials science letters*, 7(10), 1056-1057.

McCarter, W. J., and Garvin, S. (1989). Dependence of electrical impedance of cement-based materials on their moisture condition. *Journal of Physics D: Applied Physics*, 22(11), 1773.

McCarter, W. J., Chrisp, T. M., Starrs, G., Basheer, P. A. M., and Blewett, J. (2005). "Field monitoring of electrical conductivity of cover-zone concrete." *Cement and Concrete Composites*, 27(7), 809-817.

McCarter, W. J., Starrs, G., Chrisp, T. M., and Banfill, P. F. G. (2009). "Complex Impedance and Dielectric Dispersion in Carbon Fiber Reinforced Cement Matrices." *Journal of the American Ceramic Society*, 92(7), 1617-1620.

Minsk, L. D. (1968). "Electrically Conductive Asphalt for Control of Snow and Ice Accumulation." *502 Highway Research Record*, 227, 57–63.

Minsk, L. D. (1971). *Electrically Conductive Asphaltic Concrete*, U.S. Patent 3,573,427.

Mo, L., S. Wu, X. Liu, and Z. Chen (2005). "Percolation Model of Graphite-Modified Asphalt Concrete." *Journal of Wuhan University of Technology Materials Science Edition*, 20 (1), pp. 111–113.

NAPA (2009). Black and Green: *Sustainable Asphalt, Now and Tomorrow,* National Asphalt Pavement 507 Association, Lanham, Md.

Nemat-Nasser, S., Nemat-Nasser, S., Plaisted, T., Starr, A., and, Amirkhizi, A. V. (2005). 509 "Multifunctional materials." *Biomimetics: Biologically Inspired Technologies*, Taylor and 510 Francis Group, Boca Raton, London, New York, 309-340.

Newcomb, D. E., Buncher, M., and Huddleston, I. J. (2001). "Concepts of perpetual pavements." *512 Transportation Research Circular*, 503, 4-11.

Nixon, W. A. (1993). "Improved cutting edges for ice removal." *Strategic Highway Research Program 514 Report*, SHRP-H-346, Washington, D.C.

Norambuena-Contreras, J., and Garcia, A. (2016). Self-healing of asphalt mixture by microwave and induction heating. *Materials & Design*, 106, 404-414.

Norambuena-Contreras, J., and Garcia, A. (2017). Crack-healing evaluation of fibre-reinforced asphalt mixtures using microwave and induction heating. *Road Materials and Pavement Design*, 1-11.

Ozyurt, N., Mason, T. O., and Shah, S. P. (2006). "Non-destructive monitoring of fiber orientation using AC-IS: an industrial-scale application." *Cement and Concrete Research*, 36(9), 1653-1660.

Pan, P., Wu, S., Xiao, F., Pang, L., and Xiao, Y. (2015). Conductive asphalt concrete: A review on structure design, performance, and practical applications. *Journal of Intelligent Material Systems and Structures*, 26(7), 755-769.

Park, P. (2012). "Characteristics and applications of high-performance fiber reinforced asphalt concrete." University of Michigan at Ann-harbor.

Park, P., El-Tawil, S., Park, S.-Y., and Naaman, A. E. (2015). "Cracking resistance of fiber reinforced asphalt concrete at −20°C." *Construction and Building Materials*, 81, 47-57.

Park, P., Rew, Y., and Baranikumar, A. (2014). "Controlling Conductivity of Asphalt Concrete with Graphite." Citeseer.

Park, S., Ahmad, S., Yun, C. B., and Roh, Y. (2006). "Multiple crack detection of concrete structures using impedance-based structural health monitoring techniques." *Experimental Mechanics*, 46(5), 609-618.

Peled, A., Torrents, J. M., Mason, T. O., Shah, S. P., and Garboczi, E. J. (2001). "Electrical impedance spectra to monitor damage during tensile loading of cement composites." *ACI Materials Journal*, 98(4), 313-322.

Providakis, C. P., Stefanaki, K. D., Voutetaki, M. E., Tsompanakis, Y., & Stavroulaki, M. (2014). Damage detection in concrete structures using a simultaneously activated multi-mode PZT active sensing system: numerical modelling. *Structure and Infrastructure Engineering*, 10(11), 1451-1468.

Qiu, J., Zhang, C., Wang, B., and Liang, R. (2007). "Carbon nanotube integrated multifunctional multiscale composites." *Nanotechnology*, 18(27), 275708.

Rew, Y., Baranikumar, A., Tamashausky, A. V., El-Tawil, S., and Park, P. (2017). "Electrical and mechanical properties of asphaltic composites containing carbon based fillers." *Construction and Building Materials*, 135, 394-404.

RSMeans. (2002). *Heavy civil construction cost data*. Kingston, MA.

Sandler, J. K. W., Kirk, J. E., Kinloch, I. A., Shaffer, M. S. P., and Windle, A. H. (2003). "Ultra-low electrical percolation threshold in carbon-nanotube-epoxy composites." *Polymer*, 44(19), 5893-5899.

Sanzo, D., and Hecnar, S. J. (2006). "Effects of road de-icing salt (NaCl) on larval wood frogs (Rana sylvatica)." *Environ Pollut*, 140(2), 247-256.

Serin, S., Morova, N., Saltan, M., and Terzi, S. (2012). "Investigation of usability of steel fibers in asphalt concrete mixtures." *Construction and Building Materials*, 36, 238-244.

Shi, X. (2014). "Controlling thermal properties of asphalt concrete and its multifunctional applications." *Master Thesis*, Texas A&M University.

Shi, X., Rew, Y., Ivers, E., Shon, C. S., Stenger, E. M., and Park, P. (2017). “Effects of thermally 527 modified asphalt concrete on pavement temperature.”

*International Journal of Pavement 528 Engineering*, DOI: 10.1080/10298436.2017.1326234.

Singla, M., Chang, C., Song, G., Yang, Z., and Ge, X. (2013). "Automatic controls for the carbon fiber tape-based deicing technology." *Journal of Cold Regions Engineering*, 28(1), 04013001.

Stratfull, R. F. (1974). "Experimental cathodic protection of a bridge deck." *Transportation Research Record*. 500, Transportation Research Board, Washington, D.C.

Thostenson, E. T., Ziaee, S., and Chou, T.-W. (2009). "Processing and electrical properties of carbon nanotube/vinyl ester nanocomposites." *Composites Science and Technology*, 69(6), 801-804.

U.S. Bureau of Labor Statistics. (2013). "National Occupational Employment and Wage Estimates, 533 May 2013." (http://www.bls.gov/oes/current/oes_nat.htm). 534

U.S. Energy Information Administration. (2014). "Average price of electricity to ultimate customers by 535 end-use sector." 536 (https://www.eia.gov/electricity/monthly/epm_table_grapher.cfm?t=epmt_5_6_a)

Vaidya, S., and E. Allouche (2011). "Experimental Evaluation of Electrical Conductivity of Carbon Fiber Reinforced Fly Ash Based Geopolymer." *Smart Structure and Systems*, 7 (1), pp. 27–40.

Wandowski, T., Malinowski, P., Skarbek, L., and Ostachowicz, W. (2016). "Moisture detection in carbon fiber reinforced polymer composites using electromechanical

impedance technique." *Proceedings of the Institution of Mechanical Engineers, Part C: Journal of Mechanical Engineering Science*, 230(2), 331-336.

Wang, K., Nelsen, D. E., and Nixon, W. A. (2006). "Damaging effects of deicing chemicals on concrete materials." *Cement and Concrete Composites*, 28(2), 173-188.

Wang, H., Yang, J., Liao, H., & Chen, X. (2016). Electrical and mechanical properties of asphalt concrete containing conductive fibers and fillers. *Construction and Building Materials*, 122, 184-190.

Wen, S., and D. D. L. Chung (2001a). "Effect of Admixtures on the Dielectric Constant of Cement Paste." *Cement and Concrete Research*, 31 (4), pp. 673–677.

Wen, S., and D. D. L. Chung (2001b). "Effect of Stress on the Electric Polarization in Cement." *Cement and Concrete Research,* 31 (2), pp. 291–295.

Wen, S., and Chung, D. (2001c). "Electric polarization in carbon fiber-reinforced cement." *Cement and Concrete Research*, 31(1), 141-147.

Wen, S., and Chung, D. D. L. (2004). "Effect of fiber content on the thermoelectric behavior of cement." *Journal of materials science*, 39(13), 4103-4106.

Wen, S., and Chung, D. D. L. (2006). "The role of electronic and ionic conduction in the electrical conductivity of carbon fiber reinforced cement." *Carbon*, 44(11), 2130-2138.

Wen, S., and Chung, D. D. L. (2007a). "Electrical-resistance-based damage self-sensing in carbon fiber reinforced cement." *Carbon*, 45(4), 710-716.

Wen, S., and Chung, D. D. L. (2007b). Double percolation in the electrical conduction in carbon fiber reinforced cement-based materials. *Carbon*, 45(2), 263-267.

Williams, D. D., Williams, N. E., and Cao, Y. (2000). "Road salt contamination of groundwater in a major metropolitan area and development of a biological index to monitor its impact." *Water Research*, 34(1), 127-138.

Wu, S.-p., Liu, X.-m., Ye, Q.-s., and Ning, L. (2006). "Self-monitoring electrically conductive asphalt-based composite containing carbon fillers." *Transactions of Nonferrous Metals Society of China*, 16, s512-s516.

Wu, S., Mo, L., Shui, Z., and Chen, Z. (2005). "Investigation of the conductivity of asphalt concrete containing conductive fillers." *Carbon*, 43(7), 1358-1363.

Wu, S., Y. Zhang, and M. Chen (2010). "Research on Mechanical Characteristics of Conductive Asphalt Concrete by Indirect Tensile Test." *Proceedings of SPIE*, pp. 752265-752265.

Wu, S., Pan, P., Chen, M., and Zhang, Y. (2012). "Analysis of characteristics of electrically conductive asphalt concrete prepared by multiplex conductive materials." *Journal of Materials in Civil Engineering*, 25(7), 871-879.

Wu, S. P., Mo, L., and Shui, Z. (2003) "Piezoresistivity of graphite modified asphalt-based composites." *Proc., Key Engineering Materials*, Trans Tech Publ, 391-396.

Xiangyang, W. and Yuxing, G. (2010). "Research on the preparation of conductive asphalt concrete for 546 deicing and snow melting." *Proceedings of Advanced*

*Computer Theory and Engineering 547 (ICACTE) 3rd International Conference*, V2-381-V2-384.

Yang, Z. J., Yang, T., Song, G., and Singla, M. (2012). "Experimental study on an electrical deicing technology utilizing carbon fiber tape."

Ye, L., Lu, Y., Su, Z., and Meng, G. (2005). "Functionalized composite structures for new generation airframes: a review." *Composites Science and Technology*, 65(9), 1436-1446.

Yehia, S., and Tuan, C. (2000). "Thin conductive concrete overlay for bridge deck deicing and anti-icing." *Transportation Research Record: Journal of the Transportation Research Board*(1698), 45-53.

Zaleski, P. L., Derwin, D. J., and Flood, W. H. (1998). "Electrically Conductive Paving Mixture and 558 Paving System." U.S. Patent 5,707,171.

Zenewitz, J. A. (1977). "Survey of Alternatives to the use of Chlorides for Highway Deicing." *FHWA-560 RD-77-52, U.S. Dept. of Transportation*, Federal Highway Administration, Offices of 561 Research and Development, Washington, D.C.

Zhang, H., X. H. Wu, and X. L. Wang, (2011). "Conductivity mechanism of asphalt concrete with the PANI/PP compound conductive fiber." *In Materials Science Forum*, Vol. 689, pp. 69-73.

Zhao, X. H., and Zhang, X. D. (2011). "The research on the anti-icing and pavement performance of the chloride-stored asphalt mixture." *Applied Mechanics and Materials*, 97, 321-326.

Zhu, X.-K., and Joyce, J. A. (2012). "Review of fracture toughness (G, K, J, CTOD, CTOA) testing and standardization." *Engineering Fracture Mechanics*, 85, 1-46.

Ziegler, W. (2013). "A solar thermal approach to runway ice management." *FAA Design Competition for Universities.*